Technische Universität München

Lehrstuhl für Bioverfahrenstechnik

Membrane functionalization of nano-scale enzyme membrane reactors for asymmetric syntheses

Tom Sebastian Schwarzer, M.Sc.

Vollständiger Abdruck der von der Fakultät für Maschinenwesen der Technischen Universität München zur Erlangung des akademischen Grades eines

Doktors der Naturwissenschaften

genehmigten Dissertation.

Vorsitzender:		Prof. Dr.-Ing. Dirk Weuster-Botz
Prüfer der Dissertation:	1.	TUM Junior Fellow Dr. rer. nat. Kathrin Castiglione
	2.	Prof. Dr. rer. nat. Michael Groll

Die Dissertation wurde am 15.05.2017 bei der Technischen Universität München eingereicht und durch die Fakultät für Maschinenwesen am 09.10.2017 angenommen.

Acknowledgements

This doctoral thesis was prepared at the Institute of Biochemical Engineering (Prof. Dr.-Ing. Dirk Weuster-Botz) of the Technical University of Munich as part of the junior research group of Dr. rer. nat. Kathrin Castiglione. It is my pleasure to thank the many people who contributed to this work.

My sincerest gratitude goes to Dr. rer. nat. Kathrin Castiglione for the possibility to realize this project. I would like to thank her for her help and guidance, for many lively discussions and the vast knowledge she shared.

I would like to thank Prof. Dr. Michael Groll for his role as committee member and Prof. Dr.-Ing. Dirk Weuster-Botz for his role as chairman. Furthermore, I would like to thank Prof. Dr.-Ing. Dirk Weuster-Botz for providing the necessary equipment and lab space to work on this thesis.

I thank the the BMBF (German Federal Ministry of Education and Research) for funding.

Special thanks go to all of my former colleagues, most of all Dr.-Ing. Sarah Poschenrieder, Dr. rer. nat. Ludwig Klermund and Florian Sedlmaier, for all the discussions and debates and the excellent collaboration. I would also like to thank Ingmar Polte and Dr. Ludwig Klermund for carefully proofreading the manuscript.

The knowledgeable support of Swati Krishnan of the Chair of Systems Biophysics and Bionanotechnology (TUM) for the acquisition of numerous TEM images and of electrophysiological data on OprG is greatly appreciated. I also thank Dr. rer. nat. Marianne Hanzlik of the Institute of Electron Microscopy (TUM) for the acquisition of TEM images of purified polymersomes and Vera Arnaut and Dr. rer. nat. Martin Langecker of the Chair of Systems Biophysics and Bionanotechnology (TUM) for their help with the acquisition of electrophysiological data on FocA. The freedom of access to the ultracentrifuges at the Chair of Biochemistry (TUM), the Chair of Biomolecular Nano-Technology (TUM) and the Chair of Biotechnology (TUM) is also gratefully acknowledged.

I deeply acknowledge my students for their great experimental assistance, especially Maria Hermann and Daniel Wehrle, but also Daniele De Donato, Thomas Meier, Peter Sinner, Vivian Würf, Fabian Seebacher and Lena Träger.

Furthermore, I would like to thank Ellen Truxius, Gabriele Herbrik, Markus Amann, Georg Kojro and Norbert Werth for their support in administrative and technical issues.

Last and most important, I would like to thank my family, most of all my wife and my son. How would I have fared without their endless support of love and bliss?

Table of contents

1 Introduction

It has been known for decades that chiral molecules can evoke different sensory and pharmacological effects. The biological differences between enantiomers led to an increased interest in the synthesis of enantiopure compounds (Kroutil *et al.*, 2004). This is particularly true for the pharmaceutical industry, because in most cases only one enantiomer mediates the desired effect, while the other enantiomer can be inactive, at best, or even cause severe side effects (Faber, 2011, Goswami, 2011). As a consequence of their complex chiral constitution, enzymes are inherently suited for the synthesis of optically pure compounds. The use of enzymes to catalyze the conversion of organic compounds is called biocatalysis. Technological advances in the fields of biotechnology and bioprocess engineering helped to create efficient and profitable biocatalytic processes, and biocatalysis has become an established technology for the industrial manufacturing of fine or even of bulk chemicals (Panke *et al.*, 2004, Meyer, 2011, Santacoloma *et al.*, 2011). This development is driven by a strong societal emphasis on greener and environmentally benign manufacturing. Due to their exquisite selectivity and their preference for mild reaction conditions, biocatalysts can offer less side products, fewer processing steps, higher yields at each step, lower material and energy costs and less waste production (Bommarius and Riebel, 2004). Without the need for extreme temperatures, strong acids or bases and large amounts of organic solvents, the goals of sustainable development, green chemistry and environmentally friendly manufacturing are easier to achieve than with chemical processes (Bommarius and Riebel, 2004).

The growing demand for the synthesis of optically pure or increasingly complex molecules using enzymes on the one and the necessity for economic and competitive processes on the other hand calls for innovative strategies (Santacoloma *et al.*, 2011). As a result, next generation processes are sought for, such as novel reactor concepts and the coupling of multiple reactions in time and space (Vriezema *et al.*, 2005). Coupled multienzyme syntheses in one pot can shift an unfavorable equilibrium towards the desired product by linking consecutive reaction steps or by coupling one endergonic step with another exergonic auxiliary reaction (Faber, 2011). The immediate consumption of reaction intermediates is particularly beneficial if these intermediates are unstable or toxic. A further advantage is the elimination of successive separation and purification steps. This leads to a considerable process improvement, reducing downstream processing and associated costs (Santacoloma *et al.*, 2011).

Despite the generalization that most enzymes operate under similar conditions, this is not always entirely true in all respects. The activity and stability of enzymes is influenced for example by the buffer composition, the pH and the temperature, and each enzyme has its own preferences. Therefore, the combination of multiple enzymes in one pot usually requires a compromise between the different requirements, and incompatibilities can ensue and manifest in a less-than-optimal activity of some enzymes, inhibitory as well as inactivation effects and loss of stability. An innovative reactor design and/or immobilization on one or more supports can further assist in improving the process performance of multienzyme syntheses (Santacoloma *et al.*, 2011, Garcia-Urdiales *et al.*, 2012).

2 Motivation and objectives

Novel biotechnological processes can be designed by improving and rearranging existing biological systems and combining them with artificial components. Compartmentalization and selective mass transport represent two basic design principles of all living systems. Compartmentalization has several advantages in the context of cellular metabolism: toxic metabolites formed in one compartment are confined, subcompartments offer optimal reaction conditions for different enzymes, competition for substrates by different pathways is avoided and isoenzymes can be differentially regulated within each compartment (Schmitt *et al.*, 2016). Selective channel or transport proteins effectively regulate the exchanges of various substrates across the confines of different compartments while maintaining essential chemical gradients. These two principles allow for a tight control over the occurring reactions and facilitate the simultaneous procession of essentially incompatible reactions.

The generation of artificial reaction compartments based on the encapsulation of enzymes in the lumen of polymersomes approaches the problem of more efficient multienzyme syntheses from a synthetic biology perspective. In view of the often drastically reduced permeability of polymeric nanocompartments, the specific exchange of substrates and products across the nanoreactor boundary represents a major determinant for the success of future reactor systems. So far, most nanoreactor studies relied on the unspecific exchange of compounds across the membrane, mediated by chemical means to increase the permeability of the polymer shell (e.g. glassy polystyrene-based membranes or stimuli-responsive polymers) or by the incorporation of unspecific channel proteins into the membrane (Gaitzsch *et al.*, 2016, Schmitt *et al.*, 2016). Polymersomes composed of the amphiphilic block copolymer poly(2-methyloxazoline)-poly(dimethylsiloxane)-poly(2-methyloxazoline) (PMOXA-PDMS-PMOXA) display a low permeability compared to liposomes and allow the functional incorporation of different channel proteins (Nardin *et al.*, 2000b, Discher and Eisenberg, 2002, Nallani *et al.*, 2006, Kumar *et al.*, 2007), both important prerequisites for a controlled and selective mass transport. Early studies with β-lactamase-loaded PMOXA-PDMS-PMOXA polymersomes functionalized with the unspecific porin OmpF demonstrated that the functional reconstitution of channel proteins can be realized and improves the activity of mass-transfer-limited systems (Nardin *et al.*, 2000b). This is not self-evident, given that polymer membranes can be significantly thicker than natural lipid membranes. The difference between the thickness of the hydrophobic domains of the channel protein and the membrane is called hydrophobic mismatch. A large hydrophobic mismatch in combination with a low compressibility of the membrane is energetically unfavorable (Andersen and Koeppe, 2007). Nevertheless, a high degree of compressibility and polydispersity of the polymer chains serve to accommodate membrane proteins even in very thick polymer membranes (Pata and Dan, 2003, Srinivas *et al.*, 2005, Itel *et al.*, 2015). The number of membrane proteins which have been successfully incorporated into polymer membranes has risen in the past decade (Habel *et al.*, 2015), yet no more than 10 different channel proteins (not counting proton pumps or pore-forming peptides) have been utilized so far. Of these, none is particularly selective for small organic acids/anions or known to facilitate the

transport of hydrophobic molecules, substrate classes which are of great interest for a number of biocatalytical applications. Besides, only a fraction of the reports involving the reconstitution of channel proteins in polymer membranes contains quantitative information about the degree of functionalization, with most studies only indicating the initial protein:polymer ratio.

As a model system for the study of selective mass transport of chemically diverse substrates, i.e. anions and hydrophobic compounds, through different channel proteins, the asymmetric reduction of prochiral ketones within the lumen of $PMOXA_{15}$-$PDMS_{68}$-$PMOXA_{15}$-based nano-scale enzyme membrane reactors was chosen. The reduction should be catalyzed by the 3-ketoacyl-[acyl-carrier-protein]-reductase (KR) from the cyanobacterium *Synechococcus elongatus* PCC7942 with internal cofactor regeneration by an engineered formate dehydrogenase (FDH). The KR has proven its merit for the enantiopure synthesis of chiral building blocks, especially of certain halogenated compounds, such as ethyl-*(S)*-4-chloro-3-hydroxy-butyrate, ethyl-*(S)*-3-hydroxy-3-phenylpropionate and *(S)*-1-(2',3',4',5',6'-pentafluorophenyl)ethanol (*(S)*-PFE) (Hölsch *et al.*, 2008). Regeneration of the otherwise expensive cofactor nicotinamide adenine dinucleotide phosphate (NADPH) was to be accomplished by an $NADP^+$-accepting mutant of an FDH from *Mycobacterium vaccae* N10 (Hölsch *et al.*, 2013, Sührer *et al.*, 2014). Since it was reported that the encapsulation of proteins in polymersome can vary (Onaca *et al.*, 2006), a colocalization of both enzymes should be ensured by the use of an artificial fusion construct (Hölsch and Weuster-Botz, 2010, Sührer *et al.*, 2014). Encapsulation of the fusion enzyme and of the cofactor should be investigated and the results were to be implemented into the scalable production process for uniform polymersomes established by Poschenrieder *et al*. (2016).

The central objective of this thesis was to diversify the available toolbox of channel proteins for a selective mass transport of the hydrophobic KR substrate 2',3',4',5',6'-pentafluoroacetophenone (PFAP) and the corresponding alcohol as well as formate across the polymer membrane. Channel proteins for the functionalization of the nano-scale enzyme membrane reactors to be used in this study should be specific for these substrates, while retaining the encapsulated cofactor $NADP^+$. In order to be able to study the different channel proteins in polymer membranes, efficient strategies for the production of sufficient amounts of these proteins were to be devised. The reconstitution was then to be assessed in terms of influencing factors, efficiency and the maximal degree of functionalization (i.e. channels per polymersome as well as functionality per channel). The performance of the channels in terms of an enhanced activity of the nanoreactors was to be compared with the unfunctionalized system, and plain as well as membrane-functionalized nanoreactors should also be compared to the non-compartmentalized enzyme system and to whole cells. Since no membrane-specific permeability data for substrates of the reaction were available, it remained to be assessed which type of channel would have a greater impact on the activity of the nanoreactors, or whether a combination of both channel types would be beneficial. Besides, it should be investigated how the combination influences the relative reconstitution of both channels, another aspect not well-studied to date, with the only reported channel

pair being bacteriorhodopsin and an F_0F_1-ATPase (Choi and Montemagno, 2005). The envisioned configuration of an FDH-KR-loaded nano-scale enzyme membrane reactor functionalized with channel proteins specific for both anions and hydrophobic substrates is depicted in Figure 2-1.

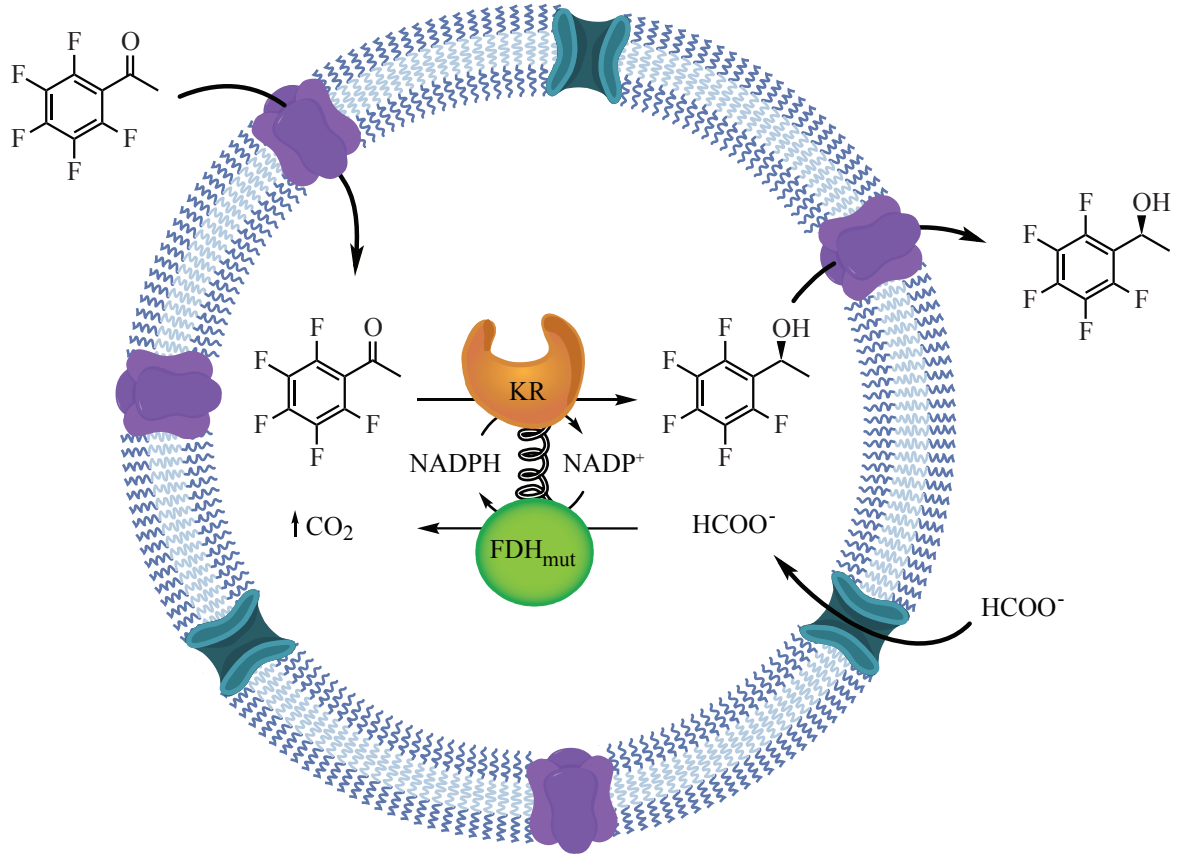

Figure 2-1. Schematic representation of the proposed nano-scale enzyme membrane reactor with an FDH-KR fusion enzyme in its lumen and channel proteins specific for formate or hydrophobic KR substrates reconstituted in its membrane. Upon entering the nanoreactor, the substrate 2',3',4',5',6'-pentafluoracetophenone is converted to *(S)*-1-(2',3',4',5',6'-pentafluorophenyl)ethanol by the KR under concomitant NADPH consumption, which is regenerated in the secondary FDH reaction by a mutant FDH accepting $NADP^+$ (FDH_{mut}).

In short, this thesis is divided into the following work packages:

- Identification of putative, selective channel proteins for the transport of formate or PFAP
- Establishment of suitable conditions for the preparative isolation and purification of channel proteins
- Establishment of an efficient production process for nano-scale enzyme membrane reactors loaded with the FDH-KR fusion enzyme and $NADP^+$
- Investigation of the reconstitution of channel proteins into nano-scale enzyme membrane reactors, either with a single channel protein species or with a combination of two different channel protein types

- Analysis of the membrane-specific permeability of formate and $NADP^+$ in the absence or presence of selected channel proteins
- Implementation of the synthesis of the chiral alcohol *(S)*-1-(2',3',4',5',6'-pentafluorophenyl)ethanol using plain or membrane-functionalized nano-scale enzyme membrane reactors
- Evaluation of the effect of different channel proteins on the activity of the nano-scale enzyme membrane reactors
- Comparison of the nano-scale enzyme membrane reactors with the free enzyme system and with whole cells

3 Theoretical background

3.1 Biocatalysis

Although not a new technology, biocatalysis has gained much importance during the past decades, fueled by the advances in biotechnology. The increasing demand for enantiopure building blocks in the pharmaceutical, cosmetics, food and fine chemical industry alongside with the recognition that biocatalytic processes can be greener and competitive even on an industrial scale have contributed to this development (Woodley, 2008, Meyer, 2011, Gröger and Asano, 2012). Chemical syntheses often require organic solvents, strong acids/bases, heavy metal catalysts and extreme temperatures as well as pressures (Liese *et al.*, 2000). In addition, especially the synthesis of complex compounds requires numerous process steps, including a number of protection and subsequent deprotection steps, causing a lot of (toxic) waste and increasing production costs. Enzymes on the other hand are completely biodegradable and can be produced from renewable resources (Woodley, 2008). They usually (but not necessarily always) operate in an aqueous environment, at moderate pH and at temperatures between 20 and 40 °C (Faber, 2011). Under these conditions, the occurrence of side reactions, such as decomposition, isomerization, racemization and rearrangement, is minimized (Faber, 2011). Because of the similar reaction conditions most enzymes require, sequential reactions are more easily combined in one batch. Such cascade reactions eliminate the need for the repeated purification of intermediates, thus increasing yields and reducing costs (Nestl *et al.*, 2014). The greatest advantage of enzyme-catalyzed reactions is that enzymes are highly chemo-, regio- and stereoselective. A higher selectivity also translates into fewer byproducts, which otherwise complicate the downstream processing and cause additional costs in chemical processes. Enzymes are even able to catalyze reactions which are hardly accessible by chemical means, such as the selective functionalization of complex aliphatic or aromatic compounds (Rozzell, 1999, Schmid *et al.*, 2001, Faber, 2011, Nestl *et al.*, 2014). The acceptance of non-natural substrates is an additional bonus which broadens the potential use of enzymes considerably (Bradshaw *et al.*, 1992, Gröger and Asano, 2012).

The greatest challenge for enzyme-based processes is the low volumetric productivity often encountered. Possible reasons include the low solubility of many substrates and products in aqueous media, substrate- or product inhibition or an insufficient stability of the enzyme (Goswami, 2011). Furthermore, many enzymes require cofactors such as adenosine triphosphate (ATP), nicotinamide adenine dinucleotides ($NAD(P)^+$ / NAD(P)H), flavin adenine dinucleotides (FAD / $FADH_2$) or flavin mononucleotides (FMN / $FMNH_2$), which are expensive in their own right and need to be recycled during the process (Faber, 2011). Depending on the expression yield and the required purity, which are responsible for most of the costs of the biocatalyst, its recycling might also be required to create an economically competitive process (Faber, 2011, DiCosimo *et al.*, 2013).

3.1.1 Enzyme classification

According to the International Union of Biochemistry and Molecular Biology (IUBMB, 1992a), enzymes are classified into six main classes, depending on the reaction they catalyze (*cf.* Table 3-1). The IUBMB classing system is reflected in the four-digit enzyme commission (EC) number. Within the main classes, subclasses exist, which correspond to the second and third digit and specify the reaction in greater detail. The last digit corresponds to a serial number. It is of note that due to the function-oriented approach of the IUBMB nomenclature system, the identifier is not unambiguous and entirely different enzymes might be assigned the same EC number. On the other hand, a single enzyme might also possess multiple EC numbers, if it catalyzes more than one reaction (IUBMB, 1992b). The system is demonstrated by taking the example of the 3-ketoacyl-[acyl-carrier-protein]-reductase (KR), EC number 1.1.1.100):

EC 1	Oxidoreductases
EC 1.1	Acting on the CH-OH group of donors
EC 1.1.1	With NAD^+ or $NADP^+$ as acceptor
EC 1.1.1.100	3-Ketoacyl-[acyl-carrier-protein] reductase

Table 3-1. Classification of enzymes according to the International Union of Biochemistry and Molecular Biology (IUBMB, 1992a, modified from Gröger and Asano, 2012).

EC Number	Enzyme class	Catalyzed reaction
1	Oxidoreductases	Reduction of C=O and C=C; reductive amination of C=O; oxidation of C-H, C=C, C-N, and C-O; cofactor reduction/oxidation
2	Transferases	Transfer of functional groups, such as amino, acyl, phosphoryl, methyl, glycosyl, nitro and sulfur-containing groups
3	Hydrolases	Hydrolysis of esters, amides, lactones, lactams, epoxides, nitriles, etc., as well as the reverse reactions
4	Lyases	Addition of small molecules to double bonds such as C=C, C=N and C=O
5	Isomerases	Transformation of isomers (isomerizations) such as racemizations, epimerizations and rearrangement reactions
6	Ligases	Formation or cleavage of C-O-, C-S-, C-N or C-C-bonds with concomitant ATP consumption

3.1.2 Asymmetric synthesis of chiral alcohols

Chiral alcohols constitute important building blocks for the synthesis of pharmaceuticals, agrochemicals, fragrances and flavors (Nakamura *et al.*, 2003, Daußmann *et al.*, 2006). One reason for this versatility is that the chiral hydroxyl group is easily converted to other chemical functionalities, such as chlorides (Lewis and Boozer, 1952), amines (Degerbeck *et al.*, 1992), azides (Fabiano *et al.*,

1987) and fluorides (Leroy *et al.*, 1979). The production of chiral alcohols can either be achieved by reduction of a prochiral ketone, by the kinetic resolution of the racemic alcohol or by chromatographic separation of the latter using chiral chromatography media. Ryōji Noyori developed a chemical process for the stereospecific hydrogenation of prochiral ketones using a chiral, ruthenium-based catalyst (Noyori and Ohkuma, 2001, Noyori *et al.*, 2001). Depending on the substrate, this Nobel-prize awarded process results in moderate to high enantiomeric purity and good yields (Etayo and Vidal-Ferran, 2013), but the metal catalyst, based on a very rare and expensive metal, is itself expensive and causes the production of a lot of toxic waste.

The enzymatic synthesis of chiral alcohols presents an attractive and environmentally friendly alternative to the chemical synthesis route and is now used at an industrial scale on numerous occasions (Liese *et al.*, 2000, Breuer *et al.*, 2004). Of the six enzyme classes introduced in chapter 3.1.1, hydrolases, lyases and oxidoreductases can be used to this end (Goldberg *et al.*, 2007). The enzymatic reduction of prochiral ketones by oxidoreductases, in particular alcohol dehydrogenases and more recently also ketoreductases, to yield the respective *(R)*- or *(S)*-alcohols with high purity have gained the greatest importance (Goldberg *et al.*, 2007, Goswami, 2011, Nestl *et al.*, 2014). These two enzyme subclasses are ubiquitous in bacteria, yeasts and fungi and well accessible by biotechnological means (Goswami, 2011). Both require a supply of reduction equivalents in the form of NAD(P)H, which functions as donor for the transfer of a hydride ion to the carbonyl group of the substrate (Nakamura *et al.*, 2003, Kroutil *et al.*, 2004). Different enzymes have differing preferences for either NADH or NADPH, but they also differ with respect to the stereochemistry of the hydride transfer. The possible transfer reactions are depicted in Figure 3-1. The sp^2-hybridized, planar prochiral ketone can be attacked from either the re- or the si-face, resulting in a sp^3-hybridized, asymmetrically substituted alcohol. Most oxidoreductases catalyze an attack from the re-face, thus producing the *(S)*-alcohol (Bradshaw *et al.*, 1992, Nakamura *et al.*, 2003). Far fewer enzymes, such as the alcohol dehydrogenase of *Lactobacillus brevis*, catalyze an attack from the si-face and the production of the *(R)*-alcohol (Hummel, 1997). The stereoselectivity of this reaction is often remarkable, and even substrates such as ethylpropylketone can be reduced with a high enantiomeric excess (*ee*, *cf.* Equation 3-1), while the similar size of both substituents results in a low selectivity by chemical reduction (Nakamura *et al.*, 2003).

$$ee = \frac{|n_R - n_S|}{n_R + n_S} \cdot 100\% \qquad \text{Equation 3-1}$$

With n_R Amount of *(R)*-enantiomer, mol

n_S Amount of *(S)*-enantiomer, mol

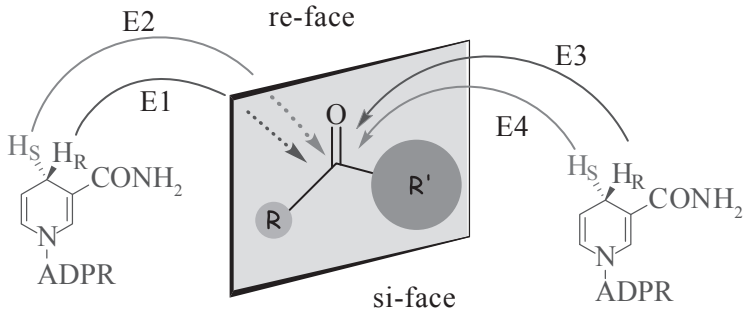

Figure 3-1. Stereochemistry of the hydride transfer from NADPH to the carbonyl carbon of the substrate. Only the nicotinamide moiety is drawn, the phosphorylated adenosine ribose is abbreviated by ADPR. Different enzymes (E1-E4) catalyze different transfer reactions (modified from Nakamura *et al.*, 2003).

A versatile enzyme for the synthesis of chiral alcohols is the 3-ketoacyl-[acyl-carrier-protein]-reductase (KR) from the freshwater cyanobacterium *Synechococcus elongatus* PCC7942. The KR belongs to the short chain dehydrogenase/reductase superfamily and originates from the anabolic fatty acid synthesis pathway. It is part of the multifunctional fatty acid synthase (FAS) II complex, which is found in plants and most bacteria. Within this complex, the KR catalyzes the reduction of 3-keto-acids, activated by their conjugation to the acyl carrier protein (ACP), to the corresponding *(R)*-3-hydroxyacyl-ACP (*cf.* Figure 3-2) (Ren *et al.*, 2000, Wright, 2004, White *et al.*, 2005).

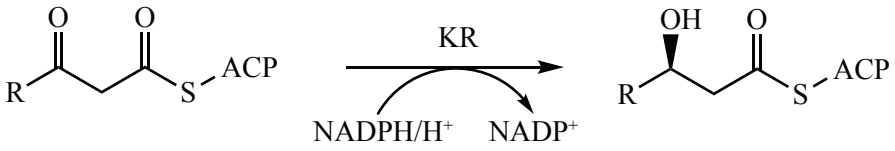

Figure 3-2. KR-catalyzed reduction of a 3-keto-acid conjugated to the acyl carrier protein (ACP).

The KR from *Synechococcus elongatus* PCC7942 was first isolated and described by Havel (2006). It was described as a potentially membrane-associated protein with a *Grand Average of Hydropathicity* (GRAVY) score (Kyte and Doolittle, 1982) of +0.457, which is exceptionally high for a non-membrane protein. Accordingly, it could only be expressed and purified in soluble form after fusion to the solubility-enhancing maltose-binding protein. The 25 kDa enzyme is usually present as a homotetramer (or rather a dimer of dimers, *cf.* Figure 3-3), which dissociates into active dimers upon purification by size exclusion chromatography (SEC) and only slowly reassociates. The specific activity of the dimers was found to be at least 79 % of that of the tetramer (Hölsch *et al.*, 2008, Hölsch, 2009). As a member of the oxidoreductases and because it is involved in an anabolic pathway, the KR requires NADPH as a cofactor (Hölsch *et al.*, 2008).

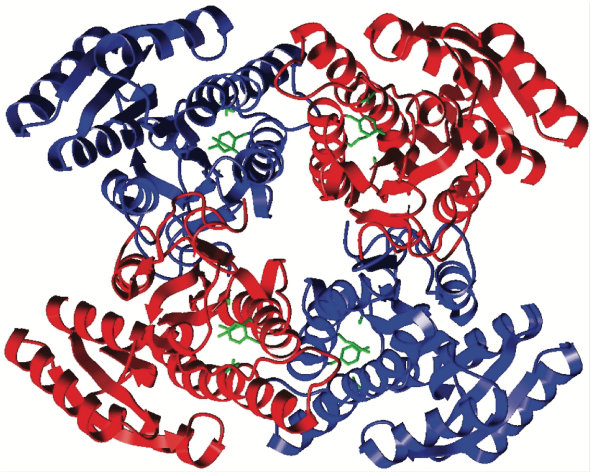

Figure 3-3. Modelled quaternary structure of the KR from *Synechococcus elongatus* PCC7942 with active site residues highlighted in green (from Hölsch, 2009).

As non-natural substrates, the KR accepts mono- and multihalogenated ketones, which are reduced to the respective *(S)*-alcohols with good to excellent enantiomeric excess. 2',3',4',5',6'-Pentafluoracetophenone was reduced to *(S)*-1-(2',3',4',5',6'-pentafluorophenyl)ethanol (*cf.* Figure 3-4) with an enantiomeric excess of >99.8 % at a maximal rate of 3.93 U mg^{-1} (at 30 °C and pH 7; Hölsch *et al.*, 2008). The catalytic mechanism of the two-substrate reaction was determined to be a steady-state *ordered bi-bi* mechanism, with NADPH binding occurring before binding of the ketone (Hölsch and Weuster-Botz, 2011).

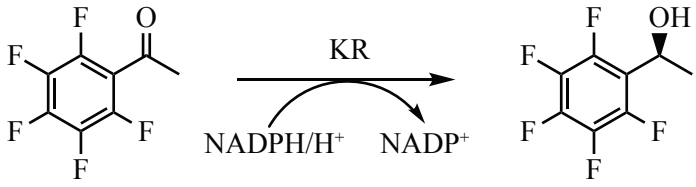

Figure 3-4. KR-catalyzed reduction of 2',3',4',5',6'-pentafluoracetophenone to *(S)*-1-(2',3',4',5',6'-pentafluorophenyl)ethanol.

3.1.3 Cofactor recycling

Compared to other production methods, the synthesis of chiral alcohols from prochiral ketones by oxidoreductases features higher yields from a variety of substrates. The downside is the strict requirement for expensive cofactors, usually NADH or NADPH. Due to the high costs, a stoichiometric addition of these cofactors is not feasible (Seelbach *et al.*, 1996, Goldberg *et al.*, 2007). Therefore, *in situ* cofactor regeneration is a necessity, allowing for a catalytic rather than stoichiometric cofactor addition. Apart from cofactor regeneration by the endogenous metabolism of whole cell biocatalysts, various chemical, photochemical and enzymatic approaches have been developed to work with isolated

enzymes (Chenault and Whitesides, 1987, Seelbach *et al.*, 1996, van der Donk and Zhao, 2003). A simple enzymatic approach is the substrate-coupled cofactor regeneration, where the cofactor is consumed and regenerated by the same enzyme (Hummel and Kula, 1989). This approach has been used successfully in conjunction with alcohol dehydrogenases from horse liver and from the bacterium *Lactobacillus brevis* (Schubert *et al.*, 2002). Inexpensive cosubstrates such as ethanol or isopropanol can be used (Schubert *et al.*, 2001), which are oxidized to acetaldehyde or acetone, respectively (*cf.* Figure 3-5). A drawback of dehydrogenase-catalyzed reactions is that the equilibrium often lies on the side of the reduced product (Faber, 2011), so the cosubstrate needs to be added in great excess to overcome thermodynamic limitations. High cosubstrate or coproduct concentrations can, however, have an impact on the enzyme activity (van der Donk and Zhao, 2003).

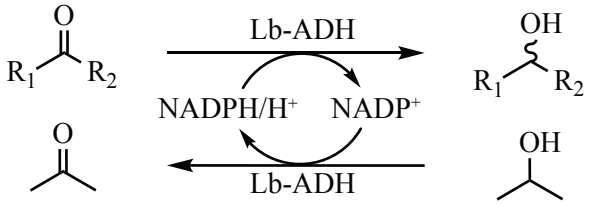

Figure 3-5. Substrate-coupled NADPH regeneration using the alcohol dehydrogenase from *Lactobacillus brevis* (Lb-ADH).

Most cofactor regeneration systems are based on an additional enzyme catalyzing the cofactor regeneration (enzyme-coupled approach) (Hummel and Kula, 1989, Goldberg *et al.*, 2007). The second enzyme is often a dehydrogenase, such as a formate dehydrogenase (FDH) (*cf.* Figure 3-6), a phosphite dehydrogenase or a glucose/glucose-6-phosphate dehydrogenase (GDH/G6PDH), requiring formate, phosphite or glucose/glucose-6-phosphate as cosubstrates (van der Donk and Zhao, 2003). These systems are attractive because they feature low-cost substrates and nearly irreversible reactions, resulting in a strong thermodynamic driving force for the ketone reduction. This is because the coproducts are either volatile (CO_2) or subsequently hydrolyze to the corresponding acids (from gluconolactone/6-phosphogluconolactone to gluconic acid/6-phosphogluconic acid) (van der Donk and Zhao, 2003, Goldberg *et al.*, 2007). The latter reaction causes an acidification of the medium, which is not always well-tolerated. On the other hand, most formate dehydrogenases originate from catabolic pathways and favor NAD^+/NADH over $NADP^+$/NADPH (Popov and Lamzin, 1994), while most enzymes used for the asymmetric synthesis of chiral alcohols require NADPH (Chenault and Whitesides, 1987, Kataoka *et al.*, 2003, van der Donk and Zhao, 2003), which can be generated by the GDH/G6PDH system (Goldberg *et al.*, 2007). To overcome the low activity towards $NADP^+$/NADPH displayed by most FDHs, efforts have been made to alter the cofactor specificity of FDHs by protein engineering.

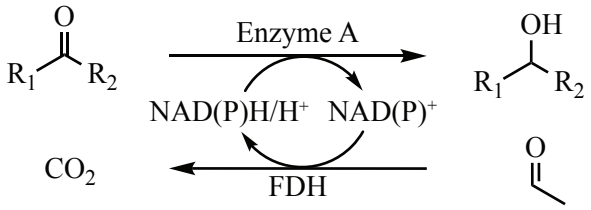

Figure 3-6. Enzyme coupled NAD(P)H regeneration using a formate dehydrogenase (FDH). Note that most FDHs have a high preference for NAD^+/NADH over $NADP^+$/NADPH.

In this thesis, an engineered variant of the FDH of *M. vaccae* N10 (EC 1.2.1.2) was used. The 44 kDa FDH exhibits a comparatively high specific activity of 10 U mg^{-1} (Tishkov and Popov, 2004). Like most formate dehydrogenases, which are found ubiquitously in plants, fungi, yeasts and bacteria, this enzyme forms an active dimer and follows a rapid equilibrium random *bi-bi* mechanism employing no metal ions and a limited number of conserved residues for catalysis (Tishkov *et al.*, 1989, Lamzin *et al.*, 1994, Popov and Lamzin, 1994). The hydride transfer is facilitated by a polarization of the substrates (Tishkov *et al.*, 1993, Popov and Lamzin, 1994). Cofactor discrimination is primarily mediated by an aspartate at position 221, which interacts with the adenosine ribose moiety of NAD^+ and repels the negatively charged phosphate group of $NADP^+$ (Carugo and Argos, 1997). An exchange to glutamine resulted in a more than 100-fold lower half-saturation constant (K_M) for $NADP^+$ (0.39 vs. >40 mM; Hölsch *et al.*, 2013). Additional mutations of two cysteines (C145S/C225V) had a synergistic effect on the catalytic activity, leading to a specific activity of the C145S/D221Q/C225V mutant with $NADP^+$ which was comparable to the wild type with NAD^+ (Hölsch *et al.*, 2013). Furthermore, the mutant was also more tolerant towards the presence of α-haloketones (Hölsch *et al.*, 2013), since the low operational stability of many FDHs results from the chemical oxidation or modification of solvent-accessible cysteines (Tishkov and Popov, 2006).

The fusion of two enzymes, one for synthesis and one for cofactor regeneration, combines elements of the two aforementioned approaches and represents a third approach to the cofactor regeneration problem. Typically, fusion enzymes are created by connecting both enzymes through a short linker sequence. This strategy mimics naturally occurring enzyme complexes with multiple catalytically active domains on a single polypeptide, such as the fatty acid synthase complex I of animals and fungi. The close proximity of the domains is thought to increase the selectivity and the productivity of the reaction (Conrado *et al.*, 2008). A bifunctional fusion enzyme for the asymmetric reduction of prochiral ketones with internal cofactor regeneration based on the *Synechococcus elongatus* PCC7942 KR and the *M. vaccae* FDH, connected by a short serine-glycine linker, was created by Hölsch and Weuster-Botz (2010). While the KR activity was independent of the particular connectivity, the FDH was only active at the N-terminal end of the fusion enzyme (Hölsch and Weuster-Botz, 2010). The FDH-SG-KR fusion enzyme was still to be improved, because it was shown to be prone to proteolytic degradation, mediated

by amino acids at the C-terminus of the FDH. Mutation of K395, F396, K397 and K398 resulted in a stabilized fusion protein. The *7M* mutant combining the K395G/F396S/K397S/K398S with the additional C145S/D221Q/C225V mutations displayed an improved chemical stability but only 70 % of the activity of the unstabilized enzyme and a moderately increased K_M (0.44 vs. 0.39 mM). Despite a lower performance of the FDH part, this fusion enzyme could outcompete the corresponding free enzyme system, probably due to a locally enhanced substrate concentration and an improved K_M of the KR towards its substrate ethyl benzoyl acetate (Sührer *et al.*, 2014, Sührer, 2015).

3.1.4 Enzyme kinetics

The classical approach to the analysis of enzyme kinetics is based on the work of Michaelis and Menten (1913) on invertase and describing the simplest form of an enzyme-catalyzed reaction, an irreversible conversion of one substrate to one product (*cf*. Figure 3-7).

$$S + E \underset{k_{-1}}{\overset{k_1}{\rightleftharpoons}} ES \xrightarrow{k_2} E + P$$

Figure 3-7. Schematic representation of an irreversible reaction where one substrate S is converted to one product P. The substrate binds the enzyme E, forming an enzyme-substrate complex ES. The enzyme-substrate complex may then undergo reversible dissociation or the substrate may be transformed into the product, which then desorbs from the enzyme. k_1, k_{-1} *and* k_2 denote the rate constants for each step.

The known form of the Michaelis-Menten equation (Equation 3-2) was derived by Briggs and Haldane (1925) under the following assumptions:

- One substrate molecule (S) binds one enzyme molecule (E), forming the activated enzyme-substrate complex (ES).
- The ES complex is in a steady-state equilibrium, $\frac{d[ES]}{dt} = 0$.
- The reaction proceeds far from thermodynamic equilibrium so that a possible reverse reaction of the last step can be neglected. For reversible reactions, this condition is satisfied when measuring initial reaction rates where $[P] \cong 0$.

$$v = v_{max} \cdot \frac{[S]}{K_M + [S]} \qquad \text{Equation 3-2}$$

With

v	Reaction rate, U mg^{-1}
v_{max}	Maximal reaction rate, U mg^{-1}
[S]	Substrate concentration, mol L^{-1}
K_M	Half-saturation constant, mol L^{-1}

The half-saturation constant K_M derives from the rate constants for each step and denotes the substrate concentration where the activity is half-maximal (Equation 3-3)

$$K_M = \frac{k_2 + k_{-1}}{k_1}$$ Equation 3-3

The maximal reaction rate v_{max} is dependent on the catalytic constant k_{cat}, which denotes the catalytic turnover of one substrate by one active site per second, and the molecular mass (MM) of one active monomeric unit of the enzyme (Equation 3-4).

$$v_{max} = \frac{k_{cat}}{M_E}$$ Equation 3-4

With k_{cat} Catalytic constant, s^{-1}

MM_E Molecular mass of the enzyme, g mol^{-1}

Enzyme kinetics are usually determined by measuring initial reaction rates. The Michaelis-Menten model is only valid for irreversible one-substrate reactions. In reality, this is rarely the case, since usually more than one substrate is involved in the majority of enzymatic reactions. This greatly complicates the mathematical description of the reaction. As a consequence, only one of the substrates is varied, while the other substrates are kept in excess (usually $10 \cdot K_M$). With this constraint, the enzyme activity with respect to the other substrate can be determined using classical Michaelis-Menten kinetics (Bisswanger, 2000). Kinetic parameters are usually determined by non-linear regression. Because the concentration of free substrate $[S]$ is not readily accessible, the initial substrate concentration $[S]_0 = [S] + [ES]$ is commonly used in enzymological studies instead. This simplification is legitimate if the amount of enzyme-bound substrate $[ES]$ can be neglected, which is true if $[E]_0 \ll [S]$ (Bisswanger, 2000).

Both enzymes employed in this thesis catalyze two-substrate/two-product reactions, which are called *bi-bi* reactions.

$$A+B \xrightleftharpoons{E} P+Q$$

Figure 3-8. Schematic representation of a reaction where the two substrates A and B are converted to the two products P and Q.

Binding of the substrates and desorption of the products can either occur in an ordered fashion, resulting in an ordered *bi-bi* mechanism, or randomly, resulting in a random *bi-bi* mechanism. A mechanism where the first product is released before the second substrate binds is called a *ping-pong* mechanism (Bisswanger, 2000).

3.1.5 Enzyme stability

Non-physiological pH, high temperatures, but also chemicals can cause inactivation of the enzyme by denaturation (Bisswanger, 2000). Under constant conditions, the inactivation can be expressed as a first-order decay function of the enzyme activity according to Equation 3-5.

$$v = v_0 \cdot e^{-(k_{inact} \cdot t)} \qquad \text{Equation 3-5}$$

With

v	Reaction rate, U mg^{-1}
v_0	Initial reaction rate at $t = 0$, U mg^{-1}
k_{inact}	Inactivation constant, h^{-1}
t	Time, h

The half-life $\tau_{1/2}$ of an enzyme denotes the time required for the initial enzyme activity to be reduced by a factor of 2 and is thus a useful indicator of the enzyme stability under the chosen process conditions. The half-life $\tau_{1/2}$ can be obtained from the inactivation constant k_{inact} using Equation 3-6.

$$\tau_{1/2} = \frac{ln\ 2}{k_{inact}} \qquad \text{Equation 3-6}$$

3.2 Polymersomes

The term polymersome was coined when Discher *et al.* (1999) described the preparation of liposome-like vesicles from amphiphilic block copolymers. Like liposomes, these self-assembled structures are essentially hollow spherical particles with an aqueous core separated from the outer medium by a membrane. As such, polymersomes can entrap hydrophilic molecules in their lumen, while hydrophobic molecules can be incorporated into the membrane (Palivan *et al.*, 2012). The versatility of the polymersome concept lies in the fact that the membrane properties depend on the composition and the structure of the amphiphilic copolymer used and can consequently be manipulated to meet the needs of the particular application (Soo and Eisenberg, 2004). In particular, the thickness of the membrane is an important determinant of many of the polymersomes' characteristics. In contrast to lipid membranes, which have a fairly uniform thickness of 3-5 nm (Le Meins *et al.*, 2011), the thickness of a polymer membrane can be tuned by changing the block length of the copolymer, and membranes ranging from 2.4-40 nm have been reported (Battaglia and Ryan, 2005, Chen *et al.*, 2009b). It has been established both theoretically (Srinivas *et al.*, 2004) as well as experimentally (Bermudez *et al.*, 2002) that the membrane thickness depends on the molecular mass of the polymer. With increasing molecular mass, the fluidity (Lee *et al.*, 2002) and the permeability (Bermudez *et al.*, 2004) of the membrane decreases, while its stability increases (Bermudez *et al.*, 2002), as illustrated in Figure 3-9. An increased stability of the membrane was for example demonstrated by a higher resistance of poly(butadiene)-poly(ethylene glycol) (PB-PEG) vesicles to lysis by the non-ionic detergent Triton X-100 with increasing membrane

thickness (Pata *et al.*, 2004). Due to the low solubility of the hydrophobic block of the polymer in water, the critical aggregation concentration (CAC) of amphiphilic polymers employed in polymersomes is usually also very low and decreases with increasing molecular mass of the polymer, making the supramolecular assembly, i.e. the polymersome, stable even at high dilutions (Discher and Ahmed, 2006). After their preparation, chemical cross-linking can be employed to further enhance the stability of the polymersomes, either by cross-linking the hydrophobic (Discher and Eisenberg, 2002) or the hydrophilic part (Nardin *et al.*, 2000a) of the polymer or by creating an interpenetrating network (Li *et al.*, 2007).

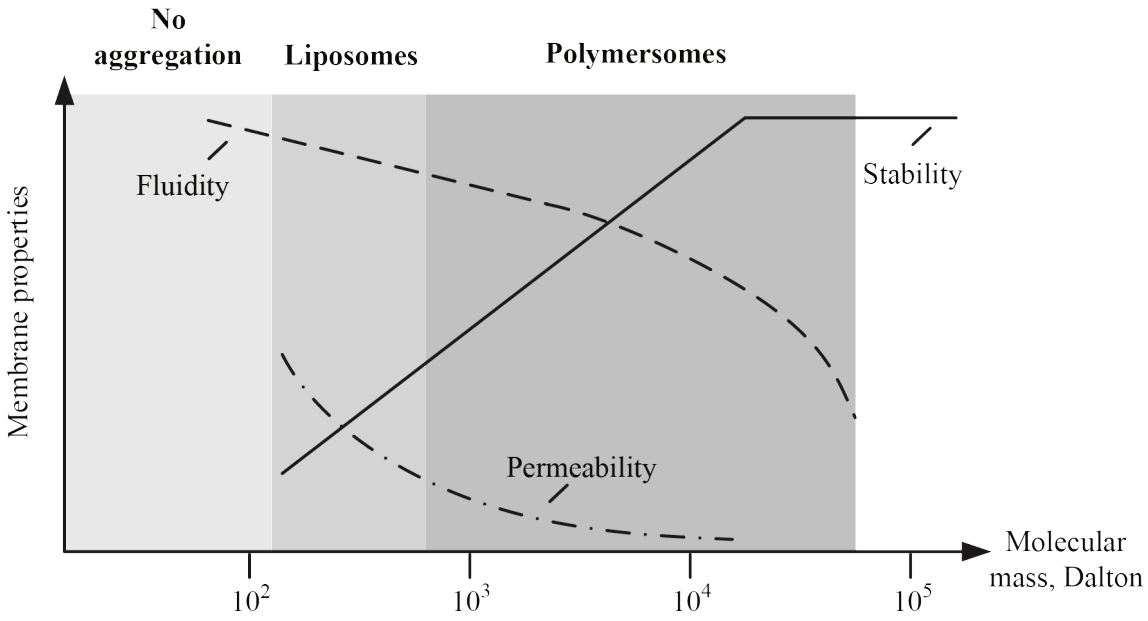

Figure 3-9. Fluidity, stability and permeability of membranes as a function of the molecular mass of the constituent amphiphilic molecule. With increasing molecular mass of the amphiphilic molecule, the stability of the membrane increases, while the fluidity and the permeability decrease (modified from Discher and Eisenberg, 2002).

The techniques described for polymersome formation are essentially the same ones used for liposome formation, although polymersomes can also be formed during the polymerization of the monomers (extensively reviewed by Gaitzsch *et al.*, 2016). Solvent-free techniques include the direct dispersion of the solid polymer in an aqueous solution (Ahmed and Discher, 2004), film rehydration (Ranquin *et al.*, 2005, Battaglia *et al.*, 2006) and electroformation (Angelova *et al.*, 1992, Discher *et al.*, 1999). Solvent-mediated techniques include the injection of a polymer dissolved in a non-selective solvent, such as ethanol, chloroform or tetrahydrofuran, into an aqueous environment as well as microemulsion/microfluidic techniques (Brown *et al.*, 2010, Marguet *et al.*, 2012). Most of these techniques require an energy input by shaking, stirring or sonication (Farquhar *et al.*, 1996). The characteristics of the particle size distribution are greatly affected by the formation process, with diameters ranging from 100 nm to 10 µm, although micrometer-sized, giant polymersomes are only

obtained by electroformation or microfluidic techniques (LoPresti *et al.*, 2009). The other techniques generally lead to smaller particles, often with rather broad particle size distributions. To reduce the polydispersity of the resulting polymersome suspensions, post-processing steps are often necessary (Kita-Tokarczyk *et al.*, 2005). Apart from the classical sonication (Kita-Tokarczyk *et al.*, 2005) or repeated freeze-thaw cycles (Napoli *et al.*, 2004a, Rank *et al.*, 2009), extrusion is often the method of choice to yield uniform polymersome dispersions (Nardin *et al.*, 2000a, Nardin *et al.*, 2001, Ranquin *et al.*, 2005).

A one-step, solvent-mediated process for the production of uniform PMOXA-PDMS-PMOXA polymersomes was introduced by Poschenrieder *et al.* (2016). The scalable process involves the injection of the polymer into a standard bioreactor under vigorous stirring and results in high-quality polymersomes after one hour, obviating the need for post-processing steps and greatly facilitating the preparation of polymersomes on a larger scale (Poschenrieder *et al.*, 2016, Poschenrieder *et al.*, 2017).

3.2.1 Amphiphilic block copolymers

Copolymers are polymers composed of two or more different monomer units, which can be arranged alternating (ABABAB), statistical (ABBAAB) or in blocks (AAABBB). The latter polymers are called block copolymers, and only these can form amphiphilic superstructures if a hydrophilic and a hydrophobic polymer block are joined.

The self-assembly of amphiphilic block copolymers in an aqueous environment is a result of the low solubility of the hydrophobic block in water, which is a selective solvent for the hydrophilic block only, and thus of the low CAC of the polymer. In order to minimize the contact area between the hydrophobic regions of the polymer and the selective solvent, polymer strands aggregate and form higher-order structures. Which structures are formed basically depends on the molecular shape of the polymer, which can be a cylinder, a wedge or a cone, expressed as the hydrophilic fraction *f*. Vesicles are formed if the hydrophilic fraction is 25-40 %, while worm micelles are formed at hydrophilic fractions of 40-50 %. If *f* becomes even higher, only spherical micelles can be formed (Discher and Ahmed, 2006). Once formed, polymersomes are characterized by a low rate of molecular interchange between aggregates and are thus nonergodic, which distinguishes them from liposomes and micelles (Gaitzsch *et al.*, 2016).

By varying the polymer chemistry (i.e. the nature, length and sequence of the blocks as well as possible modifications), the properties of the copolymer can be finely tuned (Schrage, 2002). For one, the membrane can be composed of di- or triblock copolymers, which can adopt different conformations, as depicted in Figure 3-10. Diblock copolymers are similar to lipids since they also form bilayers. These bilayers may or may not be interdigitated, which becomes more likely the higher the molecular mass of the polymer becomes (Battaglia and Ryan, 2005, Discher and Ahmed, 2006). Triblock copolymers may either adopt a hairpin conformation, which also leads to a bilayer structure, or a linear conformation,

which then leads to a monolayer. ABA triblock copolymers coexist in both conformations, although the current opinion is that the hairpin conformation is thermodynamically favored (Wang *et al.*, 1992, Nguyen-Misra *et al.*, 1996, Srinivas *et al.*, 2005, Itel *et al.*, 2014).

The plethora of available polymers has led to the development of responsive polymersomes, which respond to stimuli such as pH (Giacomelli *et al.*, 2007, Lomas *et al.*, 2011), temperature (Qin *et al.*, 2006, Zhou *et al.*, 2007), light (Liu *et al.*, 2014) or the presence of chemical triggers (Kim *et al.*, 2009, Kim *et al.*, 2012). The unifying theme in these polymersomes is that the hydrophobic block of the polymer contains certain chemical groups which can alter the hydrophobicity of the block, such as boronic acid (Kim *et al.*, 2009) or tertiary amines (Lomas *et al.*, 2008, Gaitzsch *et al.*, 2011, Yassin *et al.*, 2012). At basic or acidic pH, respectively, these become charged, resulting in a completely hydrophilic polymer and ultimately in polymersome disassembly.

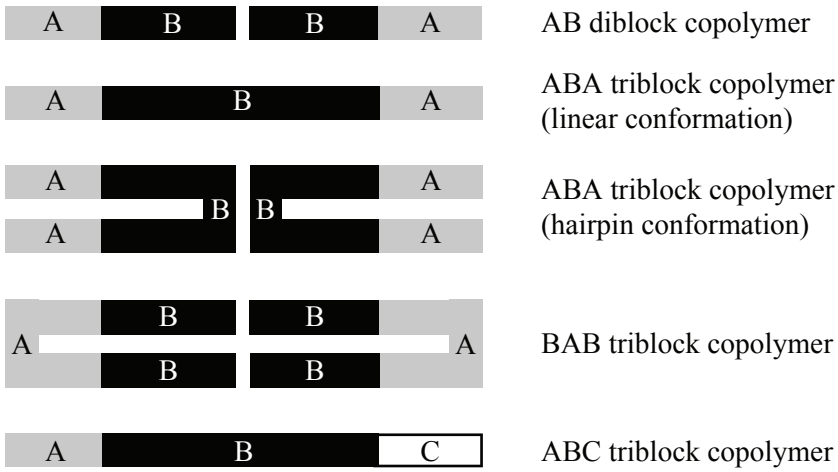

Figure 3-10. Structures of membranes composed of diblock and triblock copolymers. While diblock copolymers form bilayers similar to lipid membranes, triblock copolymers can adopt two conformations and thus form either bilayers or monolayers. In ABA triblock copolymers, both conformations can coexist, although the hairpin conformation is thermodynamically favored (adapted from Klermund, 2017).

Amphiphilic block copolymers composed of PMOXA-PDMS-PMOXA are of particular importance for biotechnological applications. The hydrophobic PDMS block is a chemically inert silicone with a high biocompatibility (Yilgor *et al.*, 1989) and practically insoluble in water (Desai and Hubbell, 1991). A very low glass transition temperature of -123 °C and a high flexibility of the polymer chain result in a high fluidity of the membrane (Prinos and Panayiotou, 1995), making this soft polymer ideally suited for the incorporation of membrane proteins. In fact, PDMS, in conjunction with the hydrophilic PMOXA block, was used repeatedly and nearly exclusively for the reconstitution of transmembrane proteins (Tanner *et al.*, 2011a, Gunkel-Grabole *et al.*, 2015), although the use of some other polymers, such as poly(butadiene)-poly(ethylene oxide) (PB-PEO), is reported (for an overview, see Habel *et al.*, 2015).

On the other side, the hydrophilic PMOXA blocks also have favorable properties. Due to their slightly basic character they are highly water-soluble. Most important for biotechnological applications is their low toxicity and their low protein binding capacity (Desai and Hubbell, 1991, Woodle *et al.*, 1994, Broz *et al.*, 2005). In this thesis, an amphiphilic ABA triblock copolymer with 68 central PDMS units and 15 PMOXA units on each side (depicted in Figure 3-11) was used.

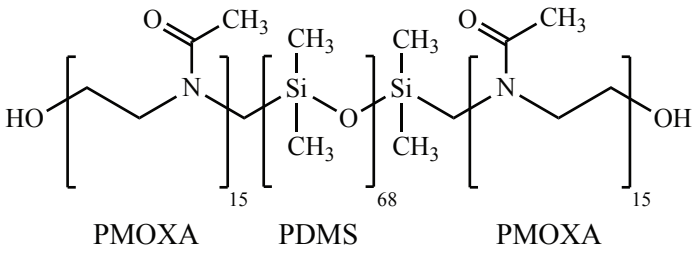

Figure 3-11. Structure of the amphiphilic triblock copolymer poly(2-methyloxazoline)-poly(dimethylsiloxane)-poly(2-methyloxazoline) ($PMOXA_{15}$-$PDMS_{68}$-$PMOXA_{15}$) used in this thesis.

3.2.2 Applications

As a consequence of the high degree of control that can be exerted on the membrane properties by simply changing the polymer chemistry and because of the high biological, chemical and physical stability, polymersomes show great promise for various applications, mainly in the fields of medicine and biotechnology (Discher and Eisenberg, 2002, Discher and Ahmed, 2006, Palivan *et al.*, 2016).

Polymersomes can be used for drug delivery, which represents a more targeted approach than the systemic application of drugs. Since the cargo, which can be small molecules or even proteins/enzymes, is only released at the intended site of action upon degradation of the polymer, fewer side effects are expected (Ahmed *et al.*, 2006, Broz *et al.*, 2006, Discher and Ahmed, 2006, Christian *et al.*, 2009, Kim and Lee, 2010). Despite the improved stability and retention of the cargo compared to liposomes, this approach still suffers from drawbacks such as an uncontrolled release or degradation at the wrong site (Baumann *et al.*, 2011). A functionalization of the polymersomes with tissue-specific targeting signals significantly improves the selectivity of the approach (see e.g. Pangburn *et al.*, 2012, Lu *et al.*, 2015) and also extends the range of possible targets beyond mere tumor tissues (see e.g. Broz *et al.*, 2005, Ben-Haim *et al.*, 2008). Release of the cargo can be achieved by altering the membrane permeability or by disassembly of the polymersomes upon internalization. The most commonly employed strategy for an intracellular release relies on the acidification of endosomes after internalization of the polymersomes (LoPresti *et al.*, 2009), making pH-responsive polymersomes well-suited to the task (Akinc and Battaglia, 2013, Canton *et al.*, 2013). Upon a pH change, the hydrophobic part of pH-sensitive polymers becomes hydrophilic, which is then no longer able to form polymersomes, leading to disassembly (Lomas *et al.*, 2008, De Oliveira *et al.*, 2012, Pawar *et al.*, 2013, Messager *et al.*, 2014). Other triggers

might be a change in temperature (Zhou *et al.*, 2007) or an oxidative environment, such as is found at the site of an inflammation or within endolysosomes (Napoli *et al.*, 2004a, Napoli *et al.*, 2004b).

A release of the cargo is not always desirable, especially if enzymes are delivered as a form of prodrug therapy. Baumann *et al.* (2014) reported on the successful intracellular production of reactive oxygen species upon irradiation of internalized polymersomes containing a photosensitizing enzyme. A further development of the concept of internalized entrapped enzymes are artificial organelles. In 2008, a primitive artificial peroxisome composed of $PMOXA_{15}$-$PDMS_{110}$-$PMOXA_{15}$ polymersomes containing Cu,Zn-superoxide dismutase was described (Axthelm *et al.*, 2008). Some years later, a more elaborate model of an artificial peroxisome was created using a cascade reaction of xanthine-oxidase, Cu,Zn-superoxide dismutase and lactoperoxidase contained within $PMOXA_{12}$-$PDMS_{55}$-$PMOXA_{12}$ polymersomes whose membrane had been permeabilized by means of reconstituted OmpF channels. These were shown to detoxify superoxide and H_2O_2 after endosomal escape and protect cells from oxidative stress (Tanner *et al.*, 2011b, Tanner *et al.*, 2013). Entrapped enzymes can also be used for diagnostic purposes to act as biosensors for a number of applications (Lecommandoux *et al.*, 2005, Ghoroghchian *et al.*, 2007, Gonzalez-Perez *et al.*, 2009, Grzelakowski *et al.*, 2009, Morton *et al.*, 2015, Zhang *et al.*, 2016).

The activity of enzymes encapsulated within polymersomes can be leveraged to create enzyme membrane nanoreactors for organic syntheses, thereby protecting them from adverse external conditions, proteolytic degradation or inhibition (Spulber *et al.*, 2014). These systems can be quite simple, but more elaborate multicompartment nanoreactors have also been realized, combining nature's principles of compartmentalization and selective mass transport. Enzyme membrane nanoreactors created from polystyrene-poly(isocyanoalanine(2-thiophene-3-yl-ethyl)amide) PS-PIAT are characterized by a semi-porous membrane and were used for model-type multienzyme syntheses. One example for a three-enzyme cascade reaction involved encapsulated glucose oxidase (GOx), membrane-integral *Candida Antarctica* lipase B (CalB) and horseradish peroxidase (HRP) anchored to the outside of the membrane. In this example, glucose acetate was converted to glucose by the CalB, which was then further oxidized to gluconolactone by the GOx. The H_2O_2 produced in this reaction was finally used by the HRP to oxidize a chromogenic substrate (van Dongen *et al.*, 2009). Meeuwissen *et al*. (2011) implemented a cofactor regeneration system where a phenylacetone monooxygenase (PAMO) was contained within PS-PIAT polymersomes, while the cofactor NADPH was recycled either by a fused phosphite dehydrogenase or by an external glucose-6-phosphate dehydrogenase. It is of note that although the cofactor was able to cross the polymer membrane, the reaction rates were reduced, particularly for the spatially separated enzyme system, which was 200-fold slower compared to both enzymes in solution. Multicompartment enzyme membrane nanoreactors were also created based on PS-PIAT polymersomes. In one recent example, three different types of small PS-PIAT polymersomes, each containing one enzyme, either PAMO, CalB/alcalase or an alcohol dehydrogenase (ADH), were

combined in larger PB-PEO polymersomes to convert a profluorescent substrate to the fluorescent dye resorufin. In this case, cofactor regeneration was successful even across different compartments, with the compartmentalized reaction only slightly slower than the uncompartmentalized one. In an attempt to implement selective mass transfer within multicompartmentalized enzyme membrane nanoreactors, Siti *et al.* (2014) encapsulated $PMOXA_{12}$-$PDMS_{55}$-$PMOXA_{12}$ polymersomes containing HRP together with GOx into semi-porous PS-PIAT polymersomes. The membrane of the PMOXA-PDMS-PMOXA polymersomes was functionalized with the channel protein OmpF, thus facilitating the influx of the substrate amplex red and the release of the fluorescent product resorufin (*cf.* Figure 3-12).

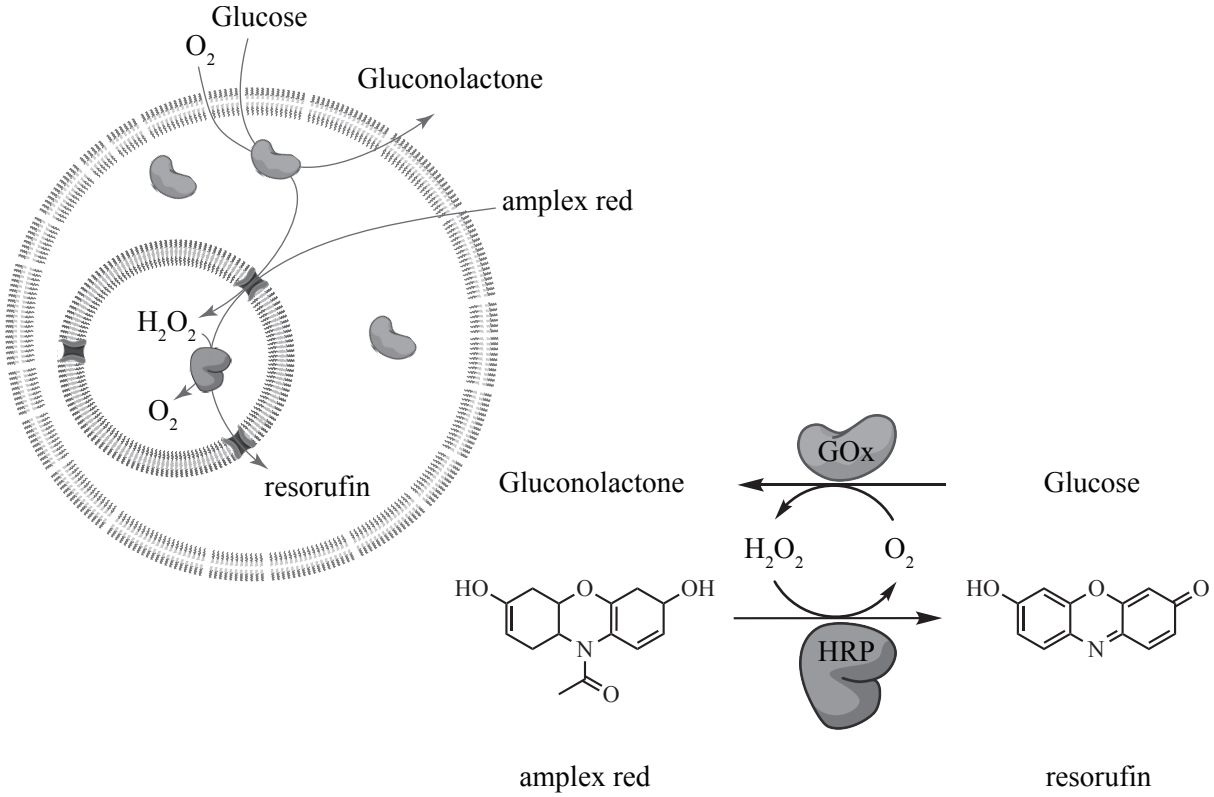

Figure 3-12. Illustration of the multicompartmentalized enzyme membrane nanoreactors implemented by Siti *et al.* (2014). The outer, porous polymer shell is composed of PS-PIAT and encloses glucose oxidase (GOx) as well as smaller, OmpF-functionalized PMOXA-PDMS-PMOXA polymersomes containing horseradish peroxidase (HRP). The net reaction from the nonfluorescent substrate amplex red to the fluorescent resorufin is also depicted for clarity.

Apart from those examples already mentioned before, a great number of different enzyme membrane nanoreactors have been created up to now, encapsulating for example α-chymotrypsin (Chen *et al.*, 2010), acetylcholinesterase (Ruysschaert *et al.*, 2005), acid and alkaline phosphatase (Broz *et al.*, 2009, Yildiz *et al.*, 2014), β-galactosidase (Chuanoi *et al.*, 2014), β-lactamase (Nardin *et al.*, 2000b), catalase (Axthelm *et al.*, 2008, Onaca *et al.*, 2010, Louzao and van Hest, 2013, Tanner *et al.*, 2013), laccase (Spulber *et al.*, 2014), lysozyme (Liu *et al.*, 2014), penicillin acylase (Langowska *et al.*, 2013) and trypsin (Chen *et al.*, 2009a) within their lumen. The following systems performed even better than their

non-encapsulated counterparts. Laccases, for example, are versatile enzymes with a wide range of substrates. Encapsulation of laccases served to protect them from inactivation by external proteases and small molecule inhibitors, which were claimed to be relevant factors limiting the enzyme performance in real-life applications (Spulber *et al.*, 2014). In some cases, the activity of the encapsulated enzyme can also be increased by the confinement in a limited volume due to an enhanced rate of enzyme–substrate and molecule–wall collisions inside the nanoreactors. Encapsulation of trypsin within polystyrene-poly(acrylic acid) (PS-PAA) polymersomes of different sizes improved the catalytic properties of the enzyme significantly, most prominently in the smallest vesicle system studied. The specific activity of the enzyme towards the fluorogenic substrate R110-Arg_2 was increased up to 4.6-fold compared to the bulk reaction, while the K_M was decreased by a factor of up to 24 (Chen *et al.*, 2009a). Similarly, k_{cat} and K_M of α-chymotrypsin were improved up to 14- and 25-fold when encapsulated within PS-PAA polymersomes (Chen *et al.*, 2010).

3.2.3 Membrane functionalization

So far, the permeability of polymer membranes has only been examined for a limited number of compounds. However, for the use of polymersomes as enzyme membrane nanoreactors, this particular membrane property is of the utmost importance, at least if mass transport phenomena represent an issue for the desired reaction. Fischer *et al.* (2007) used experimentally derived permeability coefficients (*Pe*) to classify the permeability of natural membranes towards a compound as low ($Pe < 10^{-7}$ cm s^{-1}), moderate (10^{-7} cm $s^{-1} \leq Pe \leq 10^{-6}$ cm s^{-1}) or high ($Pe > 10^{-6}$ cm s^{-1}). Compared to permeability coefficiencts of 10^{-2}-10^{-3} cm s^{-1} for typical lipid membranes (Mathai *et al.*, 2008), polymersomes prepared from $PMOXA_{15}$-$PDMS_{110}$-$PMOXA_{15}$ have been demonstrated to be significantly less permeable for water with a permeability coefficient of 10^{-5} cm s^{-1} (Kumar *et al.*, 2007). Furthermore, the same authors also showed that the polymersomes were virtually impermeable for molecules such as glucose, glycerol and urea (Kumar *et al.*, 2007). On the other hand, the term “impermeable” becomes a relative term when considered on a longer timescale, especially since polymersomes have a huge surface with regard to their volume as a consequence of their nm-scale dimensions. PMOXA-PDMS-PMOXA membranes have been shown to be intrinsically permeable for certain compounds such as superoxide anions, molecular oxygen, guanidine hydrochloride, fluorescein and the hydrophobic protease substrate BZiPAR (bis-(CBZ-Ile-Pro-Arg)- Rhodamin110) (Axthelm *et al.*, 2008, Ben-Haim *et al.*, 2008, Renggli *et al.*, 2011, Spulber *et al.*, 2013).

Nevertheless, the application of enzyme membrane nanoreactors based on polymersomes can benefit from an improved mass transfer across the membrane, ideally even a selective one. One approach to increase the permeability of the polymer membrane towards smaller molecules makes use of the earlier mentioned stimuli-responsive polymers, resulting in “breathing” polymersomes. If the membrane of such responsive polymersomes is chemically cross-linked, the membrane becomes swollen and much

more permeable rather than to disassemble (Gaitzsch *et al.*, 2011, Gaitzsch *et al.*, 2012). A similar effect is observed when PS-based polymers are mixed with stimuli-responsive polymers, creating physically cross-linked membranes due to the strong adhesive forces in the glassy polystyrene part (Kim *et al.*, 2009, Yu *et al.*, 2009). A more selective approach involves the integration of ionophores into the polymer membrane, which can shuttle ions across the membrane with a range of selectivities, depending on the choice of ionophore employed. Sauer *et al*. (2001) used two different ionophores, lasocalid A (an unselective cation carrier, Hinds and Vincenzi, 1985) and ETH5234 (a highly calcium-selective cation-carrier, Qin *et al.*, 2000), to mediate the influx of calcium ions into giant unilamellar PMOXA-PDMS-PMOXA polymersomes in order to promote a localized precipitation of calcium phosphate within their lumen. Ionophores have, however, a rather limited substrate spectrum with little relevance to biotechnological applications.

Channel-forming peptides represent another alternative with greater potential to transport relevant substrates. An advantage of peptides over the larger channel proteins is that they can often be prepared by chemical synthesis and thus their properties can be altered accordingly (Vijayan *et al.*, 2005). Gramicidin A, for example, forms a dimeric, cation-selective channel with a narrow pore of around 4 Å in diameter (Wallace, 1990). The functionality of gramicidin A inserted into $PMOXA_7$-$PDMS_{60}$-$PMOXA_7$ membranes was demonstrated by conductance measurements (Gonzalez-Perez *et al.*, 2009). Similarly, alamethicin (a peptide produced by the fungus Trichoderma viride and forming unselective, oligomeric channels; Mathew and Balaram, 1983) proved functional in membranes composed of $PMOXA_{16}$-$PDMS_{74}$-$PMOXA_{16}$ (Sauer *et al.*, 2001) and $PMOXA_{13}$-$PDMS_{33}$-$PMOXA_{13}$ (Wong *et al.*, 2006) membranes, although incorporation was shown to be significantly slower compared to lipid membranes in the latter case. Interestingly, the activity of channel forming peptides seems to depend strongly on the interaction between the peptide and the particular polymer studied, possibly due to the need for oligomerization. In polymersomes composed of polyethylethylene$_{37}$-poly(ethylene oxide)$_{40}$ (PEE_{37}-PEO_{40}) and PB_{125}-PEO_{80}, alamethicin was shown to rupture rather than selectively permeabilize the membrane, while mellitin and mastoparan, two pore-forming peptides from the venom of bees (Yang *et al.*, 2001) and wasps (Arbuzova and Schwarz, 1999), showed no activity at all (Vijayan *et al.*, 2005).

Possibly the greatest degree of control over the membrane permeability with a plethora of different substrates and selectivities can be introduced by the reconstitution of channel proteins into the polymer membrane. It has already been noted that most transmembrane proteins have so far been reconstituted into PMOXA-PDMS-PMOXA membranes (*cf.* Habel *et al.*, 2015). It is remarkable that membrane proteins have been reconstituted into membranes up to 10 times thicker than typical lipid membranes (Kumar *et al.*, 2007) and, more usually, of thicknesses of at least 6-16 nm (Itel *et al.*, 2014, Itel *et al.*, 2015). Transmembrane proteins, as well as naturally occurring channel-forming peptides, have evolved to match the dimensions of the membranes they naturally occur in. Thicker membranes result in a *hydrophobic mismatch* between the hydrophobic domain of the transmembrane protein and the

hydrophobic membrane core, which must be compensated by a compression of the membrane (*cf.* Figure 3-13). In incompressible membranes, such as lipid membranes, this results in a considerable energy penalty and can theoretically lead to the extrusion of the protein (Andersen and Koeppe, 2007). A partial embedding of the protein results in an increased surface tension between hydrophobic and hydrophilic regions of the protein and the membrane and is equally unfavorable (Pata and Dan, 2003). The reason why transmembrane proteins could still be successfully reconstituted in polymer membranes lies in the fact that the polymer chains feature a considerable degree of compressibility (Discher and Eisenberg, 2002, Pata and Dan, 2003, Srinivas *et al.*, 2005). Besides, the polydispersity of the polymers further increases the apparent compressibility of the membrane, because shorter polymer chains can segregate into the vicinity of the transmembrane protein (Discher and Eisenberg, 2002, Itel *et al.*, 2015). In PMOXA-PDMS-PMOXA membranes, this is promoted by the high fluidity and lateral mobility of polymer chains (Itel *et al.*, 2014). Even though transmembrane proteins are generally one to two orders of magnitude less deformable in terms of bending and stretching than lipid membranes (Andersen and Koeppe, 2007), a certain strain on the protein might still be exerted. Reconstituted respiratory complex I, for example, displayed an activity profile in PMOXA-PDMS-PMOXA membranes that was positively dependent on the molecular mass of the polymer and the membrane thickness (Graff *et al.*, 2010). If channel proteins are reconstituted, longer flexible polymer chains can fold back into the lumen of an integrated channel protein and block it despite a functional reconstitution (Srinivas *et al.*, 2005, Wong *et al.*, 2006). Interestingly, a high fluidity of the membrane is not always required for a protein to be reconstituted into polymersomes in an active conformation, as demonstrated for proteorhodopsin in polystyrene-poly(4-vinyl-*N*-methylpyridine iodide)$_2$ (PS-P4MVP$_2$) polymersomes (Kuang *et al.*, 2014).

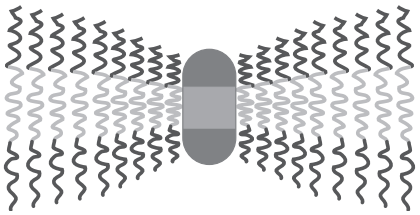

Figure 3-13. Illustration of the hydrophobic mismatch between an integral membrane protein and a polymer membrane with greater thickness than a naturally occurring lipid membrane.

The reconstitution of membrane proteins into polymersomes can be accomplished by different means. One possibility is the mixing of protein and polymer prior to polymersome formation by a solvent-based technique (Nardin *et al.*, 2000b, Choi and Montemagno, 2005). However, the formation of aquaporin Z-functionalized polymersomes by dialysis, starting from a detergent-solubilized polymer-protein mixture, has also been demonstrated (Kumar *et al.*, 2012). Alternatively, the membrane proteins can also be reconstituted into preformed polymersomes, often aided by the addition of low detergent concentrations (e.g. 0.5 % w/v Triton X-100) and ultrasound (Nallani *et al.*, 2006). The spontaneous integration of the channel protein OmpG into planar PMOXA-PDMS-PMOXA membranes, in this case only aided by

traces of detergent introduced from the protein stock and a moderate direct current (DC) voltage, has also been reported (Wong *et al.*, 2006). Even the spontaneous insertion of *in vitro* synthesized claudin-2 into PB_{21}-PEO_{12} polymersomes (Nallani *et al.*, 2011) and of the G-protein coupled dopamine receptor D2 into $PMOXA_{20}$-$PDMS_{54}$-$PMOXA_{20}$ and PB_{22}-PEO_{13} polymersomes (May *et al.*, 2013) using cell-free wheat-germ extract was recently accomplished. In the absence of any directory signals, the reconstitution of membrane proteins into polymersomes usually results in an undirected integration of the protein. This is not always detrimental, particularly if channel proteins with an asymmetric binding site or a vestibule are involved and a bidirectional mass transfer is desired. A directed insertion of a membrane protein can, however, only be accomplished by the use of asymmetric ABC triblock copolymers. Using PMOXA-PDMS-PEG with different lengths of the PMOXA and the PEG blocks, Stoenescu *et al*. (2004) could clearly demonstrate the directed insertion of aquaporin 0. In one instance, a directed integration of the F_0F_1 ATPase and bacteriorhodopsin (BR) has been observed even in the presence of a symmetrical poly(2-ethyl-2-oxazoline)-polydimethylsiloxane-poly(2-ethyl-2-oxazoline) (PEtOz-PDMS-PEtOz) membrane (Choi and Montemagno, 2005). The bulky head of the F_0F_1 ATPase is possibly responsible for the directed integration, but the surplus activity of BR proteins with their C-terminus on the outside is quite exceptional.

Another aspect of importance is the protein:polymer ratio and the ensuing degree of functionalization of the membrane. In a study with aquaporin Z, polymersomes were formed up to a very high molar protein:polymer ratio of 1:15. At even higher ratios, more complex structures including planar membranes and eventually 2D membrane protein crystals were formed (Kumar *et al.*, 2012). On a functional level, the reconstitution of OmpF at a protein:polymer ratio of 1:10 resulted in a superior permeability compared to polymersomes where the protein had been reconstituted at a ratio of 1:100 (Ranquin *et al.*, 2005). Conversely, an optimal permeability increase upon aquaporin Z reconstitution was obtained at a ratio of 1:50 (Kumar *et al.*, 2007).

A number of other membrane proteins have been successfully reconstituted into polymersomes, most of the latter composed of PMOXA-PPDMS-PMOXA. All channel proteins known to be functionally reconstituted in polymer membranes until now (not including pore-forming peptides and proton channels/pumps) are summarized in

Table 3-2. The reconstitution of the maltodextrin transporter LamB represents one of the earliest examples in which the channel was employed to direct the injection of DNA from a λ phage into the polymersome lumen (Graff *et al.*, 2002). Subsequently, the reconstitution of the nucleoside transporter Tsx (Ranquin *et al.*, 2005), cytochrome *c* oxidase (Ho *et al.*, 2005), the pore-forming toxin α-hemolysin (Wong *et al.*, 2006), the ferric hydroxamate uptake component A (FhuA) (Nallani *et al.*, 2006, Onaca *et al.*, 2008), the ion channel MspA of *M. smegmatis (Morton et al., 2015)* and the *Escherichia coli* glycerol facilitator GlpF (Zhang *et al.*, 2016) were also reported. Even such complex proteins as a photosynthetic reaction center have been reconstituted in a functional form, although the authors demonstrated that this

protein found its niche in the outer PMOXA region of the polymersome membrane rather than in the inner PDMS core (Tangorra *et al.*, 2015).

Table 3-2. Overview of channel proteins, not including proton channels/pumps, which have been functionally reconstituted in polymer membranes (mainly, but not exclusively, composed of PMOXA-PDMS-PMOXA) so far. A brief description of their natural function and exemplary applications of the channel in polymer membranes are included.

Channel	**Natural function**	**Measured activity in polymer membrane**	**Literature**
Aquaporin 0	Selective water transport	Vesicle swelling	(Stoenescu *et al.*, 2004)
Aquaporin Z	Selective water transport	Vesicle swelling	(Kumar *et al.*, 2007)
FhuA (Δ1-129 and Δ1-160 mutants)	Uptake of iron-siderophore complexes (mutants without cork domain form large hydrophilic pores for molecules ≤ 740 Da)	Transport of calcein, sulforhodamine B and 3,3',5,5'-tetramethylbenzidine	(Nallani *et al.*, 2006)
GlpF	Transport of glycerol and other sugar alcohols	Transport of ribitol	(Zhang *et al.*, 2016)
LamB	Maltoporin	Transport of phage λ DNA	(Graff *et al.*, 2002)
MspA	Major diffusion channel of the *M. smegmatis* outer membrane	Electrical current	(Morton *et al.*, 2015)
OmpF	Major porin of the *E. coli* outer membrane forming a large hydrophilic pore for molecules ≤ 600 Da	Transport of ampicillin	(Nardin *et al.*, 2000b)
OmpG	Monomeric porin for the uptake of mono-, di- and trisaccharides	Electrical current	(Wong *et al.*, 2006)
TsX	Transport of nucleosides/nucleotides	Transport of nucleosides and nucleoside analogues	(Ranquin *et al.*, 2005)
α-Hemolysin	*S. aureus* exotoxin forming large heptameric pores	Electrical current	(Wong *et al.*, 2006, Morton *et al.*, 2015)

3.3 Channel proteins of gram-negative bacteria

3.3.1 General function and classification of channel proteins

All cells are enclosed by a lipid membrane, which separates the cytoplasm with all its cellular components from the outside environment. This allows the cell to exist far from thermodynamic equilibrium, but it also implies that information and nutrients cannot be freely exchanged between the inside and the outside. The cytoplasmic membrane is selectively permeable and transport of molecules which are unable to cross this barrier due to their size or their polarity is facilitated by a number of specialized transport proteins, many of them characterized by a high substrate specificity (Alberts *et al.*, 2007, Berg *et al.*, 2007, Chen, 2007). While the cytoplasmic membrane primarily represents a barrier to hydrophilic but not to hydrophobic molecules, gram-negative bacteria have evolved a second membrane beyond the cell wall with drastically different properties. The architecture of this outer membrane is asymmetric, with the outer leaflet mainly composed of lipopolysaccharide (LPS) (Koebnik *et al.*, 2000). The lipid A component of the LPS consists entirely of unsaturated fatty acids, which are also more densely packed than in normal phospholipids, thus creating a highly-ordered membrane of low fluidity and low permeability. The hydrophilic polysaccharide structures of the LPS are negatively charged and bridged by divalent cations. This feature creates a quasi-crystalline structure and further limits the permeation rate of hydrophobic molecules, which is 50-100-fold lower compared to phospholipid membranes (Nikaido, 1994b, Hancock, 1997, Chen, 2007). Mass transport across the outer membrane is still very efficient and rather unspecific for small molecules due to the presence of high levels of porins and other transport proteins (Nikaido, 1992, Koebnik *et al.*, 2000).

The importance of membrane proteins for the proper functioning of the cell is epitomized by the fact that about one third of a cell's proteins are integral membrane proteins (Krogh *et al.*, 2001, Tan *et al.*, 2008), and of these, about one third is involved in the transport of molecules across membranes (Paulsen *et al.*, 1998a, Paulsen *et al.*, 1998b). Membrane proteins are structurally distinct from soluble proteins because they exist in the partially hydrophobic membrane environment. Thus, they resemble inverse micelles, exposing a hydrophobic surface to the membrane interior. In order to satisfy the hydrogen bonding potential of the protein backbone, membrane protein structures are restricted to regular secondary structure elements, i.e. α-helices or β-sheets (Rosenbusch, 1988). On a functional level, membrane transport proteins can be classified into channels, carriers, primary active transporters and group translocators (secondary active transporters) (*cf.* Figure 3-14).

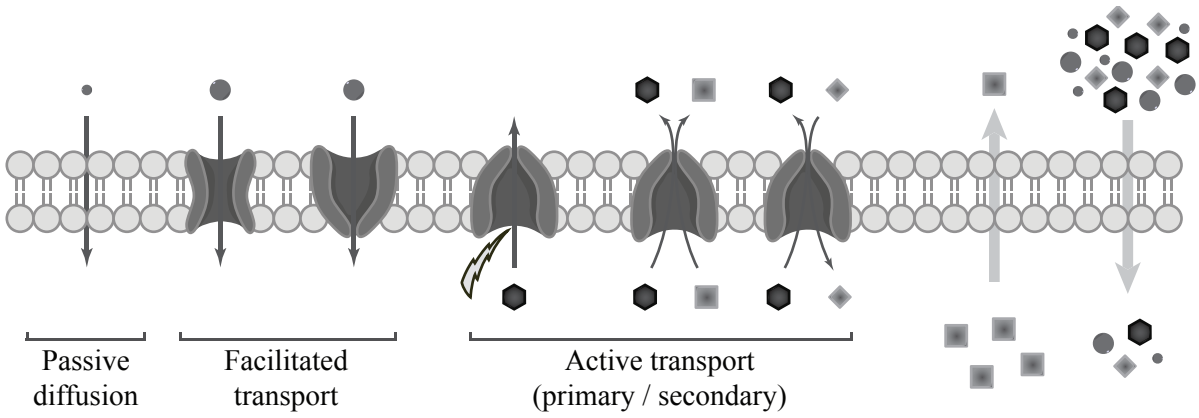

Figure 3-14. Classes of membrane transport proteins and their mode of transport. Simple passive diffusion, channel mediated and carrier-mediated facilitated transport occur along a concentration gradient. Active transport of a molecule against the concentration gradient can be coupled to the hydrolysis of ATP (primary active transport) or to the cotransport of another molecule along its concentration gradient (secondary active transport). Depending on the direction of the secondary gradient, the latter can either be unidirectional (symport) or bidirectional (antiport). The respective concentration gradients are indicated on the right.

Channel proteins can be further divided into five functional types according to structure, function, site of action and size (Saier, 2000). Channel proteins of the α-type consist of bundles of amphipathic α-helices. These are found in the cytoplasmic membranes of all organisms and are particularly important for eukaryotes owing to the great number of specialized channels with bioelectric and sensory activity (Saier, 2000). Channel proteins of a β-barrel-type consist of an even number (8-22) of antiparallel amphipathic β-sheets which form a closed barrel structure. Proteins of this class are almost exclusively found in the outer membrane of gram-negative bacteria, mitochondria and chloroplasts. Most β-barrel-type channels are far less hydrophobic than typical α-type channels. The membrane-domain is rather conserved within this group, while the extracellular domains are very diverse. The differential localization of α-type and β-barrel-type channels is assumed to originate from their biogenesis, because the polypeptide chain of the latter type has to cross the cytoplasmic membrane and the periplasm where it could get stuck if the protein was too hydrophobic (Koebnik *et al.*, 2000). Another important characteristic of β-barrel-type channels is their high stability. The sturdy general porins for example can withstand denaturation in the presence of 5 M guanidine hydrochloride or 2 % w/v SDS at 70 °C (Koebnik *et al.*, 2000). A third type of channel, also α-helical but exclusively found in bacteria and their viral parasites, are referred to as holins. These proteins form oligomeric pores in the membrane and allow the export of autolytic enzymes and the free flow of ions and other solutes, thus mediating cellular self-destruction (Young and Blasi, 1995). In contrast to holins, toxins are directed against other cells and can thus be considered agents of biological warfare. Channel-forming protein and peptide toxins represent the fourth and fifth type of channel proteins (Saier, 2000).

The channel proteins chosen for reconstitution into nano-scale enzyme membrane reactors to facilitate the mass transfer of the hydrophobic substrates of the 3-ketoacyl-(acyl-carrier-protein)-reductase and the cosubstrate formate are mainly β-barrel-type outer membrane proteins. The only exception is FocA, which is an α-type channel residing in the cytoplasmic membrane of *E. coli*. An overview of these channels can be found in Table 3-3, and a more detailed description will ensue in the subsequent chapters 3.3.2 and 3.3.3.

Table 3-3. Overview of the channel proteins used in this thesis. Name, origin, function, tertiary and quaternary structure as well as selected references are indicated.

Channel	**Organism**	**Function**	**Tertiary structure**	**X-mer**	**Literature**
OmpF	*Escherichia coli*	Diffusion pore for small hydrophilic molecules, slightly cation-selective	16-stranded β-barrel	Trimer	(Garavito and Rosenbusch, 1980, Nikaido and Rosenberg, 1983)
PhoE	*Escherichia coli*	Diffusion pore for small hydrophilic molecules, moderately anion-selective	16-stranded β-barrel	Trimer	(Nikaido and Rosenberg, 1983, Tucker *et al.*, 1991)
FocA	*Escherichia coli*	Formate transport, strictly anion-selective	6-stranded α-helical bundle	Pentamer	(Wang *et al.*, 2009, Falke *et al.*, 2010)
OprP	*Pseudomonas aeruginosa*	Transport of phosphate, strictly anion-selective	16-stranded β-barrel	Trimer	(Hancock *et al.*, 1982, Moraes *et al.*, 2007)
AlkL	*Pseudomonas putida* GPo1	Transport of alkanes	8-stranded β-barrel	Monomer	(Julsing *et al.*, 2012, Grant *et al.*, 2014)
OprG	*Pseudomonas aeruginosa*	Transport of small amino acids/ hydrophobic substrates	8-stranded β-barrel	Monomer	(Touw *et al.*, 2010, Kucharska *et al.*, 2015b)
OmpW	*Escherichia coli*	Transport of hydrophobic substrates	8-stranded β-barrel	Monomer	(Hong *et al.*, 2006, Burgess *et al.*, 2008)
TodX	*Pseudomonas putida*	Transport of toluene/ hydrophobic substrates	14-stranded β-barrel	Monomer	(Wang *et al.*, 1995, Hearn *et al.*, 2008)

3.3.2 General porins and anion-selective channel proteins

Perhaps the most important general porin of the *E. coli* cell envelope is OmpF, which mediates the passive diffusion of small, mainly hydrophilic molecules with a molecular mass below 600 Da across the outer membrane (Nikaido, 1992). It was also among the first membrane proteins whose structure had been solved (Garavito and Rosenbusch, 1980, Garavito *et al.*, 1983). The trimeric 38 kDa outer membrane protein with a 16-stranded β-barrel structure (*cf.* Figure 3-15A) forms a water-filled pore in the outer membrane, which measures 7 x 11 Å at its narrowest position. The channel is constricted at half its height by the extracellular loop L3, which folds back into the channel and contributes significantly to the permeability and selectivity of the channel (Cowan *et al.*, 1992). Even within the exclusion limit of the pore, solute permeability decreases sharply over several orders of magnitude with increasing size, probably influenced by the presence of several ordered water molecules in the constriction zone (Nikaido, 1994a). Due to a slightly larger channel cross-section, OmpF is also more efficient in transporting solutes than OmpC, the second important general *E. coli* porin (Nikaido and Rosenberg, 1983). OmpF, although primarily an unselective diffusion pore, exhibits a slight cation-selectivity due to a strong transversal electrostatic field generated by two acidic residues located in L3 and four basic residues at the opposite barrel wall (Cowan *et al.*, 1992). Minor changes in the constriction zone can lead to a reversal of the ion selectivity. Indeed, the moderately anion-selective phosphoporin PhoE, which is induced under phosphate starvation (Tommassen *et al.*, 1982), is structurally very similar to OmpF, and the preference for anions is primarily based on the presence of a lysine residue substituting for G131 in OmpF (Bauer *et al.*, 1989). Additional charged residues in the channel and the extracellular rim of the channel contribute further to the different ion-selectivity of PhoE and OmpF (Bauer *et al.*, 1989, Saint *et al.*, 1996, van Gelder *et al.*, 1997). First evidence for the anion-selectivity of PhoE was presented by Nikaido and Rosenberg (1983) by means of liposome-swelling assays. From their experiments, they concluded that the rate of diffusion of anions through PhoE was several times faster than through OmpF.

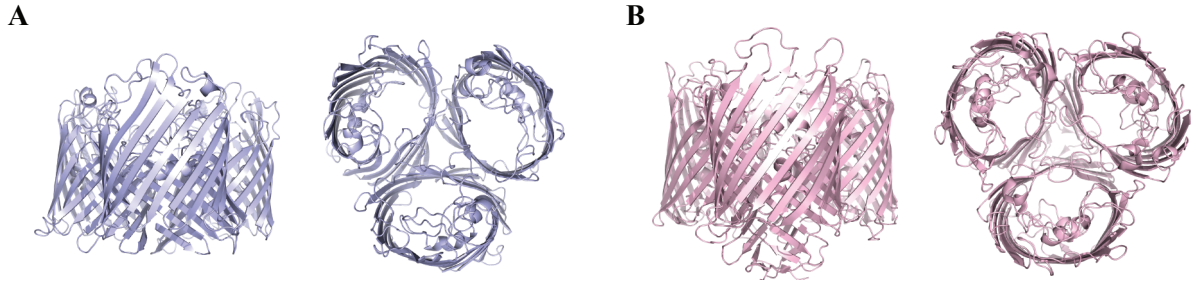

Figure 3-15. Crystal structures of (A) *E. coli* OmpF (PDB: 2OMF) and (B) *P. aeruginosa* OprP (PDB: 2O4V). Both channels are shown in side and top view.

The trimeric 48 kDa outer membrane protein OprP from *P. aeruginosa* is another anion-selective porin with a much more pronounced anion-selectivity than PhoE. It is also induced under phosphate starvation (Siehnel *et al.*, 1988, Sukhan and Hancock, 1996) and essential for growth under low-phosphate conditions. Unlike the former, OprP contains a high-affinity binding site for phosphate ions with a K_D of approximately 0.1 mM at neutral pH and displays a saturation behavior for other anions at high substrate concentrations (i.e. >300 mM for chloride) similar to enzymes (Benz *et al.*, 1993). The channel was shown to be virtually impermeable for cations (Hancock *et al.*, 1982, Hancock *et al.*, 1983, Benz *et al.*, 1984b, Benz *et al.*, 1985) and to discriminate between anions of different sizes (Benz and Hancock, 1987). Furthermore, the high affinity for phosphate results in a strong inhibition (half-maximal inhibition at a phosphate concentration of approximately 0.5 mM) of the flux of other ions in the presence of this preferred substrate (Hancock and Benz, 1986). Structurally, the special transport characteristics of OprP are based on the presence of a 9-residue arginine ladder spanning the extracellular surface of the channel down to the constriction zone where phosphate is coordinated. Lysine residues located in the periplasmic half of the channel create an electropositive sink, pulling the substrate into the periplasm. Besides, the OprP trimer is also distinct from those of OmpF and PhoE due to an extended, periplasmatically located N-terminus which is involved in stabilization of the trimer through a tricorn-like strand-exchange (*cf.* Figure 3-15B) (Moraes *et al.*, 2007).

Another anion-specific channel which displays a substrate-specific saturation behavior is the formate channel FocA (Lu *et al.*, 2012). The 31 kDa protein was identified by the characterization of hypophosphite-resistant *E. coli* mutants and is an α-type channel responsible for the transport of formate across the cytoplasmic membrane (Suppmann and Sawers, 1994). Sometimes welcome as a valuable electron donor for many anaerobic bacteria, its substrate formate (or rather formic acid) is also produced during the mixed-acid fermentation, which can lead to a severe acidification of the cytoplasm (Lu *et al.*, 2012, Hunger *et al.*, 2014). Therefore, both import and export of formate by FocA are important in a cellular context. FocA does not conduct cations or divalent anions, but apart from the main substrate formate, other products of the mixed-acid fermentation (acetate, lactate and pyruvate) as well as chloride are also accepted. The relative yields of the mixed-acid fermentation products roughly match the relative affinities of FocA for them. The K_D of FocA towards formate could be determined to be 11.7 mM. Each of the five protomers of the pentameric complex forms a separate channel, while the central pore is apparently non-conducting. Furthermore, the channels appear to be in a closed state with fast rearrangements to allow for substrate passage rather than being permanently opened. An open pore would not be able to exclude the passage of water molecules and the formation of a water chain, resulting in the degradation of the proton-motive force across the cytoplasmic membrane (Wang *et al.*, 2009, Lu *et al.*, 2012). Structural analysis of FocA from *E. coli* (Wang *et al.*, 2009), *Vibrio cholerae* (Waight *et al.*, 2009) and *Salmonella enterica ssp. enterica* serovar Typhimurium (Lu *et al.*, 2012) revealed a homopentamer of six membrane-spanning α-helices with structural resemblance to aquaporins and glyceroporins (*cf.* Figure 3-16).

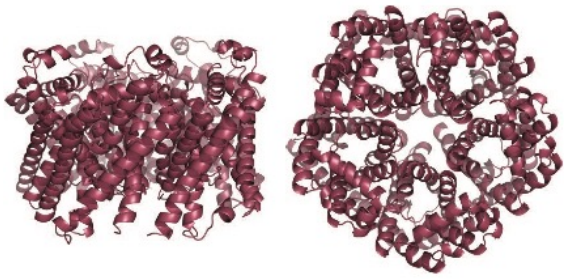

Figure 3-16. Crystal structure of *E. coli* FocA (PDB: 3KCV) in side and top view.

3.3.3 Channel proteins for hydrophobic substrates

As discussed in chapter 3.3.1, the outer membrane of gram-negative bacteria represents a major barrier to the diffusion of hydrophobic molecules. Presumably, a number of hydrophobic substrates are therefore transported by members of the FadL family of monomeric outer membrane proteins (van den Berg, 2005). In accordance with the asymmetric structure of the outer membrane and considering that the hydrophilic LPS layer rather than the hydrocarbon part of the membrane is transport-limiting, Hearn *et al*. (2009) proposed a lateral diffusion transport model for the action of these transporters (*cf*. Figure 3-17). In this model, the substrate is first bound by a low-affinity binding site at the extracellular face of the channel and then transferred to a second, high-affinity binding site further down the channel. Upon spontaneous conformational changes in the N-terminal hatch domain, a continuous passageway to a lateral opening in the channel-wall is created, releasing the substrate into the outer leaflet of the outer membrane. Subsequently, the substrate can move to the inner leaflet and diffuse into the periplasm. Lateral diffusion transport is also known from multidrug efflux transporters, so this mechanism was proposed to be a universal strategy for the transport of hydrophobic compounds across the outer membrane (Hearn *et al.*, 2008).

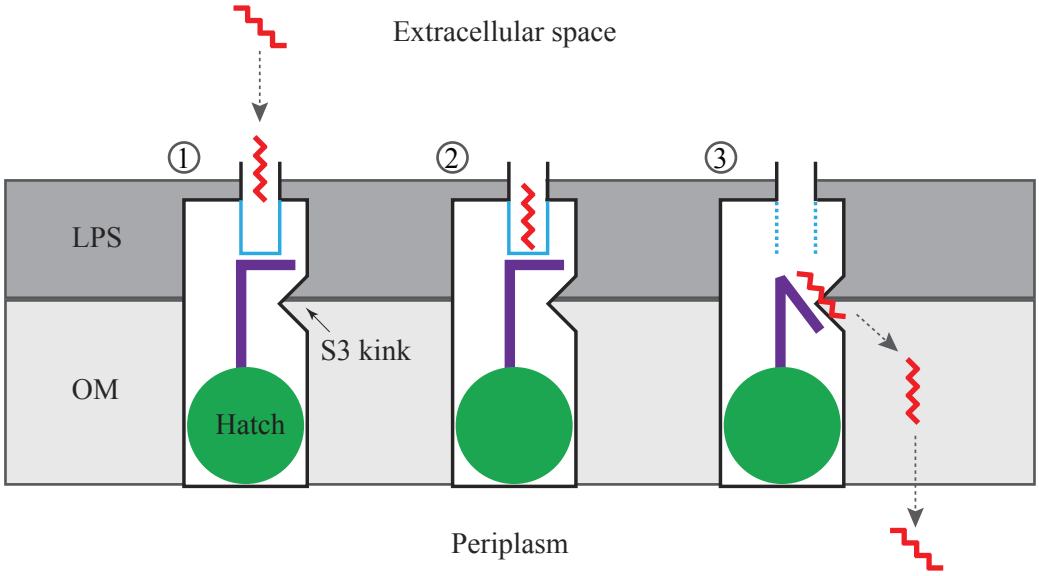

Figure 3-17. Lateral diffusion transport model for the transport of hydrophobic molecules across the outer membrane by FadL, exemplified for octane. (1) The substrate first binds to a low-affinity site and (2) then relocates to a second, high-affinity binding site. (3) This causes a conformational change in the hatch domain, opening a passage in the barrel wall. From there, the substrate partitions into the membrane and then into the periplasm (modified from Hearn *et al.*, 2009).

TodX is a member of the FadL family. This 48 kDa protein forms a 14-stranded β-barrel with a lateral opening in the channel wall and a hatch domain similar to FadL. The channel is part of the toluene dioxygenase (*tod*) pathway in *P. putida* and it was shown that TodX is responsible for the transport of substrates such as toluene into the cell (Wang *et al.*, 1995). In contrast to FadL, where the hatch domain blocks a periplasmatic exit of the channel, the TodX hatch domain contains a narrow continuous channel which might also serve as a traditional channel (Hearn *et al.*, 2008). Since the channel interior is relatively polar, this channel might have evolved to facilitate the uptake of more water-soluble monoaromatic hydrocarbons. With regard to ions, however, TodX appeared to be non-conductive (Hearn *et al.*, 2009).

Structural features resembling those of the FadL family, i.e. a lateral opening in the channel wall, are also found in the widespread OmpW family (Busch and Saier, 2004) of monomeric, eight-stranded β-barrel channels (Hong *et al.*, 2006). The eponymous, 23 kDa channel OmpW (*cf.* Figure 3-18) was originally described as the receptor for colicin S4 in *E. coli* (Pilsl *et al.*, 1999) and forms a hydrophobic channel with a lateral opening into the hydrocarbon region of the membrane, which was speculated to serve as a passageway for hydrophobic molecules across the outer membrane (Hong *et al.*, 2006). The same authors also demonstrated that OmpW forms a transient pore (as opposed to a permanently open pore) with a low ion-conductance of 18 pS at 1 M KCl. Hard evidence for its function is still scarce, and not all assigned functions of OmpW are obviously transport-related or particularly well-understood on a mechanistic level. It seems to be involved in a number of immune-escape related functions, such as

the efflux of quaternary cationic compounds (Beketskaia *et al.*, 2014), resistance to phagocytosis (Wu *et al.*, 2013) as well as complement-mediated killing by binding to the alternative complement pathway component factor H (Li *et al.*, 2016) and iron homeostasis (Lin *et al.*, 2008) in *E. coli*. In other gram-negative bacteria, OmpW or OmpW-homologs were shown to be involved in the escape from phagocytic cells by mediating the influx and subsequent sensing of H_2O_2 and HOCl in *S. enterica ssp. enterica* serovar Typhimurium (Morales *et al.*, 2012), in the stress-response to trinitrotoluene in *Stenotrophomonas sp*. (Ho *et al.*, 2004) or to salinity in *V. cholerae* (Nandi *et al.*, 2005) and *V. alginolyticus* (Xu *et al.*, 2004, Xu *et al.*, 2005), in biofilm formation (Ritter *et al.*, 2012) and finally also in the uptake of hydrophobic substrates such as benzothiophene in *P. putida* (Eaton and Nitterauer, 1994) and naphthalene in *P. fluorescens* (Neher and Lueking, 2009).

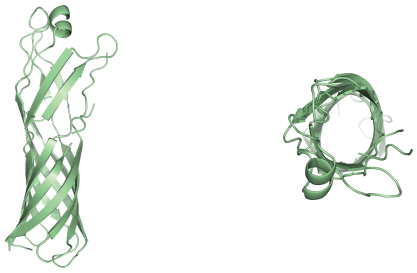

Figure 3-18. Crystal structures of *E. coli* OmpW (PDB: 2F1V) in side and top view.

The 25 kDa channel protein OprG is the closest OmpW homolog in the opportunistic pathogen *P. aeruginosa* and one of its major outer membrane proteins (Gensberg *et al.*, 1999). Similar to OmpW, the OprG channel is lined with hydrophobic amino acids and the crystal structure indicates the presence of a lateral opening (Touw *et al.*, 2010). The function of OprG was long speculative, ranging from an iron-uptake transporter (Yates *et al.*, 1989) or a cation-channel (McPhee *et al.*, 2009) to a transport facilitator for hydrophobic compounds (Touw *et al.*, 2010). Furthermore, OprG was also described to be an important factor for biofilm formation (Ritter *et al.*, 2012) and its downregulation was linked to an increased resistance to antimicrobial compounds such as kanamycin and tetracycline (Peng *et al.*, 2005) or benzalkonium chloride (Machado *et al.*, 2013). Recently, Kucharska *et al.* (2015b) investigated the structure of OprG by solution NMR and found significant structural differences between their structure and the crystal structure solved by Touw *et al.*, particularly the lack of a lateral opening in the barrel wall and a generally shorter barrel with extended flexible loops. They proposed that the main function of OprG might rather lie in the uptake of small amino acids, which they demonstrated by means of liposome swelling and bacterial growth assays.

Another close OmpW homolog from *P. putida* GPo1 (formerly known as *P. oleovorans*) is AlkL. The 25 kDa outer membrane protein AlkL is part of the *alk*-operon necessary for hydrocarbon utilization by this strain (Eggink *et al.*, 1987, van Beilen *et al.*, 1992). As such, its role probably lies in the transport of hydrocarbon substrates across the outer membrane (e.g. van Beilen *et al.*, 1992, Schneider *et al.*,

1998, Grant *et al.*, 2011, Julsing *et al.*, 2012). Although the natural substrates of AlkL are still unknown, its function as a transport facilitator has been utilized by several groups to improve whole-cell biocatalysts for various products (*cf.* chapter 3.3.4).

3.3.4 Membrane channel proteins and their use for biocatalytic applications

The employment of a number of channel proteins to mediate mass transport into and out of enzymatically active polymersomes has already been outlined in chapter 3.2.3. But being an integral part of bacterial membranes, the importance of channel proteins for whole-cell-mediated bioconversions is not to be overlooked. Biocatalytic processes involving whole cells have several advantages over the use of isolated enzymes, including the elimination of the need to isolate and purify said enzymes, an increased stability of the biocatalyst and facile cofactor regenerations (Chen, 2007). However, whole-cell bioconversions of hydrophobic or large hydrophilic compounds are often limited by the barrier-function of the outer membrane of gram-negative bacteria (Chen, 2007). Accordingly, strategies for the permeabilization of whole-cell biocatalysts are often necessary. Popular methods include the use of detergents, organic solvents, EDTA or freeze-thaw cycles (Chen, 2007). Apart from these rather crude methods, cell envelope engineering represents another possibility to overcome mass transfer limitations. An alteration of the LPS structure or deletion of Braun's lipoprotein is one example where the overall permeability of the outer membrane was altered to improve uptake of toluene and other substrates (Ni and Chen, 2004, Ni and Chen, 2005).

Recently, transport proteins for hydrophobic substrates have gained more attention. Overexpression of the *E. coli* long-chain fatty acid transporter FadL was used to increase the uptake of medium-chain alkanes (Call *et al.*, 2016) and the microbial production of hydroxylated long-chain fatty acids (Bae *et al.*, 2014), while its deletion served to increase free fatty acid secretion into the medium of an engineered *E. coli* strain by means of a reduced reuptake (Meng *et al.*, 2013). The small outer membrane protein AlkL from the *P. putida* OCT plasmid was found to increase oxygenation of alkanes (Julsing *et al.*, 2012, Grant *et al.*, 2014), fatty acids or fatty acid methyl esters (Julsing *et al.*, 2012, Scheps *et al.*, 2013, Schrewe *et al.*, 2014, Kadisch *et al.*, 2016) and limonene (Cornelissen *et al.*, 2013). In a membrane proteome study on phenylpropanoid producing *E. coli* strains, Zhou *et al.* (2015) identified and functionally validated several outer membrane proteins involved in the import or export of these phytochemicals. Interestingly, even the use of an engineered FhuA variant which forms a very wide hydrophilic channel in the outer membrane proved effective to alleviate mass transfer limitations of cytochrome P450 substrates. In the presence of the channel, the regiospecific hydroxylation of the aromatic compounds toluene and anisole as well as the oxidation of the terpenes (α)-pinene and *(R)*-limonene with an engineered *E. coli* strain was moderately (1.4-2.1-fold) increased (Ruff *et al.*, 2016).

3.4 Protein refolding

Protein overexpression in *E. coli* is a standard technique to produce recombinant proteins. Depending on the protein and the expression conditions, the formation of insoluble protein aggregates in the form of cytoplasmic or periplasmatic inclusion bodies is a frequently encountered side effect (De Bernardez-Clark, 2001, Jungbauer and Kaar, 2007). Due to their hydrophobicity and their special biogenesis, membrane proteins are particularly prone to aggregate, which presents a major problem for the production of larger amounts of stable and functional protein (Junge *et al.*, 2008, Solov'eva *et al.*, 2012). Most bacterial outer membrane proteins are first synthesized as unfolded precursor proteins with an N-terminal leader peptide, targeting them to the outer membrane. This is accomplished by binding to chaperones and transport across the cytoplasmic membrane by the Sec system, where the leader peptide is cleaved off. The still unfolded polypeptide is subsequently bound by periplasmatic chaperones, which prevent aggregation and promote the early stages of folding. Insertion into the outer membrane and proper folding is accomplished by the barrel assembly (Bam) complex (Solov'eva *et al.*, 2012). Unfortunately, the capacity of this system is rather limited, causing the observed problems during the overexpression of membrane proteins. Other reasons for the often extremely low yields are that excessive amounts of a membrane protein often prove toxic to the cell, as well as the need to solubilize the protein from the membrane, which requires a suitable detergent (Junge *et al.*, 2008).

The formation of inclusion bodies can also be turned into an advantage, because inclusion bodies provide a means of producing the target protein in high amounts in an easy to isolate, albeit still unfolded form. Apart from the often considerably higher yields, inclusion bodies protect the target protein from proteases and allow for the expression of otherwise toxic proteins (Choe *et al.*, 2006). Many membrane proteins can be efficiently directed to form cytoplasmic inclusion bodies by removal of the leader peptide sequence (Bannwarth and Schulz, 2003). Due to their high density and the high target protein content (up to 95 %, Valax and Georgiou, 1993), inclusion bodies represent an elegant way of enriching the target protein simply by centrifugation. Most contaminants are not incorporated and adsorb to the inclusion bodies only after cell disruption, so they are readily removed (De Bernardez-Clark, 2001, Middelberg, 2002). On the downside, inclusion body based protein production requires additional downstream processing steps, i.e. the solubilization of the unfolded protein by guanidine hydrochloride or urea and their subsequent refolding.

Generally, protein folding *in vitro* corresponds to a conversion of the protein from a denatured state to its folded, native conformation. This process is driven by the free energy difference between the two states, which is caused by the formation of hydrogen bonds, electrostatic, hydrophobic and van-der-Waals interactions (Jaenicke, 1996). The formation of disulfide bridges is another significant factor for protein folding, but since no disulfide bridges are present in the outer membrane proteins to be refolded in this thesis, this aspect will not be discussed any further. A characteristic of protein folding is that it is reversible (Anfinsen *et al.*, 1961). Protein folding is usually a fast process, which takes place at the scale

of microseconds to seconds. The vast number of theoretically possible conformations cannot be sampled at random in this short time, which is known as the Levinthal paradoxon (Levinthal, 1969). Levinthal also proposed that "*protein folding is speeded and guided by the rapid formation of local interactions which then determine the further folding of the peptide*" (Levinthal, 1968). Accordingly, the energy landscape of protein folding can be envisioned as a funnel with a rough surface, where the initial and the ensuing interactions within the protein rapidly collapse the conformational space (*cf.* Figure 3-19). The protein arrives at a stable local minimum after passing through a number of less stable conformations or intermediates along one or several alternative preferred folding pathways (Dill and Chan, 1997). Some of the intermediates are more stable than others, such as the molten globule state, and some might even trap the protein in an incorrect conformation, leading to a misfolded protein (Schultz, 2000).

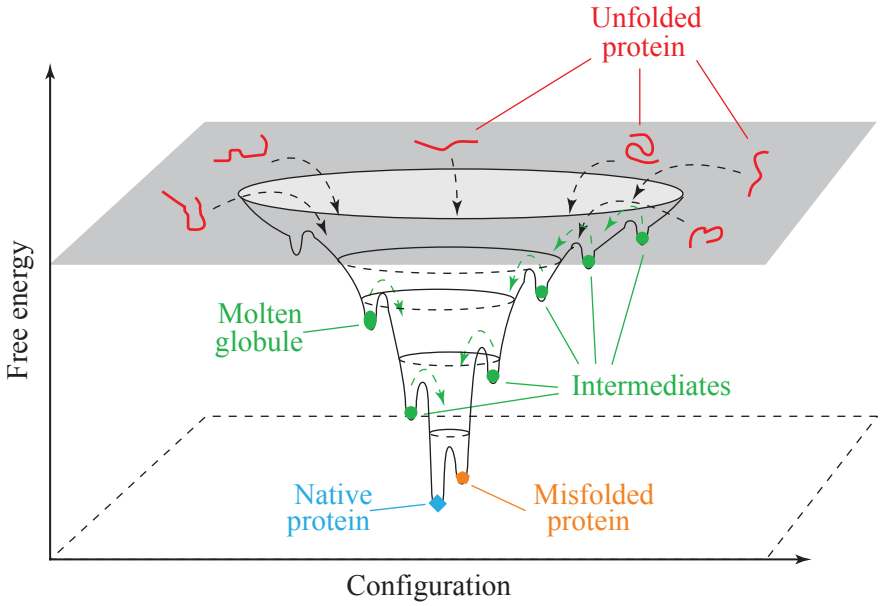

Figure 3-19. Schematic energy landscape of protein folding. The unfolded protein states collapse into a folding funnel with a rough surface representing local minima. Most of these represent transient folding intermediates. Some intermediates retain a more stable structure such as the molten globule, whereas other local minima irreversibly trap the protein in a misfolded state (from Schultz, 2000).

The presence of intermediates and misfolded states is of great significance to the *in vitro* refolding of proteins, because the formation of aggregates from partially folded intermediates or misfolded protein compete with the formation of the correctly folded protein (Rudolph and Lilie, 1996). Because protein folding mainly involves intramolecular interaction, it follows first-order kinetics, whereas aggregation is an intermolecular process and thus of higher order (Zettlmeissl *et al.*, 1979, Goldberg *et al.*, 1991, Kiefhaber *et al.*, 1991, De Bernardez-Clark *et al.*, 1998). As a result, folding yields are usually negatively affected by higher concentrations of the folding protein (Vallejo and Rinas, 2004), necessitating low protein concentrations or other ways of reducing the undesired aggregation.

3.4.1 Refolding methods

Refolding of proteins from solubilized inclusion bodies is usually achieved by removal of the denaturant (Rudolph and Lilie, 1996). This is most commonly achieved by dilution of the denatured protein into a non-denaturing refolding buffer. Due to the kinetics of refolding and aggregate formation, rapid dilution of the protein is usually performed at protein concentrations between 10 and 100 mg L^{-1} (Jungbauer and Kaar, 2007). Avoidance of high local protein concentrations is especially important during the initial renaturation when the protein is most prone to aggregate. Therefore, uniform mixing is essential, particularly on larger scales (De Bernardez-Clark, 2001, Jungbauer and Kaar, 2007). Refolding by dilution is attractive due to its simplicity, but the low protein concentrations also result in excessively high reaction volumes and so the refolded protein usually needs to be concentrated after refolding (De Bernardez-Clark, 2001). The volumetric yields can be improved by slow continuous or discontinuous addition of the denatured protein to the refolding buffer, because completely folded proteins are usually not prone to aggregate with yet unfolded proteins (Rudolph and Lilie, 1996). If the correct folding reaction is faster than the aggregation, removal of the denaturant can also be performed by one-step or stepwise dialysis or diafiltration. With this technique, misfolded states may revert to the productive folding pathway due to the action of the denaturant (Tsumoto *et al.*, 2003). Compared to the denaturant removal by dilution, the protein is exposed to intermediate denaturant concentrations for an extended period of time. This circumstance can be an advantage of the dialysis/diafiltration approach, because some proteins tend to aggregate only under strongly native conditions. For other proteins, aggregation-prone folding intermediates dominate under these conditions, and those are consequently better refolded by dilution (Rudolph and Lilie, 1996).

Alternatively, refolding can also be performed by size-exclusion chromatography (SEC) or even after binding to a chromatography matrix. The former technique involves the application of the denatured protein to a column equilibrated with refolding buffer. During the column evolution, the denaturant is retarded and the proteins can fold, isolated by the porous matrix. Protein aggregates stuck in the matrix can be resolved once the denaturant catches up, resulting in a higher fraction folded. Besides, the different hydrodynamic radii of the folded and unfolded protein results in a separate elution of both species, which renders a subsequent clean-up unnecessary (Vallejo and Rinas, 2004). Matrix-assisted refolding also assures a spatial isolation of the refolded protein and prevents the formation of aggregates. On-column refolding can be performed with most binding chromatography techniques, including ion exchange chromatography (Wang *et al.*, 2014), immobilized metal affinity chromatography (Shi *et al.*, 2003) and hydrophobic interaction chromatography (Li *et al.*, 2004). Apart from reduced aggregation, on-column refolding also facilitates a subsequent buffer exchange, higher protein concentrations by step elution and short process times. However, the compatibility of column material and refolding buffer or a possible interference of the affinity tag with refolding may limit the scope of this approach (Jungbauer *et al.*, 2004).

Protein folding is a complex process and depends both on the properties of the protein and environmental factors, such as temperature, pH and ionic strength (Rudolph and Lilie, 1996, Vallejo and Rinas, 2004). At lower temperatures, folding is slower and hydrophobic interactions between folding intermediates are reduced, leading to less aggregation (Xie and Wetlaufer, 1996). Stable proteins may, however, require higher temperatures to fold properly (Sakamoto *et al.*, 2004). The pH and the ionic strength have an impact on the solubility of the folded protein and of the folding intermediates (Vincentelli *et al.*, 2004). Furthermore, low molecular mass additives, such as guanidine hydrochloride, urea or arginine, are commonly utilized to improve the refolding yield. Folding additives may affect the stability and/or the solubility of the unfolded or folded state of the protein as well as of any folding intermediates, or they may solubilize aggregates (De Bernardez-Clark *et al.*, 1999, De Bernardez-Clark, 2001). Hamada *et al*. (2009) proposed a general classification into denaturants (guanidine hydrochloride, urea, strong ionic detergents), stabilizers (certain amino acids, sugars, polyhydric alcohols, osmolytes and kosmotropic salts) and mixed-class additives (arginine, $MgCl_2$, ethylene glycol, non-ionic detergents, non-detergent sulfobetaines, amino acid derivatives, polyamines and certain amphiphilic polymers), which have marginal effects on the protein structure and stability, but are able to disrupt protein interactions. Denaturants applied at non-denaturing concentrations mainly act on folding intermediates and aggregates by solubilizing solvent-exposed hydrophobic regions, thus stabilizing these protein species (Hamada *et al.*, 2009). Stabilizers may promote folding by preferential hydration or through the osmophobic effect. The former is based on the preferential exclusion of the additive from the hydrophobic surface of the unfolded protein, leading to an increased concentration of water molecules in the vicinity of the peptide chain. This may happen because of unfavorable electrostatic interactions, a steric exclusion of the additive or an increased surface tension of the solvent. Since the hydrophobic surface area of the unfolded protein is larger than in the folded state, more water molecules are concentrated around the protein. This results in a shift of the equilibrium towards the folded state (Timasheff, 2002, Chi *et al.*, 2003). The related osmophobic effect favors the folded state primarily by the highly unfavorable transfer of the polypeptide backbone from water to the cosolvent system, thereby again destabilizing the unfolded state (Liu and Bolen, 1995). The main mechanism of action of those folding additives employed in this thesis are summarized in Table 3-4.

Table 3-4. Folding additives used in this thesis and their proposed mechanism of action.

Additive	Mechanism of action
NaCl	Stabilization of the natively folded state by preferential hydration at high concentrations (Arakawa and Timasheff, 1983).
Glycerol	Stabilization of the natively folded state by the osmophobic effect (Bolen and Baskakov, 2001).
PEG 4000	Stabilization of the natively folded state by preferential hydration due to a steric exclusion (Cleland and Wang, 1990) and inhibition of unspecific aggregation by binding to exposed hydrophobic areas of folding intermediates (Cleland and Wang, 1990).
Urea	Inhibition of unspecific aggregation by chaotropic solubilization of aggregation-prone, unfolded protein species and folding intermediates (Tsumoto *et al.*, 2003).
NDSB-201	Inhibition of unspecific aggregation (Expert-Bezançon *et al.*, 2003).
Glycine	Stabilization of the natively folded state by preferential hydration (Arakawa and Timasheff, 1983).
Arginine	Inhibition of unspecific aggregation by binding to exposed hydrophobic areas of folding intermediates (Tsumoto *et al.*, 2003).
Glutamine	Stabilization of the natively folded state by the osmophobic effect (Bolen and Baskakov, 2001).
Glutamate	Stabilization of the natively folded state by preferential hydration at high concentrations (Arakawa and Timasheff, 1983).

3.4.2 Refolding of outer membrane proteins

As a result of their hydrophobic environment, membrane protein folding is intimately linked to the presence of lipid membranes or at least membrane surrogates, e.g. detergent micelles. Therefore, although classically considered as folding enhancers, detergents or lipids are a necessity for membrane protein refolding (Popot and Engelman, 2016). The process of outer membrane protein folding was investigated in micellar detergent systems as well as in lipid membranes (Kleinschmidt *et al.*, 1999, Tamm *et al.*, 2004) and can be divided into three phases. Initially, hydrophobic side chains spontaneously partition into the interface region of the membrane, which is driven by the hydrophobic effect. Secondary structure elements (i.e. β-strands) then form upon insertion into the hydrophobic core of the membrane. The final step consists of a complete insertion into the membrane, accompanied by closure of the barrel and tertiary structure formation.

Membrane protein refolding was first demonstrated for the α-helical bacteriorhodopsin (Huang *et al.*, 1981), but the strategy is also well suited for the production of large amounts of outer membrane proteins with their β-barrel architecture. A number of these proteins are easily foldable in principle, provided that their basic requirements are met (Otzen and Andersen, 2013). The nature of the denaturant influences the outcome of the refolding experiments, and while α-helical membrane proteins appear to

refold best when denatured and solubilized by sodium dodecyl sulfate (SDS), outer membrane proteins are more often refolded from a urea-, or sometimes guanidine hydrochloride-denatured state (Popot, 2014). Reports about refolded membrane proteins have dramatically increased over the past 20 years and so far, at least 40 different β-barrel membrane proteins have been refolded successfully (Popot, 2014). Generally, the refolding of monomeric as well as oligomeric outer membrane proteins is feasible, but due to the secondary oligomerization step in the latter, the folding reaction becomes more complicated. As a result, folding is slower and refolding yields are often lower than for monomeric proteins (Surrey *et al.*, 1996). *In vivo*, outer membrane protein folding occurs in the periplasm where the pH varies considerably in response to the environment. Still, many outer membrane proteins fold best at a slightly basic pH of 8-10, where they are often negatively charged (Burgess *et al.*, 2008). With regard to the refolding temperature, many outer membrane proteins have been refolded at room temperature (Buchanan, 1999), but higher temperatures up to 50 °C improved the refolding of some outer membrane proteins (Burgess *et al.*, 2008). The inherent stability of outer membrane proteins has also provided the basis for the classical test of outer membrane protein folding, which is the temperature modifiability on semi-native SDS-PAGE, originally developed by Schweizer *et al*. (1978). The folded state of outer membrane proteins is usually resistant to denaturation by SDS at room temperature, therefore SDS traps the differently folded populations of the protein present in the sample at the time of its addition. The differential running behavior of the folded and unfolded protein species by SDS-PAGE can thus be used to analyze the folding of the sample (Otzen and Andersen, 2013).

4 Materials and methods

4.1 General materials

Lists of all materials used in this thesis can be found in the appendix A. General equipment is listed in Table A 1. Chromatography equipment is listed in Table A 2, bioREACTOR 48 equipment in Table A 3, gas chromatography equipment in Table A 4 and equipment for electrophysiological measurements in Table A 5. Consumables can be found in Table A 6, chemicals in Table A 7. The composition of buffers and media is given in Table A 11 - Table A 28.

4.2 Special materials

4.2.1 ABA triblock copolymer

Polymer vesicles were produced using an ABA triblock copolymer comprised of poly(2-methyloxazoline) (PMOXA) and poly(dimethylsiloxane) (PDMS) with average chain lengths of 15 and 68, respectively. The polymer has a total mass of 7600 g mol^{-1} with block masses of 1300 g mol^{-1} for the outer PMOXA blocks and 5000 g mol^{-1} for the PDMS middle block. $PMOXA_{15}$-$PDMS_{68}$-$PMOXA_{15}$ was purchased from Polymer source (Dorval, Canada). The polymer has an M_W/M_N of 1.23, where M_W is the mass-average molecular mass and M_N is the number-average molecular mass. The polymer contains hydroxyl end groups on both sides and the blocks are linked by methyl groups (*cf*. Figure 3-11).

4.2.2 Detergents and lipids

Table 4-1 contains all detergents and lipids used in this thesis. The classification of the detergents and their critical micelle concentrations (CMCs) are listed separately in Table A 13.

Table 4-1. Detergents and lipids.

Detergent/Lipid	Purity	Art.-No.	Supplier
1,2-Diphytanoyl-*sn*-glycero-3-phosphocholine (DPhPC)	≥ 99 %	850356	Avanti Polar Lipids
1-Palmitoyl-2-oleoyl-*sn*-glycero-3-phosphocholine (POPC)	≥ 99 %	850375	Avanti Polar Lipids
3-[(3-Cholamidopropyl)dimethyl-ammonio]-1-propane sulfonate (CHAPS)	Pufferan, ≥98 %, for biochemistry	1479	Carl Roth
Dodecyl-*β*-D-maltoside (DDM)	≥ 99 %, for biochemistry	CN26	Carl Roth

Detergent/Lipid	Purity	Art.-No.	Supplier
N,N-Dimethyldodecylamine *N*-oxide (LDAO)	-	40236	Sigma-Aldrich
N-Lauroylsarcosine sodium salt	BioXtra	L5777	Sigma-Aldrich
n-Octylpolyoxyethylene (O-POE)	-	P-1140.0100	Bachem
Nonidet P40 substitute (NP-40)	-	NIDP40	Anatrace
n-Octyl-*β*-D-glucopyranoside (OG)	≥ 99 %, for biochemistry	CN23	Carl Roth
n-Octyl-*β*-D-thioglucopyranoside (OTG)	≥ 95 %, for biochemistry	4139	Carl Roth
Polyethylene glycol alkylphenyl ether (Triton X-100)	Extra pure	3051	Carl Roth
Polyoxyethylene lauryl ether (Brij-35)	For biochemistry	CN21	Carl Roth
Polyoxyethylene (20) sorbitan monolaureate (Tween 20)	Pure, Ph. Eur., USP	37470.01	Serva
Polyoxyethylene (80) sorbitan monolaureate (Tween 80)	Pure, Ph. Eur., USP/NF	37475.01	Serva

4.2.3 Biological materials

The channel protein genes cloned in this thesis are listed in Table 4-2. Genomic template DNA was purchased from the Leibniz Institute DSMZ-German Collection of Microorganisms and Cells. The *alkL* gene was synthesized by Eurofins Genomics (Ebersberg, Germany) with minor modifications from the original gene to introduce a standard ATG start codon and to remove NdeI and NheI restriction enzyme cleavage sites. Bacterial strains for cloning and expression can be found in Table A 8. Commercial enzymes, standards and kits are listed in Table A 9 and Table A 10. Oligonucleotides for cloning and gene sequencing are listed in Table A 29 - Table A 32. Plasmids used and generated in this thesis are summarized in Table A 33. Finally, the nucleotide sequences and the peptide sequences of the cloned genes are listed in Table A 34 - Table A 35 and Table A 36 - Table A 37. Table A 38 contains useful physicochemical properties of the proteins.

Table 4-2. Gene names, host organism, DSMZ accession (where applicable) and database accessions of the channel proteins cloned in this thesis.

Gene	Organism	Accession
alkL	*P. putida* (OCT plasmid)	GenBank: AJ245436.1; region 14924 to 15616
ompW	*E. coli* MG1655 (DSM 18039)	NCBI RefSeq: NC_000913.3; region 1314020 to 1314658
oprG	*P. aeruginosa* PAO1 (DSM 22644)	NCBI RefSeq: NC_002516.2; region 4544607 to 4545305
todX	*P. putida* F1 (DSM 6899)	GenBank: U18304.1; region 2147 to 3508
foca	*E. coli* MG1655 (DSM 18039)	NCBI RefSeq: NC_000913.3; region 953609 to 954466
oprP	*P. aeruginosa* PAO1 (DSM 22644)	NCBI RefSeq: NC_002516.2; region 3671227 to 3672549
phoE	*E. coli* MG1655 (DSM 18039)	NCBI RefSeq: NC_000913.3; region 259045 to 260100
ompF	*E. coli* MG1655 (DSM 18039)	NCBI RefSeq: NC_000913.3; region 985894 to 986982

4.2.4 Software

The software used to run particular applications is listed in the respective equipment sections in the appendix A. Software for general applications is listed in Table 4-3.

Table 4-3. Software for general applications.

Software	Application	Source
Basic Local Alignment Search Tool (BLAST)	DNA sequence alignment	http://blast.ncbi.nlm.nih.gov/Blast.cgi
GENtle	Cloning	Magnus Manske (http://gentle.magnusmanske.de)

Software	Application	Source
ImageStudio Lite Version 5.2	Densitometric image analysis	Licor Bioscience, Lincoln, NE
Magellan v6.6	MTP-photometer software	Tecan, Männedorf, Switzerland
Sigma Plot 12.3	Data analysis	Systat Software, Chicago, USA
SkanIt FC	MTP-photometer software	Thermo Fisher Scientific, Braunschweig, Germany
Zetasizer 7.01	Dynamic light scattering	Malvern Instruments, Worcestershire, UK

4.3 Molecular biological methods

4.3.1 Isolation of plasmid DNA from *Escherichia coli*

For the isolation of plasmid DNA from *E. coli*, 4 mL Terrific Broth (TB) supplemented with the appropriate antibiotics (50 mg L^{-1} ampicillin or 30 mg L^{-1} kanamycin) were inoculated with a single colony of the desired plasmid and grown overnight at 37 °C. Plasmid DNA was then isolated using the GenElute HP Plasmid Miniprep Kit according to the manufacturer's instructions.

4.3.2 Polymerase chain reaction

DNA amplification was performed by polymerase chain reaction (PCR) in a MJ Mini Thermal Cycler with Phusion High-Fidelity DNA polymerase. The reaction was performed with 0.02 U μL^{-1} DNA polymerase in 1x Phusion HF buffer with 0.2 mM desoxyribonucleotide triphosphates (dNTPs), 0.5 µM of each primer and 0.5 µL template DNA. Cycling times were chosen according to the manufacturer's instructions and the lengths of the amplicons. Annealing temperatures were chosen according to the melting temperatures of the primers calculated using the GENtle software package.

Assembly PCR was performed according to the Assembly PCR Oligo Maker instructions (http://www.yorku.ca/pjohnson/), except that Phusion High-Fidelity DNA polymerase was used as well.

4.3.3 Agarose gel electrophoresis

DNA fragments were analyzed by agarose gel electrophoresis in 1x Tris-acetate-ethylenediaminetetraacetic acid (TAE) buffer. Fragments of more than 500 bp were run on a 1 % agarose gel at 120 V for 30-45 min, for smaller fragments a 2 % agarose gel was used. DNA samples were mixed with 1/10 volume of 11x DNA loading dye to assist loading. For visualization of the DNA, the agarose gel was supplemented with Roti GelStain prior to casting, so that DNA bands were subsequently visible upon UV illumination. A 100 bp extended DNA ladder was loaded to determine the size of the fragments.

4.3.4 DNA purification

DNA purification was performed using the GenElute PCR Clean-up Kit. Alternatively, DNA was purified from excised bands after agarose gel electrophoresis using the GenElute Gel Extraction Kit. In both cases, the purification was performed using spin-protocols according to the manufacturer's instructions.

4.3.5 Restriction and ligation of DNA

PCR products and plasmids were digested with the required restriction enzymes at 37 °C for 1 h according to the manufacturer's instructions. 10 µL of PCR product or approximately 500 ng of plasmid DNA were digested in a total volume of 20 or 50 µL, respectively, with the appropriate restriction buffer and 10 U of each restriction enzyme. The digested plasmid was subsequently dephosphorylated with 5 U of Antarctic Phosphatase in 60 µL 1x Antarctic Phosphatase buffer at 37 °C for 15 min. After dephosphorylation, the phosphatase was heat-inactivated at 65 °C for 5 min. Following these procedures, DNA fragments were purified using the GenElute PCR Clean-up Kit, while plasmid DNA was first run on a gel and then purified using the GenElute Gel Extraction Kit. PCR products and plasmids were ligated using a T4 DNA Ligase or the Quick Ligation Kit according to the manufacturer's instructions.

4.3.6 Preparation of electrocompetent cells

Electrocompetent bacteria were mainly used for cloning purposes due to their superior competency. For the preparation of electrocompetent bacteria, the respective strain was grown at 37 °C in 200 mL LB medium to an optical density at 600 nm (OD_{600}) of 0.4-0.5, at which the cultivation was stopped and the cell suspension was chilled on ice for 20 min. Cells were pelleted at 3200 x g for 10 min and resuspended in 100 mL sterile, chilled 10 % v/v glycerol. After another washing step with 8 mL chilled sterile 10 % v/v glycerol, the cells were finally resuspended in 0.8 mL chilled sterile 10 % v/v glycerol, aliquoted in 20 µL batches and shock-frozen in liquid nitrogen. All centrifugation steps were performed at 2 °C. After preparation, cells were stored at -80 °C until use, but not for more than 2 months.

4.3.7 Transformation of electrocompetent cells

The electroporation of cells with DNA required an essentially salt-free DNA preparation, so ligation reactions were desalted using the GenElute PCR Clean-up Kit prior to mixing with the cells. 20 µL electrocompetent cells were thawed on ice, mixed with 2-3 µL of a desalted ligation product and transferred to an electroporation cuvette. Cells were shocked using the default exponential decay function for *E. coli* of the Electroporator GenePulser Xcell. After the pulse has been delivered, cells were immediately recovered in 800 µL sterile and pre-warmed SOC medium. After 1 h incubation at 37 °C and 600 min^{-1} in a thermomixer, the cell suspension was gently spun down in a microcentrifuge at 1000 min^{-1} for 10 min, resuspended in 200 µL of the supernatant and plated onto LB agar plates containing the respective antibiotic (30 mg L^{-1} kanamycin or 50 mg L^{-1} ampicillin). Plates were incubated at 37 °C over night.

4.3.8 Preparation of chemically competent cells

Chemically competent bacteria were primarily used for the generation of expression strains. For the preparation of chemically competent bacteria, the respective strain was grown at 37 °C in 100 mL LB medium to OD_{600} of 0.3-0.6, at which the cells were harvested at 3200 x g for 10 min and resuspended in 20 mL chilled sterile 0.1 M $CaCl_2$. After 30 min incubation on ice, the cells were centrifuged again and resuspended in 10 mL chilled sterile 0.1 M $CaCl_2$ supplemented with 10 % v/v glycerol, aliquoted in 90 µL batches and shock-frozen in liquid nitrogen. After preparation, chemically competent cells were stored at -80 °C until use.

4.3.9 Transformation of chemically competent cells

90 µL chemically competent cells were thawed on ice and mixed with 1 µL of plasmid DNA or 20 µL of a ligation product. The cells were chilled on ice for 30 min before being heat-shocked at 42 °C for 1 min in a water bath. The cells were then briefly chilled on ice before 800 µL SOC medium were added. To develop the resistant phenotype, cells were incubated for 1 h at 37 °C and 600 min^{-1} in a thermomixer. For the introduction of plasmid DNA, 200 µL of the cell suspension were directly plated onto LB agar plates containing the respective antibiotic (30 mg L^{-1} kanamycin or 50 mg L^{-1} ampicillin). For the introduction of a ligation product, the cell suspension was gently spun down in microcentrifuge at 1000 min^{-1} for 10 min, resuspended in 200 µL of the supernatant and then plated onto LB agar plates containing the respective antibiotic. Plates were incubated at 37 °C over night.

4.3.10 Colony polymerase chain reaction

Bacterial colonies were screened for the correct insert by colony polymerase chain reaction (colony PCR). The reaction was performed with 1.25 U Taq DNA polymerase in 1x ThermoPol buffer, 0.2 mM dNTPs and 0.2 µM of the T7 and T7 terminator primers (Table A 32) and a single resuspended colony. After an initial denaturation step of 10 min at 95 °C, the colony PCR was run for 30 cycles (denaturation for 30 s at 95 °C, annealing for 1 min at 55 °C and elongation for 1 min per kbp at 68 °C). A final elongation step was performed for 7 min at 68 °C.

4.3.11 DNA sequencing

DNA sequencing was performed by Eurofins Genomics and sequencing results were verified using the GENtle software package.

4.3.12 Cloning of expression constructs for channel proteins

The PHT modules for the introduction of an N-terminal His_6-tag to proteins with a cleavable leader sequence were generated by assembly PCR (primers are listed in Table A 29) according to the Assembly PCR Oligo Maker (http://www.yorku.ca/pjohnson/) and were introduced into pET21a via NdeI/BamHI (PHT1) or NdeI/HindIII (PHT2).

Expression vectors for His_6-tagged OmpF, PhoE and OprP were generated by fusing the sequences of their mature gen products with the PHT-modules. The respective genes were amplified from genomic DNA (*cf.* Table 4-2) using the primers listed in Table A 30. The *ompF* and *phoE* PCR products were digested using BamHI/HindIII and ligated with BamHI/HindIII-linearized pET21a-PHT1 to generate pET21a-PHT1-*phoE* and pET21a-PHT1-*ompF*, respectively. In analogy, the *oprP* PCR product was digested using NheI/SacI and ligated with NheI/SacI-linearized pET21a-PHT2 to generate pET21a-PHT2-*oprP*.

Expression vectors for His-tagged AlkL, FocA, OmpW, OprG and TodX were generated by C-terminal fusion with a His_6- or a His_8-tag. The respective genes were amplified from genomic DNA (*cf.* Table 4-2) using the primers listed in Table A 30. The *alkL* gene was synthesized by Eurofins Genomics, so in this case the gene was amplified from the vector pEX-A-*P. oleovorans alkL* instead. The PCR products were digested using NdeI/HindIII and ligated with NdeI/HindIII-linearized pET21a to generate pET21a-*alkL*, pET21a-*focA*, pET21a-*ompW*, pET21a-*oprG* and pET21a-*todX*, respectively (*cf.* Table A 33). The nucleotide sequences of the coding region of these constructs are listed in Table A 34, the corresponding peptide sequences in Table A 36. A His_8-tagged variant of FocA was also generated using NdeI and XhoI, resulting in pET21a-*focA*2-H8.

For the expression of AlkL, OmpW, OprG and TodX in inclusion bodies, the leader peptide was omitted to promote inclusion body formation (AlkL: ΔAA 2-27, OmpW: ΔAA 2-20, OprG: ΔAA 2-27, TodX: ΔAA 2-21, *cf.* Table A 36). The respective genes were amplified from genomic DNA (*cf.* Table 4-2) using the primers listed in Table A 31. All PCR products were digested using NdeI/HindIII and ligated with NdeI/HindIII-linearized pET21a to obtain constructs with a C-terminal His_6-tag (-IB1). His_8-tagged variants (-IB2) were subsequently created using the original forward primer and the generic primer pET28a_His8_rev (XhoI) on the subcloned genes. The nucleotide sequences of the coding regions of these constructs are listed in Table A 35, the corresponding peptide sequences in Table A 37.

4.4 Microbiological methods

4.4.1 Strain maintenance

Bacterial cultures were stored on agar plates containing the appropriate antibiotics (30 mg L^{-1} kanamycin or 50 mg L^{-1} ampicillin) at 4 °C, but not for more than 2 weeks if protein expression was intended afterwards, especially for the strain *E. coli* BL21 omp8, because older colonies did not grow in suspension anymore. For long-term storage, cryo-stocks in 25 % v/v glycerol were generated. For this purpose, 4 mL Terrific Broth (TB) supplemented with the appropriate antibiotics were inoculated with a single colony of the desired strain and grown overnight at 37 °C. After addition of sterile 60 % v/v glycerol, the cells were frozen and stored at -80 °C. All strains used in this thesis are listed in Table A 8.

4.4.2 Precultures for heterologous protein expression

A single colony was used to inoculate 50 mL TB supplemented with the appropriate antibiotics (50 mg L^{-1} ampicillin or 30 mg L^{-1} kanamycin). The preculture was grown overnight at 30 °C at 250 min^{-1} (3.5 cm excentricity). The main culture was inoculated with 5-10 mL L^{-1} of the preculture.

4.4.3 Heterologous expression of enzymes

The wild-type FDH and the FDH-KR fusion protein were expressed by *E. coli* BL21. This strain as well as the other expression strains BL21 omp8 and C43 (see chapters 4.4.4 and 4.4.5) contain the λDE3 lysogen carrying the gene for the T7 polymerase under control of the lacUV5 promoter (the λDE3 designation is omitted from here on for reasons of clarity). Expression was performed in TB medium supplemented with the appropriate antibiotics (50 mg L^{-1} ampicillin or 30 mg L^{-1} kanamycin, respectively) in 1,000 mL shake flasks with a filling volume of 200 mL. The cells were grown at 37 °C and 250 min^{-1} (3.5 cm excentricity) to an OD_{600} of 0.6-0.8 before protein expression was induced by the addition of 1 mM isopropyl-*β*-D-1-thiogalactopyranoside (IPTG) and the temperature was reduced to 20 °C. Expression was allowed to proceed for at least 16 h.

4.4.4 Heterologous expression of oligomeric channel proteins

Native channel proteins were expressed in *E. coli* BL21 omp8, an expression strain optimized for the expression of membrane proteins, and importantly, deficient of a number of major outer membrane proteins (Prilipov *et al.*, 1998). Expression was performed in TB medium supplemented with 50 mg L^{-1} ampicillin, 5 g L^{-1} glycerol, 0.5 g L^{-1} glucose and 1 g L^{-1} lactose in 1,000 mL unbaffled shake flasks with a filling volume of 200 mL. The medium composition was adopted from Gordon *et al.* (2008) due to its self-inducing properties. Accordingly, cells were grown for 1 h at 30 °C and 250 min^{-1} (3.5 cm excentricity) after inoculation and then at 20 °C for 24 h without further interference.

4.4.5 Heterologous expression of monomeric channel proteins in inclusion bodies

Truncated channel proteins were expressed in *E. coli* C43. Expression was performed in TB medium supplemented with 50 mg L^{-1} ampicillin in 1000 mL unbaffled shake flasks with a filling volume of 200 mL. For the expression of TodX, the medium was also supplemented with 1 g L^{-1} glucose and 1 mM $MgSO_4$. Cells were grown at 37 °C and 250 min^{-1} until a cell density (OD_{600}) of 0.5-0.6 was reached. Protein expression was induced by the addition of 1 mM IPTG and expression was allowed to proceed for 4 h at 37 °C and 250 min^{-1}.

4.4.6 Determination of optical density

The optical density (OD_{600}) of bacterial cultures was measured photometrically at 600 nm. Measurements exceeding an OD_{600} of 0.3 were appropriately diluted with medium.

4.4.7 Determination of cell dry weight

The cell dry weight (cdw) of bacterial cultures was determined by harvesting 1 mL aliquots of the culture in pre-weighed 1.5 mL tubes and discarding the supernatant. The pellet was dried at 80 °C over night and then weighed again.

4.4.8 Cell harvest and lysis

After protein expression, cells were harvested by centrifugation for 20 min at 3260 x g and 4 °C and then frozen at -20 °C. The cell pellets were resuspended in 5-10 mL g^{-1} (cell wet weight) lysis buffer, supplemented with 1 mM phenylmethylsulfonyl fluoride (PMSF), 1 mg g^{-1} lysozyme and 4 U g^{-1} DNAse I. The lysis buffer basically consisted of the respective binding buffer in case of enzymes and native channel proteins. The composition of lysis buffer for the isolation of inclusion bodies is listed in Table A 16. After 1 h incubation at 20 °C, cells were lysed by sonication with a Sonoplus HD 2070 equipped with a sonotrode MS73 (10 min, 0.5 s cycles, 90 % power) on ice and cleared by centrifugation at 25,400 x g for 30 min at 4 °C, except for inclusion body isolation, which is described in section 4.5.2.

4.5 Protein purification

4.5.1 Bacterial membrane enrichment and solubilization of channel proteins

Bacterial membranes were isolated using preparative ultracentrifugation of cleared cell lysate at 140,000-180,000 x g and 4 °C for 1 h. For preparative purifications, the resulting membrane pellet was detached with a glass rod after addition of 1/5 of the original volume of MP IMAC buffer A supplemented with an appropriate detergent (*cf.* Table A 14) and transferred to a 40 mL dounce homogenizer. After homogenization, the membrane suspension was incubated for 1 h at room temperature in a head-over-end shaker at 8 min^{-1} and was then cleared of non-solubilized membrane proteins by another ultracentrifugation step at 100,000 x g and 4 °C for 1 h. The cleared membrane protein extract was applied to an IMAC column for further purification.

For detergent screening experiments, the membrane pellet was resuspended in MP IMAC buffer A without any detergent and the total protein content was determined using a BCA assay. The protein concentration was adjusted to 20 g L^{-1}, 1 mM PMSF was added and the membrane extract was divided into 750 µL aliquots and stored at -80 °C until use. For solubilization, the membrane extracts were thawed on ice and mixed with an equal volume of MP IMAC buffer A supplemented with a single detergent at twice the desired concentration. The membrane suspension was incubated for 1 h at room temperature in a head-over-end shaker at 8 min^{-1} and was then cleared of non-solubilized membrane proteins by another ultracentrifugation step at 100,000 x g and 4 °C for 1 h. Detergents and their concentrations used in these screening experiments are listed in Table A 13. Usually, 400 µL of the

cleared membrane protein extracts were applied to Mobicol "Classic" 1 mL spin colums filled with 50 µL Profinity IMAC beads for further purification.

4.5.2 Isolation and solubilization of inclusion bodies

After the addition of 1/3 volume of 4x membrane extraction buffer to the cell lysate and incubation for 1 h on ice, the lysate was centrifuged at 25,400 x g for 30 min at 4 °C. The resulting pellet was resuspended in IB washing buffer I using an Ultra-Turrax (Ika, Staufen, Germany) and centrifuged again. This step was repeated twice with IB washing buffer II. The final pellet was dissolved in 18 mL IB solubilization buffer at 4 °C over night. The protein solution was cleared by centrifugation as before and applied to an IMAC column for further purification.

4.5.3 Immobilized metal affinity chromatography

Protein purification was performed on an ÄKTA Pure platform via immobilized metal affinity chromatography (IMAC) using 1 mL or 5 mL HisTrap FF columns at a flow rate of 1 or 5 mL min^{-1}, respectively. Columns were equilibrated with at least 5 column volumes (CVs) of IMAC binding buffer, supplemented with an appropriate detergent (if applicable; *cf.* Table A 11-Table A 14). After protein loading, the columns were washed with another 10 CVs of IMAC binding buffer. Proteins were eluted with a linear gradient of 0-100 % IMAC elution buffer over 20 CVs. 1 or 5 mL fractions were collected during the gradient elution and fractions containing the target protein were pooled. All solutions were filtered (0.22 µm) and purifications were performed at room temperature.

For detergent screening, all MP IMAC buffers were supplemented with the respective detergents listed in Table A 13. The clarified membrane protein extracts (400 µL per column) were applied to Mobicol "Classic" 1 mL spin colums filled with 50 µL Profinity IMAC beads equilibrated with the respective MP IMAC binding buffer. After 5 min incubation, the columns were centrifuged at 1,000 x g for 30 s at 4 °C to remove unbound protein and were washed twice with 400 µL MP IMAC washing buffer. Protein elution was achieved by the addition of 75 µL MP IMAC elution buffer, 5 min incubation and centrifugation at 1,000 x g for 1 min at 4 °C, which was repeated once more to elute all bound protein.

4.5.4 Anion exchange chromatography

Anion exchange (AEX) chromatography was performed as a concentrating step for membrane proteins or to exchange one detergent for another. Anionic detergents as well as salts had to be avoided, so all protein solutions were extensively dialyzed against AEX binding buffer containing 0.05 % w/v LDAO. Because LDAO is hardly dialyzable, the respective amount was also added directly to the protein solution inside the dialysis bag. AEX chromatography was either performed manually or on an ÄKTA Pure platform with a flow rate of 1 mL min^{-1}. The protein solution was applied to a 1 mL HiTrap Capto Q column. The column was washed with 10 CVs of AEX washing buffer and eluted with 2 CVs of AEX elution buffer in peak fractionation mode. For elution, the flow rate was lowered to 0.5 mL min^{-1}, while manual elution was paused for about 2 min after each 0.5 mL fraction.

4.5.5 Size exclusion chromatography

Size exclusion chromatography (SEC) was mainly performed as an analytical technique to assess membrane protein homogeneity or as a polishing step for applications such as circular dichroism (CD) spectroscopy or electrophysiology. SEC was performed on an Äkta Pure platform with a Superdex 200 Increase 10/300 GL column at a flow rate of 0.75 mL min^{-1}. The column was equilibrated with 10 mM sodium phosphate buffer pH 8 (for CD spectroscopy) or 20 mM Tris-HCl pH 8 (for other applications) containing 50 mM NaCl and 0.05 % w/v LDAO (or 0.03 % w/v DDM for FocA). 100-500 µL protein solution were loaded and eluted isocratically with 2 CVs buffer and 0.5 mL fractions were collected.

4.5.6 Refolding of monomeric channel proteins

Refolding conditions were screened on a 1.2 mL-scale using rapid dilution of the unfolded protein into different refolding buffers. Basically, the refolding was performed by dilution into TE buffer (20 mM Tris-HCl, 1 mM EDTA) at pH 8, except for OmpW, which was folded at pH 9. TE buffer was supplemented with various detergents (*cf.* Table A 13) and an optional folding additive (*cf.* Table A 20). If not stated otherwise, the proteins were diluted 8.5-25-fold, starting from protein stock solutions of 2.5-9.5 g L^{-1}. However, the protein concentrations of OmpW, OprG and TodX were successively increased in between experiments (for clarity, the exact protein concentration is indicated in the respective figure legend). For higher dilutions, the proteins were previously diluted with IB IMAC buffer A. To achieve rapid mixing of the protein solution and the refolding buffer, the latter was quickly added to the protein solution, which was at the bottom of a 4 mL glass vial, at one dash using a pipette. Afterwards the reaction mixture was stirred for at least 30 min at 200 min^{-1} with cross-shaped magnetic stirrers at room temperature (*cf.* Figure 4-1).

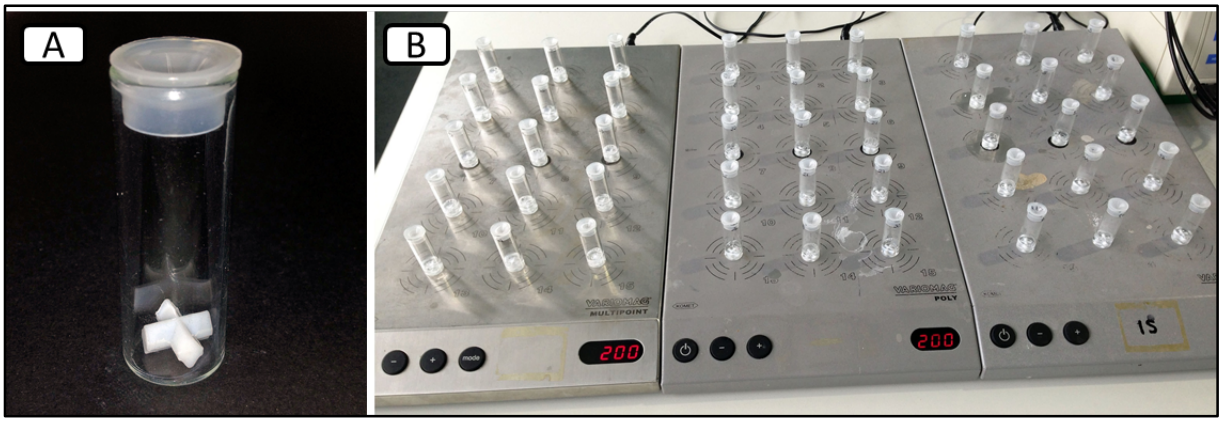

Figure 4-1. Setup for 1.2 mL scale refolding. (A) 4 mL glass vial with cross-shaped stirrer and (B) typical array of refolding reactions on multipoint stirrer plates.

Larger-scale refolding was performed in the bioREACTOR 48 system using unbaffled polystyrene reactors with a working volume of 10 mL. Temperature control of the refolding buffer was realized with a heat exchanger integrated into the reactor block. The lid of the reactor block was equipped with

apertures to comply with the use of a liquid handler (Weuster-Botz *et al.*, 2005). The refolding buffer (*cf.* Table A 21) was stirred at 500 rpm using an S-shaped stirrer (Riedlberger *et al.*, 2012) while the protein solution (3 g L^{-1}) was continuously or intermittently added with a commercial dosage pump or a liquid handler. Feeding rates were 16 µL min^{-1} with the dosage pump and 2 or 10 µL min^{-1} in 10 µL-steps with the liquid handler. The folding reaction was routinely performed overnight.

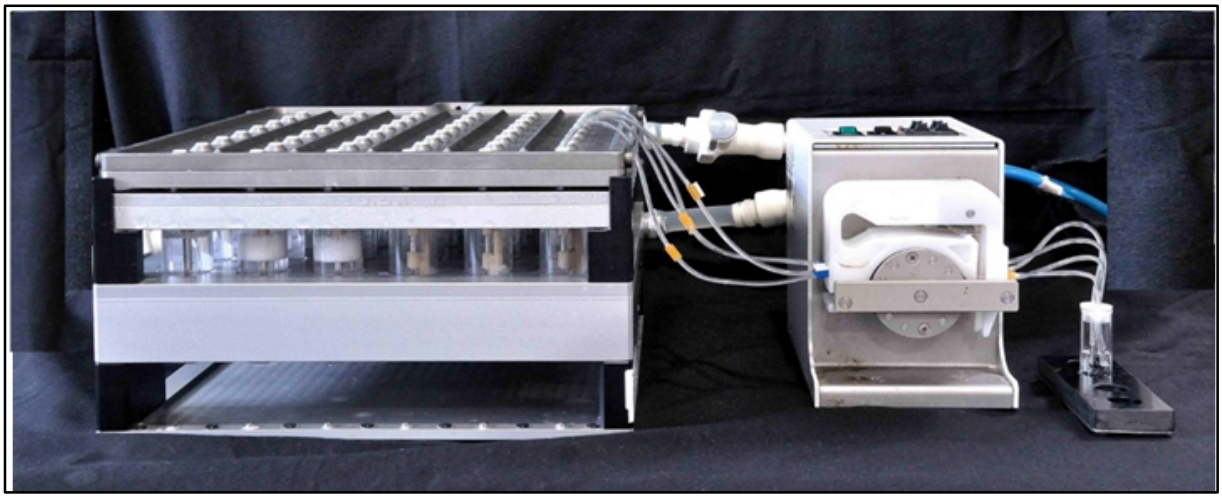

Figure 4-2 bioREACTOR 48-based refolding with a peristaltic pump.

4.5.7 Dialysis

Dialysis was used as a means of exchanging buffer components and, most importantly, to remove excess detergent, folding additives and guanidine-HCl from refolded proteins. The latter compound was able to precipitate SDS and needed to be removed in order to analyze protein folding by semi-native SDS-PAGE. For analytical purposes, 600 µL of the protein preparation were dialyzed against 30 volumes of TE buffer supplemented with the respective detergent at twice the CMC at 4 °C overnight. Small-scale dialysis was performed in custom-made high-density polyethylene dialysis chambers equipped with a 14 kDa T4 dialysis membrane.

Preparative dialysis was performed in a 14 kDa T4 dialysis bag against at least 100 volumes of stirred buffer at 4 °C over night.

4.5.8 Concentration of proteins

Proteins were concentrated using Amicon Ultra centrifugal filter devices with various cut-offs. AlkL, OmpW, OprG and TodX were concentrated using filters with a 10,000 MMCO; FDH_{wt}, OmpF, OprP and PhoE were concentrated using filters with a 30,000 MMCO and FocA as well as the FDH-KR fusion protein were concentrated using filters with a 100,000 MMCO. Concentration of the proteins was achieved by centrifuging the devices at 4 °C and at no more than 3,000 x g for a certain period until the

desired concentration was reached. Generally, the membrane protein solutions needed to be mixed after about 15 min to avoid aggregation near the membrane.

4.5.9 Storage of proteins

Proteins were stored at 4 °C in their respective buffers. FDH-KR was stored in PBS pH 7.5 at concentrations above 1 g L^{-1}, while membrane proteins were always stored in buffer containing an appropriate detergent at a concentration above the CMC.

4.6 Protein analytics

4.6.1 Determination of protein concentrations

Channel protein concentrations were primarily determined by their absorbance at 280 nm using quartz cuvettes or the Eppendorf µCuvette G 1.0 according to the Lambert-Beer-law (Equation 4-1) with molar extinction coefficients ε listed in Table A 38. Measurements were always blanked against the respective storage buffer of the protein.

$$c_{Protein} = \frac{A_{280}}{\varepsilon \cdot d} \qquad \text{Equation 4-1}$$

Alternatively, protein concentrations were determined using the bicinchoninic acid (BCA) Assay Kit according to the manufacturer's instructions. Bovine serum albumin served as reference protein. For the evaluation of membrane protein solubilization with different detergents, the respective elution buffer containing the detergent served as a blank.

4.6.2 Sodium dodecyl sulfate polyacrylamide gel electrophoresis

Protein folding was assessed by semi-native sodium dodecyl sulfate polyacrylamide gel electrophoresis (SDS-PAGE) (Noinaj *et al.*, 2015). This technique is based on an important characteristic of many outer membrane proteins called heat-modifiability. Because of the stability of the barrel, the proteins retain their high content of β-structure in the presence of SDS below a certain temperature and thus appear more compact and migrate faster through the gel. Only after denaturation at high temperatures do they lose their native structure and migrate according to their true molecular mass (Inouye and Yee, 1973, Nakamura and Mizushima, 1976, Ohnishi *et al.*, 1998). A representative SDS-PAGE showing both the native and the denatured form of a monomeric outer membrane protein is shown in Figure 4-3. Because of the ease of distinction between the folded and the unfolded species, this method is considered a standard technique to assess outer membrane protein folding (Burgess *et al.*, 2008). Similarly, the oligomeric state of the trimeric channel proteins OmpF, OprP and PhoE could be determined because the native trimer runs much slower than the monomers. Refolded or solubilized proteins were mixed with an equal amount of 2x Laemmli buffer, incubated at 37 °C for 15 min and loaded on polyacrylamide gels. For most applications, a 13.5 % resolving gel and a 4 % stacking gel was used (*cf.* Table A 22).

Polymerization of the polyacrylamide was induced by the addition of 50 µL 10 % w/v ammonium persulfate (APS) and 5 µL tetramethylethylenediamine (TEMED) per gel. For denaturing SDS-PAGE, protein samples were incubated with 1x Laemmli buffer for 5 min at 99 °C prior to loading, but channel proteins were denatured for at least 15 min. SDS-PAGE was performed in Rotiphorese 1x SDS-PAGE buffer at 40 mA per gel and max. 300 V for 50-60 min.

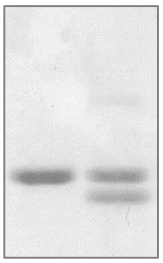

Figure 4-3. Semi-native SDS-PAGE of a monomeric outer membrane protein. The left sample was denatured for 15 min at 99 °C, the right sample was incubated at 37 °C. The lower band represents the folded and the upper the unfolded form of the protein.

4.6.3 Blue native polyacrylamide gel electrophoresis

Blue native polyacrylamide gel electrophoresis (BN-PAGE) (Schagger *et al.*, 1994, Wittig *et al.*, 2006) was performed to assess the oligomeric state of FocA after solubilization with different detergents. Protein samples were mixed with 1/10 volume of 10x sample loading buffer and applied to a TG PRiME 4-20 % precast gel. The composition of BN-PAGE buffers is given in Table A 23. Electrophoresis was performed in a cold room at 100 V for 15 min and then at 300 V for 4 h. Bovine serum albumin (BSA), yeast alcohol dehydrogenase (ADH) and β-Amylase were used as reference proteins.

4.6.4 Coomassie staining and densitometry

Polyacrylamide gels were stained according to Fairbanks *et al.* (1971). The gels were boiled successively in Fairbanks' solutions A, B and C (*cf.* Table A 24) with intervening incubation times of 5 min at a gentle agitation. Afterwards, the gels were digitalized by scanning or photography. Densitometry was performed using ImageStudio Lite (Version 5.2) and folding efficiency was defined as the intensity of the native protein band divided by the sum of the intensities of the native and aggregated/denatured protein bands. The oligomeric content of native protein preparations was assessed analogously.

$$\text{Fraction folded} = \frac{Intensity_{native}}{Intensity_{native} + Intensity_{denatured}} \cdot 100\% \qquad \text{Equation 4-2}$$

4.6.5 Circular dichroism spectroscopy

Circular dichroism (CD) spectra were recorded on a Jasco J-815 spectrophotometer in a 0.5 mm quartz cuvette. Ten spectra were accumulated per measurement, using a data pitch of 0.1 nm, a scan speed of

100 nm min^{-1}, 1 nm slit width and a response time of 1 s. Proteins were purified by size-exclusion chromatography prior to analysis and protein concentrations were kept between 0.1 and 0.4 g L^{-1}. Protein spectra were corrected for the buffer spectrum (10 mM sodium phosphate pH 8 containing 50 mM NaCl and 0.05 % w/v LDAO or 0.03 % w/v DDM).

4.6.6 Determination of the thermal stability of channel proteins

To assess protein stability, samples were incubated at various temperatures from 20-99 °C for 30 min before semi-native SDS-PAGE. After electrophoresis and densitometric analysis, stability data were fit to a sigmoidal curve of the form displayed below using nonlinear regression with GraphPad Prism.

$$\text{Fraction folded} = \frac{100}{1 + 10^{((T_m - T) * Hill\ slope)}} \qquad \text{Equation 4-3}$$

With T_m Melting temperature, °C

T Temperature, °C

Because the protein stability was analyzed based on incompletely folded samples, the initial fraction of folded protein at 20 °C incubation was used as a reference for this sort of analysis.

4.6.7 Protease resistance of channel proteins

To assess the protease resistance of channel proteins, 1 g L^{-1} of the respective protein was incubated with 0.1 g L^{-1} ptrypsin at 37 °C for 2 h and then analyzed by semi-native SDS-PAGE.

4.6.8 Electrophysiology

Electrophysiological experiments were performed at the Chair of Systems Biophysics and Bionanotechnology (TUM). The activity of refolded and SEC-purified channel protein OprG was checked by observing its ability to allow K^+ ions to pass through a lipid bilayer. The flow of ions caused by insertion of the protein channel was recorded as an increase in current (ΔI) which is dependent on the applied voltage. The Orbit mini system from Nanion technologies was employed, which is based on the painted bilayer technique on a MECA recording chip containing a 2 x 2 array of circular microcavities in a highly inert polymer. Each cavity contains an individual integrated Ag/AgCl microelectrode. The bilayer was formed by painting with 1,2-diphytanoyl-*sn*-glycero-3-phosphocholine (DPhPC) dissolved in octane at a concentration of 1 g L^{-1}. About 0.6 mg L^{-1} of the refolded protein were added to the *cis* chamber of a bilayer-sealed chip. The voltage across the bilayer was periodically changed to assist protein insertion and to determine the conductance of a single channel. The signal was recorded using a Dagan PC one patch clamp amplifier, GePulse software and a 3k low pass Bessel filter. Further data processing was performed using Matlab. In order to deduce a single channel conductance, ΔI was divided by the applied voltage. The mean conductance values were obtained by fitting the histograms with a sum of two Gaussians. The conductance G of a single protein channel was obtained from the

distance between the histogram peaks. Electrical recordings with detergent solution only were made to ensure that the increase in current is due to protein insertion and not due to surfactant-mediated pores in the bilayer.

The activity of purified FocA was checked in a similar fashion, but with a classical vertical black lipid membrane (BLM) setup, consisting of a home-made measurement chamber with a central 0.2 mm aperture in a Teflon support between two buffer-filled compartments. Due to the anion-selectivity of FocA, salt-bridged Ag/AgCl electrodes (embedded in a 3 M KCl / 1.5 % agarose matrix) were used. The aperture was prepainted with 1 µL of 2 % v/v *n*-hexadecane in *n*-heptane and dried under vacuum. Afterwards, both compartments were filled with 40 mM sodium formate. The bilayer was formed by the classical Montal-Mueller technique. First, 1 µL 1,2-diphytanoyl-*sn*-glycero-3-phosphocholine (DPhPC), 1-palmitoyl-2-oleoyl-*sn*-glycero-3-phosphocholine (POPC) or a 1:2 mixture thereof dissolved in pentane at a concentration of 5 g L^{-1} was added to the surface of the *cis* compartment. After about 5 min to evaporate the pentane, the fluid level was lowered below the aperture, creating a lipid monolayer. By raising the fluid level once more, a bilayer forms. About 3 mg L^{-1} of the SEC-purified protein were added to the *cis* side of the bilayer-sealed chamber at a holding potential of 100 mV. The signal was recorded using an Axopatch 200B amplifier, a home-made Matlab measurement script and a 10k low pass Bessel filter.

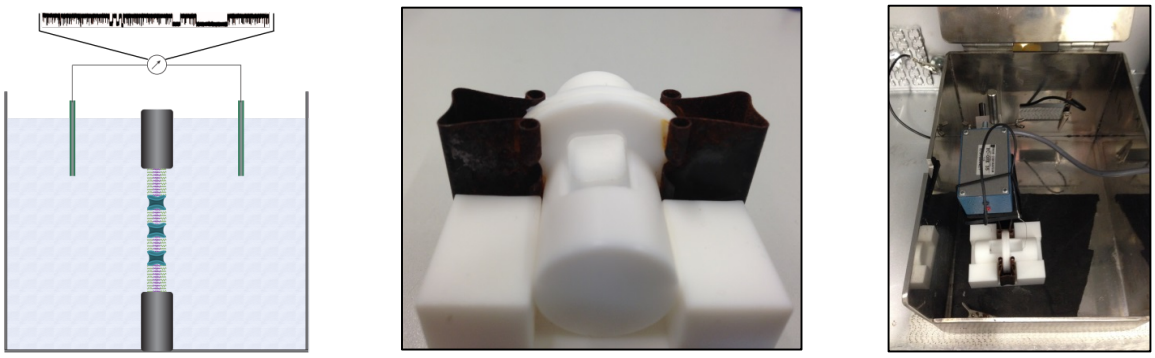

Figure 4-4. Classical BLM setup for the analysis of FocA. The left image shows a schematic illustration of the setup with electrodes on both sides of the membrane and inserted channel proteins. The middle image shows the measurement chamber with the Teflon aperture clamped in between both compartments. The right image depicts the faraday cage with the measurement chamber and the signal converter.

4.7 Gas chromatographic analytics

4.7.1 Sample preparation

Because chiral columns are easily damaged by water, the analytes were extracted from the aqueous phase with ethyl acetate. Samples containing enzymes or whole cells were extracted directly in the reaction vial by adding 167 µL of ice-cold ethyl acetate (containing 10.8 mM acetophenone as an

internal standard) to 500 µL of sample and vortexing briefly to inactivate the enzyme. Samples were then stored on ice until they were extracted for 10 min in a mixer mill at 1,500 min^{-1} at room temperature and phase separated in a centrifuge at 3,250 x g for 10 min. For gas chromatographic analyses, 33 µL of the organic phase were diluted with 66 µL ethyl acetate dried with potassium carbonate, resulting in a final concentration of 3.6 mM of the internal standard.

Polymersome suspensions could not be extracted directly because even the presence of traces of polymersomes resulted in an emulsion that could not be phase-separated. Therefore, a strategy was devised to remove the polymersomes before extraction. To this end, 500 µL of the polymersome suspension were transferred to Amicon Ultra-0.5 centrifugal filter units with a 100,000 MMCO. These were then centrifuged for 1 h at 10 °C and 5,000 x g and 420 µL of the permeate were extracted with 140 µL ethyl acetate containing 10.8 mM acetophenone and diluted as described above.

Recycling of the centrifugal filter units was achieved by first rinsing and then centrifuging the filters with ddH_2O, incubating them in 70 % ethanol for 1 h and finally storing them in 20 % ethanol.

4.7.2 Detection of 2',3',4',5',6'-pentafluoroacetophenone and 1-(2',3',4',5',6'-pentafluorophenyl)ethanol

The analysis of the substrate 2',3',4',5',6'-pentafluoroacetophenone (PFAP) and the product (1*S*)-(2',3',4',5',6'-pentafluorophenyl)ethanol *(S)*-PFE) was performed on a Varian CP-3800 gas chromatograph equipped with a chiral BGB-174 column. Injector and detector were always kept at 250 °C. The split was set to 20 before 0.01 and after 1 min. To account for variation during the sample preparation, an internal standard of 3.6 mM acetophenone (after dilution with dried ethyl acetate) was present in every sample. Analyte concentrations were determined from a standard curve with known PFAP or *(S)*-PFE concentrations in the range of 0-5 mM. For centrifugal filter unit permeate samples, a separate standard curve was prepared. The analytes were separated according to the method of Havel and Weuster-Botz (Havel and Weuster-Botz, 2007) with minor modifications:

Sample injection	5 µL, Split 50
Column flow	5 mL min^{-1} Helium
Temperature profile	80-100 °C at 1 °C min^{-1}, 2 min isothermal; 100-150 °C at 15 °C min^{-1}, 2 min isothermal
Retention times	PFAP 10.7 min; acetophenone 11.9 min; *(S)*-PFE 20.8 min

The (R)-enantiomer was not detected in any experiment. The usual product concentrations achieved with nano-scale enzyme membrane reactors were too low for a proper assessment of the enantiomeric access. However, in experiments with whole cells or purified enzyme, the enantiomeric access was always >99 % (as assessed by the limit of detection).

4.7.3 Determination of the maximal solubility of 2',3',4',5',6'-pentafluoroacetophenone

The maximal solubility of PFAP in PBS pH 7.5 was determined by adding a large excess of PFAP to the buffer, resulting in a two-phase system. The system was mixed thoroughly for 30 min in a mixer mill at 1,500 min^{-1} at room temperature and then phase-separated in a centrifuge at 3250 x g for 10 min. 500 µL of the aqueous phase were then extracted as described in chapter 4.7.1.

4.8 Enzyme characterization

4.8.1 Photometric determination of enzyme activities

During the reduction of ketones catalyzed by the ketoreductase, the cofactor NADPH is oxidized to $NADP^+$, while the cofactor regenerating enzyme (a mutant FDH derived from *M. vaccae*) is again reducing the $NADP^+$ to NADPH. The ensuing change in the absorbance at 340 nm can be followed photometrically. The reactions were carried out in PBS pH 7.5 at 25 °C in transparent 96 well plates as soon as the target temperature was reached, usually after 5 min equilibration. Specific enzyme activities were derived from the photometric data by applying the Lambert-Beer-law (Equation 4-4).

$$v = \frac{\Delta c_{NAD(P)H}}{\Delta t \cdot c_{Protein}} = \frac{\Delta A_{340} \cdot 10^6}{\Delta t \cdot \varepsilon_{NAD(P)H} \cdot d \cdot c_{Protein}} \qquad \text{Equation 4-4}$$

With

v	Reaction rate, U mg^{-1}
$\frac{\Delta c_{NAD(P)H}}{\Delta t}$	Change of NAD(P)H concentration over time, µM min^{-1}
$c_{Protein}$	Protein concentration, mg L^{-1}
$\frac{\Delta A_{340}}{\Delta t}$	Change of absorbance at 340 nm over time, min^{-1}
$\varepsilon_{NAD(P)H}$	Molar extinction coefficient of NADPH, 6,220 L mol^{-1} cm^{-1}
d	Layer thickness, cm (0.6 cm for 200 µL reaction volume)

When specific activities of whole-cell biocatalysts were determined, the protein concentration in Equation 4-4 was replaced by the cell dry weight concentration.

4.8.2 Determination of enzyme kinetics

Enzyme kinetics were determined by measuring initial reaction rates. Both the reactions of FDH and KR are in fact two-substrate reactions, so in order to ensure applicability of the Michaelis-Menten relationship, one of the two substrates had to be kept in excess. With this constraint, the enzyme activity with respect to the other substrate was determined using classical Michaelis-Menten kinetics (Bisswanger, 2000) according to Equation 3-2. Kinetic parameters were determined by non-linear regression using a least square fit with SigmaPlot 12.8. The FDH reaction was analyzed photometrically at a protein concentration of 50 mg L^{-1} FDH-KR. The KR reaction was analyzed by gas chromatography

at a protein concentration of 10 mg L^{-1} FDH-KR. According to Hölsch (2009), the activity of the KR was proportional to its concentration up to concentrations of 125 mg L^{-1}. The protein concentration was corrected for the densitometrically determined purity of the enzyme (85 %). For reasons of comparability with the single enzymes, specific activities were calculated for the respective part of the enzyme, which means that enzyme concentrations used for the calculation were corrected by a factor of 0.65 for the FDH part and 0.35 for the KR part.

Ideally, enzyme kinetics are analyzed at substrate concentrations ranging from 0.2-5 $\cdot K_M$ with several concentrations above and below the half-saturation concentration (Segel, 1996) and at least 10 concentrations in total. The concentration of the excess substrate was kept above $10 \cdot K_M$, if possible. The reaction rate at this excess of substrate is still only about 90 % of the maximal reaction rate at an infinite substrate excess (Bisswanger, 2000), so specific activities were multiplied by an appropriate correction factor to maintain comparability of enzyme kinetics determined with varying excess of the second substrate. The correction factor could be deduced from the non-linear regression of activity data generated with the other substrate in excess. This was particularly important for the analysis of the KR reaction with an excess of PFAP, since that substrate had a limited solubility of 6 mM in buffer. Another correction for the concentration-dependent activity of the KR was taken into account using Equation 8-2.

For the analysis of the FDH activity, samples were equilibrated for 5 min before measurements were started by the addition of substrate or cosubstrate. Measurements were performed photometrically at 25 °C without agitation. Due to the limited solubility of the substrate PFAP, samples for GC analysis were equilibrated with PFAP for at least 1 h in GC vials at 25 °C and 600 min^{-1} and the reaction was started by the addition of cosubstrate or enzyme. The duration of the reaction before samples were extracted was chosen to be within the linear range in an iterative fashion.

4.8.3 Selection of optimal buffer conditions

For the assessment of suitable buffer conditions for the reaction system, freshly purified FDH-KR was dialyzed against one of the following buffers at a concentration of 0.5 g L^{-1}: 0.1 M sodium phosphate (pH 7, 7.5 and 8), PBS (pH 7, 7.5 and 8), 0.1 M 3-(*N*-morpholino)propanesulfonic acid (MOPS; pH 6.5, 7 and 7.5) and 0.1 M *N*-Tris-(hydroxymethyl)-methyl-glycine (Tricine; pH 7.5, 8 and 8.5). After one week, the relative activity of both enzyme parts was determined photometrically in the respective buffers according to section 4.8.1. The FDH activity was determined at 50 mg L^{-1} with 1 M formate and 4 mM $NADP^+$, the KR activity was determined at 100 mg L^{-1} with 3 mM PFAP and 2 mM NADPH. The latter reaction was carried out in a volume of 100 µL to account for the high NADPH concentration.

4.8.4 Determination of enzyme stability

Due to the long reaction times needed to investigate the nano-scale enzyme membrane reactors, the stability of the FDH-KR fusion enzyme was an important factor. Experimentally, the inactivation of the fusion enzyme was investigated at 25 °C with 0.8 g L^{-1} of the fusion enzyme and 0, 1 or 6 mM PFAP

with or without 1 M formate in PBS pH 7.5. Enzyme activities were measured over a period of 96 h. FDH activities were determined photometrically according to section 4.8.1 at a fusion protein concentration of 40 mg L^{-1} with 5 mM $NADP^+$ and 1 M formate. KR activities were determined by gas chromatography at a fusion protein concentration of 40 mg L^{-1} with 5 mM NADPH and 4 mM PFAP after 30 min at 25 °C and 600 min^{-1}. Determination of the inactivation constant k_{inact} was performed by non-linear regression using Equation 3-5. The half-life τ was then obtained from the inactivation constant k_{inact} using Equation 3-6.

4.9 Polymersome production and characterization

4.9.1 Polymersome production

Polymersomes were prepared in the bioREACTOR 48 system according to the method described by Poschenrieder *et al*., which yields particles with a narrow, monomodal size distribution in a single step. The average aggregation number of these particles has been determined to be 43,000 polymer units per polymersome (Poschenrieder *et al.*, 2016). 0.6 mL of a filtered solution (0.2 µm) of 20 % $PMOXA_{15}$-$PDMS_{68}$-$PMOXA_{15}$ polymer in ethanol (99.8 %) were injected into 11.4 mL of the solution to be encapsulated in a stirred tank reactor at 4,000 rpm with an S-type stirrer for 1 h at room temperature to yield a 1 % w/v polymersome dispersion. Higher concentrations, for example for a subsequent size exclusion purification, were achieved by concentrating the polymersome dispersion using Amicon Ultra centrifugal filter devices with a 100,000 MMCO at no more than 3,000 x g. When enzymes or $NADP^+$/NADPH were encapsulated, all steps were performed at 4 °C. For the production of the final nano-scale enzyme membrane reactors, 4.5 mM $NADP^+$ and 0.60 g L^{-1} FDH-KR in PBS pH 7.5 were encapsulated during 2.5 h at 4 °C.

4.9.2 Extrusion of polymersomes

Polymersomes were usually used without further particle size distribution refinement. However, for the permeability assay polymersomes were extruded to yield a highly homogeneous polymersome dispersion. Extrusion was achieved by successively forcing the polymersome suspension through 1.2, 0.4 and 0.2 µm Isopore polycarbonate membranes supported by a Swinnex filter holder for use with a syringe.

4.9.3 Dynamic light scattering

The particle sizes of polymersome dispersions were determined using dynamic light scattering (DLS) on a ZetaSizer Nano-S. Light scattering was measured at an angle of 173 ° with 500 µL of a 0.05-0.1 % w/v polymersome suspension in standard half micro cuvettes. Each measurement was performed at 25 °C with 10 accumulations and automatic determination of the measurement position and attenuation at least in triplicate. Samples of enzyme-containing preparations out of the reactor that had not been

processed further had to be centrifuged at 16,200 x g for 5 min at room temperature due to occasional enzyme aggregates.

The polymersomes used in this thesis were usually of a monomodal particle size distribution with a polydispersity index (PDI) ≤ 0.25, an intensity-based mean hydrodynamic diameter (z-average) of 170 nm and a number-based mean diameter (d_N) around 100 nm.

4.9.4 Polymersome concentration measurements

The concentration of a polymersome preparation was determined via absorbance at 340 nm against a standard of polymersomes (0.1-1% w/v) prepared in buffer by applying a second-order polynomial fit. Samples exceeding a concentration of 1 % w/v were diluted accordingly.

4.9.5 Polymersome purification

Polymersomes were separated from non-encapsulated molecules or non-integrated channel proteins by size exclusion chromatography (SEC). Small-scale purifications were performed on 2.5 or 12.5 mL laboratory columns packed with Sepharose 4B by gravitational flow. 100-200 or 500-1,000 µL sample, respectively, were applied on the top frit of the column. Once the liquid had passed through, 1.5 CVs of buffer, usually PBS, were added in 200 or 500 µL increments, respectively, and fractions were collected using microcentrifuge tubes. Polymersome-containing fractions were identified by their absorbance at 340 nm and pooled afterwards.

Larger-scale purification of volumes up to 10 mL was performed on an Äkta Pure platform with a 25x500 mm preparative column packed with 140 mL Sepharose 4B at a flow rate of 1 mL min^{-1}. All solutions were filtered (0.22 µm) before they were used.

Due to problems with an incomplete removal of FDH_{wt} or FDH-KR by SEC, polymersome preparations containing these enzymes were first treated with 250 mg L^{-1} proteinase K (+1 mM $CaCl_2$) at 4 °C for at least 1 h at 80 min^{-1} after their production (while still in the stirred tank reactors) and were then centrifuged at 4,200 x g for 20 min to remove larger aggregates before being further purified.

4.9.6 Determination of enzyme loading of polymersomes and whole cells

Enzyme loading of purified polymersomes was assessed based on a photometric FDH assay. To this end, polymersomes were disintegrated by the addition of 1 % w/v *n*-octylpolyoxyethylene (O-POE) and the FDH activity was determined with 4.5 mM $NAD(P)^+$ and 400 mM formate at 30 °C by following the absorbance at 340 nm. The concentration of encapsulated enzyme was obtained by comparison with an enzyme standard, which also contained 1 % w/v O-POE. To account for incompletely removed non-encapsulated enzyme, the activity of intact polymersomes was used for correction. Due to the dissociation of the KR part of the fusion enzyme at low concentrations, the KR activity could not be determined independently in polymersomes. The enzyme content of whole cells was determined analogously, but without correcting for the activity of unlyzed cells.

The (absolute) encapsulation efficiency was defined as the enzyme concentration of a 1 % w/v polymersome suspension $E_{encapsulated}$ with regard to the initially applied enzyme concentration $E_{applied}$ (Equation 4-5):

$$Encapsulation\ efficiency = \frac{E_{encapsulated}}{E_{applied}} \cdot 100\% \qquad \text{Equation 4-5}$$

Furthermore, the statistical encapsulation efficiency defines the observed encapsulation efficiency with regard to the theoretically expected encapsulation efficiency if no interaction between the polymer and the protein occurs (*cf.* Equation 4-6). If $E_{inside} = E_{applied}$, the statistical encapsulation would be 100 %.

$$Statistical\ encapsulation\ efficiency = \frac{E_{encapsulated} \cdot V_{total}}{E_{applied} \cdot V_i} \cdot 100\% \qquad \text{Equation 4-6}$$

A 1 % w/v polymersome suspension with a mean particle diameter d_N of 100 nm, a membrane thickness d_M of 14 nm and an aggregation number N_{Agg} of 43,000 (Poschenrieder *et al.*, 2016) would encapsulate 0.36 % of the total volume according to Equation 4-7. The number of polymersomes per volume $N_{Polymersomes}$ was estimated from the concentration of the polymer, the molecular mass (MM) of the polymer (7600 g mol^{-1}), N_{Agg} and the Avogadro constant N_A according to Equation 4-8. Furthermore, the internal volume of 1 polymersome $V_{i,\ 1\ Polymersome}$ can be calculated from the given information according to Equation 4-9.

$$V_i = N_{Polymersomes} \cdot V_{i,1\ Polymersome} \qquad \text{Equation 4-7}$$

$$N_{Polymersomes} = \frac{c_{Polymer} \cdot N_A}{MM_{Polymer} \cdot N_{Agg}} \qquad \text{Equation 4-8}$$

$$V_{i,1\ Polymersome} = \frac{4}{3} \cdot \pi \cdot (d_N/2 - d_M)^3 \qquad \text{Equation 4-9}$$

4.9.7 Channel protein reconstitution

Channel proteins were reconstituted into the polymer membrane after polymersome production at a molar ratio of 1:1000-1:100. Usually, channel proteins were reconstituted at a polymersome concentration of 2 % w/v. The volumetric ratio of protein stock to polymersome dispersion was always kept below 10 % to avoid damaging concentrations of the detergents contained. Since the reconstitution of membrane proteins is a non-equilibrium process due to dilution of the detergent necessary to stabilize the protein in solution, a proper mixing is essential. To achieve rapid mixing of the protein stock solution and the polymersome dispersion, the latter was quickly added to the protein solution, which was at the bottom of a microcentrifuge tube, at one dash using a pipette. The mixture was incubated for 30-60 min at 30 °C under agitation in a thermo shaker at 800 min^{-1}, centrifuged for 10 min at 4 °C and 5,000 x g and then SEC-purified.

Quantification of the reconstituted channels was achieved by densitometry. Routinely, 400 µL of a 0.3 % w/v polymersome suspension with reconstituted channel proteins were ultracentrifuged at 125,000 and 4 °C for 60 min. At 180,000 x g, 30 min of centrifugation were sufficient for pelleting the polymersomes. The pelleted polymersomes were resuspended in 80 µL 1x Laemmli and samples were denatured for 15 min at 99 °C, except for FocA-containing samples, which were only treated at 37 °C to avoid total precipitation of the protein. Protein concentrations were calculated after SDS-PAGE and densitometry by comparison with a standard of Perfect Protein Marker (0.2-1 µg of each marker protein per lane, 0.4-2 µg of the 50 kDa marker protein) on the same gel. For a more precise quantification, the 25, 35 and 50 kDa marker protein bands were used for quantification. To calculate the number of channels per polymersome, the channel protein concentration in the sample was then correlated to the number of polymersomes per volume according to Equation 4-8.

4.9.8 Permeability assay

The permeability of the $PMOXA_{15}$-$PDMS_{68}$-$PMOXA_{15}$ polymer membrane towards formate as well as $NADP^+$ was determined by measuring the influx of the substance into empty plain polymersomes or empty polymersomes functionalized with a channel protein. The principle of the assay is outlined in Figure 4-5. Empty and extruded polymersomes with or without reconstituted channel proteins in PBS pH 7.5 at a final concentration of 1 % w/v were mixed with 200 mM formate or 20 mM $NADP^+$ and were incubated for up to 30 h at 25 °C. Immediately after mixing and at certain intervals afterwards, 200 µL samples were taken and SEC-purified on 2.5 mL lab columns as described in section 4.9.5 to remove free formate/$NADP^+$. The polymersome-containing fractions were pooled, disintegrated with 1 % O-POE and the concentration of formate was determined using an FDH assay, while the concentration of $NADP^+$ was determined by measuring the absorbance at 260 nm. For quantification, a standard of 0.004-0.250 mM formate or 0.0003-0.0200 mM $NADP^+$ was spiked into the first sample taken directly after mixing. For determination of the formate concentration, the polymersome samples were mixed with 1 % O-POE, 1.4 mM NAD^+ and 0.25 g L^{-1} FDH_{wt} in a pre-chilled 96 well plate to avoid a premature reaction start (the subsequent addition of one component to start the reaction was not feasible under the circumstances). After a brief equilibration to 30 °C, the reduction of NAD^+ to NADH was followed photometrically and the formate concentration in the polymersome samples was calculated from the kinetics of the absorbance at 340 nm.

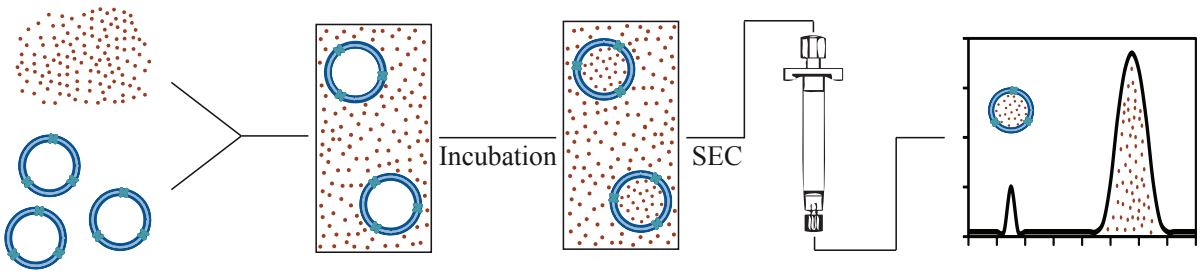

Figure 4-5. Principle of the permeability assay with polymersomes.

The kinetics of the passive diffusion of formate/$NADP^+$ into spherical vesicles can be described by the dimensionless acceptor number $AC_{vesicle}$, which is defined as follows:

$$AC_{vesicle} = \frac{c_A}{c_{eq}} \qquad \text{Equation 4-10}$$

With
c_A Concentration in the acceptor phase, mol cm^{-3}
c_{eq} Equilibrium concentration, mol cm^{-3}

Under the condition that the concentration inside the vesicles cannot be greater than c_{eq}, it holds that:

$$0 \leq AC_{vesicle} \leq 1 \qquad \text{Equation 4-11}$$

The formate/$NADP^+$ concentrations in the samples could also be used to calculate the permeability Pe according to Equation 4-12 (Avdeef, 2012).

$$Pe = -\frac{V_A \cdot V_D}{(V_A + V_D) \cdot A \cdot t} \cdot \ln\left(1 - \frac{c_A}{c_{eq}}\right) \qquad \text{Equation 4-12}$$

With
Pe Permeability, cm s^{-1}
V_A Total volume of the acceptor phase, cm^3
V_D Total volume of the donor phase, cm^3
A Total surface area of the polymer membrane, cm^2
t incubation time, s

V_A is the sum of the inner volume of all polymersomes present in the sample analogous to V_i. The inner volume of a single polymersome of $1.96 \cdot 10^{-16}$ cm^3 was calculated from the number-based mean diameter d_P of 100 nm and the membrane thickness d_M of 14 nm (Poschenrieder *et al.*, 2016). With a 1 % w/v polymersome suspension and a total sample volume of $2 \cdot 10^{-1}$ cm^3, $V_{A,}$ derived from the inner polymersome diameter, was equal to $7.23 \cdot 10^{-4}$ cm^3. The membrane itself occupied a volume of $1.21 \cdot 10^{-3}$ cm^3. V_D was calculated by subtracting the total volume of all polymersomes (V_A+$V_{membrane}$) from the total sample volume and amounted to $1.98 \cdot 10^{-1}$ cm^3. The total outer surface area of the polymersomes was 1,160 cm^2. The formate concentration in the acceptor phase was calculated by dividing the measured formate concentration in the sample by V_A/V_{total}. The equilibrium concentration c_{eq} was determined according to Equation 4-13, assuming that no significant membrane retention occurred, and amounted to 201.22 mM. Due to the volume occupied by the polymersomes, the initial concentration in the donor phase c_D amounted to 201.95 mM.

$$c_{eq} = \frac{c_D \cdot V_D}{V_A + V_D} \qquad \text{Equation 4-13}$$

With c_D Concentration in the donor phase, mol cm^{-3}

For weak acids and bases, it is usually only the uncharged species which contributes to the flux (Walter *et al.*, 1982). Accordingly, the permeability becomes pH-dependent. For simple, monoprotic acids, the permeability of the membrane at any given pH can be described as a function of the intrinsic permeability Pe_0 of the uncharged species, the pH and the pk_A of the acid (Avdeef *et al.*, 2004, Avdeef and Tsinman, 2006):

$$Pe = \frac{Pe_0}{10^{(pH-pK_A)} + 1}$$ Equation 4-14

With Pe_0 Intrinsic permeability, cm s^{-1}

Another important parameter for the description of the mass transfer across the membrane is the flux density J, which can also be described as a function of the permeability Pe using Equation 4-15.

$$J = -\frac{dc_A}{dt} \cdot \frac{V}{A} = Pe \cdot (c_D - c_A)$$ Equation 4-15

With J Flux density, mol cm^{-2} s^{-1}

4.9.9 Calcein and fluorescein leakage experiments

Calcein and fluorescein leakage experiments were employed to analyze possible damaging effects, e.g. of detergents or $NADP^+$, to polymersomes. Calcein or fluorescein were encapsulated at a self-quenching concentration (15 mM or 60 mM in 0.1 M Tris-HCl pH 8, respectively) according to the method described in 4.9.1 and the calcein-loaded polymersomes were SEC-purified and stored at 4 °C in the dark until use. Fluorescein-loaded polymersomes had to be prepared freshly because of the higher permeability of the polymersome membrane towards the dye. 50 µL of the polymersome suspension were added to 50 µL of the analyte solution in 96 well, half-area, chimney, black polystyrene assay plates. The sample fluorescence was recorded immediately after 30 s mixing on an Infinite M200 microplate reader for up to 2 h. Measurements were taken in intervals from 30 s to 3 min with excitation and emission wavelengths of 485 and 515 nm, respectively, in top fluorescence mode at a gain of 80. Dye release resulted in an increase of fluorescence due to a local dilution of the dyes below the self-quenching concentration. Negative controls (buffer) and positive controls (1 % O-POE to disintegrate the polymersomes) were included to calculate the relative release of calcein or fluorescein.

4.9.10 Electron microscopy

A visual characterization of polymersomes by transmission electron microscopy (TEM) was performed at the Chair of Electron Microscopy (TUM) or at the Chair of Systems Biophysics and Bionanotechnology (TUM). Polymersome samples were diluted to a concentration of 0.01 % w/v with PBS pH 7.5 and 2 µL of the suspension were added to a carbon-coated and plasma-treated copper grid. After 60 s of adsorption to the grid the liquid was drained with a filter paper and a drop of 2.5 % w/v uranyl acetate (or uranyl formate, respectively, was added. The uranyl acetate/formate was removed likewise after 30 s, the grid was dried and then imaged with a Jeol JEM 100 CX or a Philips CM100 electron microscope at an acceleration voltage of 100 kV.

4.10 Synthesis of 1-(2',3',4',5',6'-pentafluorophenyl)ethanol

4.10.1 1-(2',3',4',5',6'-Pentafluorophenyl)ethanol synthesis with nano-scale enzyme membrane reactors

The reduction of PFAP to yield *(S)*-1-(2',3',4',5',6'-pentafluorophenyl)ethanol (*(S)*-PFE) with purified nano-scale enzyme membrane reactors was routinely performed in GC vials in a reaction volume of 500 µL with 0.2-0.4 % w/v polymersome suspensions in PBS pH 7.5. Under standard conditions, 6 mM PFAP and 0.1 M formate were used, while the nano-scale enzyme membrane reactors were prepared with 0.60 g L^{-1} FDH-KR and 4.5 mM $NADP^+$. If the concentration of the substrate or the cosubstrate was varied the other concentration was kept constant. The reaction was usually allowed to proceed for 112 h at 25 °C and with gentle agitation at 450 min^{-1} on a MTS 2/4 digital shaker. After this period, the entire reaction was transferred to Amicon Ultra-0.5 centrifugal filter units with a 100,000 MMCO to prepare the samples for extraction as described in section 4.7.1.

4.10.2 1-(2',3',4',5',6'-Pentafluorophenyl)ethanol synthesis with free enzymes

The reduction of PFAP to yield *(S)*-PFE with purified FDH-KR was performed analogously to section 4.10.1. Since no $NADP^+$ was present in the enzyme preparation, the reaction buffer was additionally supplemented with 4.5 mM $NADP^+$. The enzyme loading of the nano-scale enzyme membrane reactors was used for the comparison of activities. However, the employed concentration of 7.5 mg L^{-1} FDH-KR was about 10 times higher than the amount of enzyme contained within a 0.2 % w/v polymersome suspension and was chosen because of the dissociation of the enzyme at low concentrations. Reactions containing only the free enzyme were extracted directly as described in section 4.7.1.

4.10.3 1-(2',3',4',5',6'-Pentafluorophenyl)ethanol synthesis with whole cells

Whole cells containing the FDH-KR fusion enzyme were produced as described in section 4.4.3. The cells were resuspended in chilled PBS on ice after being harvested and their activity was determined

according to section 4.9.6. The reduction of PFAP to yield *(S)*-PFE was performed analogously to section 4.10.1 with 0.024-0.18 g_{cdw} L^{-1} cells. Reactions containing whole cells were extracted directly as described in section 4.7.1.

4.11 Statistics

The effect of different additives in the initial refolding experiments was assessed using multiple t-tests with correction for multiple comparisons by the Holm-Sidak method with α = 0.001 using GraphPad Prism (Version 6; GraphPad Software, CA).

Enzyme stability in the presence of substrates of the reaction was assessed based on the non-linear regression of activity data with GraphPad Prism using Equation 3-5. The fits of stability data obtained under different conditions were compared using an extra sum-of-squares F-test. The half-life of enzymes was considered statistically different if $p<0.05$.

Measurement uncertainties are indicated in the form of standard deviations. If required for more complex calculations, the propagation of measurement uncertainties *s(f)* for a function $f(a,b,c)$ were calculated by Gaussian error propagation (Equation 4-16).

$$s(f) = \sqrt{\left(\frac{\partial f}{\partial a} \cdot \Delta_a\right)^2 + \left(\frac{\partial f}{\partial b} \cdot \Delta_b\right)^2 + \left(\frac{\partial f}{\partial c} \cdot \Delta_c\right)^2} \qquad \text{Equation 4-16}$$

5 Expression and purification of channel proteins

5.1 Selection of channel proteins

Channel proteins for the membrane-functionalization of nano-scale enzyme membrane reactors containing the FDH-KR fusion protein had to meet three basic requirements: They had to allow the passage of the formate as well as the passage of substrates of the KR across the polymersome membrane, while retaining the cofactor $NADP^+$. The latter requirement only meant that the exclusion limit of the channel proteins had to be smaller than the molecular mass of $NADP^+$ of 744.41 Da. The general porin OmpF with a molecular mass cut-off (MMCO) of 600 Da is not expected to allow the passage of the cofactor, while the channel of the Δ1-160 FhuA mutant is too wide (Koebnik *et al.*, 2000). On the other hand, OmpF is neither particularly selective, nor does it appear to be well-matched to transport the specified substrates very efficiently. At a neutral to slightly basic pH, where the stability of the cofactor is higher than at a slightly acidic pH (Wu *et al.*, 1986), the cosubstrate formic acid (pK_A=3.75) is almost entirely deprotonated and therefore negatively charged, whereas OmpF is slightly cation-selective (Benz *et al.*, 1985). Transport of hydrophobic molecules is also impaired, because the passage of hydrophobic molecules is assumed to disturb the energetically favorable array of ordered water molecules in the channel constriction. Nikaido and Rosenberg (1983) investigated the passage of different monoanionic cephalosporins through OmpC, OmpF and PhoE and concluded that diffusion rates were negatively correlated with the log*P* of the substrates. For these reasons, the reconstitution of anion-selective channel proteins for the transport of formate and of channel proteins of the FadL or OmpW family for the transport of the rather hydrophobic KR substrates represented a promising strategy to improve the performance of the nanoreactors.

Apart from the general porin OmpF (Nikaido and Rosenberg, 1983, Nikaido, 1992), which was chosen for reference, three anion-selective channel proteins and four channel proteins that were shown or at least suspected to transport hydrophobic compounds were chosen from the literature. The anion-selective channels comprised the formate channel FocA (Suppmann and Sawers, 1994, Wang *et al.*, 2009) and the phosphoporin PhoE from *E. coli* (Nikaido and Rosenberg, 1983, Benz *et al.*, 1985) as well as the outer membrane protein OprP from *P. aeruginosa* (Hancock *et al.*, 1982, Moraes *et al.*, 2007). The channel proteins for hydrophobic substrates comprised the alkane transporter AlkL from *P. putida* GPo1 (van Beilen *et al.*, 1992, Julsing *et al.*, 2012), the outer membrane protein OmpW from *E. coli* (Pilsl *et al.*, 1999, Hong *et al.*, 2006), the outer membrane protein OprG from *P. aeruginosa* (McPhee *et al.*, 2009, Touw *et al.*, 2010) and the toluene transporter TodX from *P. putida* (Wang *et al.*, 1995, Hearn *et al.*, 2008). Neither of these channel proteins (except OmpF) had been reconstituted into polymer membranes before. On the other hand, all of these proteins, except AlkL, had been purified before and crystal structures were available. Nevertheless, the expression and purification of all eight channel proteins had to be established and adapted to meet the specific needs of the project. In particular,

the low production yields generally associated with membrane proteins presented an obstacle. Therefore, two strategies for the production of the channel proteins were devised. The ion channel proteins were to be produced in native form, requiring the establishment of a suitable solubilization protocol. The channel proteins for hydrophobic compounds AlkL, OmpW, OprG and TodX are all monomeric and thus represented promising candidates for the production by refolding from inclusion bodies. The protocol development for both strategies is described in the next sections.

5.2 Expression and purification of ion channels

5.2.1 Expression constructs

The oligomeric ion channel proteins FocA, OmpF, OprP and PhoE were expressed in native form in *E. coli* BL21 omp8, a strain developed for the expression of membrane proteins and deficient in most major outer membrane proteins (Prilipov *et al.*, 1998). The latter trait prevents the formation of heterotrimers between the recombinant and endogenous porins. For ease of purification, all expression constructs for ion channel proteins contained a His-tag. FocA does not contain a cleavable leader peptide and has been shown to be functional with a C- or N-terminally attached Strep-tag (Falke *et al.*, 2010). The created plasmids pET21a-*focA* and pET21a-*focA*2 contained a C-terminal His_6- or His_8-tag, respectively. The creation of His-tagged OmpF, OprP and PhoE was less straightforward. These three proteins contain a cleavable leader peptide, precluding the use of a simple N-terminal tag. On the other hand, the barrel of OmpF and PhoE is closed by a salt-bridge between the N- and C-terminus (Cowan *et al.*, 1992), and the C-terminal phenylalanine was shown to be important for a proper assembly in the outer membrane (Struyve *et al.*, 1991, deCock *et al.*, 1997). Van Gelder *et al.* (1996) proposed the introduction of a His-tag between the PhoE leader peptide and the mature protein and could show that the resulting protein was functional. Following their example, two modified expression vectors, pET21a-PHT1 and pET21a-PHT2, were generated. The PHT modules consist of the sequence for the PhoE leader peptide, followed by a His_6-tag and a tobacco etch virus protease (TEV) cleavage site for optional tag removal and are fused with the sequence of the mature membrane protein via BamHI (PHT1) or NheI (PHT2) sites. A schematic representation of the generated expression constructs for ion channel proteins are illustrated in Figure 5-1. The structure of the pET21-based PHT cloning site is shown in Figure B 1.

Expression of all constructs could be achieved in the chosen expression strain using a self-inducing medium, but the expression temperature was crucial for obtaining properly folded membrane proteins. Cultures were usually inoculated and initially incubated at 30 °C, but if the temperature was not lowered to 20 °C after 1 h the isolated protein yields decreased radically. Even so, most of the OmpF, OprP and PhoE appeared to be sequestered in inclusion bodies as assessed by visual examination of SDS-PAGEs.

Figure 5-1. Cartoon representations of expression constructs for the ion channel proteins. The mature protein is represented in green, the PhoE leader peptide in grey, the His-tag in red and the TEV cleavage site in black.

5.2.2 Detergent selection

The selection of an appropriate detergent for the extraction of native channel protein complexes out of the *E. coli* membrane is vital for a successful purification of the protein (Seddon *et al.*, 2004). The efficiency of extraction of the four ion channel proteins by a number of detergents (the nonionic detergents Brij-35, DDM, NP-40, OG, OTG, O-POE, Triton X-100, Tween 20 and Tween 80; the zwitterionic detergents CHAPS and LDAO and the anionic detergent *N*-lauroylsarcosine) was determined by a combination of BCA and densitometry after solubilization of membrane extracts, miniaturized IMAC and semi-native SDS-PAGE. The isolated protein yields were determined using the densitometric estimate for the protein purity based on the denaturing SDS-PAGE, while semi-native or BN-PAGE were employed for quality control. For solubilization, a concentration of 2 % w/v was chosen for most detergents except for *N*-lauroylsarcosine, which was applied at a concentration of 1 % w/v to avoid damage to the IMAC resin. For all subsequent steps, a concentration around twice the CMC was applied (a detailed list of the concentrations of all detergents can be found in Table A 13). It was demonstrated in pre-trials that a solubilization for 1 h at room temperature was generally sufficient. The quaternary structure of OmpF, OprP and PhoE could be deduced from the semi-native SDS-PAGE due to the high stability of the native trimer, while the oligomeric state of FocA could only be investigated by BN-PAGE. SDS-PAGE analysis of FocA was complicated by the strong propensity of the protein to aggregate and precipitate in the presence of SDS, especially if boiled. The SDS-PAGEs displayed in Figure 5-2, Figure 5-3, Figure 5-4 and Figure 5-5 do not contain a marker for reasons of completeness, but the respective protein bands were assigned by their molecular mass and, in case of OmpF, OprP and PhoE also their heat-modifiability, on a number of SDS-PAGEs which included a marker. Examples can be found in Figure B 2 in the supplement.

FocA was apparently extracted from the *E. coli* membrane with most of the investigated detergents (except for OTG and O-POE) to some extent (*cf.* Figure 5-2). Most promising were the glycosidic detergents DDM and OG with similar isolated protein yields of 0.47 ± 0.03 and 0.48 ± 0.03 mg L^{-1} shake flask culture, respectively. These were also the only detergents where a band of the approximate size of the FocA oligomer (164 kDa) was detected by BN-PAGE. There was a single prominent band of around 140 kDa present for the DDM-solubilized protein, while the OG-solubilized protein appeared less

homogeneous with two major bands around 130 and 160 kDa and a third one with a very high molecular mass. It is known that the presence of different detergents can cause significant differences in the migration distance of membrane proteins (Wittig *et al.*, 2006). Even so, the DDM-extracted protein band appeared slightly smaller than expected, so the protein was further characterized by protein biochemical and biophysical methods (see 5.2.3). The isolated protein yield obtained after preparative production, isolation and purification using DDM amounted to 4.0 mg L^{-1} shake flask culture and was thus higher than the originally estimated isolated protein yield determined in the small-scale experiments. This is primarily due to a more carefully controlled expression temperature profile during the expression (i.e. only 1 h adaption at 30 °C after inoculation and then a constant temperature of 20 °C until harvest), but also to a more facile handling of the membrane extracts on the large scale, the use of a preparative rather than an analytic ultracentrifuge and the use of a dounce homogenizer. Besides, with reference to the stabilizing effect of the natural substrates of the related hydrosulphide ion channel of *C. difficile* (Czyzewski and Wang, 2012), 5 mM formate were added to all chromatography buffers to stabilize the protein.

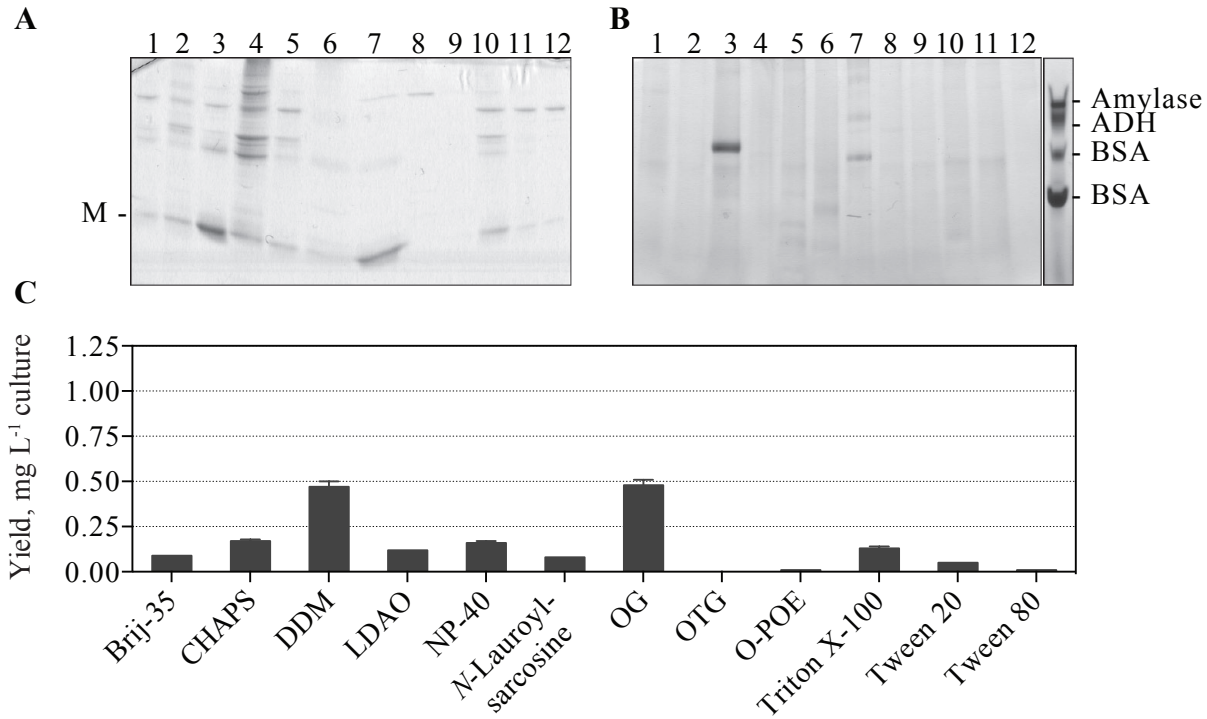

Figure 5-2. Solubilization and purification of FocA with different detergents. (A) Denaturing SDS-PAGE and (B) BN-PAGE after solubilization and IMAC. BSA (66 / 132 kDa), ADH (150 kDa) and β-amylase (200 kDa) were used as marker proteins for BN-PAGE. The position of monomeric FocA (M) is indicated. 1: Brij-35, 2: CHAPS, 3: DDM, 4: LDAO, 5: NP-40, 6: *N*-lauroylsarcosine, 7: OG, 8: OTG, 9: O-POE, 10: Triton X-100, 11: Tween 20, 12: Tween 80. (C) Isolated protein yields of the purified FocA (mg L^{-1} shake flask culture) as determined by BCA and densitometry. N=3.

OmpF was extracted from the *E. coli* membrane with the zwitterionic detergent LDAO as well as with the glycosidic detergents DDM, OG and OTG with isolated protein yields of 0.50 ± 0.02, 0.53 ± 0.02, 1.0 ± 0.1 and 0.85 ± 0.05 mg L^{-1} shake flask culture (*cf.* Figure 5-3). OmpF extracted with LDAO showed the highest trimer content with 41 ± 4 %. The trimer content of OG- or OTG-extracted OmpF was lower and amounted to 28 ± 0.3 % and 30 ± 0.6 %, while the DDM-extracted protein apparently contained only higher molecular mass aggregates but no trimers. The preparative expression, solubilization and purification by IMAC of OmpF using OG and subsequent polishing and detergent exchange into LDAO by AEX yielded 1.0 mg L^{-1} shake flask culture with a trimeric content of 52 %. The final exchange of OmpF into LDAO was performed primarily because this detergent appeared more suitable to retain the trimeric structure of the protein, but also to harmonize the subsequent reconstitution into polymersomes. As a result of the improved temperature profile during the expression, the better handling on the preparative scale using a preparative ultracentrifuge and a dounce homogenizer, the final isolated protein yield after polishing is almost identical to the isolated protein yield of the small-scale experiment with OG, which was performed without a polishing step and yielded a slightly lower trimer content.

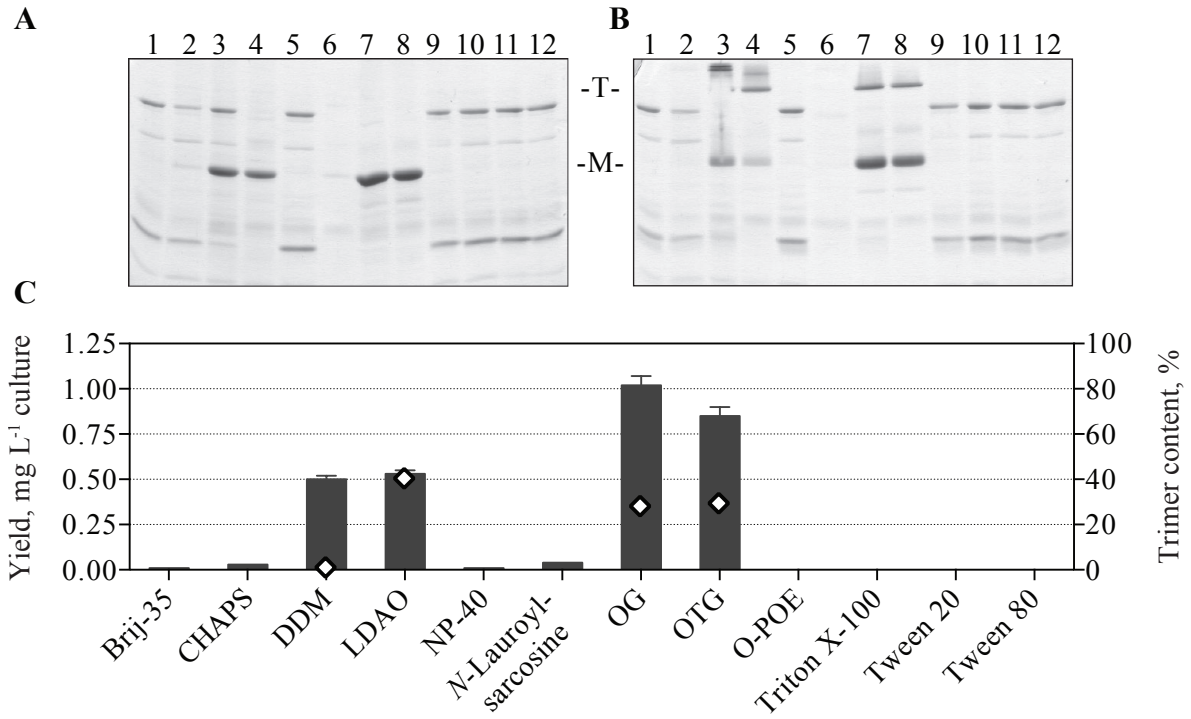

Figure 5-3. Solubilization and purification of OmpF with different detergents. (A) Denaturing and (B) semi-native SDS-PAGE after solubilization and IMAC. The position of monomeric (M) and trimeric (T) OmpF is indicated. 1: Brij-35, 2: CHAPS, 3: DDM, 4: LDAO, 5: NP-40, 6: *N*-lauroylsarcosine, 7: OG, 8: OTG, 9: O-POE, 10: Triton X-100, 11: Tween 20, 12: Tween 80. (C) Isolated protein yields (bars; mg L^{-1} shake flask culture) and trimer content (◇) of the purified OmpF as determined by BCA and densitometry. N=3.

Like OmpF, OprP could be extracted from the *E. coli* membrane with DDM, LDAO, OG and OTG, but with isolated protein yields of only 0.06 ± 0.02, 0.05 ± 0.01, 0.12 ± 0.01 and 0.08 ± 0.01 mg L^{-1} shake flask culture (*cf.* Figure 5-4). OprP extracted with OG or OTG exhibited a high trimer content with 89 ± 1 % and 91 ± 4 %. The trimeric content of OprP extracted with LDAO was 48 ± 6 % and the one obtained with DDM was 36 ± 2 %. Despite the highly native extraction of OprP with OG or OTG, no preparative expression and purification of OprP was performed because the isolated protein yields were too low to produce the necessary amounts of the protein with reasonable effort.

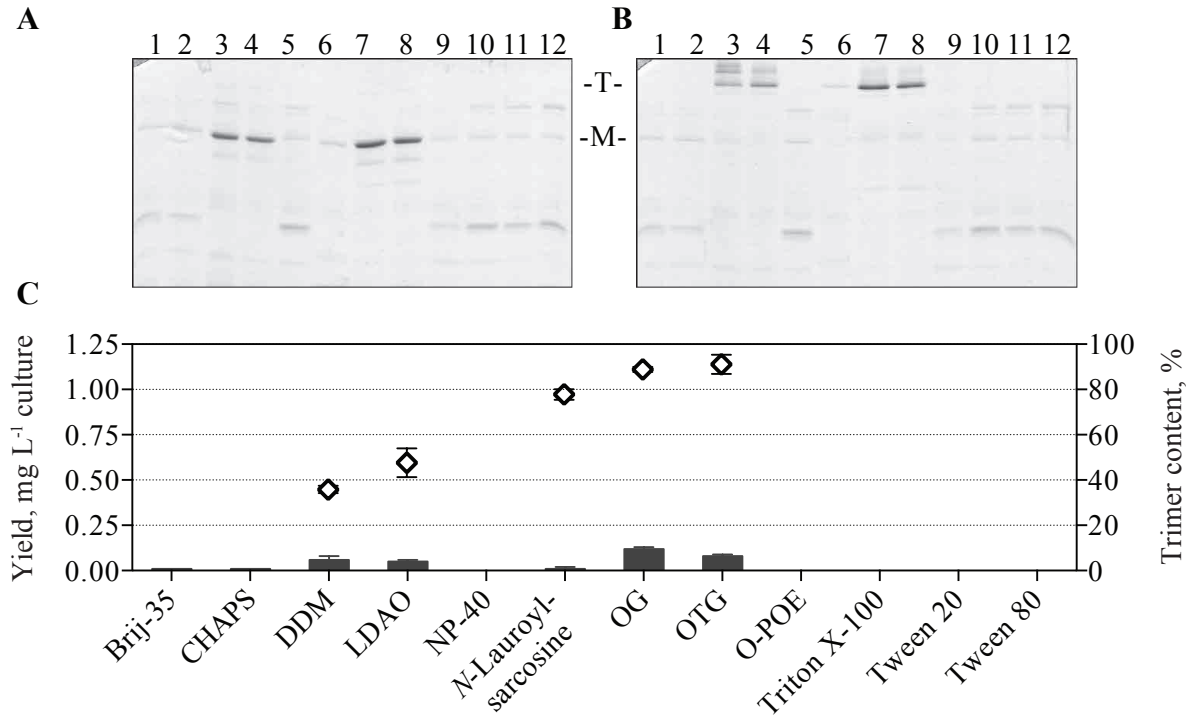

Figure 5-4. Solubilization and purification of OprP with different detergents. (A) Denaturing and (B) semi-native SDS-PAGE after solubilization and IMAC. The position of monomeric (M) and trimeric (T) OprP is indicated. 1: Brij-35, 2: CHAPS, 3: DDM, 4: LDAO, 5: NP-40, 6: *N*-lauroylsarcosine, 7: OG, 8: OTG, 9: O-POE, 10: Triton X-100, 11: Tween 20, 12: Tween 80. (C) Isolated protein yields (bars; mg L^{-1} shake flask culture) and trimer content (◇) of the purified OprP as determined by BCA and densitometry. N=3.

PhoE was extractable from the *E. coli* membrane with the zwitterionic detergents CHAPS and LDAO as well as with the glycosidic detergents DDM, OG and OTG and with the non-ionic detergent O-POE (*cf.* Figure 5-5). The isolated protein yields were highest with LDAO (0.75 ± 0.04 mg L^{-1} shake flask culture) and OG (0.67 ± 0.02 mg L^{-1} shake flask culture). PhoE extracted with LDAO was also most native with a trimer content of 95 ± 2 %. O-POE, albeit less effective in extracting PhoE from the membrane, was also very gentle and preserved 95 ± 4 % of the trimers. The trimer content of the OG- or OTG-extracted PhoE was lower and amounted to 70 ± 2 % and 73 ± 2 %, respectively. As for FocA and OmpF, the preparative expression, solubilization and purification of OmpF by IMAC using LDAO

and subsequent polishing by AEX was more efficient than on the small scale described above and yielded 2.5 mg L^{-1} shake flask culture with a trimeric content of 97 %.

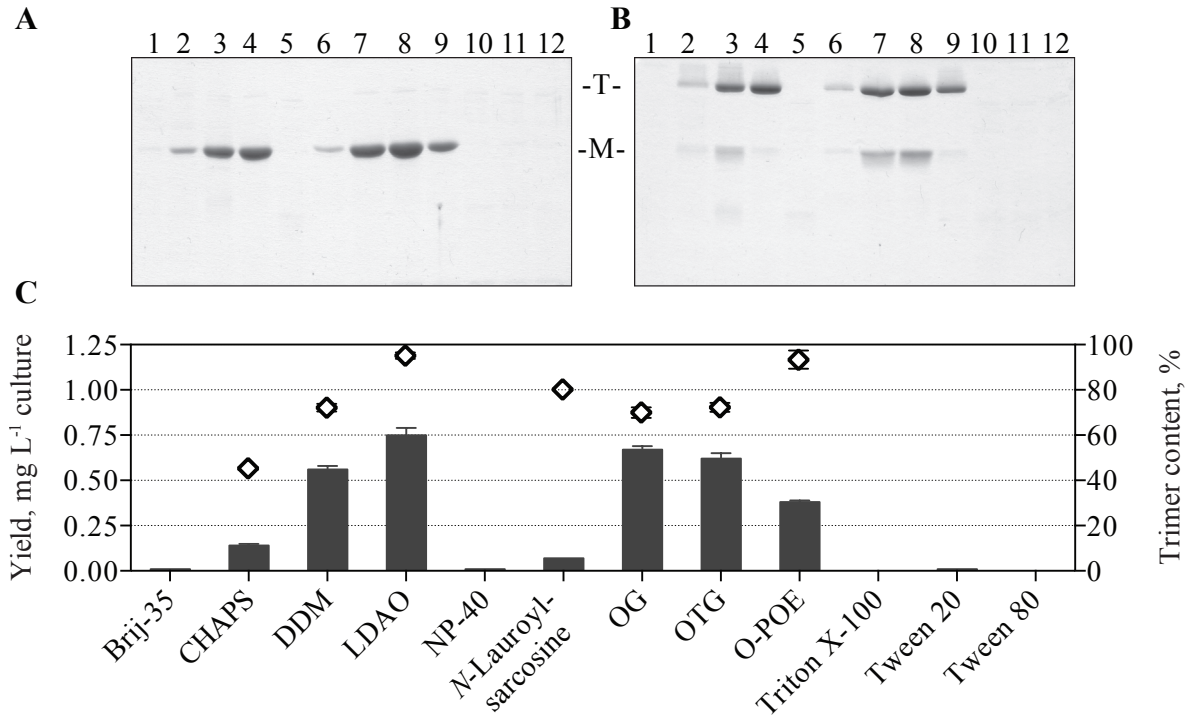

Figure 5-5. Solubilization and purification of PhoE with different detergents. (A) Denaturing and (B) semi-native SDS-PAGE after solubilization and IMAC. The position of monomeric (M) and trimeric (T) PhoE is indicated. 1: Brij-35, 2: CHAPS, 3: DDM, 4: LDAO, 5: NP-40, 6: *N*-lauroylsarcosine, 7: OG, 8: OTG, 9: O-POE, 10: Triton X-100, 11: Tween 20, 12: Tween 80. (C) (bars; mg L^{-1} shake flask culture) and trimer content (◇) of the purified PhoE as determined by BCA and densitometry. N=3.

Some additives which have been reported to improve the solubilization of outer membrane proteins and/or the stability of solubilized membrane proteins, such as EDTA (e.g. Hindahl *et al.*, 1984, Worobec *et al.*, 1988) or non-detergent sulfobetaines (NDSBs; Vuillard *et al.*, 1995) were also investigated. The addition of EDTA to the solubilization buffer had a negative impact on the purity of OmpF, OprP and PhoE rather than improving the isolated protein yield (data not shown). Neither NDSB-201 nor NDSB-221 (both 0.75 M) had any influence on the isolated protein yield of FocA, OmpF, OprP and PhoE (data not shown).

5.2.3 Structural and functional characterization of FocA

To investigate whether FocA was in its native state after extraction with DDM, additional investigations on this protein were undertaken. The CD-spectrum (*cf.* Figure 5-6) displayed two minima at 209 and 222 nm and a maximum at 195 nm typical for mainly α-helical membrane proteins (Miles and Wallace, 2016).

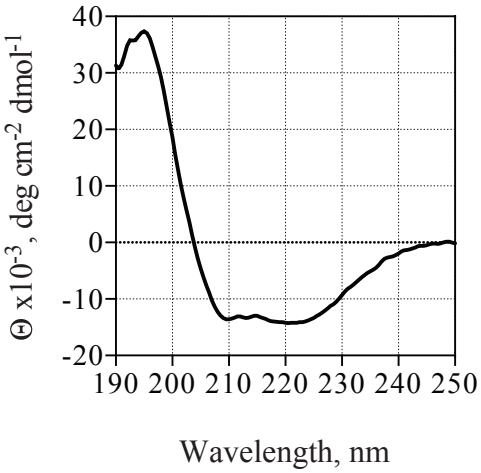

Figure 5-6. CD spectrum of SEC-purified FocA in DDM (in mean molar residue ellipticities).

The functionality of DDM-extracted FocA was subsequently assayed using electrophysiology. DPhPC formed stable membranes, but the spontaneous integration of added protein was insufficient. On the other hand, the protein integrated well into a planar bilayer composed of POPC. However, the POPC membrane proved to be rather unstable, so most measurements were performed with a bilayer composed of a mixture of POPC and DPhPC at a ratio of 1:2. Planar bilayers composed of this mixture were stable for hours, could be reformed once broken and facilitated the spontaneous integration of FocA. With a symmetric formate concentration of 40 mM, several conductance states could be observed (*cf.* Figure 5-7), indicating that the protein was indeed functional. In addition, fast gating was observed, and most of the time only a fraction of the integrated protomers was opened. Since a FocA pentamer contains five protomers, the reconstitution of even a single channel complex can have up to 5 conductance states, although the simultaneous opening of all five protomers is unlikely. The conductance of a single FocA protomer was estimated to be approximately 22 pS under these conditions.

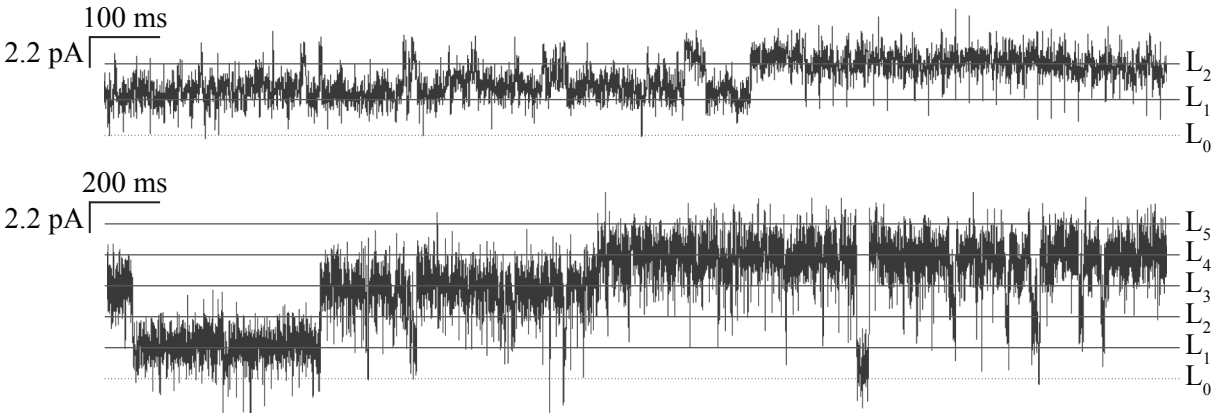

Figure 5-7. Electrophysiological measurements with DDM-extracted FocA in 40 mM formate. About 3 mg L^{-1} of the SEC-purified protein were added to the cis side of the bilayer-sealed chamber. Two representative traces with FocA in a planar bilayer of POPC and DPhPC (1:2) at 100 mV are shown. L_0-L_4 denote the estimated conductance states of several pore protomers.

5.3 Expression, purification and refolding of channel proteins for hydrophobic substrates[1]

5.3.1 Selection of the expression system

A native expression of AlkL, OmpW, OprG and TodX was initially attempted, but only AlkL and OmpW could be isolated with 2 % LDAO, and only in minute amounts (data not shown). One possible option would have been a comprehensive detergent screening as performed for the oligomeric ion channel proteins. But since a number of outer membrane proteins have been successfully refolded from inclusion bodies (Otzen and Andersen, 2013, Popot, 2014) and no secondary oligomerization to yield the final product had to be considered, this approach seemed more suitable for the goal of producing large amounts of channel proteins. At the time, OmpW (Albrecht *et al.*, 2006, Burgess *et al.*, 2008) and TodX (Hearn *et al.*, 2008) had already been reported to refold successfully from inclusion bodies. The expression constructs for both approaches are depicted in Figure 5-8A.

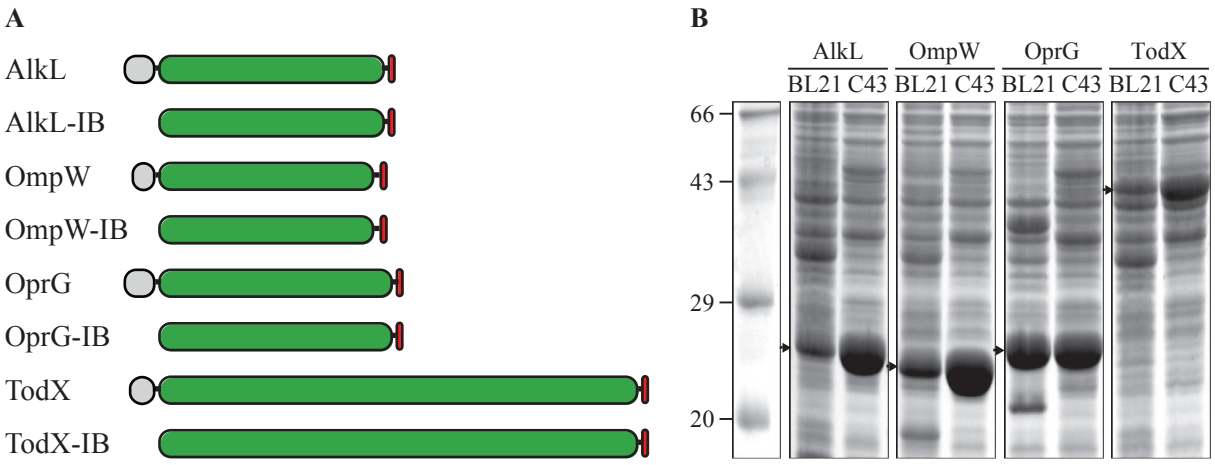

Figure 5-8. (A) Cartoon representations of expression constructs for monomeric channel proteins for hydrophobic substrates. The mature protein is represented in green, the natural leader peptides in grey and the His-tag in red. Constructs without a leader peptide are designated for the production of inclusion bodies and are thus termed "-IB". (B) SDS-PAGE of the truncated monomeric channel proteins expressed in *E. coli* BL21 and *E. coli* C43 4 h after induction with 1 mM IPTG at an OD_{600} of 0.6 and expression at 37 °C. Whole cell lysates were adjusted (according to the OD_{600} of the cultures) and boiled for 10 min at 99 °C. Roti-Mark STANDARD was loaded as a visual guide to the observer. The positions of the overexpressed proteins are indicated by arrows.

The expression of channel proteins without leader peptides in the form of inclusion bodies was examined in different expression strains. Interestingly, a far better expression than in the classical expression strain *E. coli* BL21 was observed in *E. coli* C43 (*cf.* Figure 5-8B), a strain usually associated with an improved

[1] A large part of the results presented in this chapter has recently been published (SCHWARZER, T. S., HERMANN, M., KRISHNAN, S., SIMMEL, F. C. & CASTIGLIONE, K. 2017. Preparative refolding of small monomeric outer membrane proteins. *Protein Expression and Purification,* 132**,** 171-181.)

expression of native membrane proteins. In addition, the use of an octahistidine tag could further increase the final isolated protein yield and the purity of the protein after inclusion body isolation, purification and IMAC compared to the His_6-tagged variant, presumably due to an improved binding to the IMAC column. Typical isolated protein yields of both variants of the four proteins are summarized in Table 5-1.

Table 5-1. Typical isolated protein yields of denatured monomeric channel proteins expressed in inclusion bodies. The isolated protein yields were calculated for the IMAC-purified His_6- and the His_8-tagged variants per liter shake flask culture.

Protein	**Isolated protein yield His_6-variant, mg L^{-1}**	**Isolated protein yield His_8-variant, mg L^{-1}**
AlkL	125	218
OmpW	160	233
OprG	70	144
TodX	60	70

5.3.2 1.2 mL-scale refolding

Refolding of the truncated monomeric channel proteins AlkL, OmpW, OprG and TodX was optimized in several stages. The composition of the folding buffer as well as the influence of the protein concentration were investigated on a 1.2 mL scale. To illustrate the heat-modifiability of the proteins used for the assessment of protein folding, the native and denatured forms of AlkL, OmpW, OprG and TodX are exemplarily depicted in Figure 5-9.

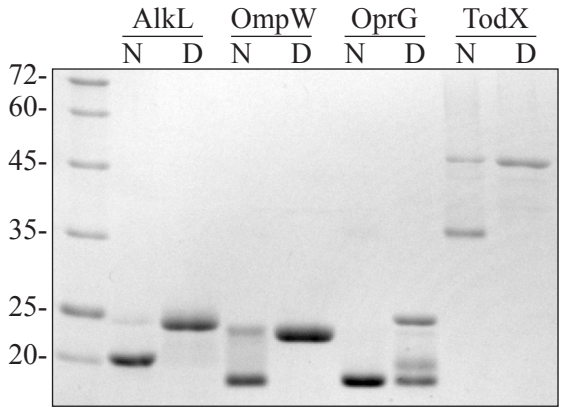

Figure 5-9. Semi-native SDS-PAGE showing native (N) and denatured (D) AlkL, OmpW, OprG and TodX. Native/denatured samples were incubated at 37/99 °C for 15 min. Note that OprG is not completely denatured after 15 min incubation at 99 °C. Just Blue Protein Marker was loaded as a visual guide to the observer.

The selection of an appropriate detergent is the starting point for most refolding studies (Buchanan, 1999). Protein folding was assessed in the presence of six nonionic detergents (Brij-35, DDM, NP-40, Triton X-100, Tween 20 and Tween 80), two zwitterionic detergents (CHAPS and LDAO) and the anionic detergent *N*-lauroylsarcosine. The results of these experiments are summarized in Figure 5-10A. The broadest detergent preference was observed for OprG, which folded with all investigated detergents, although to a varying degree. In the presence of *N*-lauroylsarcosine the folding of OprG was almost complete (90 %), while around 80 % folding were observed with Brij-35, DDM and LDAO. Although less complete, AlkL folding was similarly robust, with a slight preference for LDAO (62 % folding). The folding of OmpW was more delicate, with folding efficiencies of more than 20 % only in the presence of DDM, LDAO and *N*-lauroylsarcosine, with the latter again being optimal (29 % folding). Interestingly, folding of TodX was only achieved with *N*-lauroylsarcosine (65 % folding) and to a minor degree (10 %) with LDAO. It seems as if the C_{12}-detergents DDM, LDAO and *N*-lauroylsarcosine were most effective for folding the small monomeric β-barrel proteins, and that a negatively charged head group is an additional prerequisite for folding the larger TodX.

After the identification of suitable detergents, i.e. LDAO for AlkL and *N*-lauroylsarcosine for OmpW, OprG and TodX, the influence of the concentration of those detergents was examined in closer detail (*cf.* Figure 5-10B). Below a concentration of 1 % w/v, which is 2.5 times the critical micelle concentration, the folding efficiency of OprG and TodX decreased noticeably, while higher concentrations could not really improve the folding further, so the originally chosen concentration of 2 % w/v was already sufficient and was maintained for further experiments. Similarly, AlkL folding was much less efficient below 2 % w/v LDAO, which is about 100 times the critical micelle concentration. In contrast, the folding of OmpW was much more dependent on the concentration of *N*-lauroylsarcosine and rose from 25 % at 2 % w/v to 38 % at 5 % w/v. For OmpW, a concentration of 4 % w/v was considered to be sufficient for further experiments.

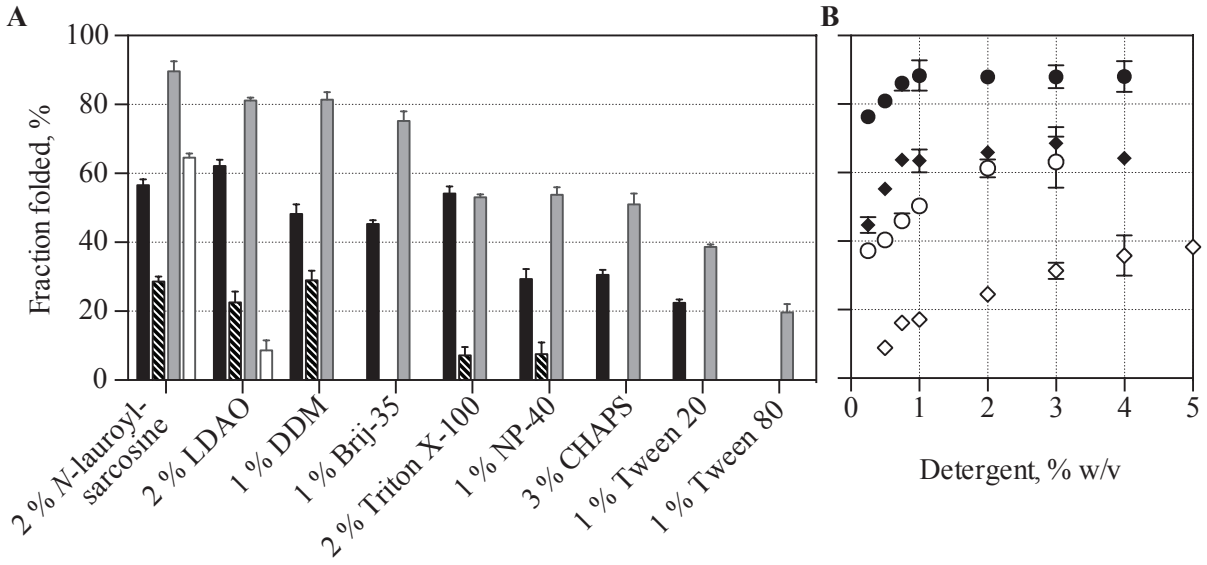

Figure 5-10. Detergent preferences for the refolding reaction. (A) Refolding of 0.1 g L^{-1} AlkL (black bars), 0.38 g L^{-1} OmpW (streaked bars), 0.34 g L^{-1} OprG (grey bars) and 0.21 g L^{-1} TodX (white bars) in the presence of different detergents. (B) Refolding of 0.1 g L^{-1} AlkL (○) with various concentrations of LDAO and 0.47 g L^{-1} OmpW (◇), 0.5 g L^{-1} OprG (●) or 0.27 g L^{-1} TodX (◆) at various concentrations of *N*-lauroylsarcosine. Results are given as the fraction folded observed after dialysis and semi-native SDS-PAGE. N=3.

Following classical refolding screens (e.g. De Bernardez-Clark *et al.*, 1999, De Bernardez-Clark, 2001, Anselment *et al.*, 2010), the inclusion of several low molecular mass additives at different concentrations in the refolding buffer composition was also investigated (*cf.* Figure 5-11). Although very common when refolding soluble proteins, this approach has not yet been widely applied to the refolding of membrane proteins. One of the few examples from the literature is the addition of 0.6 M arginine to the refolding buffer for OprG and OprH by Kucharska *et al.* (2015a). The folding of AlkL was most affected by different additives: 0.5-1 M urea, 0.5-1.5 M NDSB-201, 0.025 M glycine, 0.1-0.5 M arginine and 0.05 M glutamine all improved the folding significantly. The greatest effect (1.5-fold control) was observed upon addition of 1 M urea. The same additive improved the folding of OmpW by a factor of 1.3, however, this was not significant due to a larger variation in the control. A significant improvement of the folding of OprG was observed with 0.1 M glutamate (1.09-fold control, i.e. from 88 % to 96 %) and with 0.1 M arginine (1.05-fold control, i.e. to 92 %), but not with 0.5 M arginine. The folding of TodX improved 1.2-fold by the addition of 0.025-0.1 M glycine.

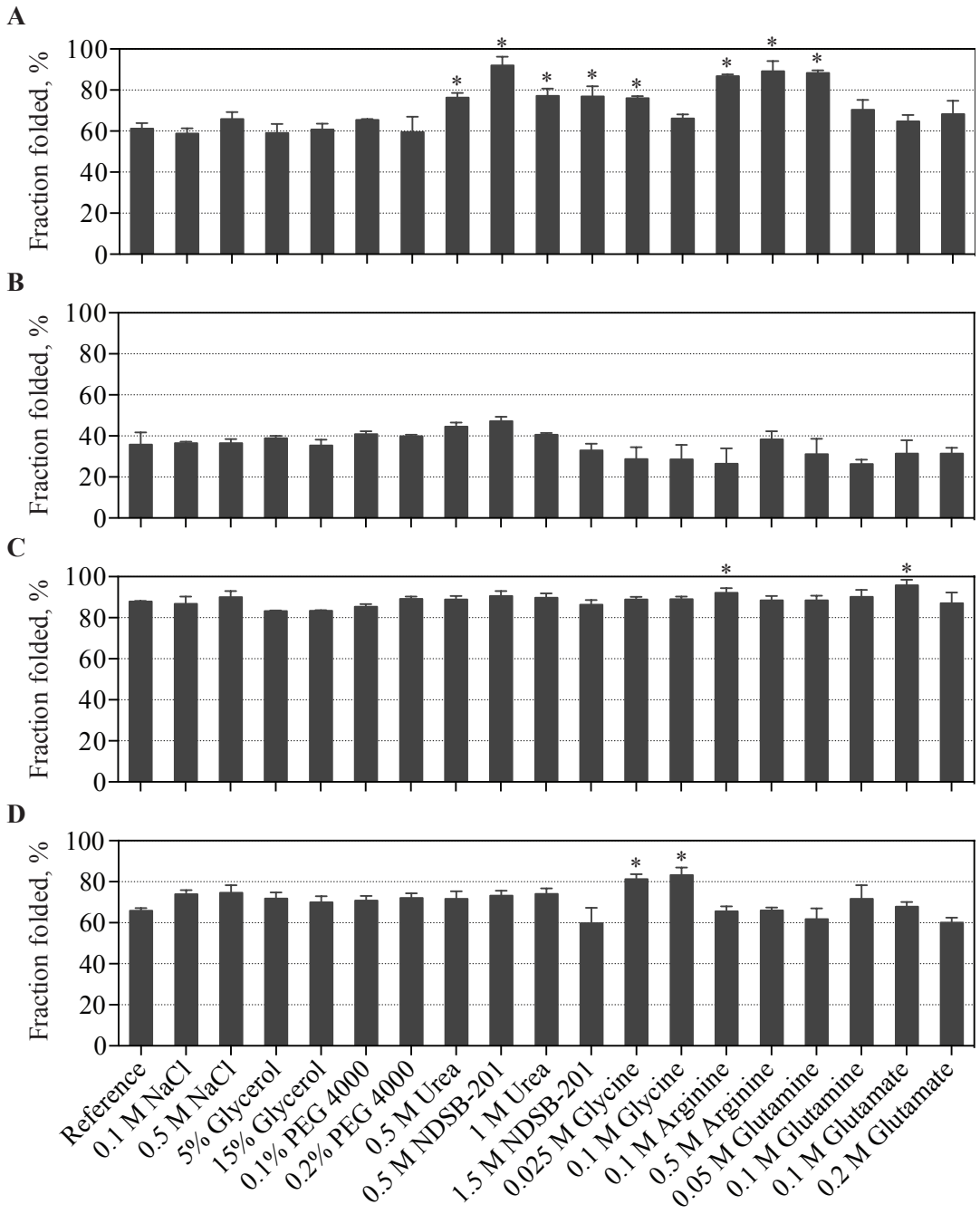

Figure 5-11. Effect of low molecular mass additives on the folding efficiency. The refolding of (A) 0.1 g L^{-1} AlkL in the presence of 2 % LDAO, (B) 0.47 g L^{-1} OmpW in the presence of 4 % *N*-lauroylsarcosine, (C) 0.5 g L^{-1} OprG in the presence of 2 % *N*-lauroylsarcosine and (D) 0.27 g L^{-1} TodX in the presence of 2 % *N*-lauroylsarcosine was assisted by adding various low molecular mass additives to the folding buffer. Results that were significantly different from the reference condition ($p < 0.001$) are indicated by an asterisk. N=3.

The last stage that was investigated on the 1.2 mL scale was the effect of varying protein concentrations in the presence or absence of the best additive for each protein (*cf.* Figure 5-12). The folding of AlkL followed a clear trend towards lower folding at higher protein concentrations and an improved folding with urea across the entire concentration range. The effect of the added urea tended to increase with the

protein concentration. The other proteins displayed an optimal folding at a concentration of 0.3 g L^{-1}, above and below which the folding efficiency decreased. The decline was most pronounced at low concentrations for OmpW and at high concentrations for TodX. Interestingly, the effect of 1 M urea on OmpW folding was also more pronounced below 0.3 g L^{-1}, whereas 0.1 M glutamate was more beneficial for the folding of TodX above 0.3 g L^{-1}. OprG folded best at 0.3-0.5 g L^{-1}, but in the presence of glutamate, folding still remained above 80 % at all investigated concentrations.

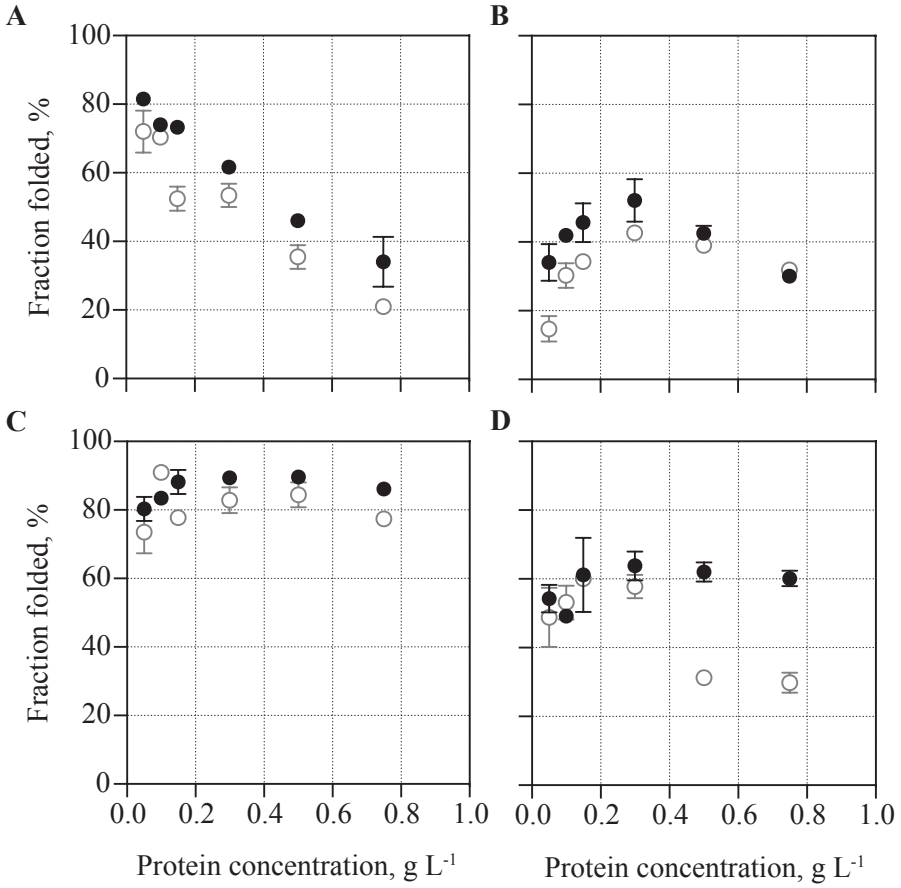

Figure 5-12. Refolding at different protein concentrations with (●) and without (○) additives. The refolding of (A) AlkL in the presence of 2 % LDAO ± 1 M urea, (B) OmpW in the presence of 4 % *N*-lauroylsarcosine ± 1 M urea, (C) OprG in the presence of 2 % *N*-lauroylsarcosine ± 0.1 M glutamate and (D) TodX in the presence of 2 % *N*-lauroylsarcosine ± 25 mM glycine was performed at protein concentrations ranging from 0.075-0.75 g L^{-1}. N=3.

5.3.3 10 mL-scale refolding

After the identification of suitable folding conditions on the 1.2 mL-scale, the next step was to transfer the folding reaction to larger volumes. An additional requirement was the achievement of reasonable refolding efficiencies at higher protein concentrations to facilitate further processing of the proteins. It is understood that high local protein concentrations during the dilution of the denaturant lead to aggregation of the protein, so a proper mixing is essential when using the rapid dilution technique, especially with larger volumes (De Bernardez-Clark, 2001, Jungbauer and Kaar, 2007). The

bioREACTOR 48 system (Weuster-Botz *et al.*, 2005) enables the parallel refolding on a 10 mL-scale under defined conditions. The use of an S-shaped stirrer was the best available option from a number of different stirrer variants (summarized by Poschenrieder *et al.*, 2016) to achieve fast and reliable mixing while maintaining relatively low shear rates (Riedlberger *et al.*, 2012) (data not shown). A first assessment of the transferability of results from the 1.2 mL scale to larger volumes was made by using a peristaltic pump to feed the protein solution into the stirred refolding buffer. This change was necessary because rapid mixing by pipetting proved to be no option when working with volumes much greater than 1 mL. With a relatively low feed rate of 16 µL min^{-1} and a final protein concentration of 0.5 g L^{-1} (AlkL and OprG) or 0.3 g L^{-1} (OmpW and TodX), it was possible to reproduce the refolding efficiencies from the 1.2 mL-scale perfectly (*cf.* Figure 5-13A). But although this approach enabled the reproducible refolding at a larger scale, the peristaltic pump still represented a bottleneck for the parallelization of the process.

The integration of a commercial liquid handler greatly enhanced the flexibility and the throughput of the experiments. Since the minimal dispensable volume of the employed liquid handler corresponds to 10 µL, the resulting process is actually an intermittent fed batch process. To standardize the folding experiments, the following experiments were performed with a final protein concentration of 0.5 g L^{-1} of the His_8-tagged variants, yet the folding efficiencies of AlkL, OmpW and OprG were still better than those obtained with the peristaltic pump and a protein concentration of 0.3 g L^{-1}. A feed rate of 2 µL min^{-1} was preferable for all four proteins (*cf.* Figure 5-13B-E).

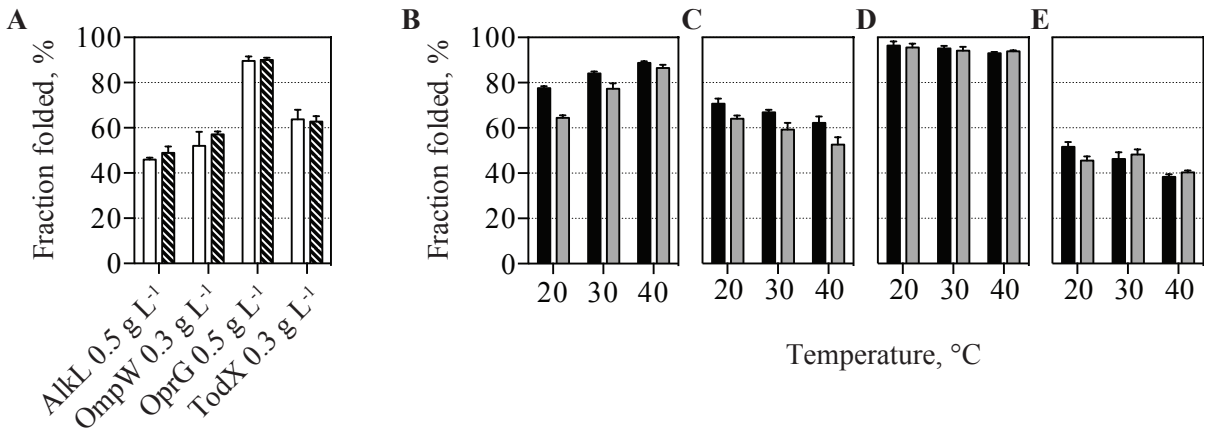

Figure 5-13. Refolding of outer membrane proteins at the 10 mL-scale. (A) Comparison of the folding efficiencies of AlkL (0.5 g L^{-1}, 2 % LDAO,1 M urea), OmpW (0.3 g L^{-1}, 4 % *N*-lauroylsarcosine, 1 M urea), OprG (0.5 g L^{-1}, 2 % *N*-lauroylsarcosine, 0.1 M glutamate) and TodX (0.3 g L^{-1}, 2 % *N*-lauroylsarcosine, 25 mM glycine) obtained by batch dilution at the 1.2 mL-scale (white bars) or by fed-batch dilution using a peristaltic pump with protein stocks of 3 g L^{-1} and a feed rate of 16 µL min^{-1} at the 10 mL-scale (streaked bars). (B-E) Automatized refolding of (B) AlkL, (C) OmpW, (D) OprG and (E) TodX at the 10 mL-scale with a final protein concentration of 0.5 g L^{-1}. The protein solution was slowly fed to the stirred refolding buffer using a liquid handler with a flow rate of 2 or 10 µL min^{-1} (black or grey bars, respectively) at three different temperatures. N=3.

AlkL folding further improved at increased temperatures, with a maximum folding efficiency of 89 % at 40 °C and a feed rate of 2 µL min^{-1}. At this temperature, the effect of the feed rate was not pronounced (84 % with 10 µL min^{-1}), whereas the difference was much greater at 20 °C (78 vs. 65 % at 2 and 10 µL min^{-1}, respectively).

In contrast, the temperature dependence of the folding of OmpW was negative between 20 and 40 °C. A further decrease below 20 °C was not only impractical due to the need for active cooling, the folding efficiency of OmpW also dropped considerably to 46 % at a feed rate of 10 µL min^{-1} when the folding was performed at 10 °C (data not shown). With a feed rate of 2 µL min^{-1}, OmpW could be folded with a folding efficiency of 71 %, which is a considerable improvement with respect to the starting conditions shown in Figure 5-10 (29 % folding). More importantly, the volumetric yield of properly folded protein was also satisfactory due to the refolding at a protein concentration of 0.5 g L^{-1}.

Automatized OprG folding was extremely good in general but marginally more efficient at 20 °C and a feed rate of 2 µL min^{-1} compared to 40 °C and 10 µL min^{-1} (96 vs. 94 %).

The temperature dependence of the folding reaction of TodX was negative only with a feed rate of 2 µL min^{-1} (52 % folding at 20 °C vs. 38 % at 40 °C). With a feed rate of 10 µL min^{-1} refolding was best at 30 °C (48 %). For some reason, we observed a high batch-to-batch variation in TodX folding experiments, whereas the folding experiments with the three smaller proteins AlkL, OmpW and OprG were much more consistent. It is probably due to this high variability that the folding of TodX in this experiment was lower compared to the folding with a peristaltic pump or at the 1.2 mL-scale.

5.3.4 Structural and functional characterization

When studying outer membrane proteins, utilizing the heat-modifiability of these proteins by semi-native SDS-PAGE is considered a standard technique for assessing the protein fold (Burgess *et al.*, 2008). This technique can also be used to determine the inherent stability of outer membrane proteins. The resistance to thermal denaturation of AlkL, OmpW, OprG and TodX was measured after 30 min incubation in the presence of 2 % SDS. The apparent melting temperature T_m varied considerably between the four proteins (*cf.* Figure 5-14). The best-folding protein OprG was also the most stable one and could not be denatured completely under the experimental conditions. AlkL, too, displayed a high resistance to thermal denaturation with an apparent T_m of 87 °C, which incidentally also corresponds to a good folding profile. As a side note, the formation of a very minor fraction of dimeric structures was sporadically observed when folding those two stable proteins, which are likely composed of two intertwined peptide strands. These dimers display the same heat modifiability on an SDS PAGE as the folded monomers. OmpW and TodX on the other hand folded less efficiently and displayed lower T_m values of 58 and 62 °C, respectively.

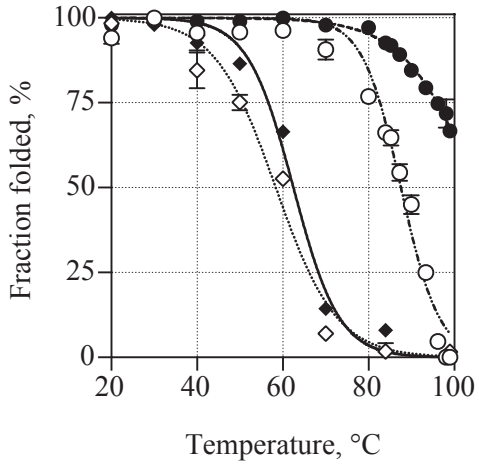

Figure 5-14. Resistance to thermal denaturation of the refolded proteins. Thermal stability of AlkL (-···○···-), OmpW (···◇···), OprG (--●--) and TodX (–◆–) was investigated by incubating aliquots of folded protein samples for 30 min at various temperatures from 20-99 °C in the presence of 2 % SDS. After semi-native SDS-PAGE, the remaining fraction folded was analyzed by densitometry, and fit to a sigmoidal function using GraphPad Prism. The observed fraction folded after incubation at 20 °C was set to 100 %. N=3.

Resistance to protease digestion is another property of a number of outer membrane proteins (Nakamura and Mizushima, 1976, Surrey *et al.*, 1996). Semi-native SDS-PAGE of the refolded AlkL, OmpW, OprG and TodX revealed that the band corresponding to the folded protein species was present even after 2 h incubation at 37 °C in the presence of 0.1 g L^{-1} trypsin, while bands corresponding to misfolded species as well as aggregates disappeared (*cf*. Figure 5-15).

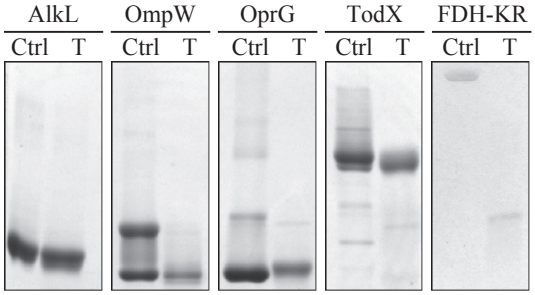

Figure 5-15. Protease resistance of the refolded proteins. Thermal stability of AlkL, OmpW, OprG and TodX was investigated by incubating aliquots of folded protein samples (c ≈ 0.3 g L^{-1}) for 2 h at 37 °C in the absence (Ctrl) or presence (T) of 0.1 g L^{-1} trypsin and semi-native SDS-PAGE. FDH-KR incubated for 1 h under the same conditions is shown as a protease activity control.

CD spectra of the folded and purified proteins were also recorded and show the characteristics of β-rich proteins with a single minimum around 216 nm, most typically that of OmpW. A slight deviation from typical β-barrel protein spectra with a steady decline of ellipticity from 240 to 216 nm was seen for AlkL, where the hint of a secondary maximum at around 230 nm sometimes found in proteins with

clustered tryptophan or tyrosine residues was present. A slight negative shoulder around 204 nm was noticeable in the OprG spectrum. However, a certain degree of unordered structure is also expected for OprG, since the measurements were performed in detergent.

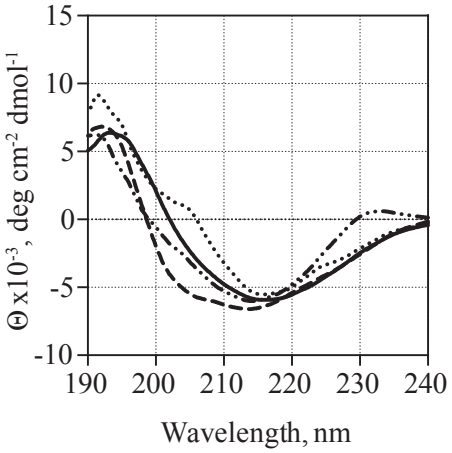

Figure 5-16. CD spectra of refolded and SEC-purified AlkL (-···-), OmpW (····), OprG (----) and TodX (—) by circular dichroism. Results are given as mean molar residue ellipticities.

True functional assays are somewhat difficult with this class of membrane proteins, because they do not have an activity apart from their possible pore-forming effect in compartmentalized systems. Besides, the substrates of these membrane proteins are for the most part only speculative. A functional assessment of the protein folding was exemplarily performed for OprG, because this protein has been shown to display a notable single-channel conductance ($G \approx 500$ pS in 1 M KCl (McPhee *et al.*, 2009)), in contrast to OmpW, which has a very low conductance of less than 20 pS under similar conditions (Hong *et al.*, 2006) and is thus much harder to measure. TodX was described to be non-conducting (Hearn *et al.*, 2008) and for AlkL, no electrophysiological measurements have been performed so far. Nevertheless, it is also rather unlikely that AlkL can be studied by electrophysiological methods, since its hydrophobic channel is even narrower than the one of OmpW (Grant *et al.*, 2014). The refolded OprG could indeed be integrated into a planar lipid bilayer and displayed a conductance of roughly 330 pS in 1 M KCl (*cf.* Figure 5-17).

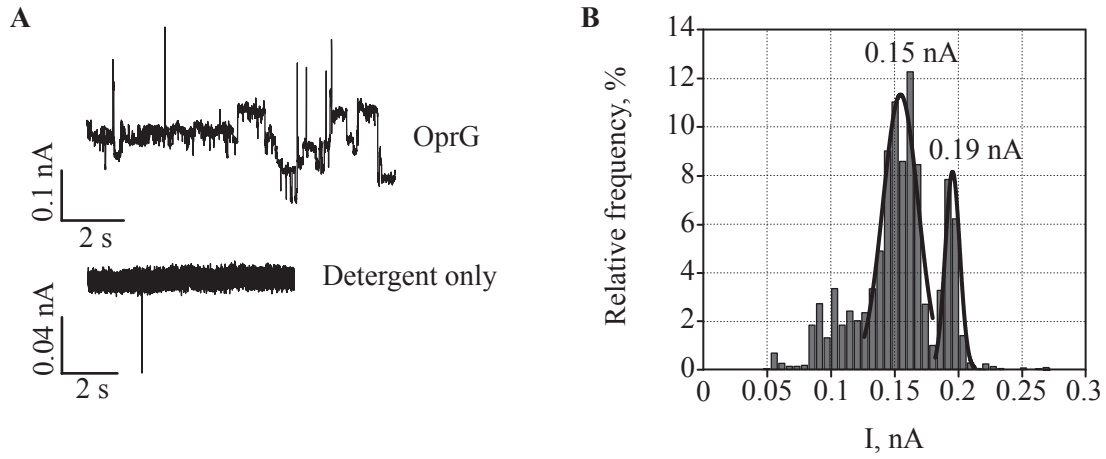

Figure 5-17. Single-channel conductance of OprG in 1 M KCl. (A) Refolded and purified protein (0.6 mg L^{-1}) was added to the cis side of a MECA chip sealed with a DPhPC bilayer. A representative recording at 150 mV is shown. The control trace, which was recorded with detergent *sans* protein channels showed no pore formation. Note that several channels were present in the bilayer. (B) Histogram of the trace shown in (A). The conductance of a single protein channel was obtained from the distance between the histogram peaks and corresponds to $G \approx 330$ pS.

5.4 Discussion

The preparation of sufficient amounts of channel proteins was an important requirement for the assembly of membrane-functionalized nano-scale enzyme membrane reactors. Typical extraction and purification protocols for outer membrane proteins are very laborious and involve multiple steps of ultracentrifugation. First, membranes are collected and preextracted successively (up to 8 times) with detergents such as 0.5 % w/v O-POE (Garavito and Rosenbusch, 1986) or 2 % w/v SDS (Rosenbusch, 1974) to remove contaminants. The protein is then extracted from the membrane fraction by increasing the detergent concentration (e.g. 3 % w/v O-POE; Garavito and Rosenbusch, 1986) or by adding EDTA (usually 20 mM; Hancock *et al.*, 1982) or salt (0.6 M NaCl; van Gelder *et al.*, 1996) to dissociate the protein from the peptidoglycan and subsequently purified by ion exchange chromatography and size exclusion chromatography. For OmpF, one of the most abundant outer membrane protein in *E. coli*, this procedure can yield up to 6.5 mg L^{-1} culture or 4.3 mg g^{-1} cell wet weight of endogenous protein (Garavito and Rosenbusch, 1986). Another study made use of the strain *E. coli* BL21 omp8 developed by Prilipov *et al*. (1998) to overexpress plasmid-borne OmpF and reported an isolated protein yield of 2-3 mg g^{-1} cell wet weight (Phale *et al.*, 1997). Often though, a few mg per liter culture or even less can be considered a good result when isolating membrane proteins (Bannwarth and Schulz, 2003). The tedious isolation procedure was greatly simplified by the introduction of an affinity tag as described by van Gelder *et al*. (1996), which allowed the extraction of OmpF, OprP and PhoE by only two ultracentrifugation steps in this thesis, one for membrane isolation and one for removal of non-solubilized proteins, followed by an IMAC purification step to yield almost pure protein. The successful extraction of OmpF with 3 % w/v OG (Garavito and Rosenbusch, 1980), 3 % w/v O-POE (Garavito and

Rosenbusch, 1986) or 2 % w/v SDS (Rosenbusch, 1974) is described in the literature. In this thesis, OmpF extraction was most successful with 2 % w/v OG, but not with 2 % w/v O-POE. As a result of the N-terminal His-tag, the protein stability appeared to be impaired, since only 52 % of the protein was still in its trimeric form. In addition, the isolated protein yield of 1.0 mg L^{-1} was much lower than those reported for untagged OmpF (see above). Purification of native OmpF via His-tag is not reported in the literature, but the original publication by van Gelder *et al*. mentions that a substantial fraction of the tagged PhoE appeared monomeric after purification. The authors argued that functional characteristics, transport across the inner membrane, trimer formation and insertion into the outer membrane were not altered, but that the protein stability was impaired by the presence of the N-terminal tag, which is located at the trimer interface. The trimer interface is an important determinant for the unusually high stability of the trimeric porins, as mutations affecting the trimer interface result in a lower stability of mutant OmpF (Phale *et al.*, 1998) and OmpF trimer dissociation was described to be accompanied by denaturation (Rosenbusch, 1974).

Interestingly, PhoE extracted with 2 % w/v LDAO or 2 % w/v O-POE displayed a much higher trimer content of 95 ± 2 % and 95 ± 4 %. PhoE was previously extracted using 2 % w/v SDS (Bauer *et al.*, 1989), 2 % w/v Triton X-100 (aided by 20 mM EDTA; Benz *et al.*, 1984a) or 3 % w/v O-POE (Dargent *et al.*, 1986). In this thesis, PhoE could not be extracted with Triton X-100, and SDS was not further evaluated since it interfered with protein binding to the IMAC column material. The highest isolated protein yield of 2.5 mg L^{-1} could be obtained with LDAO. PhoE yields are not reported in the literature, but compared to those for untagged OmpF (Garavito and Rosenbusch, 1986), extraction with LDAO yielded less PhoE, although at least more than obtained for His-tagged OmpF.

OprP stability was not drastically affected by the His-tag when extracted with OG or OTG (89 ± 1.1 % and 91 ± 4 % trimer content), probably as a result of the more periplasmic location of the N-terminus (Moraes *et al.*, 2007) but the isolated protein yields of not more than 0.12 ± 0.01 mg L^{-1} culture were extremely low. This protein had previously only been expressed in its native host, *P. aeruginosa*, and its extraction was performed with 2 % w/v Triton X-100 (Hancock *et al.*, 1982) or 2 % w/v SDS (Worobec *et al.*, 1988), in each case assisted by 20 mM EDTA. In these studies, the purification yielded 6.3 mg L^{-1} or 4.8 mg g^{-1} cell wet weight, which is comparable to reported yields for wild type OmpF. It is possible that the heterologous expression of OprP in *E. coli* was less suitable for OprP. Another possibility would be that the extraction conditions were not efficient enough, but at least EDTA did not help in solubilizing more of this outer membrane protein, so further trials were discontinued. This decision had an impact on the further exploration of suitable reaction conditions for the nano-scale enzyme membrane reactors, since the high specificity of OprP for phosphate ions over other anions (Hancock *et al.*, 1982, Hancock and Benz, 1986) would have required a completely phosphate-free system to avoid inhibitory effects on the transport of formate.

FocA purification was similar to published procedures, since FocA had been isolated using both a N/C-terminal Strep-tag or a C-terminal His-tag and using 1 % w/v DDM (Falke *et al.*, 2010) or 2 % w/v OG (Lu *et al.*, 2011) for extraction and purification. Falke *et al*. reported an isolated protein yield of 1 mg L^{-1} culture. In this thesis, the preparative purification of FocA was much more successful than the solubilization trials on a smaller scale, probably due to an expression which was very sensitive to the temperature profile during the expression. Under optimized conditions, an isolated protein yield of 4.0 mg L^{-1} culture could be obtained, which represents quite an improvement with regard to published yields. The CD-spectrum of the purified FocA was identical to the one reported by Falke *et al*., and a functional survey using electrophysiological measurements with formate yielded conductance levels of approximately 22 pS, which is similar to a conductance of approximately 21 pS under comparable conditions estimated from the data presented by Lu *et al*. (2012). Unfortunately, time and the limited access to the necessary resources did not allow for a more encompassing and complete functional characterization of the other isolated ion channel proteins.

For the other four outer membrane proteins used in this thesis, the native expression and purification was found to be problematic and probably an inferior solution to their refolding from inclusion bodies due to their monomeric nature. Depending on the particular protein and the refolding efficiency, the yields of refolded membrane proteins can be one to two orders of magnitude higher than for the native expression and extraction from the membrane (Bannwarth and Schulz, 2003). Isolated protein yields for these four proteins after inclusion body purification were indeed higher and ranged from 70 mg L^{-1} (TodX) to 233 mg L^{-1} (OmpW) when expression of the octahistidine-tagged variants was performed in *E. coli* C43. It is noteworthy that the expression of all four proteins by this particular strain, which is otherwise more renowned for its ability to express native membrane proteins, was much better than by *E. coli* BL21. However, Miroux *et al*. (1996) observed a better expression of globular non-membrane proteins and inclusion-body bound membrane proteins as well as of native membrane proteins in *E. coli* C41, which is the parent strain of the C43 strain (also described in the same publication) used in this thesis. The productive expression and purification of AlkL, OmpW, OprG and TodX from inclusion bodies generated sufficient material for the crucial determination of suitable folding conditions.

Pretrials indicated that folding of AlkL, OprG and TodX was best at pH 8, while OmpW preferred pH 9 (*cf*. Figure B 3). Outer membrane folding *in vivo* occurs in the periplasm, where the pH is subject to the environment and therefore not well-defined. Burgess *et al*. (2008) found that a number of outer membrane proteins folded best between pH 8 and pH 10. Since the pI of many outer membrane proteins lies between 5 and 6, they are negatively charged under these conditions, which was proposed to aid in the folding process. The choice of detergent is undoubtedly the most important factor for the refolding of membrane proteins. In this thesis, the influence of the detergent was also most prominent, with the best results obtained with the ionic C_{12} detergents LDAO and *N*-lauroylsarcosine. AlkL and OprG folded reasonably well in the presence of most of the investigated detergents, while OmpW and TodX folding

was more delicate. This is in good agreement with previous reports about the folding of OmpW and TodX, which were performed with LDAO (Albrecht *et al.*, 2006) and *N*-lauroylsarcosine (Hearn *et al.*, 2008), respectively. Unfortunately, these studies did not indicate the refolding efficiency or the yield in detail but referred to the lack of any precipitation instead. In this thesis, precipitation was seldom observed, but this did not correlate well with the folding efficiency. The folding of OmpW has been described as demanding by other authors in the past. Burgess *et al*. (2008) have for example reported about 95 % folding of OmpW at a final concentration of 4 µM (ca. 0.084 g L^{-1}) only in the presence of 1,2-didecanoyl-*sn*-glycero-3-phosphocholine vesicles, while all other conditions resulted in a less complete folding. They also reported that FadL, which is structurally related to TodX, folded least efficient under most conditions. The addition of low-molecular weight folding additives in addition to the folding detergent is rarely reported for the refolding of membrane proteins. Two of the few examples in the literature are OprG (Kucharska *et al.*, 2015a) and the related OprH (Edrington *et al.*, 2011) from *P. aeruginosa*, which were both refolded in the presence of 0.6 M arginine. In this thesis, arginine also resulted in a better refolding of OprG, but only with 0.1 M and not with 0.5 M. In general, the presence of a folding additive proved useful in further enhancing the folding of AlkL, OprG and TodX, while OmpW folding in the absence was less reproducible on the smaller scale, which complicated the statistical assessment of the data.

The implementation of a liquid handler to refold the proteins on the 10 mL scale using the parallel bioREACTOR 48 system proved to be most valuable to the production of larger amounts of refolded outer membrane proteins, and yields were indeed even better than on the 1.2 mL scale (except for TodX, which displayed an unusual degree of batch-to-batch variation and folded less efficiently in the respective experiments). A better refolding of lysozyme in a fed-batch process compared to simple batch dilution was also reported by Katoh and Katoh (2000). The final folding efficiencies under optimized conditions were 89 % (AlkL), 96 % (OprG), 71 % (OmpW) and 52 % (TodX). These were obtained in unbaffled reactors agitated by S-stirrers at 500 min^{-1} with an intermittent feed of 2 µL min^{-1} up to a final protein concentration of 0.5 g L^{-1} at 20 °C, except for AlkL, which folded best at 40 °C. OprG folding is in the same range as in very recent reports where OprG was refolded in the presence of the zwitterionic 1,2-di-hexanoyl-*sn*-glycero-3-phosphocholine (Kucharska *et al.*, 2015a, Kucharska *et al.*, 2015b). AlkL refolding or even its purification is unprecedented in the literature, but it appears that this outer membrane protein is generally well-suited to be produced by refolding.

In addition, AlkL and OprG were also highly resistant to thermal denaturation in the presence of 2 % w/v SDS, while OmpW and TodX appeared less, but still considerably, stable. The melting point of OmpW under these conditions amounted to 58 °C, which matches the value reported by Burgess et al. (2008), who employed the same methodology. The occasionally observed formation of dimers apparently consisting of intertwined peptide strands of the two stable proteins AlkL and OprG has also been reported for OmpA (Wang *et al.*, 2013), which is perhaps the best-studied outer membrane protein with

respect to its folding mechanism. Lower feed rates were, however, sufficient to avoid this phenomenon sufficiently. Resistance to ptrypsin digestion and CD-spectroscopy indicated properly folded proteins. Peculiarities of the observed spectra include a hinted secondary maximum of the AlkL spectrum around 230 nm and a bulge in the OprG spectrum between 200 and 210 nm. A behavior of the spectrum similar to the one of AlkL was reported for LamB (Park *et al.*, 1992), which was attributed to the positive contribution of clustered tryptophan and tyrosine residues in a β-sheet-rich environment at this wavelength (Schechter *et al.*, 1971, Lacadena *et al.*, 1995). Since AlkL is very rich in tyrosines, this explanation might very well apply to this protein, too. The bulge in the OprG spectrum hints to a higher degree of unordered structure. In a micellar environment, the extended loops are rather more flexible than under conditions in a lipid environment where the crystal structure has been solved and where the β-sheets are longer and the periplasmic loops shorter, probably due to the restricted flexibility in the crystal (Touw *et al.*, 2010, Kucharska *et al.*, 2015b). On the other hand, OmpW apparently retains partially β-structured loops in Fos-30 micelles as shown by solution-NMR (Horst *et al.*, 2014), which explains why the CD spectrum of this protein is marked by a steeper increase in ellipticity from 216 to 208 nm than those of the other proteins.

Finally, a brief functional survey of OprG functionality by electrophysiology demonstrated a conductance of ≈ 330 pS, only slightly lower than the conductance of ≈ 500 pS previously reported (McPhee *et al.*, 2009).

6 Characterization of the fusion enzyme between formate dehydrogenase and 3-ketoacyl-(acyl-carrier-protein)-reductase

6.1 pH optimum and buffer preference

The buffer preference of the FDH-KR fusion enzyme was investigated with MOPS, sodium phosphate, PBS and Tricine between pH 6.5 and 8.5 to evaluate suitable conditions for the creation of the nano-scale enzyme membrane reactors (*cf.* Figure 6-1). The FDH activity was highest at pH 7.5 in sodium phosphate buffer or PBS, indicating a preference for phosphate containing buffers for this part of the enzyme. In MOPS and Tricine, the FDH activity declined steadily with rising pH from 84 % at pH 6.5 to 28 % at pH 8.5. Conversely, the activity of the KR part was only dependent on the pH and not on the buffer substance. The highest activity was found at pH 7.5. Activities above and below were slightly lower with 75 % at pH 6.5 and 85 % at pH 8.5. Since both enzymes displayed a good activity in PBS at pH 7.5, further investigations were only performed under these conditions.

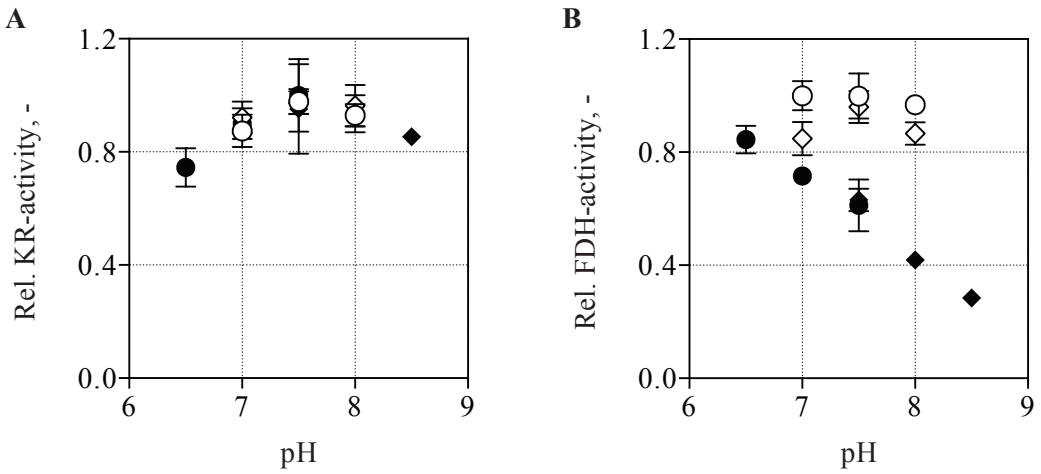

Figure 6-1. Relative activity of the (A) FDH or (B) KR part of the fusion enzyme in different buffers. (●): 50mm MOPS pH 6.5-7.5; (○): 50 mM sodium phosphate pH 7.0-8.0; (◇): PBS pH 7.0-8.0; (◆): 50 mM Tricine pH 7.5-8.5. Activities were normalized to the highest activity observed. N=3.

6.2 Kinetic parameters

An understanding of the behavior of the encapsulated fusion enzyme with regard to the employed substrates was important to the assembly and investigation of the nano-scale enzyme membrane reactors. The isolated reactions of FDH (*cf.* Figure 6-2) and KR (*cf.* Figure 6-3) were analyzed with the respective substrate (or cosubstrate) in excess and analyzed by non-linear regression. The maximal specific activities v_{max} and the half-saturation constants K_M for both enzyme parts are listed in Table 6-1. It is of note, though, that the determined v_{max} of the KR subsystem is strictly speaking only valid for high enzyme concentrations due to an observed activity loss at low enzyme concentrations, which is most

pronounced below 100 mg L^{-1} (*cf.* section 8.3). At the FDH-KR concentration (10 mg L^{-1}) used for determining the specific KR activity, the remaining activity amounts to 13 % of the maximal activity at an infinite concentration according to Equation 8-2.

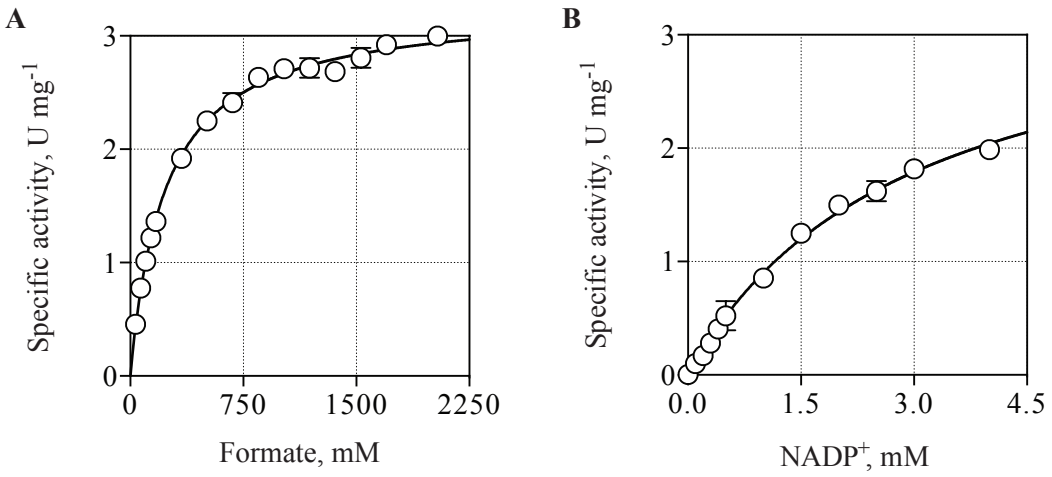

Figure 6-2. Specific activity of the FDH-part of the fusion enzyme as a function of the (A) formate or (B) $NADP^+$ concentration. The data were fitted by non-linear regression using Equation 3-2. For comparability with the isolated enzymes, specific activities refer to the mass fraction of the FDH part only. N=4.

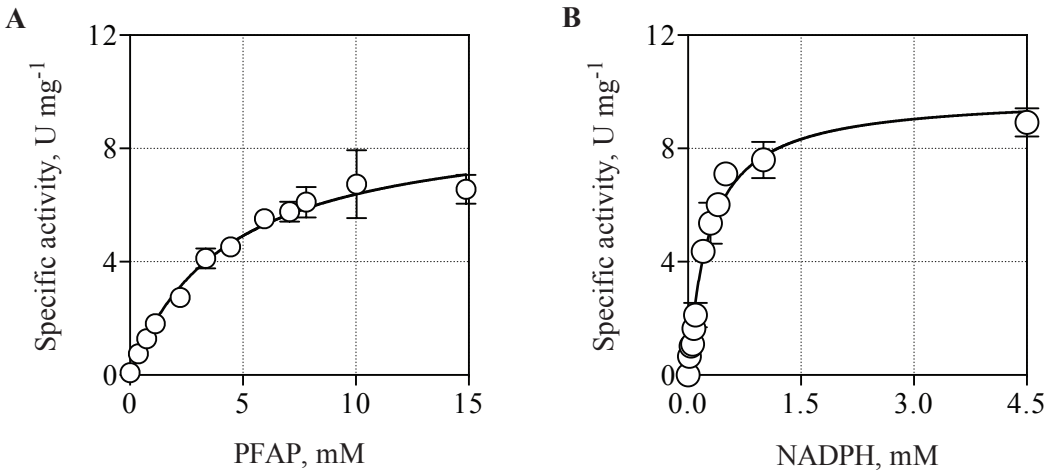

Figure 6-3. Specific activity of the KR-part of the fusion enzyme as a function of the (A) PFAP or (B) NADPH concentration. The data were fitted by non-linear regression using Equation 3-2. For comparability with the isolated enzymes, specific activities refer to the mass fraction of the KR part only. Besides, the specific activity was corrected for the observed concentration-dependent loss of activity (13 % of the maximal activity at the employed concentration of 10 mg L^{-1} according to Equation 8-2). N=3.

Table 6-1. Kinetic parameters of the FDH-KR fusion enzyme in PBS at 25 °C. * Kinetic parameters of the KR part are calculated for an infinite enzyme concentration according to Equation 8-2.

	FDH-part	**KR-part***
v_{max}, U mg^{-1}	3.75 ± 0.1	9.90 ± 0.5
k_{cat}, s^{-1}	2.77 ± 0.1	2.60 ± 0.1
$K_{M\ (NADP^+ / NADPH)}$, mM	2.91 ± 0.2	0.28 ± 0.04
$K_{M\ (Formate / PFAP)}$, mM	231 ± 6	4.26 ± 0.5

6.3 Enzyme stability

Due to the long duration (usually 112 h) of experiments with nano-scale enzyme membrane reactors, the protein stability was an important factor that needed to be investigated. Experiments were performed in PBS at 25 °C with 1 and 6 mM PFAP with or without 1 M formate (*cf.* Table 6-2). The stability of the FDH part was relatively high with a half-life of 78 h under these conditions. The addition of 1 mM PFAP with or without 1 M formate did not alter the stability significantly as judged by an extra sum-of-squares F-test comparing the k_{inact} values generated by non-linear regression.

The KR part, however, was significantly stabilized in the presence of PFAP, with a 3-fold increased half-life in the presence of PFAP. The actual PFAP concentration did not have a significant impact on the enzyme's half-life, nor did the presence of formate.

Table 6-2. Half-life $\tau_{1/2}$ of the FDH-KR fusion enzyme in the presence of different substrate concentrations in PBS at 25 °C. The data were fit by non-linear regression using Equation 3-5 and Equation 3-6. (n.d.: not determined). N=3.

	$\tau_{1/2}$ FDH-part, h	**$\tau_{1/2}$ KR-part, h**
Buffer	78 ± 8	43 ± 3
1 mM PFAP	71 ± 12	130 ± 9
1 mM PFAP + 1 M formate	51 ± 17	119 ± 27
6 mM PFAP	n.d.	115 ± 22
6 mM PFAP + 1 M formate	n.d.	123 ± 43

6.4 Discussion

A basic characterization of the FDH-KR fusion enzyme had already been performed by others (Hölsch and Weuster-Botz, 2010, Sührer *et al.*, 2014), but under somewhat different reaction conditions, i.e. in 0.1 M sodium phosphate buffer pH 7 at 22 °C or 30 °C and with ethyl 4-chloroacetoacetate or ethyl benzoyl acetate as substrates. Therefore, a kinetic characterization under the conditions used for the nano-scale enzyme membrane reactors was still required. The activity of the FDH part is comparable to results obtained by Sührer *et al*. (2014) in 0.1 M sodium phosphate, pH 7 at 22 °C (3.75 vs. 2.52 U mg^{-1}), considering that the FDH activity strongly increases with temperature (Hölsch *et al.*, 2013). On the other hand, half saturation constants for both $NADP^+$ (2.91 vs. 0.44 mM) and formate (231 vs. 170 mM) were higher than reported by Sührer *et al*. (2014), possibly as a result of higher temperature (Hölsch *et al.*, 2013) or pH. For the KR part of the fusion enzyme, no kinetic data concerning the activity with PFAP as a substrate are reported, but the activity with ethyl 4-chloroacetoacetate or ethyl benzoyl acetate was comparable to that of the single enzyme (Hölsch and Weuster-Botz, 2010, Sührer *et al.*, 2014). The reported activity of the single enzyme with PFAP amounts to 3.93 U mg^{-1} at 30 °C, which corresponds to an activity of approximately 3 U mg^{-1} at 25 °C (estimated from the data presented by Hölsch *et al.*, 2008). The KR-specific activity of the fusion enzyme with PFAP as a substrate was found to be higher with 10.5 U mg^{-1} in this thesis. The half-saturation constant for NADPH (0.28 vs. 0.57 mM) was slightly lower than previously determined for the fusion enzyme in 0.1 M sodium phosphate, pH 7 at 22 °C (Sührer *et al.*, 2014), but the single enzyme exhibited an almost comparable half-saturation constant of 0.4 mM at 30 °C (Hölsch *et al.*, 2008). The half-saturation constant towards PFAP can also only be compared to the single enzyme, which was again comparable (4.26 vs. 5.72 mM).

With regard to its stability, the fusion enzyme had not been characterized so far. However, the stability of the FDH part appeared reduced in comparison to the stabilized FDH 3M single enzyme, which corresponds to the FDH part of the FDH-KR used in this thesis. The single enzyme exhibited a half-life of more than 200 h at 30 °C (Hölsch *et al.*, 2013), while the half-life of the fusion enzyme was only 77.7 h at 25 °C. Although the stability of the version of the fusion enzyme used in this thesis had not been assessed, all initial fusion enzyme variants with a non-optimized FDH part also displayed some loss of activity compared to the single enzyme (Hölsch and Weuster-Botz, 2010). Interestingly, the stability of the KR part at 25 °C with a half-life of 42.7 h was found to be improved compared to the unfused enzyme (30.9 h; Hölsch, 2009). Even more interesting is the observation that the stability of the KR part is enhanced in the presence of the substrate PFAP, while the same substrate led to a faster denaturation of the single enzyme (personal communication Dr. Castiglione). These observations underline the notion that the influence of protein fusion on the protein properties is rather specific for each enzyme (Sührer *et al.*, 2014).

7 Production of nano-scale enzyme membrane reactors

7.1 Process conditions

Initial attempts to produce nano-scale enzyme membrane reactors loaded with FDH-KR and $NADP^+$ did not result in the same degree of uniformity of the particles described for the original polymersome preparation method (Poschenrieder *et al.*, 2016). Particular problems were the formation of a polymer or protein residue during the formation process, a higher degree of polydispersity and the encapsulation of less protein than expected. Therefore, some conditions particular to the specific production process were investigated in closer detail.

7.1.1 Buffer

Since most data for the published polymersome production process were obtained in water and by using an automatized polymer feed, the manual injection of the polymer solution into different buffers with a syringe was investigated and evaluated by dynamic light scattering (DLS) after 1.5 h. The polymersomes produced in water were comparable to those of the reference process (PDI of 0.15, z-average of 166 nm; Poschenrieder *et al.*, 2016) with a PDI slightly below 0.2 and a Z-average of 165 nm. Basically, polymersomes produced in sodium phosphate, PBS, MOPS or Bicine were of a similar size and the PDI of those polymersome preparations was only marginally higher than of the polymersomes produced in water (*cf.* Figure 7-1). A minor proportion of particles around 30 nm was only observed in MOPS, indicating that the formation process in this buffer might not be fully completed after 1.5 h. Polymersomes produced in PBS were most homogeneous with a PDI of 0.2 and a Z-average of 170 nm, confirming that high-quality polymersomes are obtained under these conditions. Further experiments were always performed in PBS pH 7.5.

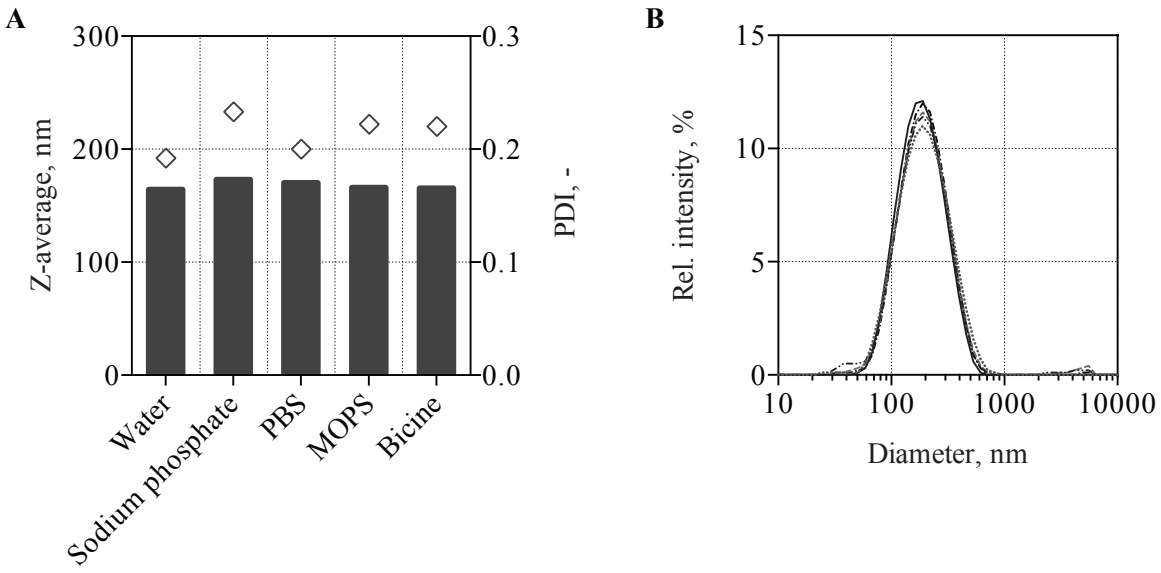

Figure 7-1. Polymersome formation in different media. (A) Z-average (bars) and PDI (◇) after 1.5 h stirring at 4000 min^{-1} and 4 °C in different buffers. (B) Intensity-based size distribution of polymersomes formed in water (—), sodium phosphate (----), PBS (-·-·), MOPS (-···-) and Bicine (····). N=2.

7.1.2 Cofactor concentration

The influence of the presence of $NADP^+$ on the polymersome formation process was so far unknown and needed experimental clarification. The production of polymersomes in PBS was investigated in the presence of up to 50 mM NAD^+ (as a cheaper substitute for $NADP^+$ in preliminary experiments). NAD^+ did not interfere with the polymersome formation up to a concentration of 10 mM, but at NAD^+ concentrations of 25 and 50 mM, a significant formation of visible polymer aggregates could be observed, while the actual concentration and the size of the polymersomes formed was severely reduced (*cf*. Figure 7-2).

An interaction between NAD^+ and already formed polymersomes was also investigated in terms of membrane integrity using polymersomes loaded with fluorescein at a self-quenching concentration. In contrast to calcein, which can be effectively retained within polymersomes for weeks at room temperature, the polymersome membrane was significantly more permeable to fluorescein. At 30 °C, around 13 % of the dye were released within 1 h. The addition of NAD^+ did not cause an increase in the dye release up to the highest concentration investigated (5 mM; *cf*. Figure 7-3).

Although these experiments were only performed with NAD^+ and not with $NADP^+$, no negative effect of the latter was observed when the nano-scale enzyme membrane reactors with a final concentration of 4.5 mM $NADP^+$ were prepared in later experiments (data not shown), indicating a transferability of the results obtained.

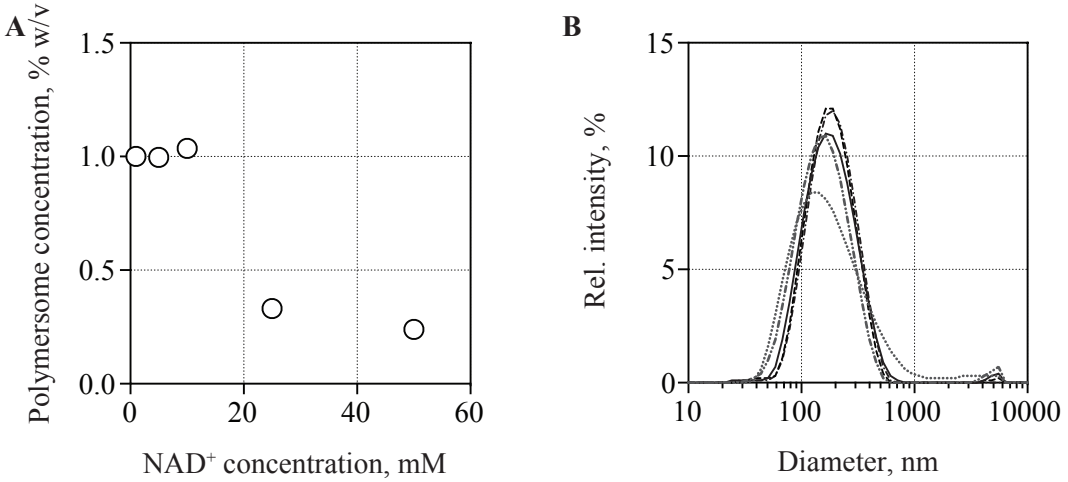

Figure 7-2. Polymersome formation in the presence of NAD^+. (A) Concentration of formed polymersomes after 1 h stirring at 4000 min^{-1} and 4 °C in PBS pH 7.5 as a function of the NAD^+ concentration. The polymersome concentration was determined by absorbance measurements of the polymersome suspension after centrifugation at 16,200 x g for 5 min. (B) Intensity-based size distribution of polymersomes formed in the presence of 1 (—), 5 (----), 10 (-·-·), 25 (-··-) and 50 mM NAD^+ (····). In contrast to the standard DLS sample preparation procedure, the polymersome suspension was centrifuged before the measurements because aggregates formed in the presence of 25 and 50 mm NAD^+ interfered with the DLS measurement. N=2.

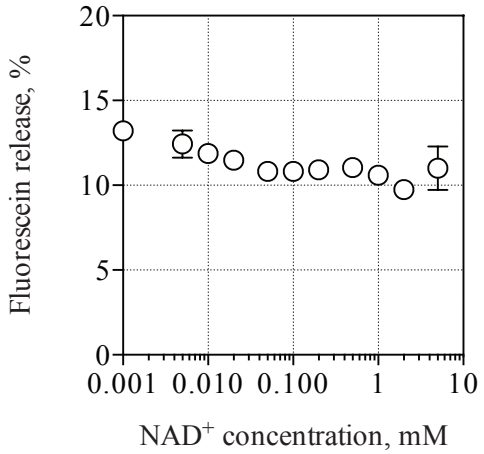

Figure 7-3. Fluorescein release from polymersomes in response to different NAD^+ concentrations at 30 °C. The release of fluorescein was assessed by fluorescence measurement after 1 h relative to polymersomes disintegrated with 1 % O-POE. Note that the polymersome membrane is permeable to fluorescein to some degree even under reference conditions. N=3.

7.1.3 Enzyme concentration and process duration

Likely the most influential factor for the formation of nano-scale enzyme membrane reactors was the enzyme to be encapsulated. Initially, the effect of the protein concentration was investigated with regard to the final polymersome concentration achievable. To account for the still observed formation of

aggregates and the necessity to remove non-encapsulated components, the polymersome formation was assessed after analytical size exclusion chromatography. Interestingly, the observed polymersome concentrations dropped radically with increasing protein concentration, particularly above 1.0 g L^{-1}. If the polymersome suspensions were treated with proteinase K prior to the purification, however, the effect seemed much reduced (*cf.* Figure 7-4), indicating that the formation of protein or protein-polymer aggregates during the process was responsible for a part of the polymersome loss. With prior proteinase K digestion, the interaction between the protein and the polymer still caused the final polymersome concentration to be reduced, but now the lowest polymersome concentration obtained after 3 h was at a protein concentration of 1.8 g L^{-1} and still amounted to 0.8 % w/v. At a protein concentration of 0.40 and 0.80 g L^{-1}, the polymersome concentration after 3 h stirring was comparable to the process without protein. This was also the process time where the PDI became minimal for those concentrations (i.e. <0.25, data not shown). Further stirring was not beneficial, and Figure 7-4 clearly shows that longer process times resulted in a reduced polymersome yield.

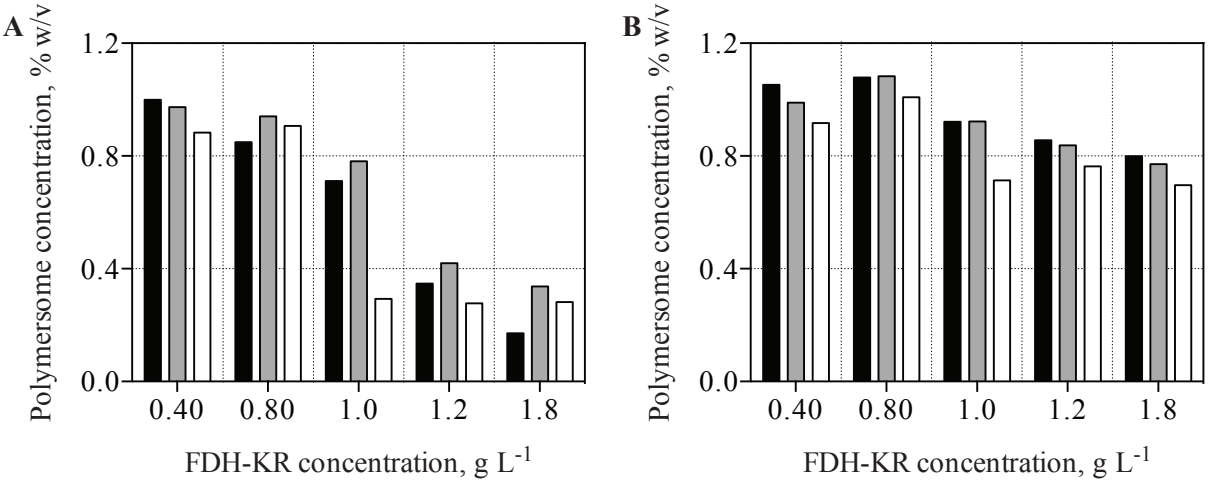

Figure 7-4. Polymersome formation in the presence of the FDH-KR fusion enzyme. Concentration of formed polymersomes after 3 h (black bars), 4 h (grey bars) and 5 h (white bars) stirring at 4000 min^{-1} and 4 °C in PBS pH 7.5 as a function of the enzyme concentration. The polymersome concentration was determined by absorbance measurements of the polymersome suspension after size exclusion chromatography (A) without or (B) with prior proteinase K digestion. N=1.

The moderately reduced polymersome concentrations at protein concentrations above 1.0 g L^{-1} would not present a problem for the production of nano-scale enzyme membrane reactors if this could be traded for a higher activity. However, further experiments revealed that the amount of encapsulated enzymes (as judged by the contained FDH activity, which was deemed appropriate because stirring under the conditions used for polymersome formation did not lead to a reduced activity of the enzyme as long as the protein concentration was above 0.50 g L^{-1}; data not shown) remained nearly constant when the protein concentration was increased from 0.60 to 0.80 or 1.8 g L^{-1} (*cf.* Figure 7-5). This discrepancy cannot be explained alone by a reduced polymersome concentration because the effect of the protein

concentration on the enzyme load was even more pronounced. It rather appears that the encapsulation efficiency is negatively correlated to the protein concentration, as becomes apparent from Figure 7-5B. In analogy to the polymersome concentration, the enzyme load also decreased over time, but again with a steeper slope than the former.

Another interesting observation was that although the encapsulation efficiencies (calculated according to Equation 4-5) decreased with the applied protein concentration, they were still higher than expected for a statistical encapsulation. Assuming a statistical encapsulation efficiency of 100 %, a 1 % w/v polymersome suspension with a mean particle diameter of 100 nm (membrane thickness: 14 nm, aggregation number: 43,000; (Poschenrieder *et al.*, 2016) would encapsulate 0.36 % of the initial volume. This is roughly the encapsulation efficiency obtained when encapsulating 0.88 g L^{-1} FDH-KR, but at a protein concentration of 0.60 g L^{-1}, the statistical encapsulation efficiency amounted to 180 ± 20 % after 3 h according to Equation 4-6.

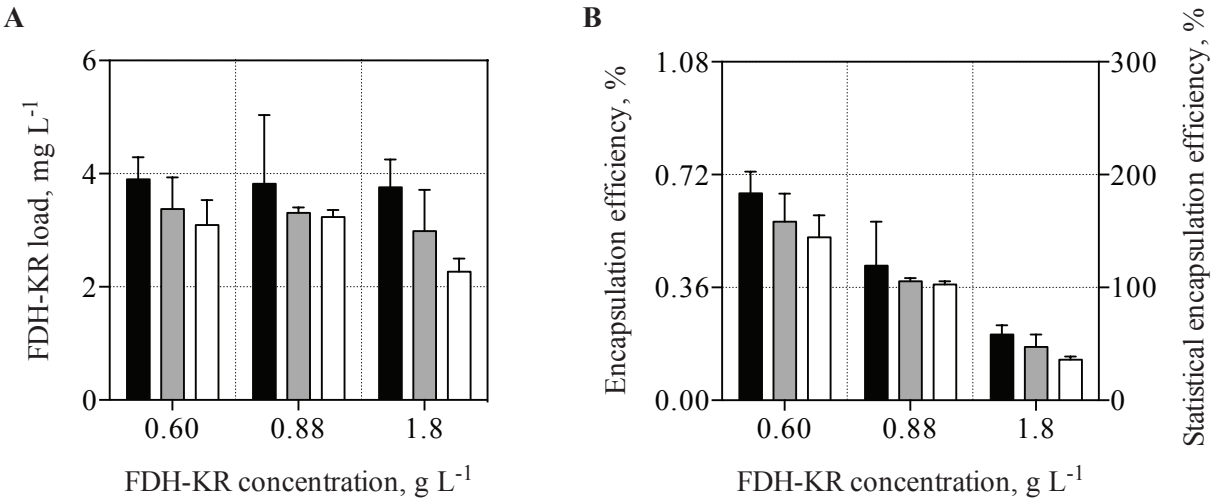

Figure 7-5. FDH-KR encapsulation as a function of the enzyme concentration. (A) Enzyme load and (B) the encapsulation efficiency as well as the statistical encapsulation efficiency after 3 h (black bars), 4 h (grey bars) and 5 h (white bars) stirring at 4000 min^{-1} and 4 °C in PBS pH 7.5. The encapsulated enzyme fraction was determined based on measurement of the FDH activity of the disintegrated polymersome suspension after size exclusion chromatography with prior proteinase K digestion. N=3.

7.1.4 Removal of non-encapsulated enzyme

The KR has been described as a peripheral membrane protein with a high affinity towards membranes (Havel, 2006, Hölsch, 2009). Although this interaction with bacterial membranes was described to be suppressed in the FDH-KR fusion protein (Hölsch and Weuster-Botz, 2010), an interaction with the nascent polymer membranes became apparent from the experiments described in section 7.1.3. Apart from the reduced polymersome concentration after SEC without prior protease treatment at higher protein concentrations, SEC alone proved insufficient to remove non-encapsulated proteins. The polymersome fraction of untreated polymersomes contained a considerable proportion of the overall

FDH activity of the sample. In comparison, the isolated free enzyme eluted exclusively in the late fractions. Proteinase K treatment of the polymersome dispersion prior to SEC resulted in a 5-fold activity reduction in the polymersome fraction and a complete reduction of the activity in the free enzyme fractions (*cf*. Figure 7-6A). These observations are also reflected by an SDS-PAGE of the relevant fractions. After 1 h incubation with ptrypsin, only a fragment of about 25 kDa remained (*cf*. Figure 7-6B). From the available data, it cannot be concluded whether the contaminating protein results from a massive adsorption of the enzyme to the outside of the polymersomes, protein-polymer aggregates or pure protein aggregates due to the fast stirring during the process. The recovery of a higher protein concentration from SEC without prior protease treatment could indicate that protein-polymer and/or protein-polymersome aggregates were involved, since aggregates of a certain size would coelute with the polymersomes. However, transmission electron microscopy did not reveal large aggregates of the latter kind, nor was an excessive alteration of the outer polymersome morphology apparent (*cf*. Figure 7-6C). Nevertheless, these mechanisms might still contribute to some degree to the observed contamination of the polymersome fraction.

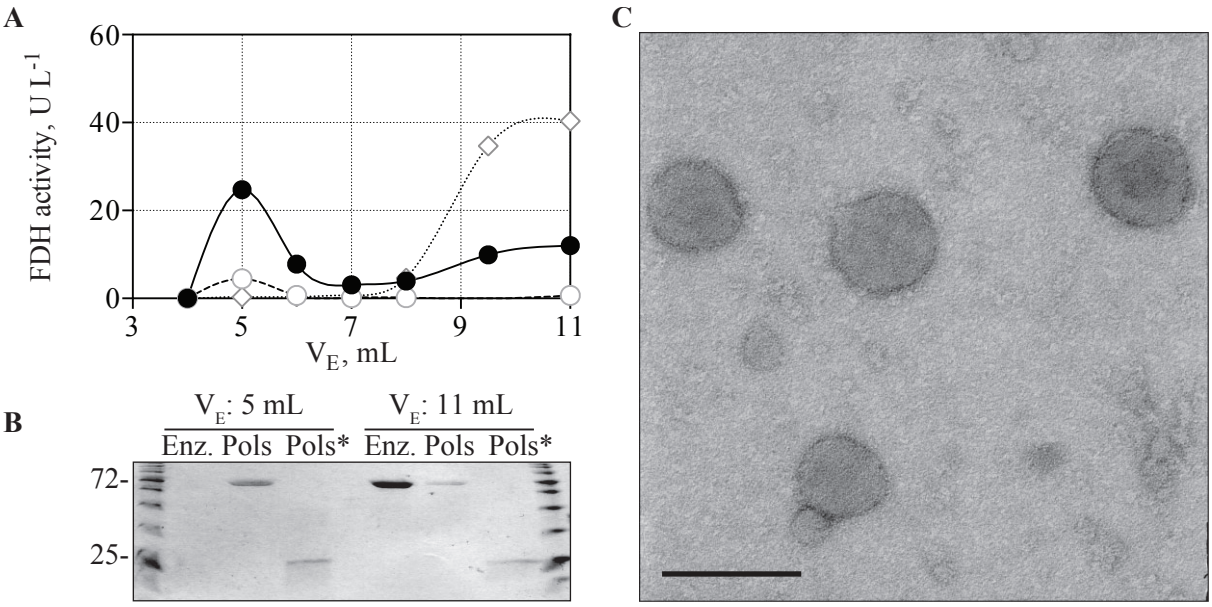

Figure 7-6. Removal of non-encapsulated FDH-KR. (A) FDH activity of SEC fractions of 0.60 g L^{-1} FDH-KR (◇) or polymersomes formed with 0.60 g L^{-1} FDH-KR with (○) and without (●) preceding ptrypsin digestion, depicted as a function of the elution volume V_E. Lines are only included as a guide to the observer. (B) SDS-PAGE of SEC fractions collected after 5mL and 11 mL (Enz: free FDH-KR, Pols: untreated polymersomes, Pols*: trypsin-digested polymersomes). (C) TEM micrograph of undigested and unpurified nano-scale enzyme membrane reactors formed with 0.60 g L^{-1} FDH-KR and 4.5 mM $NADP^+$ and contrasted with uranyl acetate. The scale bar corresponds to 100 nm.

For further characterizations of the nano-scale enzyme membrane reactors a complete removal of non-encapsulated enzyme was highly desirable, so different strategies for the enzyme removal were evaluated. Prior incubation of the polymersome suspension with an excess of IMAC beads did not result

in a reduced activity in the polymersome fraction after SEC (data not shown). Protease treatment on the other hand proved to be effective. The performance of the commercially available proteases proteinase K and ptrypsin on the inactivation of 0.60 g L^{-1} FDH-KR was compared at 4 °C. proteinase K treatment led to a complete KR inactivation within 1 h, regardless of the applied protease concentration (50 or 250 mg L^{-1}). The FDH activity was reduced to about 40 % in the same time but remained constant afterwards. Although no protein could be detected by SDS-PAGE afterwards, it appears likely that the FDH-part of the enzyme is partially proteinase K-resistant and also retains partial activity. Proteinase K activity is known to be increased rather than abolished upon heating in SDS due to a better substrate availability, which could lead to a further digestion of residual FDH during the sample preparation step. Besides, subsequent purification of proteinase K-treated polymersomes was sufficient to remove most of the residual contaminating FDH activity (data not shown). Treatment of the protein with ptrypsin led to a complete disappearance of both FDH and KR activity, but at a lower rate. A complete FDH inactivation was only observed after 24 h treatment at 4 °C, and, in contrast to the inactivation by proteinase K, there was a considerable difference between the two protease concentrations. Accordingly, proteinase K pretreatment was judged to be more suitable for an efficient production strategy of nano-scale enzyme membrane reactors.

The final production process with 3 h stirring at a protein concentration of 0.60 g L^{-1} with subsequent proteinase K treatment with 250 mg L^{-1} and SEC resulted in a high enzyme load in the range of 4.0 mg L^{-1} with less than 10 % residual FDH and no residual KR activity.

7.1.5 Discussion

The formation of high-quality nano-scale enzyme membrane nanoreactors presents a prerequisite for the successful demonstration of their usefulness for asymmetric syntheses. Furthermore, to be able to evaluate potential transport limitations, the ability to encapsulate a sufficient enzymatic activity was considered important. Due to initial problems with the achievement of these goals, the polymersome formation process was investigated with all components to analyze which factors were most influencing the polymersome quality. Different buffers had a negligible effect on the polymersome quality. The presence of small molecules on the other hand has shown potential to inhibit the polymersome formation. Calcein, a hydrophilic dye, inhibited the formation of polymersomes at a concentration of 25 mM, while 15 mM were tolerated (Poschenrieder, 2017). Similarly, the cofactor concentration influenced the polymersome formation in this thesis, but only at concentrations above 10 mM, which is sufficient for full enzymatic activity. The most important influence was found to be the presence of the fusion enzyme, which is able to interact with the polymer. Protein concentrations above 1.0 g L^{-1} during the formation process led to low polymersome recoveries in the subsequent purification. This effect was reduced when the polymersomes were protease-treated beforehand, but even then, total polymersome yields were reduced by 20 % at a protein concentration of 1.8 g L^{-1}. Klermund (2017) observed a similar

inhibition of the polymersome formation at protein concentrations exceeding 1.5 g L^{-1} when encapsulating the enzyme *N*-acetylglucosamine 2-epimerase (AGE). The AGE did not adhere to the surface of the polymersomes, which is in contrast to the FDH-KR, which displayed a significant adsorption to the polymersomes, necessitating a two-step purification process consisting of protease treatment and size exclusion chromatography. Residual binding of HRP to the surface of polymersomes was also reported by Nallani *et al*. (2006). Although the high affinity of the KR to bacterial membranes was shown to be abolished in the fusion enzyme (Hölsch, 2009), this is supposedly due to steric effects and the higher solubility of the FDH part. An interaction with the dissolved polymer or nascent polymer membranes or smaller particles with a higher curvature than bacterial membranes is therefore still conceivable and represents the most likely explanation for the observed interference with the polymersome formation and the negative effect of the protein concentration on the encapsulation efficiency. This assumption is also in agreement with the appearance of visible protein-protein, protein-polymer or protein-polymer aggregates during the formation process of FDH-KR-loaded polymersomes. The restoration of higher polymersome recoveries after protease digestion is also a strong indicator that a part of the polymersomes is initially sequestered within the formed aggregates (whatever their exact nature) and removed during the centrifugation step necessary for the subsequent SEC purification, and that these aggregates are at least in part resolved by digesting the non-encapsulated enzyme. Another aspect is the kinetics of the polymersome formation at 4 °C in the presence of protein. Klermund (2017) also observed that the formation of AGE-loaded polymersomes at 4 °C took considerably longer than the formation of empty polymersomes (7 vs. 5 h), and even then, the PDI was higher than the <0.2 described for the reference process (Poschenrieder *et al.*, 2016). At a protein concentration of 0.60 g L^{-1}, the PDI of the nano-scale enzyme membrane reactors produced in this thesis usually became minimal (i.e. <0.25) after 3 h. In general, longer process times result in a more narrow particle size distribution, which was observed by Klermund (2017) and Poschenrieder *et al*. (2016) using the same $PMOXA_{15}$-$PDMS_{68}$-$PMOXA_{15}$ polymer used in this thesis. However, process times of several hours were also described to lead to a certain degree of polymersome destruction and the formation of polymer aggregates in the latter work, and the presence of the FDH-KR fusion enzyme apparently enhanced this effect, since longer process times led to lower polymersome yields and lower encapsulation efficiencies in this thesis. The reason for the lower enzyme load after longer process times becomes evident from the observation that the larger particles disappear first during the process (Poschenrieder *et al.*, 2016). Unfortunately, the encapsulation efficiency also mainly depends on the vesicle dimensions (Rigler and Meier, 2006, Onaca *et al.*, 2010), since larger vesicles can harbor more enzyme molecules due to their lower surface-to-volume ratio and the consequently larger encapsulated volume.

As a result of the interaction of the FDH-KR and the polymersomes, the statistical encapsulation efficiency became quite high at a protein concentration of 0.60 g L^{-1}, i.e. 180 ± 20 %. In the absence of any interaction, the statistical encapsulation efficiency cannot become higher than 100 % (Wang *et al.*, 2012). Unfortunately, the negative influence on the polymersome formation and the polymersome yield

counteracted this primarily positive effect, so that actually not more than 2 FDH-KR fusion enzymes could be effectively encapsulated. The encapsulation efficiency of the FDH-KR at a process concentration of 0.60 g L^{-1} amounts to 0.69 % or 4.1 µg mg^{-1} polymer. Depending on the size of the formed polymersomes and the applied protein concentration, this result is comparable to other examples from the literature. Klermund (2017) was able to encapsulate 0.47 % of the initially added AGE within 110 nm polymersomes, which amounts to 4 AGE molecules per polymersome and a statistical encapsulation efficiency of 82 ± 17 % to 89 ± 16 %. Rigler and Meyer (2006) described the encapsulation of 0.5-10 avidin-Alexa488 conjugates per polymersome at protein concentrations ranging from 0.03-1 g L^{-1}, which corresponds to an average statistical encapsulation efficiency of 80 %. Vrizeema *et al*. (2007) encapsulated 14 GOx molecules within 517 nm PS-PIAT polymersomes, and Noor *et al*. (2012) encapsulated 2 eGFP molecules within 100 nm PIB-PEG-PIB polymersomes. Significantly higher encapsulation efficiencies can be achieved by other polymersome formation techniques, such as film rehydration. Encapsulation efficiencies for bovine serum albumin, ovalbumin and γ-globulin amounted to 15-37 %, but because the applied polymer concentration was much higher, this corresponds only to 2.4-13 µg mg^{-1} polymer. Encapsulation of the *Trypanosoma vivax* nucleoside hydrolase TvNH (Ranquin *et al.*, 2005) was actually rather efficient, since the 15 % encapsulation efficiency translate to a statistical encapsulation efficiency of 94 %. Other enzymes are apparently less efficiently encapsulated. Lee *et al*. (2001) encapsulated hemoglobin and albumin with a statistical encapsulation efficiency of 4.5 and 5 % by film rehydration, while myoglobin encapsulation by electroformation resulted in a statistical encapsulation efficiency of 55 %. These examples illustrate that most encapsulations reported so far result in a rather comparable enzyme loading per polymersome, since the film rehydration approaches only use up more of the bulk protein but do not actually produce more active nano-scale enzyme membrane reactors. A true positive interaction between the encapsulated protein and the polymersomes was shown for the encapsulation of GOx, G6PDH and CRE2-PAMO by a THF- or dioaxane-mediated formation process, respectively. Van Dongen *et al*. (2009) and Meeuwissen *et al*.(2011) found that these enzymes were encapsulated into 90-180 nm PS-PIAT polymersomes with an efficiency of 18-25 %, which is several times more than the expected efficiency of 0.1 % for a statistical inclusion. In another study, Wang *et al*. (2012) could encapsulate BSA with an efficiency 15-20 times higher than by statistical inclusion using electroporation. However, the polymersomes produced by these authors had a significantly thinner membrane (6.5 nm) than the one used in this thesis, thus requiring lower electroporation voltages. Therefore, initial attempts to incorporate FDH or AGE into polymersomes by electroporation were not successful (own experience and personal communication Ludwig Klermund, TUM). Compared to the extremely high encapsulation efficiencies just mentioned, the 1.8-fold enrichment of the FDH-KR within the polymersomes produced in this thesis is moderate, but higher than most reports nevertheless.

7.2 Membrane functionalization of polymersomes using channel proteins

The reconstitution of channel proteins was a central problem *en route* to the generation of membrane-functionalized nano-scale enzyme membrane reactors. Two different strategies were available to achieve reconstitution of the channel proteins into the polymersome membrane, either before or after the formation of polymersomes (Nardin *et al.*, 2000b). Although the former method was described to be more convenient, it requires considerable amounts of channel protein when opting for the reconstitution of the channel protein on the classical 12 mL scale employed for polymersome production, which was not desirable at the exploratory stage. A great disadvantage of this approach is the reduced tolerance for the presence of detergent during the formation of the polymersomes. While the effect of different detergents on already formed polymersomes correlated roughly with their CMC (*cf.* Figure B 5), at least LDAO, *N*-lauroylsarcosine and O-POE already interfered with the formation of polymersomes at much lower concentrations (data not shown), thus limiting the degree of functionalization which can be achieved this way. Additionally, this approach lacks the flexibility of the latter approach to integrate a number of different channel proteins under different conditions into a homogeneous polymersome preparation on a small scale. Therefore, the addition of the channel protein stock to the polymer solution in ethanol and subsequent polymersome formation was not attempted, but instead channel proteins were reconstituted into preformed polymersomes only. The reconstitution of a protein by mixing the detergent-stabilized protein stock with the polymersomes is a non-equilibrium process and is driven by the dissociation of the detergent upon dilution below the CMC, resulting in the association of the membrane protein with any membrane in the vicinity and its subsequent integration therein to reduce the contact of the exposed hydrophobic protein surface with the aqueous solvent (depicted in Figure 7-7). Non-integrated protein is usually quickly inactivated and likely to aggregate in the absence of detergent micelles or membranes.

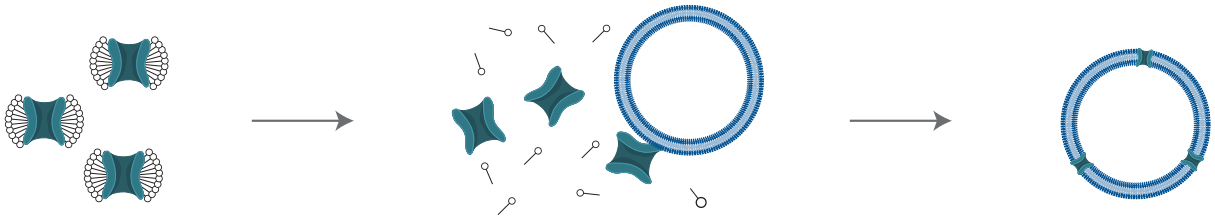

Figure 7-7. Schematic representation of the reconstitution of channel proteins into polymersomes.

7.2.1 Membrane functionalization of polymersomes using one channel protein species

The reconstitution of a single channel protein species was first studied with AlkL because the production of this protein was fairly uncomplicated and very productive due to the efficient refolding in LDAO, which is compatible with an immediate further purification and concentration by ion-exchange. Because residual detergent was not desirable in the final nano-scale enzyme membrane reactors and to be able to distinguish between integrated and non-integrated channel proteins, the polymersomes were purified

once more by SEC after channel protein reconstitution. This step also served to ensure that no cofactor or enzyme that might have been released as a consequence of locally increased detergent concentrations and the resulting disintegration of polymersome were present in the final polymersome preparations. In the absence of polymersomes, no channel protein could be detected in the early SEC fractions following ultracentrifugation and SDS-PAGE analysis (data not shown).

As an important factor of influence for the channel protein reconstitution into polymersomes, the temperature during this process step was investigated. A comparison between a short incubation at 30 °C with agitation (800 min^{-1}) and overnight incubation at 4 °C revealed a clear advantage of the higher temperature, with a 1.5-fold higher channel reconstitution into the polymersomes (data not shown). Accordingly, all further reconstitution experiments were performed under these conditions.

As a result of the additional SEC purification step and the ensuing dilution, higher polymersome concentrations were desirable for the reconstitution step and initial polymersome concentrations of 1, 2 and 3 % w/v were investigated at a constant protein:polymer ratio of 1:100. Under these conditions, the integration of AlkL could be increased 2.6-fold from 51 ± 3 to 130 ± 3 channels per polymersome if the polymersome concentration was increased from 1 % w/v to 2 % w/v. This result translates to a reconstitution efficiency of 29 ± 1 %. A further increase of the polymersome concentration to 3 % w/v did result in the reconstitution of only 112 channels per polymersome, possibly as a result of the higher detergent concentration (*cf.* Figure 7-7A).

The detergent concentration did indeed influence the reconstitution of AlkL, as shown for a 2 % w/v polymersome suspension and a protein:polymer ratio of 1:500 (*cf.* Figure 7-7B). The amount of detergent introduced with the protein results in a final concentration of roughly 0.001 % w/v LDAO. Doubling the detergent concentration led to a 1.8-fold increased AlkL reconstitution, but a further increase of the LDAO concentration to 0.004 % w/v was again slightly less conducive (1.7-fold increased reconstitution).

Variation of the AlkL concentration at a constant polymersome concentration of 2 % w/v in another experiment demonstrated a clear dependence of the reconstitution of AlkL on the protein:polymer ratio (*cf.* Figure 7-7C). Reconstitution at a protein:polymer ratio of 1:100 resulted in a 6.3-fold increased membrane functionalization compared to the reconstitution at a protein:polymer ratio of 1:1000 (150 ± 5 vs. 24 ± 3 channels per polymersome). However, the reconstitution efficiency dropped from 55 ± 6 to 35 ± 1 %.

A time-resolved investigation of the AlkL reconstitution into a 2 % w/v polymersome suspension at a protein:polymer ratio of 1:100 served to justify the chosen integration time of 1 h (*cf.* Figure 7-7D). Although a high proportion of the protein had already been associated with the polymersomes after a period of 5 min, the number of channels reconstituted could be further increased 1.3-fold from 110 ± 13 to 150 ± 17 channels per polymersome if the incubation time was prolonged to 1 h. An even longer

incubation period was not considered to avoid unnecessary damage to the encapsulated enzyme and the cofactor at 30 °C. Besides, it was observed in some experiments where detergent concentrations were critically high that the destruction of polymersomes as a result of the detergent also increased over time.

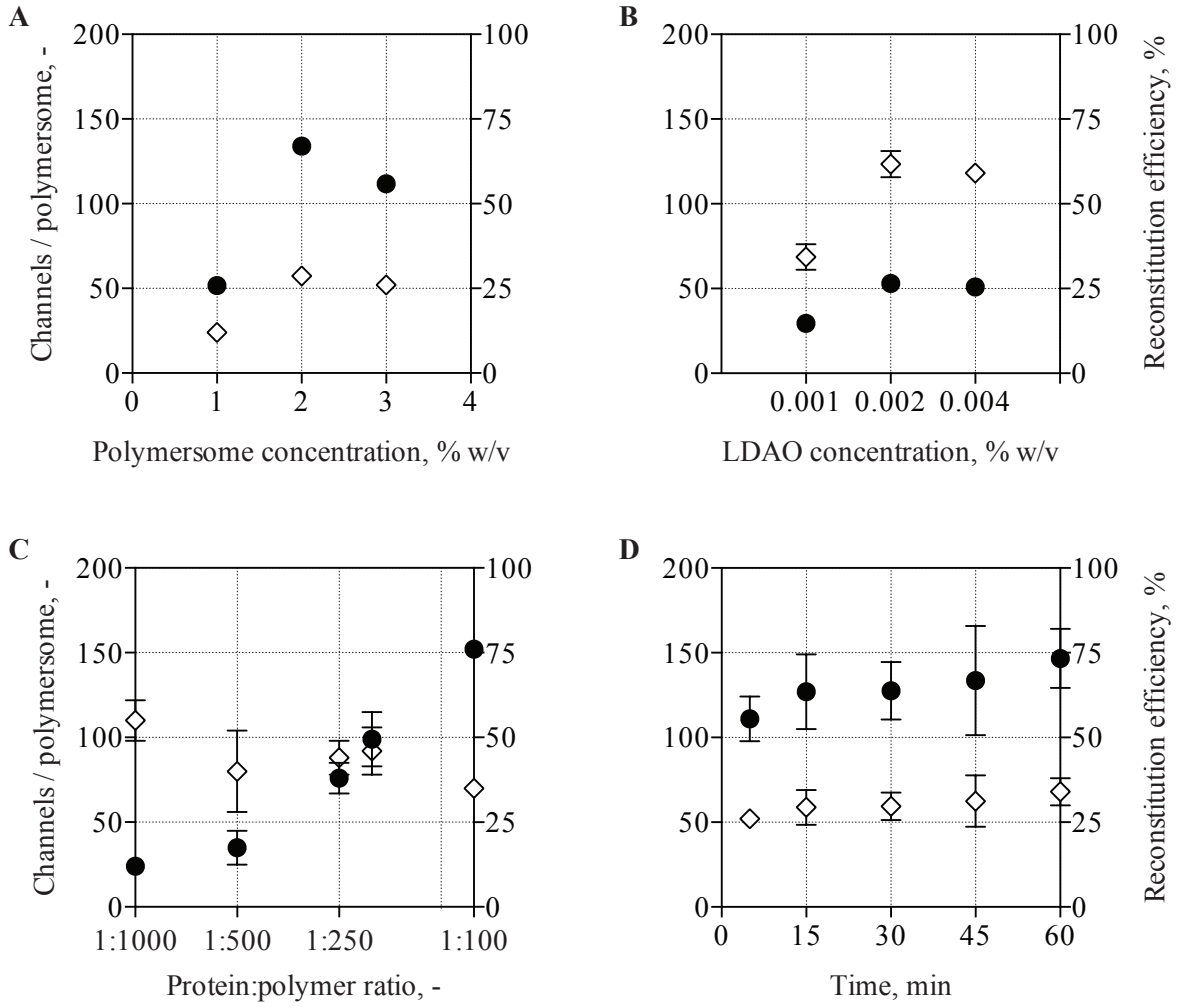

Figure 7-8. Reconstitution of AlkL (batch #1) into empty polymersomes. The number of channels per polymersome (●) and the reconstitution efficiency (◇) are shown. (A) Reconstitution at a fixed protein:polymer ratio of 1:100 as a function of the polymersome concentration. (B) Influence of the detergent (LDAO) concentration on the reconstitution of AlkL into 2 % w/v polymersomes at a protein:polymer ratio of 1:500. An LDAO concentration of 0.001 % w/v roughly corresponds to the LDAO introduced by the protein stock under the chosen conditions. (C) Reconstitution at a fixed polymersome concentration of 2 % w/v as a function of the protein:polymer ratio. (D) Reconstitution into 2 % w/v polymersomes at a protein:polymer ratio of 1:100 over time. N=3.

The maximal loading capacity of the membrane for a membrane-spanning protein was estimated from the available surface area of the inner side of the polymersome membrane and the area occupied by a single channel protein of a cylindrical shape, according to Equation 7-1 and Equation 7-3, respectively. The inner polymersome diameter d_i' (assumed to be 81 nm) was derived from the number-based mean diameter of the polymersomes d_P of 100 nm, which was measured by dynamic light scattering, the

membrane thickness of 14 nm (Poschenrieder *et al.*, 2016) and an assumed mismatch of 9 nm. The latter parameter derives from the difference between the channel protein length (5 nm) and the thickness of the polymer membrane (*cf.* Equation 7-2). Furthermore, it was assumed that the protein would insert into the center of the membrane, so that the mismatch translates into equal distances to both sides of the membrane. The relationships are illustrated in Figure 7-9.

$$A'_{Polymersome,i} = \pi \cdot d_i'^2 = \pi \cdot (d_P - 2d_M + mismatch)^2 \qquad \text{Equation 7-1}$$

$$Mismatch = d_M - L_{channel} \qquad \text{Equation 7-2}$$

$$A_{Channel\ protein} = \pi \cdot r_{channel}^2 \qquad \text{Equation 7-3}$$

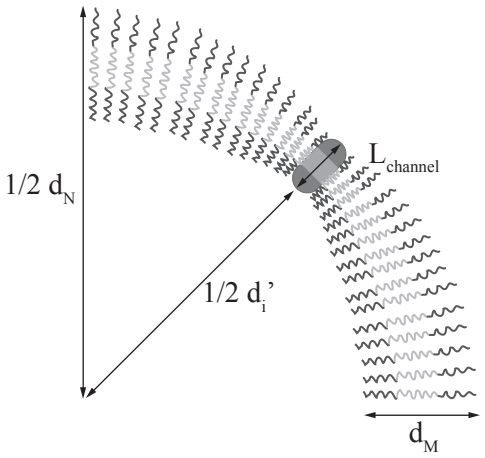

Figure 7-9. Illustration of the relationships between d_N, d_i', d_M *and* $L_{channel}$.

At the highest-density hexagonal packing arrangement of equal circles, which is equivalent to the two-dimensional packing of spheres, 90.7 % of the available surface area A_i can be covered by the channel proteins. For an average small 8-stranded outer membrane protein like OmpA (in the absence of a crystal structure of AlkL), $r_{channel}$ is approximately 1.2 nm, while it is 3.1 nm for an OmpF trimer (Rassam *et al.*, 2015). Accordingly, the membrane of a polymersome with the above dimensions could harbor about 3500 AlkL monomers or 620 OmpF trimers. The highest AlkL-loading achieved so far amounts to 150 ± 5 and thus represents a loading of about 4.3 % of the maximal capacity.

Transmission electron microscopy was again deployed to validate whether the polymersome morphology was altered upon channel protein reconstitution. Nano-scale enzyme membrane reactors functionalized with AlkL at a protein:polymer ratio of 1:100 appeared indeed comparable to their plain, unfunctionalized counterparts (*cf.* Figure 7-10). It would have been interesting to detect reconstituted

AlkL by this approach, but the limited resolution of the TEM did not allow the distinction of the smaller channel proteins in the membrane.

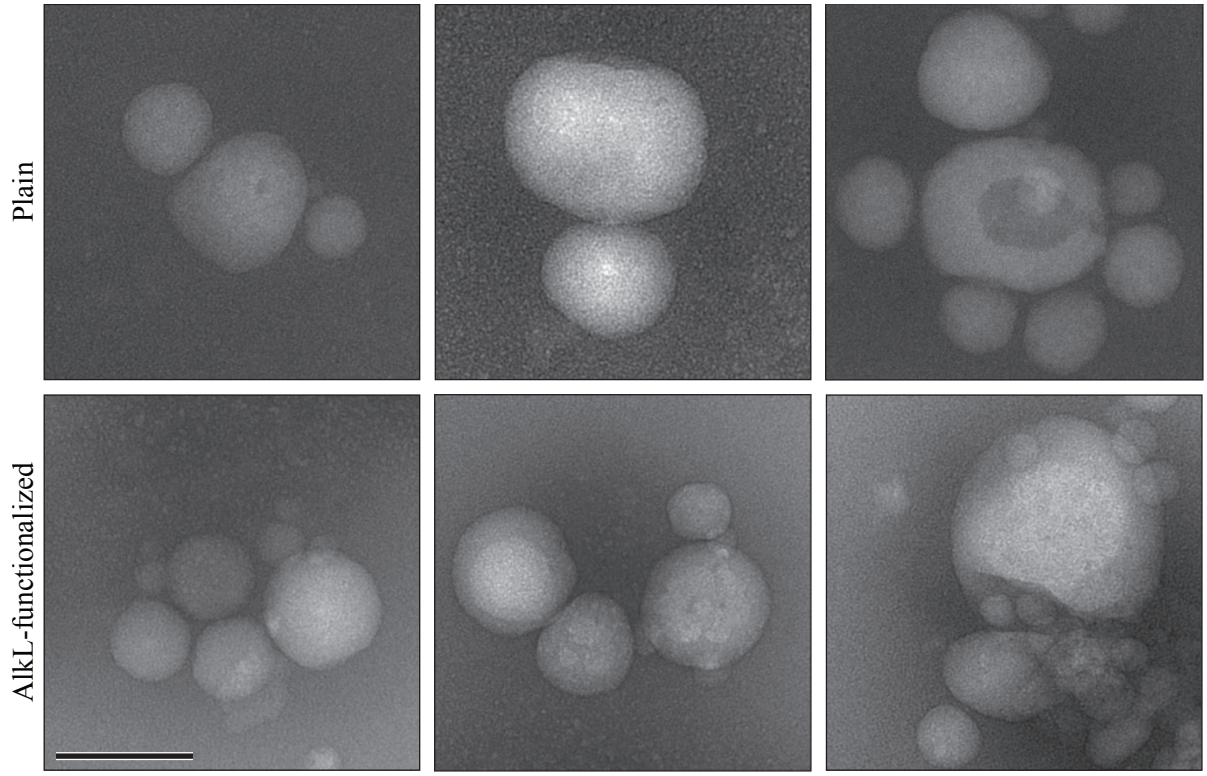

Figure 7-10. TEM micrograph of plain and AlkL-functionalized nano-scale enzyme membrane reactors formed with 0.60 g L^{-1} FDH-KR and 4.5 mM $NADP^+$ and contrasted with uranyl formate. The scale bar corresponds to 100 nm.

The reconstitution of AlkL, OmpW, OprG and TodX into nano-scale enzyme membrane reactors loaded with fusion enzyme and $NADP^+$ is displayed in Figure 7-11. Across all reconstitution experiments performed with nano-scale enzyme membrane reactors, the reconstitution of these channel proteins was usually more or less dependent on the protein:polymer ratio, but the variation within the data was far greater than in the previous experiments with AlkL reconstituted into empty polymersomes. The highest number of AlkL channels per polymersome in this setting amounted to 120 ± 6 at a protein:polymer ratio of 1:100, which is slightly lower than the 150 ± 5 channels per polymersome obtained for the functionalization of empty polymersomes. One problem that became apparent over time was that, depending on the particular channel protein stock used, a protein:polymer ratio of 1:100 often led to a partial destruction of the polymersomes, for unknown reasons particularly with TodX. As already mentioned, this effect became also more pronounced with longer incubation times. Reconstitution of OmpW and TodX was also far less successful than AlkL reconstitution, with 28 ± 2 channels per polymersome at a protein:polymer ratio of 1:200 and 19 ± 1 channels per polymersome at a protein:polymer ratio of 1:250. OprG reconstitution was intermediary with a maximum of 65 ± 2 channels per polymersome at a protein:polymer ratio of 1:200.

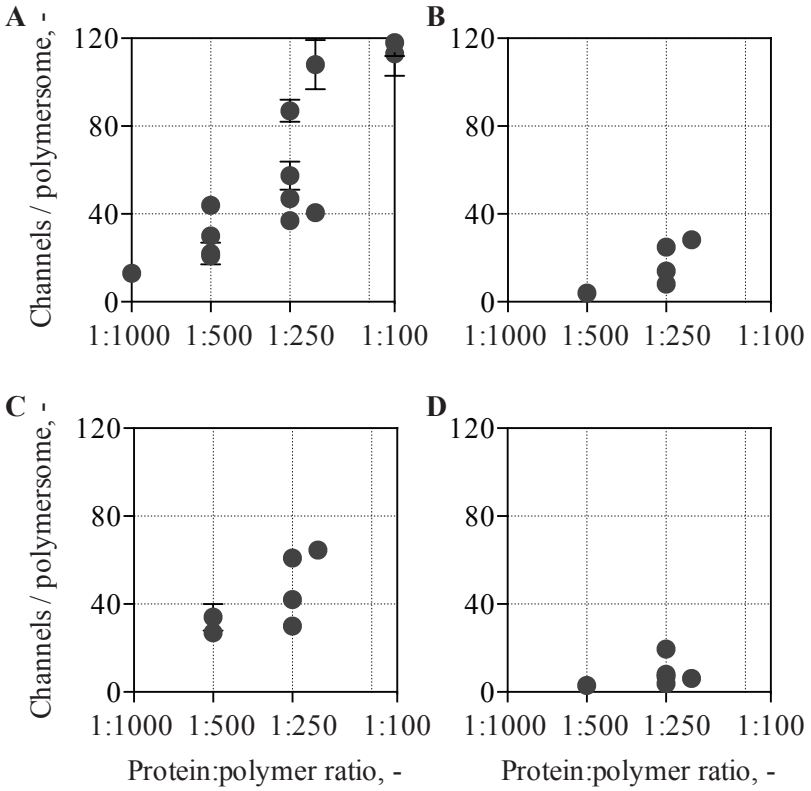

Figure 7-11. Reconstitution of (A) AlkL, (B) OmpW, (C) OprG and (D) TodX into 2 % w/v nano-scale enzyme membrane reactors loaded with 0.60 g L^{-1} FDH-KR and 4.5 mM $NADP^+$ as a function of the protein:polymer ratio. The results shown are derived from a number of experiments performed with different batches of nano-scale enzyme membrane reactors and of the channel proteins. Only AlkL was always from the same stock. N=3.

Reconstitution of the natively expressed and purified ion channel proteins into nano-scale enzyme membrane reactors loaded with fusion enzyme and $NADP^+$ was also investigated. FocA reconstitution was least successful and resulted in a maximum number of 17 ± 1 FocA channels per polymersome at a protein:polymer ratio of 1:100 (*cf.* Figure 7-12A). Even the addition of 0.02 % w/v LDAO could not improve the reconstitution of FocA (data not shown). Batch-specific differences in the reconstitution were greatest for OmpF and PhoE, with a maximum of 50 ± 5 and 80 ± 7 channels per polymersome, both achieved at a protein:polymer ratio of 1:250 (*cf.* Figure 7-12B/C). Incidentally, the number of 80 PhoE channels per polymersome also amounted to around 4.3 % of the theoretically maximal loading capacity, similar to the results obtained with AlkL.

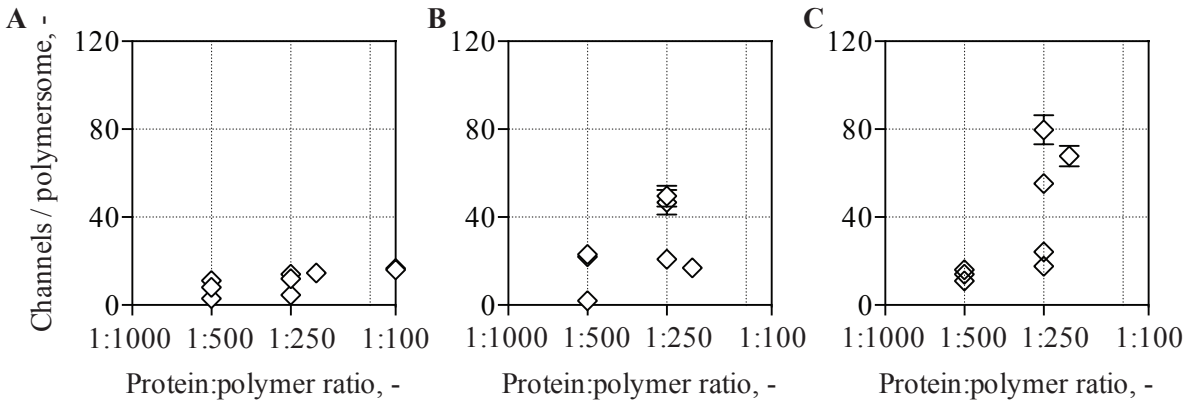

Figure 7-12. Reconstitution of (A) FocA, (B) OmpF and (C) PhoE into 2 % w/v nano-scale enzyme membrane reactors formed with 0.60 g L^{-1} FDH-KR and 4.5 mM $NADP^+$ as a function of the protein:polymer ratio. The number of channel monomers per polymersome is indicated. The results shown are derived from a number of experiments performed with different batches of nano-scale enzyme membrane reactors and of the channel proteins. N=3.

The variable success of the channel protein reconstitution into nano-scale enzyme membrane reactors loaded with fusion enzyme and $NADP^+$ is also reflected in the reconstitution efficiencies observed across all performed experiments (*cf.* Figure 7-13). AlkL and OprG reconstitution was most efficient with a median reconstitution efficiency of 33 %. OmpW, OmpF and PhoE were reconstituted with intermediate median efficiencies of 13, 27 and 17 %, while TodX and FocA were reconstituted with 7.7 and 6.8 % median efficiency.

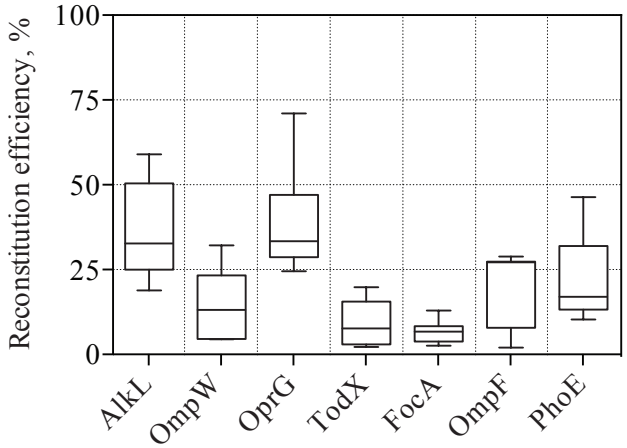

Figure 7-13. Box-whisker representation of the reconstitution efficiencies of all seven channel proteins into 2 % w/v nano-scale enzyme membrane reactors formed with 0.60 g L^{-1} FDH-KR and 4.5 mM $NADP^+$. The results shown are derived from a number of experiments performed with different batches of nano-scale enzyme membrane reactors and channel proteins at different protein:polymer ratios.

7.2.2 Membrane functionalization of polymersomes using two channel protein species

The co-reconstitution of two channel protein species, one ion channel and one channel protein for the transport of hydrophobic substrates, was also investigated. Unfortunately, combinations with FocA could not be analyzed densitometrically because the FocA band appeared rather diffuse and partially overlapped with the other channel protein bands on SDS-PAGE. The co-reconstitution with PhoE (at a fixed absolute protein:polymer ratio of 1:200; *cf*. Figure 7-14) turned out to be quite complex and unpredictable. In combination with OmpW for instance, both channels were reconstituted as efficient as when reconstituted alone. In combination with AlkL, both proteins were reconstituted more efficiently. In a combination with OprG, PhoE was reconstituted more efficiently, while the reconstitution efficiency of OprG was impaired. Finally, an impaired PhoE and improved TodX reconstitution were observed when these two channels were combined.

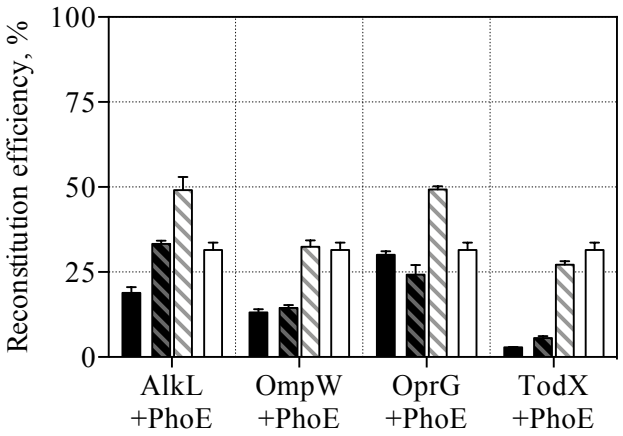

Figure 7-14. Co-reconstitution of channel proteins for hydrophobic substrates (black bars) in combination with PhoE (white bars) into 2 % w/v nano-scale enzyme membrane reactors formed with 0.60 g L^{-1} FDH-KR and 4.5 mM $NADP^+$. The overall protein:polymer ratio was kept constant at a value of 1:200, i.e. channel proteins were reconstituted alone at a protein:polymer ratio of 1:200 (plain bars) or two channel proteins were combined, each at a protein:polymer ratio of 1:400 (streaked bars). Channel proteins were of the batches: AlkL #1, OmpW #2, OprG #2, PhoE #3, TodX #2. N=3.

The co-reconstitution of PhoE and TodX was investigated more systematically at a fixed absolute protein:polymer ratio of 1:250 but with different mixtures of the channel proteins. In this experiment, PhoE reconstitution appeared to be more efficient at higher PhoE:TodX ratios, and PhoE could be reconstituted with an efficiency of 46 ± 4 % in the absence of TodX. Similarly, the reconstitution efficiency of TodX also increased at higher PhoE:TodX ratios, resulting in a maximal number of 10 ± 0.4 channels per polymersome at a PhoE:TodX ratio of 0.25.

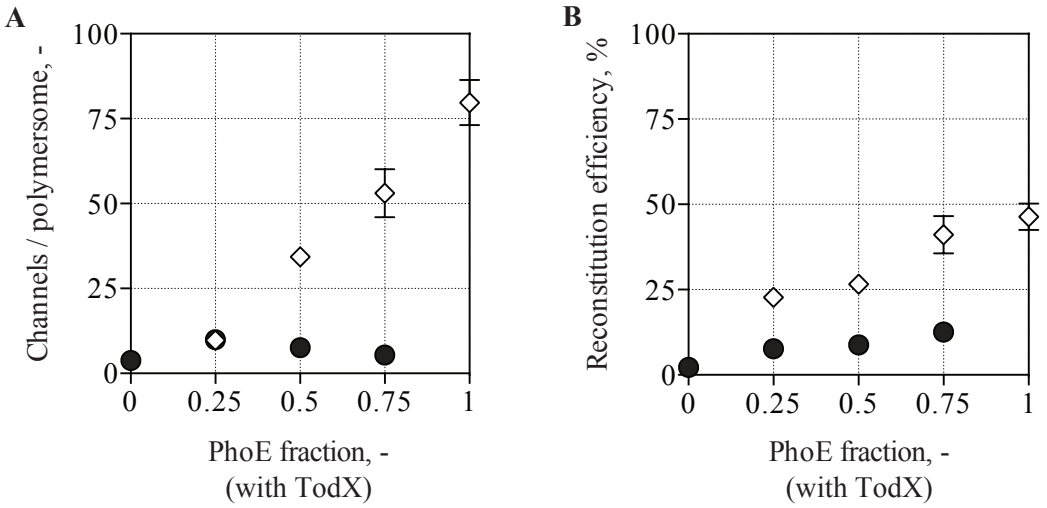

Figure 7-15. Co-reconstitution of PhoE (batch #3) and TodX (batch #2) into 2 % w/v nano-scale enzyme membrane reactors formed with 0.60 g L^{-1} FDH-KR and 4.5 mM $NADP^+$. The overall protein:polymer ratio was kept constant at a value of 1:250, but the proportion of the two protein species was varied. (A) Number of channel proteins per polymersome and (B) reconstitution efficiency for (◇) PhoE and (●) TodX. N=3.

7.2.3 Discussion

Another aspect of the production of nano-scale enzyme membrane reactors is the actual membrane functionalization with channel proteins. Using the model protein AlkL and empty polymersomes, standard conditions for the reconstitution procedure could be established which assured a substantial functionalization of the polymersomes. A temperature of 30 °C was preferable to reconstitution at 4 °C, possibly as a result of the energetically unfavorable insertion into a preformed membrane with a considerable hydrophobic mismatch (Pata and Dan, 2003). 1.3-fold higher reconstitution efficiencies were observed when the incubation period before removal of non-reconstituted channels was prolonged from 5 min to 1 h. In analogy, it was observed with different lipids that thicker membranes slow down outer membrane protein insertion and folding (Burgess *et al.*, 2008). Although no external detergent was added for most of the experiments, the integration was in fact detergent-mediated due to the relatively high protein:polymer ratios employed. Consequently, reconstitution was more efficient at a polymersome concentration of 2 % w/v compared to 1 % w/v at a fixed protein:polymer ratio. This condition represents a good compromise between a reasonable polymersome concentration after purification by SEC, the beneficial effects of moderate detergent concentrations on the protein reconstitution and the destruction of polymersomes at higher detergent concentrations. The highest protein:polymer ratio of 1:100 also led to a higher degree of functionalization, but at the cost of a lower reconstitution efficiency. This phenomenon is apparently not unique to the reconstitution into preformed polymersomes, since Erbakan *et al*. (2014) reported decreases reconstitution efficiencies for aquaporin Z at higher protein:polymer ratios using a film rehydration approach. So far, most membrane proteins were reconstituted during the polymersome formation process, but reconstitution of the *E. coli* complex

I into different preformed PMOXA-PDMS-PMOXA polymersomes was mediated by 0.5 % w/v Triton X-100 and sonication, resulting in 40-60 % reconstitution at protein:polymer ratios of 1:2,600-1:15,000, depending on the molecular mass of the polymer (Graff *et al.*, 2010). In terms of efficiency, AlkL reconstitution in 2 % w/v polymersomes ranged from 35-55 %, which is in the same range as the detergent-mediated complex I reconstitution. In terms of the absolute number of channel proteins, up to 150 ± 5 AlkL molecules per polymersome could be realized with empty polymersomes and 120 ± 6 with nano-scale enzyme membrane reactors.

Reconstitution of AlkL into FDH-KR loaded polymersomes proved slightly less efficient for unknown reasons. Furthermore, the other three monomeric outer membrane proteins OmpW, OprG and TodX as well as the ion channel proteins FocA, OmpF and PhoE were also reconstituted into FDH-KR-loaded polymersomes. Of these seven membrane proteins, only OmpF has previously been reconstituted into polymersomes. Reconstitution of the other six proteins proved less efficient than AlkL reconstitution, but to a varying degree. While up to 80 PhoE or 65 molecules of OprG per polymersome could be reconstituted, FocA, OmpW and TodX reconstitution was far less efficient (at protein:polymer ratios of 1:250-1:100). The median reconstitution efficiencies of this set of channel proteins ranged from 6.8-33 %. It is difficult to compare these results with other studies, since most publications involving the reconstitution of membrane proteins do not explicitly state the actual number or efficiency of the reconstituted membrane protein, but rather indicate only the initial protein:polymer ratio. Apparently assuming a quantitative reconstitution, polymersome functionalization with 5-20 (Nardin *et al.*, 2000b) or even 130-1,300 (Ranquin *et al.*, 2005) OmpF molecules following film rehydration was reported. Since this method involves the previous mixing of the channel protein with the polymer in an organic solvent, this method can arguably lead to denaturation of more tender membrane proteins (Choi *et al.*, 2006).

In two instances, the channel protein reconstitution was quantified by fluorescence correlation spectroscopy. Habel *et al*. (2015) calculated an average of 2.87 molecules aquaporin Z into PB_{45}-PEO_{14} polymersomes of roughly 60 nm diameter by film rehydration at a protein:polymer ratio of 1:100. A broader study with aquaporin Z, KcsA and OmpF by Itel *et al*. (2014) produced reconstitution efficiencies of 3.3-22.5 % at protein:polymer ratios from 1:200-1:650 by electroformation of the two polymers $PMOXA_7$-$PDMS_{49}$-$PMOXA_7$ and $PMOXA_{12}$-$PDMS_{63}$-$PMOXA_{12}$. The highest efficiency of 22.5 % was achieved for reconstitution of aquaporin Z into the thicker polymer at a protein:polymer ratio of 1:200, corresponding to 39 channels per polymersome or a channel density of 490 μm^{-2}. In comparison, the best condition with AlkL at a protein:polymer ratio of 1:100 corresponds to 4900 channels μm^{-2}, a roughly 10 times higher channel density. A comparably high degree of functionalization of $PMOXA_{22}$-$PDMS_{61}$-$PMOXA_{22}$ polymersomes with a photosynthetic reaction center was produced by a relatively new method for the formation of proteopolymersomes, the micelle-to-vesicle transition method. Starting from a detergent-solubilized mixture of protein and polymer,

Tangorra *et al*. (2015) induced the polymersome formation by detergent removal using SEC. The reaction center was applied at a protein:polymer ratio of 1:420, and the reconstitution efficiency amounted to 75 %. The mean size of the formed particles was 103 nm, and assuming a similar aggregation number than the polymer used in this thesis, each polymersome would contain roughly 140 channels. Despite being fully functional, this particular approach resulted in the reconstitution of the reaction center not in the hydrophobic region of the membrane, but rather in the PMOXA fraction. It is also doubtful whether this technique would be suitable for a concomitant cofactor and fusion protein encapsulation, which is a necessity for the generation of the nano-scale enzyme membrane reactors of this thesis. The same is true for a related method, which is based on the removal of the detergent by dialysis. Like the previous method, this method results in an efficient reconstitution, and since high detergent concentrations are involved from the start, the protein:polymer ratio is not limited by this factor. Using this method, Kumar *et al*. (2012) were even able to produce densely packed 2D crystals of aquaporin-0 in different polymers. However, the morphology of the resulting particles is dictated by the protein:polymer ratio, which is not desirable for the formation of nano-scale enzyme membrane reactors.

The simultaneous reconstitution of two channel proteins has only been reported in one instance, where bacteriorhodopsin and a F_0F_1 ATPase were combined in one polymersome (Choi and Montemagno, 2005, Choi *et al.*, 2006). Strangely enough, these two proteins were reconstituted in a directed fashion rather than at random. Apart from this peculiarity, nothing was mentioned about any cross interaction due to the reconstitution of more than one channel protein. Reconstitution of AlkL, OmpW, OprG or TodX in combination with FocA or PhoE was, however, very dependent on the actual protein batches involved, and no generalized behavior could be deduced. Unfortunately, it has not been possible to normalize the protein concentration of all channel protein stocks used, and it is complicated to ensure a defined detergent concentration of highly concentrated channel protein stocks if the detergent contained is not dialyzable. Therefore, the co-reconstitution of different channel proteins warrants further studies, possibly with protein stocks as homogeneous as possible.

8 *(S)*-1-(2',3',4',5',6'-Pentafluorophenyl)ethanol synthesis with nano-scale enzyme membrane reactors

The synthesis of *(S)*-1-(2',3',4',5',6'-pentafluorophenyl)ethanol from 2',3',4',5',6'-pentafluoroacetophenone was chosen as a model reaction to investigate the performance of nano-scale enzyme membrane reactors in synthesizing hydrophobic chiral alcohols for a number of reasons. With log *P* values of 2.24 and 2.34 for PFAP and PFE, respectively (calculated using Chemicalize Beta by ChemAxon Ltd.; www.chemicalize.org), both the substrate and the product of the reaction are moderately hydrophobic while still water-soluble to a certain degree. The solubility of PFAP was determined to be 6.00 ± 0.05 mM in PBS pH 7.5. But primarily, the specific activity of the 3-ketoacyl-(acyl-carrier-protein)-reductase (KR) towards this substrate is relatively high compared to other relevant substrates, although lower than towards ethyl-4-chloroacetoacetate (Hölsch *et al.*, 2008). On the other hand, the latter substrate is prone to hydrolysis in an aqueous environment, while PFAP, as a pentafluorinated compound, is fairly unreactive and so remains stable even at extended incubation times. These were required due to the usually low volumetric activity of the enzyme membrane nanoreactor preparations. The low encapsulation efficiencies already outlined in 7.1.3 were one reason for this. Besides, most experiments were performed with polymersome concentrations of less than 0.5 % w/v as a consequence of the channel protein reconstitution procedure and the limiting availability of the channel proteins.

The formation of *(S)*-PFE in the reaction buffer was usually determined after 112 h. The product concentration inside the nanoreactors was inaccessible because these needed to be separated from the buffer before the product could be analyzed to avoid emulsion of the aqueous phase and the ethyl acetate during extraction for GC analysis. To this end, a separation process based on the use of Amicon Ultra-0.5 centrifugal filter units with a 100,000 MMCO was developed, which allowed the separation of the nanoreactors within 1 h. Substrate concentrations were strongly affected as a result of binding to the centrifugal filter units, but product adsorption was below 10 %, which could be accounted for by preparing analogously-treated standard curves.

8.1 *(S)*-1-(2',3',4',5',6'-Pentafluorophenyl)ethanol synthesis with plain nano-scale enzyme membrane reactors

In order to characterize the behavior of the nano-scale enzyme membrane reactors, a number of experiments were performed with plain nanoreactors without reconstituted channel proteins.

8.1.1 Variation of the substrate and cosubstrate concentration

Initially, experiments with nano-scale enzyme membrane reactors were performed with high agitation (600 min^{-1}) and formate concentrations as high as 2.0 M due to the increased K_M of the fusion enzyme under the chosen conditions. However, the nanoreactor suspensions turned out to be more or less unstable at high formate concentrations, especially if agitated. Figure 8-1 shows exemplary reaction vessels where the damaging effect of high formate concentrations is visible. Instead of the usually turbid polymersome suspension, mainly aggregates remained. The effect was concentration-dependent. With 2.0 M formate, polymersome destruction was visible after 24 h as indicated by two ring-shaped polymer deposits at the vessel wall (corresponding to the initial fill-level before a sample was taken after 24 and the fill-level after 48 h), while the process was slower at a formate concentration of 1.5 M, where such a deposit was first seen after 48 h. At a concentration of 1.0 M, damaging effects were rarely observed, accordingly this concentration can be considered as an upper limit to the cosubstrate concentration. As an additional precaution, the agitation speed on a plate shaker was reduced to 450 min^{-1} for all further experiments.

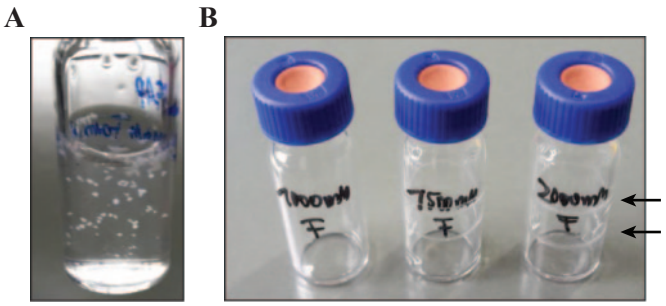

Figure 8-1. Polymersome destruction at high formate concentrations. (A) Polymersome aggregates formed in the presence of 2 M formate and 6 mM PFAP after 48 h agitation (600 min^{-1}) at 25 °C. (B). Polymersomes were incubated as before, with 1.0, 1.5 and 2.0 M formate. The ring-shaped polymer residues deposited at the vessel wall (indicated by arrows) correspond to the fill level after 24 and 48 h.

The nano-scale enzyme membrane reactors were able to synthesize *(S)*-PFE even in the absence of reconstituted channel proteins and appeared responsive towards a variation of the formate concentration up to a concentration of roughly 100 mM (*cf.* Figure 8-2). At this concentration, the reaction presumably became primarily controlled by the KR activity. The product formation by the nanoreactors was responsive towards PFAP in the range of 0-10 mM similar to the isolated KR kinetics. At the standard condition of 100 mM formate and 6 mM PFAP, 138 ± 4 µM *(S)*-PFE were produced by 0.42 % w/v nanoreactors with an enzyme load of approximately 1.7 mg L^{-1} (total enzyme content of the polymersome suspension) within 112 h. This corresponds to a specific activity of 2.8 attoU per polymersome.

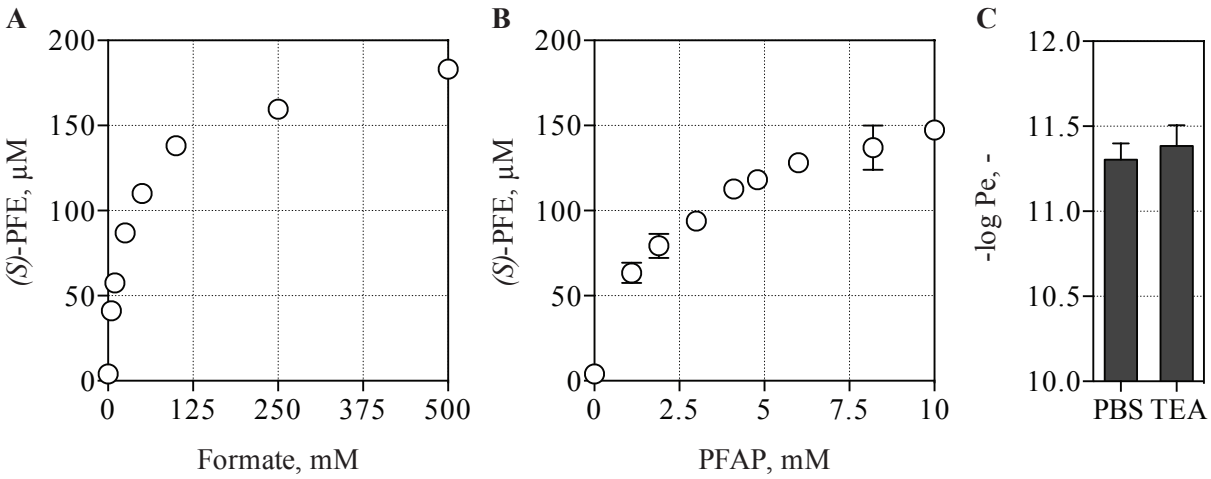

Figure 8-2. (A-B) *(S)*-PFE synthesis by 0.42 % w/v nano-scale enzyme membrane reactors after 112 h at 25 °C as a function of the substrate concentration. (A) Variable formate concentrations at a constant PFAP concentration of 6 mM (the polymersome batch used was prepared 9 days before the start of the experiment). (B) Variable PFAP concentrations at a constant formate concentration of 100 mM (the polymersome batch used was prepared 17 days before the start of the experiment). (C) Negative decadic logarithm of the permeability (cm s^{-1}) of the polymersome membrane towards formate in TEA pH 7.2 and in PBS pH 7.5. N=3.

The permeability of the polymersome membrane towards formate was probed by measuring the influx of the substrate over time as described in section 4.9.8. Initially the permeability was determined in a slightly different buffer system (TEA pH 7.2), but measurements in PBS pH 7.5 were also obtained. For plain polymersomes, passage of the negatively charged formate anion across the membrane is energetically unfavorable, so the most likely species to pass the membrane is the protonated formic acid. The fraction of the protonated compound (1-α) can be calculated from Equation 8-1.

$$(1-\alpha) = \frac{K_a}{[H_3O^+] + K_a} \qquad \text{Equation 8-1}$$

With $(1-\alpha)$ Protonated fraction

K_a Acid dissociation constant (formic acid: $2.29 \cdot 10^{-4}$ (Walter *et al.*, 1982)), M

At pH 7.2, the negative decadic logarithm of the permeability of the polymersome membrane towards formate was determined to 11.3 ± 0.1. At this pH, (1-α) is $2{,}75 \cdot 10^{-4}$, while it is $1.38 \cdot 10^{-4}$ at pH 7.5, so the permeability of the polymersome membrane towards formate in the standard PBS buffer system becomes marginally lower with –log *Pe* = 11.4 ± 0.1.

The membrane-specific permeability for formate can be used to compute the theoretical upper limit for the flux of the cosubstrate across the membrane. For simplicity, the calculation was performed for a total

volume of 1 L, which results in an active area of 2.43 10^6 cm^2 for a polymersome dispersion of 0.42 % w/v with a mean particle diameter of 100 nm. Assuming that the internal formate concentration is zero and that internal formate is rapidly converted by the FDH ($c_A = 0$, $\frac{dc_A}{dt} = 0$), the permeability determined for formate in PBS pH 7.5 would result in a maximal flux of 409 mmol formate across the membrane over a period of 112 h according to Equation 4-15 if a constant formate gradient of 100 mM was present. These assumptions are oversimplified, but they serve to assess the limits of the studied system, and since the observed product concentration of 138 µM was more than three orders of magnitude lower than the hypothetical limit, it can be assumed that the mass transport of formate across the membrane is likely not rate-limiting. The reality is of course more complex, and the real flux is a function of the actual concentration gradient, which is a steady state between formate influx and consumption and as such influenced by the K_M of the FDH as well as the cofactor consumption by the KR.

8.1.2 Kinetics of the reaction

Given the higher activity of the KR part under the chosen conditions (i.e. assuming an internal enzyme concentration of 0.60 g L^{-1}, a cofactor concentration of 4.5 mM, a steady-state formate concentration of 100 mM and a steady-state PFAP concentration of 6 mM at 25 °C in PBS pH 7.5, resulting in a 7.8-fold higher activity of the KR over the FDH), most of the cofactor is assumed to be in an oxidized state throughout the experimental time span. The half-life of the less stable, reduced form of the cofactor (NADPH) has been determined to be 107 ± 4 h in PBS pH 7.5 at 25 °C (*cf.* Figure B 4). Besides, the half-life of the KR part of the FDH-KR is in the same range as the duration of the experiment (115 ± 22-130 ± 9 h) when PFAP is present, while the half-life of the FDH-part is slightly lower (51 ± 17-71 ± 12 h, *cf.* chapter 6.3). As Figure 8-3 shows, the *(S)*-PFE concentration increased nearly linear from 8.60 µM after 24 h to 45.9 µM after 96 h. Furthermore, linear regression of the data indicates that the lag phase, during which the internal formate concentration increases, NADPH is formed and *(S)*-PFE accumulates within and diffuses out of the nanoreactors, was less than 5 h.

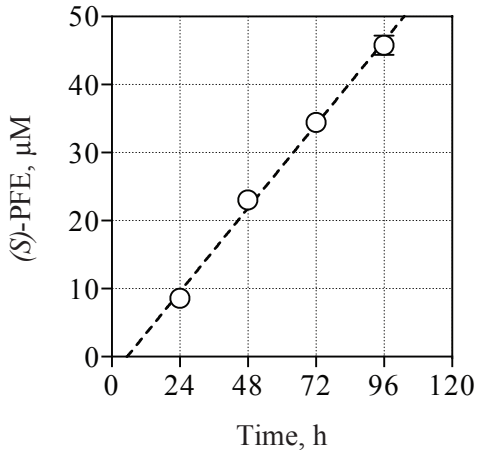

Figure 8-3. *(S)*-PFE synthesis by 0.42 % w/v nano-scale enzyme membrane reactors as a function of the incubation time at 25 °C (the polymersome batch used was prepared 70 days before the start of the experiment). The data could be adequately described by a straight line for a period between 24 and 96 h. N=3.

8.1.3 Storage stability of nano-scale enzyme membrane reactors

The preparation of nano-scale enzyme membrane reactors was always performed at the 12 mL-scale, and the further processing to produce the final catalyst was quite time-consuming. Consequently, they were routinely used for extended periods. The activity of the nanoreactors slowly decreased over time, as apparent from the results presented in chapter 8.1.1 and 8.1.2, which were all performed with a single nanoreactor batch at different time points. The activity (assuming a near-linear kinetics with a lag-phase of approximately 5 h, as demonstrated above) of this nanoreactors batch was initially $3.8 \cdot 10^{-18}$ Units per polymersome and was followed for up to 70 days post production, where the remaining activity amounted to $1.1 \cdot 10^{-18}$ Units per polymersome. The data could be fit by non-linear regression using Equation 3-5, giving a half-life of 32 ± 8 d according to Equation 3-6.

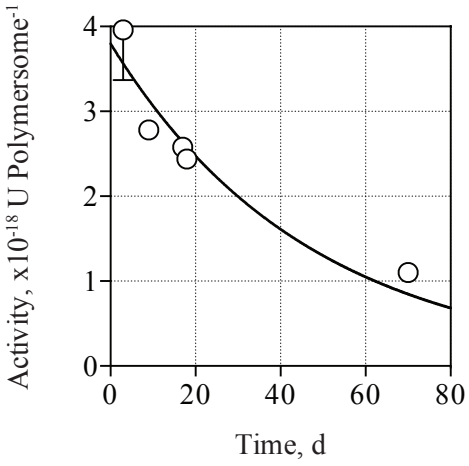

Figure 8-4. Stability of nano-scale enzyme membrane reactors at 4 °C and a concentration of 4.5 % w/v. A single batch was used repeatedly at various time points post production. *(S)*-PFE synthesis was always performed with 0.42 % w/v polymersomes, 6 mM PFAP and 100 mM formate for 112 h (96 h for the last data point) at 25 °C. The data were fitted by non-linear regression using Equation 3-5. N=3.

8.2 *(S)*-1-(2',3',4',5',6'-Pentafluorophenyl)ethanol synthesis with membrane-functionalized nano-scale enzyme membrane reactors

Based on results presented in chapter 8.1 it can be reasoned that the nano-scale enzyme membrane reactors are responsive towards changes in the PFAP and to a minor degree also the formate concentration and are consequently partially limited by the substrate availability or by the export of the product. In both cases, the membrane functionalization with a channel protein able to transport those substances should be beneficial. In order to satisfy the condition that encapsulated cofactor should be retained even in the presence of channel proteins, the permeability of polymersomes functionalized with the channel proteins AlkL, OprG, OmpF or PhoE was investigated using an influx assay. The data presented in Figure 8-5 demonstrate that no $NADP^+$ was able to diffuse into the polymersomes within 30 h, regardless whether the membrane contained channel proteins or not. Therefore, it can be concluded that leakage of the cofactor through the channels is not to be expected in the course of the experiments.

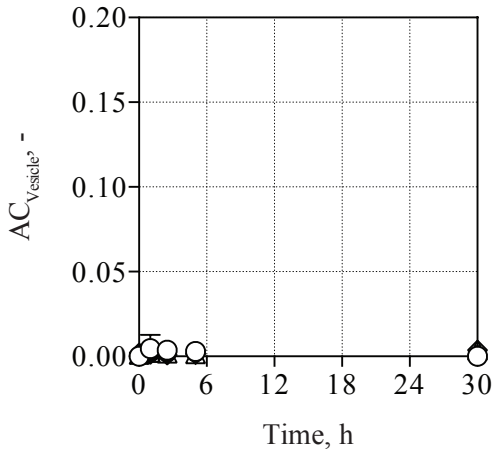

Figure 8-5. Investigation of the permeability of plain polymersomes (○) and polymersomes functionalized with AlkL (◆), OprG (●), OmpF (Δ) or PhoE (◇) using an influx assay. All channel proteins were of batch #1. AlkL was reconstituted at a protein:polymer ratio of 1:250, OprG and PhoE at 1:1000 and OmpF at 1:300. The experiment was performed with 20 mM $NADP^+$ in PBS pH 7.5. The acceptor number $AC_{Vesicle}$ represents the internal $NADP^+$ concentration, divided by the equilibrium concentration (*cf.* Equation 4-10). N=3.

8.2.1 *(S)*-1-(2',3',4',5',6'-Pentafluorophenyl)ethanol synthesis in the presence of channel proteins for hydrophobic substrates

Figure 8-6 shows the outcome of two experiments performed with nano-scale enzyme membrane reactors functionalized with either AlkL, OmpW, OprG or TodX. The experiments were performed with the same PFAP concentration of 6 mM, but the formate concentration was 100 mM in the one and 1 M in the other experiment. In addition, the age of the nanoreactors batches was also different. Accordingly, the *(S)*-PFE concentration reached after 112 h with plain polymersomes was 92 ± 9 µM in the first experiment and 227 ± 5 µM in the second. Interestingly, the product formation was increased in both

experiments if the nanoreactors were functionalized with any of the four channels. In the first experiment, the product concentration was most increased by functionalization with OmpW (2.2-fold), while AlkL had the greatest effect in the second experiment (1.6-fold). A direct comparison of these results is not straightforward, because the degree of functionalization varied greatly between the two experiments. The number of channels per polymersome had of course to be taken into account. Channel transport rates were still hardly computable since it is not known whether the substrate, the product or both are transported by the channel. In addition, the pronounced difference of the product formation by the plain nanoreactors in these experiments resulted in no uniform absolute rates for the channels. The relative effect per channel turned out to be a more reliable measure of the individual channel performance (*cf*. Figure 8-6B). The best channel in terms of performance was TodX (0.180 ± 0.04-fold higher product formation per channel), followed by OmpW (0.088 ± 0.016-fold higher product formation per channel). AlkL and OprG were almost 5-fold less efficient than TodX in transporting PFAP and/or *(S)*-PFE (0.037 ± 0.006 and 0.038 ± 0.01-fold higher product formation per channel). Yet the high reconstitution efficiency of AlkL obviously compensates the lower transport efficiency to some extent, while TodX reconstitution would need to be improved to achieve higher product concentrations.

Another aspect of interest was the scalability of the observed channel effects with the number of integrated channels. Increasing the number of AlkL channels per polymersome led to an increased product formation up to 1.8-fold when AlkL was reconstituted at a protein:polymer ratio of 1:100 (*cf*. Figure 8-6C). But as already noted, it has been suspected that the observed product concentrations are only partially limited by the PFAP/PFE transport across the membrane because the reaction system appeared to be very delicately balanced and the FDH activity might also be limiting to some extent. Besides, the baseline activity in the absence of channels was not negligible, so it is not unexpected that the relative effect per channel became lesser the more AlkL was reconstituted (*cf*. Figure 8-6D), which supports this hypothesis.

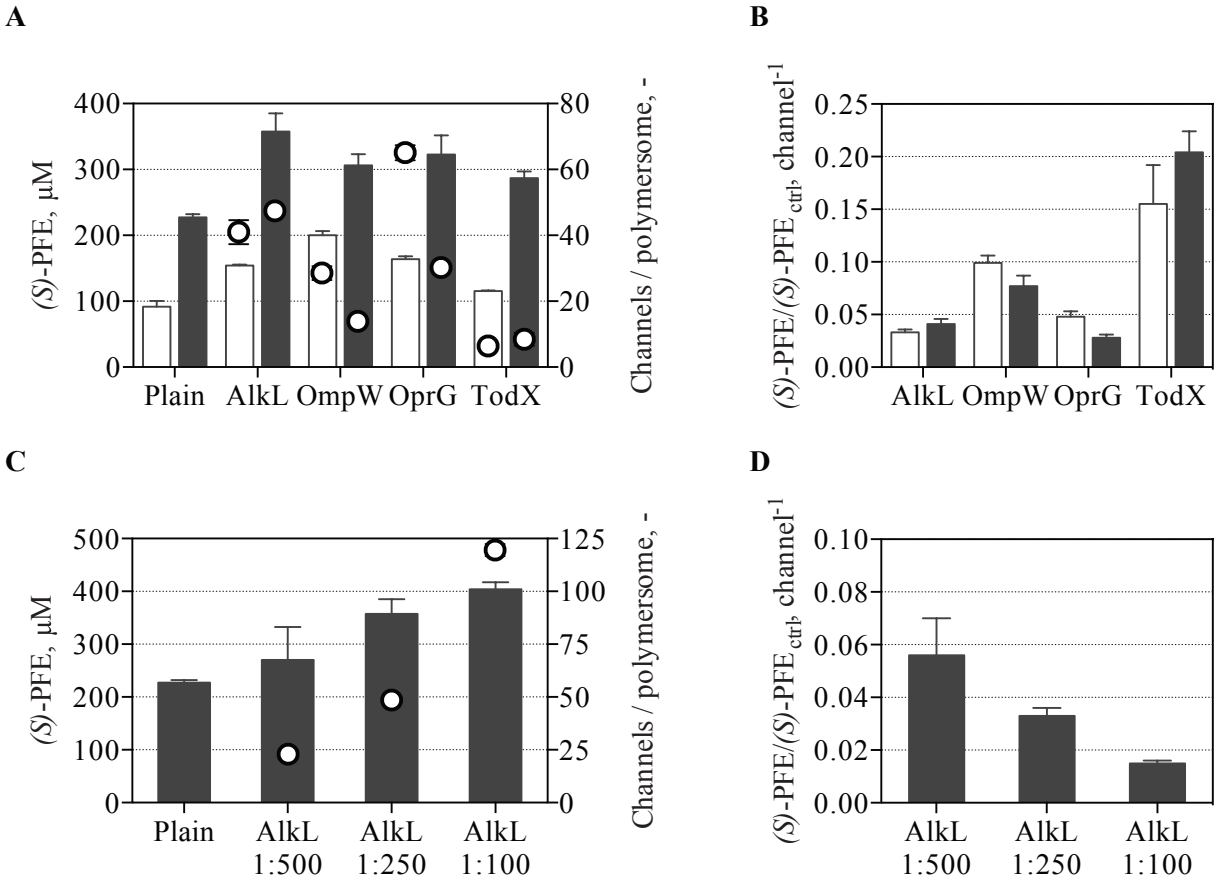

Figure 8-6. *(S)*-PFE synthesis with enzyme membrane nanoreactors functionalized with a single channel species for the transport of hydrophobic compounds. (A) *(S)*-PFE concentrations after 112 h from 2 experiments with different nanoreactors batches. One experiment was performed with 6 mM PFAP and 100 mM formate (0.42 % w/v nanoreactors, 18 days old and functionalized 1:250; white bars), one with 6 mM PFAP and 1 M formate (0.25 % w/v nanoreactors, 2 days old and functionalized 1:200; grey bars). (○): Number of channels per polymersome. Channel proteins were of the batches: AlkL #1, OmpW #2/1, OprG #2/1, TodX #2/1 (B) Ratio of the product concentrations observed with channel proteins over the control nanoreactors of the data shown in A, normalized per channel. (C) *(S)*-PFE concentrations after 112 h (6 mM PFAP and 1 M formate) for nanoreactors functionalized with varying concentrations of AlkL (nanoreactors 2 days old) and (D) *(S)*-PFE concentration fold control of the data shown in C, normalized per channel. N=3.

8.2.2 *(S)*-1-(2',3',4',5',6'-Pentafluorophenyl)ethanol synthesis in the presence of anion-selective channel proteins or OmpF

The same two experiments presented in the last section as well as an additional one with 0.25 % w/v nanoreactors 2 days old and performed with 6 mM PFAP and 100 mM formate can also be compared with nano-scale enzyme membrane reactors functionalized with the anion-selective ion channels FocA, PhoE or the unspecific porin OmpF (*cf.* Figure 8-7). Like before, the heterogeneity of the activities of the different nanoreactor batches prevents the perception of major differences at a first glance. Yet the normalized channel effects revealed a moderate but reproducible effect of the reconstituted FocA channel of 0.12 ± 0.02-fold higher product formation per channel. It must be stressed that the actual

formate concentration in the experiments had no impact on the FocA-specific effect. Despite the very low reconstitution efficiency of the FocA channel, the presence of this channel resulted in an increase of the product concentration of up to 1.7-fold. The results with PhoE are less conclusive. In one experiment, the presence of 16 PhoE channels increased the product formation 2-fold, which is equivalent to a 0.13 ± 0.01-fold higher product formation per channel, similar to the effect observed with FocA. Conversely, the presence of 68 PhoE channels in the second experiment improved the product formation only 1.3-fold (0.020 ± 0.002-fold higher product formation per channel). Both PhoE batches were freshly purified, so the most likely explanation is that the protein got inactivated during the production procedure, although the reason for this remains unclear.

Reconstitution of the unspecific porin OmpF did not lead to a pronounced improvement of the product formation, although the effect was still discernible and amounted to a 1.2-fold higher product formation in both experiments (0.060 ± 0.01-fold higher product formation per channel).

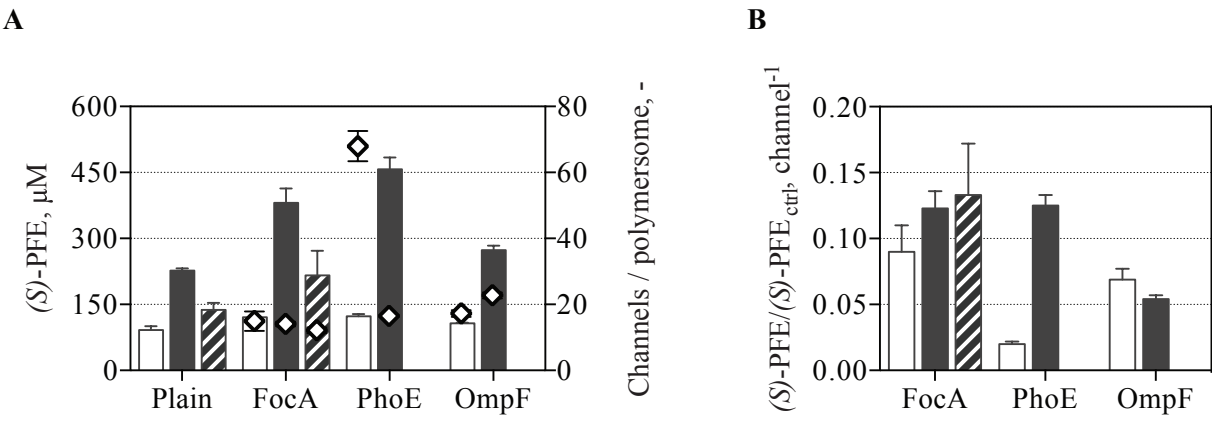

Figure 8-7. *(S)*-PFE synthesis with enzyme membrane nanoreactors functionalized with a single ion channel species. (A) *(S)*-PFE concentrations after 112 h from 3 experiments with different nanoreactors batches. Two experiment were performed with 6 mM PFAP and 100 mM formate (white bars: 0.42 % w/v nanoreactors, 18 d old; streaked bars: 0.25 % w/v nanoreactors, 2 d old), one with 6 mM PFAP and 1 M formate (grey bars: 0.25 % w/v nanoreactors, 2 d old). (◇): Number of channels per polymersome. Channel proteins were of the batches: FocA #2/1/1, PhoE #3/2/-, OmpF #3/2/-. (B) Ratio of the product concentrations observed with channel proteins over the control nanoreactors of the data shown in A, normalized per channel. N=3.

In the case of OmpF, the isolated formate transport into plain polymersomes was also investigated by an influx assay. The time course of the dimensionless acceptor number $AC_{vesicle}$ for plain and OmpF-functionalized polymersomes in TEA pH 7.2 is shown in Figure 8-8A. The functionalization of the polymersome membrane with OmpF significantly increased the permeability towards formate 2-fold ($p<0.05$). This is reflected in the negative decadic logarithm of the permeability coefficient, which is 11.3 ± 0.1 for the plain polymersome membrane and 11.1 ± 0.08 for the OmpF-functionalized polymersome membrane (*cf.* Figure 8-8B). Taking into account the number of reconstituted channels

per polymersome, the permeability difference can be converted to a flux of $1.5 \cdot 10^{-3}$ molecules s^{-1} $channel^{-1}$ at a nominal concentration gradient of 1 mM using Equation 4-15. This unexpectedly low channel activity indicates that only a fraction of the reconstituted channel protein was still functional as a result of prolonged storage.

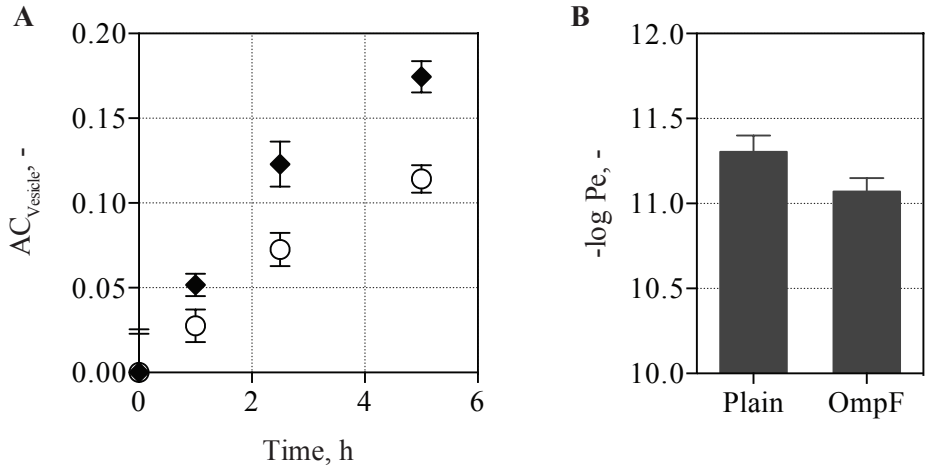

Figure 8-8. Permeability of the polymer membrane towards formate. (A) Formate influx into plain (○) or OmpF-functionalized polymersomes (◆) with 2.2 channel monomers per polymersome. OmpF was of batch #1. The experiment was performed with 200 mM formate at 25 °C in TEA pH 7.2. The acceptor number $AC_{Vesicle}$ represents the internal formate concentration, divided by the equilibrium concentration (*cf*. Equation 4-10). (B) Negative decadic logarithm of the permeability coefficients *Pe* (calculated using Equation 4-12, cm s^{-1}) derived from the experiment shown in A as well as for plain polymersomes incubated with 100 mM formate in PBS pH 7.5. N=3.

8.2.3 Combination of channel proteins

Given the moderately positive effects of both ion channels and channels for hydrophobic substrates on the *(S)*-PFE synthesis with nano-scale enzyme membrane reactors, a combination of both channel types could be expected to be even more productive. It has already been pointed out that the co-reconstitution of two channel protein species resulted in somewhat variable and unpredictable effects on the number of channels per polymersome. Another complicating factor is the interference of FocA with the quantification of reconstituted channels, making it impossible to distinguish between a mere change in the number of channels and true combinatorial effects due to an altered substrate flux.

Consequently, the results obtained with singly or doubly functionalized nanoreactors are also heterogeneous (*cf*. Figure 8-9). With AlkL, a combination with FocA further increased the product concentration 1.16-fold, while a combination with PhoE (a different batch than the apparently non-functional batch #3 used in one of the experiments shown in Figure 8-7) did not, even though the actual number of AlkL channels per polymersome was increased. A combination of OmpW with FocA did also not result in a higher product concentration, but in this case, the combination with PhoE increased the product concentration 1.19-fold, likely as a result of the 3-fold improved channel reconstitution.

Combinations with OprG and TodX were beneficial with both ion channels. The combination with FocA produced 1.2-fold more product than the nanoreactors functionalized with OprG alone, and in combination with PhoE, 1.12-fold more product was produced even though the number of OprG channels was 24 % lower. The greatest improvement was observed if TodX was combined with an ion channel. In combination with FocA, the product concentration was 1.19-fold higher, and with PhoE, the product concentration could even be increased 1.88-fold (2.3-fold higher than plain nanoreactors). Given that TodX also displayed the highest channel-specific effect in the single-channel system, this result marks TodX as the most promising candidate for further optimization of the functionalized nanoreactors.

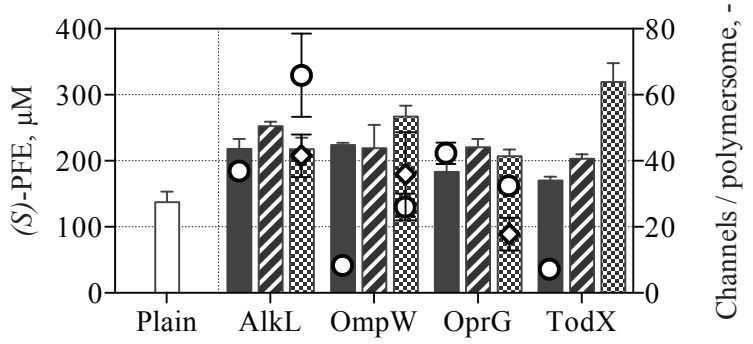

Figure 8-9. *(S)*-PFE synthesis with 0.25 % w/v enzyme membrane nanoreactors functionalized with a single channel species for the transport of hydrophobic compounds alone (grey bars) and in combination with FocA (striped bars) or PhoE (chequered bars) after 112 h. For comparison, the performance of plain enzyme membrane nanoreactors is represented by a white bar. The experiment was performed with 6 mM PFAP and 1 M formate (nanoreactors 2 days old). AlkL, OmpW, OprG and TodX were reconstituted 1:250, FocA and PhoE 1:500. The number of channels for hydrophobic substrates (○) and of PhoE (◇) per polymersome is indicated. The presence of FocA interfered with channel quantification. Channel proteins were of the batches: AlkL #1, FocA #1, OmpW #1, OprG #1, PhoE #2, TodX #1. N=3.

Combinatorial experiments with a constant overall protein:polymer ratio and varying ratios of OmpW and FocA or TodX and PhoE were performed to investigate whether there is an interaction between the effects of both channel species. However, apart from a modified reconstitution efficiency of TodX in the presence of PhoE, which has already been dealt with in section 7.2.2, no such effects were observed (*cf*. Figure 8-10). OmpW-functionalized nanoreactors produced 1.61-fold more *(S)*-PFE than the plain nanoreactors in this experiment, but possibly due to very low reconstitution efficiency of FocA in this particular experiment (although this is speculative), the achieved product concentrations steadily declined with lower OmpW:FocA ratios and became undistinguishable from the plain nanoreactors at a ratio of 0.25.

Similarly, the same possibly defective PhoE batch shown in Figure 8-7 again caused a 1.33-fold increased product concentration, which is only a 0.017 ± 0.003-fold higher product formation per channel. With TodX alone, the product concentration increased 1.63-fold, a 0.43 ± 0.075-fold higher product formation per channel. Combinations with PhoE led to a marginally lower product concentration

(it is suspected that the batch #3 used in this experiment was non-functional for unknown reasons), with a specific effect of an around 0.2-fold higher product formation per TodX channel comparable to the previously observed rate improvements.

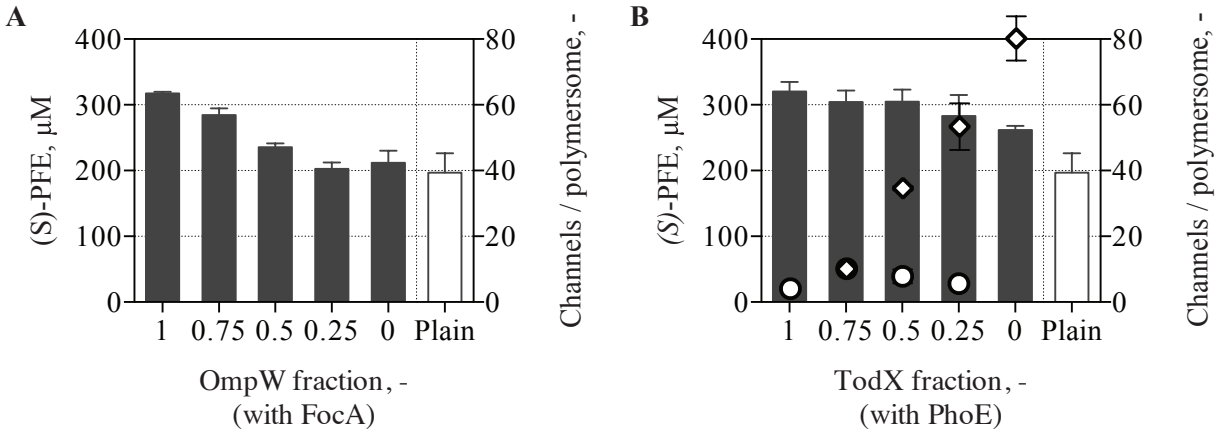

Figure 8-10. *(S)*-PFE synthesis with 0.42 % w/v enzyme membrane nanoreactors functionalized with different ratios of (A) OmpW and FocA or (B) TodX and PhoE (grey bars) as well as with plain enzyme membrane nanoreactors (white bars) after 112 h. The experiment was performed with 6 mM PFAP and 100 mM formate (nanoreactors 3 days old). The overall protein:polymer ratio was kept constant at 1:250. The number of TodX (○) and of PhoE (◇) per polymersome is indicated. The presence of FocA interfered with channel quantification. Channel proteins were of the batches: FocA #2, OmpW #2, PhoE #3, TodX #2. N=3.

8.3 Comparison with free enzymes and whole cells

A direct comparison of the nanoreactors with the free enzyme system presented a challenge because at enzyme concentrations equivalent to the nanoreactors' enzyme load (usually in the range of 2.0 mg L^{-1}), almost no product formation was observed. Product formation was only detectable above 3.0 mg L^{-1} enzyme but increased in a non-linear fashion (*cf.* Figure 8-11A). The specific activity of the FDH part of the fusion enzyme was a linear function of the enzyme concentration down to at least 0.75 mg L^{-1} (data not shown) and thus was unlikely to be responsible for this behavior. The specific KR activity was, however, subject to a concentration-dependent complex reorganization or partial dissociation with reduced activities at lower enzyme concentrations (*cf.* Figure 8-11B). Although mechanistically only valid for ligand binding, the activity could be phenomenologically best described by a general association model of the following form.

$$v = \frac{v_{max} \cdot E^n}{K_d'^n + E^n} \qquad \text{Equation 8-2}$$

With

E	Enzyme concentration
K_d'	Apparent dissociation constant, 38 ± 3 mg L^{-1}
n	Hill coefficient, 1.15 ± 0.07

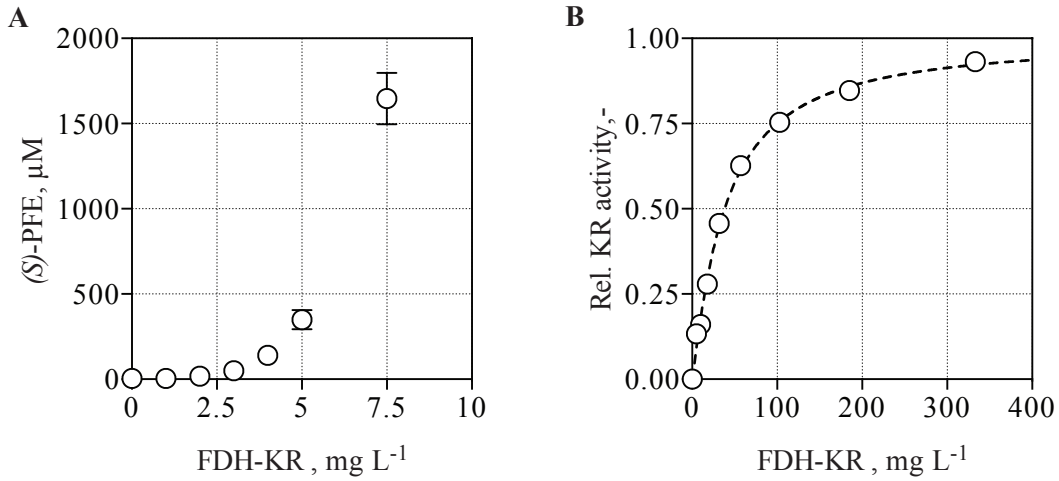

Figure 8-11. Concentration-dependent FDH-KR-dissociation. (A) Synthesis of *(S)*-PFE with the isolated FDH-KR after 112 h at 25 °C. The reaction was performed with 6 mM PFAP, 100 mM formate and 4.5 mM $NADP^+$. N=3. (B) Specific KR activity as a function of the fusion enzyme concentration relative to the activity at $c \rightarrow \infty$. The enzyme activity was determined photometrically with 1 mM NADPH and 2.6 mM PFAP. The data could be described most adequately using Equation 8-2. N=4.

In analogy to experiments with nano-scale enzyme membrane reactors, the free enzyme system was set up with variable substrate or cosubstrate concentrations at an enzyme concentration of 7.5 mg L^{-1} (*cf.* Figure 8-12). With 6 mM PFAP and 4.5 mM $NADP^+$, the product concentrations became independent of the formate concentration above 100 mM formate, which is comparable to the nanoreactor system, while the PFAP concentration was limiting up to its maximal solubility at a formate concentration of 100 mM and 4.5 mM $NADP^+$. Compared to the nanoreactor system, the limitation even appears to be more pronounced at low PFAP concentrations, which can be a result of the lower KR:FDH activity ratio in the free enzyme system. Due to the high statistical encapsulation efficiency of 180 % for the encapsulation at an initial enzyme concentration of 0.60 g L^{-1}, the nanoreactors should contain an internal concentration of 1.1 g L^{-1} FDH-KR and thus a fully active enzyme, while the KR activity of the free enzyme system at a concentration of 7.5 mg L^{-1} corresponds to 13.4 % of the nominal activity according to Equation 8-2. In contrast to the nanoreactors system with a fixed internal cofactor concentration, a variation of the cofactor $NADP^+$ was also investigated for the free enzyme system.

The maximally achieved product concentrations were almost an order of magnitude higher than the ones obtained with the nanoreactors. With 6 mM PFAP and 100 mM formate, 1620 ± 140 µM *(S)*-PFE were formed. Taking into account the concentration-dependent activity of the free KR and assuming freshly prepared nanoreactors containing 1.7 mg L^{-1} enzyme with maximal activity, the specific activity of the free enzyme system is 14-fold higher than the activity of the nanoreactors shown in Figure 8-4. However, reconstitution of channel proteins was able to alleviate the observed mass transfer limitation of the nanoreactor system to some extent, reducing the difference to the uncompartmentalized system to merely 6.4-8.6-.fold.

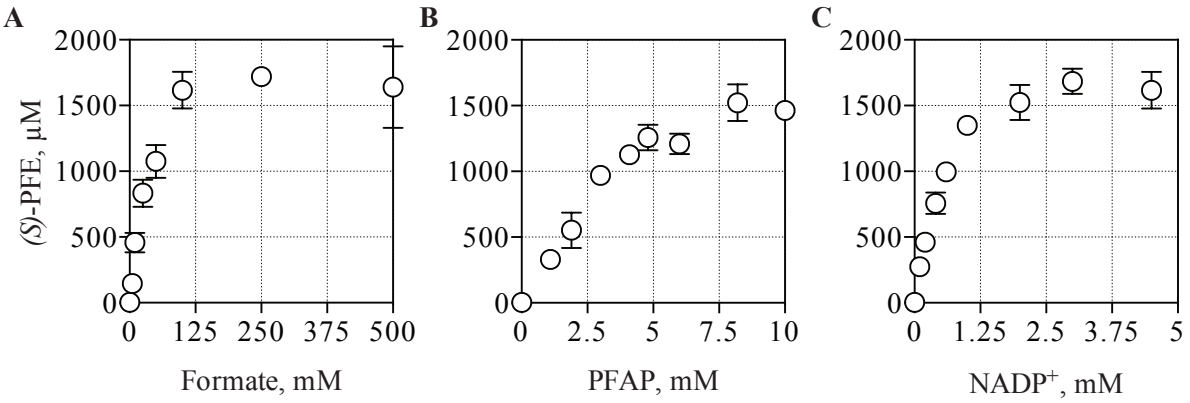

Figure 8-12. *(S)*-PFE synthesis with 7.5 mg L^{-1} free FDH-KR after 112 h at 25 °C as a function of the (A) formate, (B) PFAP and (C) $NADP^+$ concentration. The reaction was routinely performed with 6 mM PFAP, 100 mM formate and 4.5 mM $NADP^+$. In each set of experiments, the concentration of one substrate was varied while the other two were kept constant. N=3.

Whole cells with an enzyme content of 69.5 µg g_{cdw}^{-1} were incubated with 6 mM PFAP and 100 mM formate at concentrations of 0.035-0.263 g_{cdw} L^{-1} cells. The product formation per g_{cdw} after 112 h was comparable for all investigated concentrations (*cf.* Figure 8-13) and amounted to 4300 ± 800 µmol g_{cdw}^{-1} *(S)*-PFE. However, the same product formation was already obtained after 48 h. Since no more product was formed regardless of the remaining substrate concentration, it can be concluded that the whole-cell biocatalyst had lost its entire activity within 48 h. Therefore, the activity of the whole-cell biocatalyst was probably even higher than estimated from the data because no earlier samples (before the whole-cell biocatalyst lost its activity) were taken. In comparison, the nano-scale enzyme membrane nanoreactors appeared to be much more stable than the whole-cell biocatalyst, since it was demonstrated in chapter 8.1.2 that the product concentration increased linearly for a period of at least 96 h. Based on a linear interpolation of the *(S)*-PFE concentrations obtained after 48 h to 112 h, the specific activity of the whole-cell biocatalyst was at least 1.2-fold higher than that of the freshly prepared nanoreactors containing 1.7 mg L^{-1} enzyme shown in Figure 8-4, but only 0.56-0.76 of that of OmpW- or AlkL-functionalized nano-scale enzyme membrane reactors. With respect to the free enzyme system, the whole-cell biocatalyst yielded 11-fold less *(S)*-PFE under the same assumptions as before.

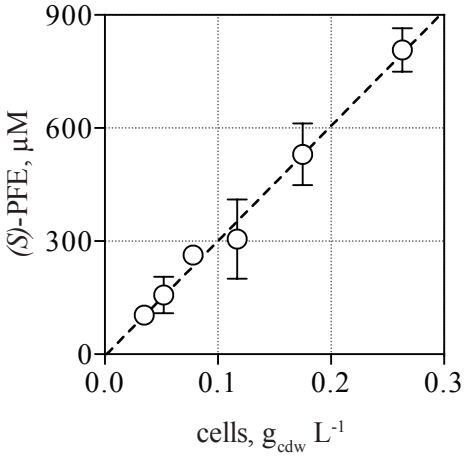

Figure 8-13. *(S)*-PFE synthesis with whole cells at 25 °C. (A) The *(S)*-PFE concentration is given as a function of the biocatalyst concentration after 48 h. The data could be described by a straight line with a slope of 1. The reaction was routinely performed with 6 mM PFAP and 100 mM formate. N=3.

8.4 Discussion

The synthesis of *(S)*-PFE from PFAP using FDH-loaded nano-scale enzyme membrane nanoreactors represents a complex system. Apart from the complex kinetics of the two coupled bisubstrate reactions of FDH and KR, the flux of both substrates into the nanoreactor as well as the efflux of the product out of the nanoreactor needed to be considered. Furthermore, high concentrations (>1 M) of the cosubstrate formate were found to be detrimental, probably due to an osmotic effect on the nanoreactors. Zhang *et al*. (2016) also reported that their $PMOXA_6$-$PDMS_{42}$-$PMOXA_6$ polymersomes were rapidly damaged by the osmotic pressure upon exposure to 400 mM ribitol.

A product formation was detectable even in the absence of any channel proteins, indicating that the nano-scale enzyme membrane reactors were functional and that substrate and cosubstrate were able to permeate across the polymer membrane. In addition, the product of the reaction must be able to diffuse back out of the nanoreactors since it could not have been detected otherwise. The passage of formate across the polymersome membrane could be further characterized by means of an influx assay, and the determined permeability (-log *Pe* of 11.4 ± 0.1 at pH 7.5) was several orders of magnitude lower than that of lipid membranes with a –log *Pe* of approximately 5.8 (calculated from the intrinsic permeability for formic acid of 10^{-2} cm s^{-1} (Walter *et al.*, 1982) using Equation 4-14). Similar differences between the permeability of polymer or lipid membranes for caffeine and propranolol have been observed by Poschenrieder (2017). Despite the very low permeability, the actual flux of formic acid across the membrane is still likely to be higher than the measured consumption by the enzymatic reaction, since the surface-to-volume ratio of the nanoreactors is exceedingly high.

A direct comparison of both systems was severely complicated by the recent proof of a concentration-dependent activity profile of the KR, which probably dissociates at lower concentrations with an

apparent K_D' of 38 mg L^{-1}. A shift in the KR:FDH-activity ratio (estimated to be 7.8 at a nominal internal protein concentration of 1.1 g L^{-1}, *cf*. chapter 8.1.2) might be responsible for the higher relative activity of the encapsulated system at low vs. high PFAP concentrations compared to the free enzyme system (with an estimated KR:FDH-activity ratio of 1.1 at a nominal protein concentration of 7.5 mg L^{-1}). Alterations in the activity of multimeric enzymes can represent a regulatory mechanism, induced either by cooperational changes in the conformation or by a change of the oligomeric state. The latter can be the result of changes in the enzyme concentration, as in the case of some β-galactosidases (Pilipenko *et al.*, 2007) or certain viral enzymes (Kadas *et al.*, 2008, Hogbom *et al.*, 2009), or by binding of an allosteric effector ligand. In most cases, the concentration-dependent oligomerization is not likely to represent an important regulatory mechanism *in vivo* (Traut, 1994). Still, a number of enzymes are known to display a loss of activity upon dilution *in vitro*, such as AMP deaminase, Ca^{2+}-ATPase, fumarase, phosphofructokinase, isocitrate dehydrogenase, glutamate dehydrogenase, glycogen phosphorylase, phosphorylase kinase, threonine dehydrase and UMP synthase (Traut, 1994). Nevertheless, the observed concentration effect is most probably only an artifact of the fusion with the FDH and of the particular process conditions. The single KR tetramer was shown to dissociate into dimers upon purification by SEC, but the dimeric enzyme retained 79 % of the specific activity of the tetramer (Hölsch *et al.*, 2008), whereas it was observed in this thesis that the dissociated form of the FDH-KR appeared nearly inactive. A concentration-independent specific activity of the dimeric FDH part indicates that no complete dissociation of the enzymes occurred, i.e. that the FDH dimer is stable in the fusion enzyme or that the FDH is also active as a monomer. It appears possible that the fusion with the FDH distorts the quaternary structure of the KR in a way that fusion enzyme dimers do not result in two catalytically active domains and that active KR dimers and tetramers rather form through a network of interconnected fusion enzymes at higher protein concentrations. The existence of such a networks has already been proposed for the KR by Hölsch *et al*. (2008). In contrast to this, the dimer-dimer interface of the non-fused enzyme must be more kinetically stable because the enzyme activity was described as a linear function of the enzyme concentration in a range of 50-125 mg L^{-1} (Hölsch, 2009).

The long-term stability of the nano-scale enzyme membrane reactors is another factor which influenced the results, because the long production times and the attempt to perform different experiments with the same batch of nanoreactors resulted in the use of nanoreactors of different age and also different activity. The effect was analyzed for one batch of nanoreactors which had been used in a number of experiments, and the half-life of these nanoreactors stored at 4 °C was 32 ± 8 days. A loss of cofactor due to leakage from the nanoreactors is unlikely, because Poschenrieder (2017) demonstrated for the similarly polar compound calcein that only 1 % was released from the polymersomes in a period of 52 days at 4 °C. However, $NADP^+$ hydrolysis represents a distinct possibility. The stability of the cofactor as well as of the purified fusion enzyme at 4 °C was unfortunately not investigated, but it was noted that the KR activity usually declined faster than the FDH activity upon longer storage. For this reason, the stability

of the KR at 4 °C can be suspected to be responsible for the observed loss of activity of the nanoreactors. The KR storage stability appears to be impaired in the fusion enzyme, because the unfused KR is quite stable with a half-life of more than 125 days (Hölsch, 2009).

An important criterion for the membrane functionalization of the nano-scale enzyme membrane reactors was the ability to retain the cofactor even in the presence of channel proteins. Using an influx assay, this could be demonstrated for all relevant channel proteins. In contrast to the cofactor, the substrate(s) would not be able to penetrate the membrane in the absence of channel proteins in an ideal system for the investigation of the membrane functionalization by channel proteins. A number of studies could demonstrate a clear benefit of the functionalization of polymersomes with OmpF because the unfunctionalized nanoreactors were impenetrable to ampicillin (Nardin *et al.*, 2001), different nucleosides (Ranquin *et al.*, 2005) and the phosphatase substrate ELF 97 (Broz *et al.*, 2006). If the polymer membrane is more permeable to the substrates, as was indeed observed for formate and PFAP, the channel effects become more subtle because they can only modulate the membrane permeability. For instance, the oxidation of various aliphatic alkanes by an engineered *E. coli* strain carrying the *P. putida* GPo1 *alk* gene cluster was primarily dependent on the presence of AlkL, but the relative improvements varied greatly depending on the permeability of the cell envelope towards the substrates. A transport limitation was shown for aliphatic alkanes longer than hexane, and the relative yield improvements by AlkL increased with increasing chain length and decreasing permeability from 1.8-fold for heptane and 10-fold for octane up to 100-1000-fold for dodecane (Grant *et al.*, 2014). PFAP reduction by the FDH-KR nanoscale enzyme membrane reactors was moderately increased when the polymer membrane was functionalized with AlkL, OmpW, OprG or TodX. In the case of AlkL, the effect per channel decreased when the number of AlkL channels per polymersome was increased, while Nardin *et al*. (2001) described a linear increase of the ampicillin hydrolysis with the number of OmpF channels (the number of channels was estimated by the authors based on the assumption of an aggregation number of 13,000 and a reconstitution efficiency of 100 %). However, these authors used a simpler model system with a substrate completely unable to enter the nanoreactor unless the transport was facilitated by the channel protein. It is thus possible that the different effect of the channel proteins (linear increase of activity with the number of OmpF channels described by Nardin *et al*. (2001) vs. saturation of the effect with higher AlkL channel densities observed in this thesis) is due to the aforementioned modulation of an already appreciable permeability (if the reaction is not fully transport-limited) rather than an absolutely channel-dependent facilitation of the mass transport.

Depending on the experiment, the greatest increase observed with nano-scale enzyme membrane reactors only functionalized with a single channel species for the transport of hydrophobic substrates was due to OmpW (2.2-fold) or AlkL (1.6-fold). As a result of the different reconstitution efficiencies, substrate transport through AlkL was found to be rather inefficient but driven by the high channel density (estimated to be 1500 μm^{-2}), whereas OmpW integrated worse (the channel density was estimated to be

900 μm^{-2}) but proved to be a better transporter for the substrate with an almost 2-fold higher productivity increase per channel than AlkL. Interestingly, the single channel effect of TodX was again about 2-fold higher than of OmpW. Reconstitution of TodX is in need of further optimization, because the channel density was far lower in the experiment (estimated to be 260 μm^{-2}). Just recently, an engineered variant of the FhuA channel was shown to improve the uptake of aromatic compounds and terpenes by an *E. coli* strain harboring a cytochrome P450 enzyme. The Δ1-160 mutant of FhuA lacks the globular N-terminal plug domain, which creates a large water-filled pore wider than the OmpF channel (14 Å vs. 12 Å diameter; Nikaido, 1992, Ruff *et al.*, 2016). The hydroxylation of toluene and anisole was improved from 35 and 25 µM to 50 and 45 µM, respectively, and oxidation of pinene and limonene was increased from 12 to 20 and 25 µM (Ruff *et al.*, 2016). The authors went so far as to quantify the number of FhuA channels in the cell envelope, which resulted in a number of roughly 44,000 per cell. Assuming a mean area of ca. 4-4.5 μm^2 per cell (Prats and Depedro, 1989), this translates to a channel density of ca. 10,000 μm^{-2}, almost an order of magnitude higher than the channel densities achieved for the nano-scale enzyme membrane reactors. It is of note that some of the most successful examples of channel-functionalized polymersomes relied on the reconstitution of a considerable number of channel proteins in the membrane of the nanoreactor. Broz *et al*. (2006) used OmpF to permeabilize their polymersomes to the phosphatase substrate ELF 97 (MM: 431 Da). They reported an average of 200 OmpF channels per nanocontainer, again only based on the protein:polymer ratio, and found that even in the presence of the porin the reaction took 3 h to completion, while the free enzyme was able to convert the substrate within 10 min. Nardin *et al*. (2001) estimated that their β-lactamase-loaded nanocontainers required about 250 OmpF channels to have the same activity as the free enzyme towards ampicillin (MM 349 Da). Finally, nucleoside transport (MM: 267-285 Da) into nanoreactors containing TvNH required a theoretical number of 1300 OmpF channels (protein:polymer ratio of 1:10) to achieve the same effect (Ranquin *et al.*, 2005). This study was also one of the first to highlight possible advantages of using specialized channels, because use of the nucleoside transporter Tsx instead of OmpF resulted in a comparable activity even at a protein:polymer ratio of 1:100.

For this reason, the possible substrate range of the channels is an important aspect to consider. OmpW was shown to be unable to facilitate the uptake of octane (Call *et al.*, 2016), and TodX was unable to transport oleic acid (Hearn *et al.*, 2008), while both substrates are transported by FadL. With regard to OprG, which also improved the reduction of PFAP to some degree, it was recently shown that its primary function in *P. aeruginosa* probably lies in the uptake of small amino acids rather than in the transport of hydrophobic compounds (Kucharska *et al.*, 2015b). The authors also reported that the lateral gate in the barrel wall described from the crystal structure (Touw *et al.*, 2010) was not confirmed by an NMR-based structure analysis in a detergent environment. These works indicate that members of the FadL and OmpW family are likely to be substrate-specific transporters. A higher specific transport of PFAP by TodX is plausible, because the natural substrate (toluene) of TodX (Hearn *et al.*, 2008) is structurally more similar to PFAP than the primarily aliphatic AlkL substrates (Julsing *et al.*, 2012, Grant *et al.*,

2014). In accordance, the CYP153A6-catalyzed hydroxylation of the more bulky *(S)*-limonene by another engineered *E. coli* strain was only improved 2-5-fold (in aqueous single-phase and two-liquid phase biotransformations, respectively) when the cells were expressing AlkL (Cornelissen *et al.*, 2013). The investigation of channel effects with other KR substrates would have been very valuable to explore their potential to facilitate the selective mass transport into synthetic reaction compartments.

An important difference between results obtained with whole cells and those with channel proteins for hydrophobic substrates reconstituted in polymer membranes is the orientation of the channels. According to the general transport model for these channels, substrate binding takes place at the outer face of the channel, and the substrate is then released into the membrane core (Hearn *et al.*, 2009). This model implies that the transport is necessarily unidirectional, because no second binding site is present at the inner face of the channel. In cells, the channels are integrated into the outer membrane in a directed fashion, so that the substrate binding site is facing the outer medium from where the substrates are to be taken up. However, reconstitution into the symmetric polymer membrane can occur in both orientations, so it can be assumed that the actual number of channels able to facilitate the substrate uptake is only about 50 % of the total reconstituted channels. Since it is not yet known whether the product of the reaction, i.e. *(S)*-PFE, is also transported by these channels, a bidirectional channel orientation is not necessarily a disadvantage, but it must be borne in mind for the assessment of the channel transport activity.

With the nanoreactors functionalized with a single ion channel species, PhoE and FocA reconstitution led to a 1.7- and 2-fold increased product concentration, which corresponds to a channel-specific effect comparable to OmpW. These results indicated that formate transport was not completely irrelevant to the performance of the nano-scale enzyme membrane reactors, although it is not clear whether these channels might also transport PFAP or *(S)*-PFE to some degree. It has been reasoned that porins such as OmpF and PhoE tend to exclude hydrophobic molecules because they contain a number of charged amino acid residues in their constriction zone, which orient water molecules in their vicinity (Schulz, 1993). Entrance of hydrophobic molecules would distort the energetically favorable orientation of the water molecules, and it was found that diffusion rates of monoanionic cephalosporins decreased about 4-fold when their log *P* was 10-fold increased (Schulz, 1993, Nikaido, 1994a). The study with FhuA Δ1-160 presented above does not present a contradiction because the channel is significantly wider, but even so, the observed increases in the product formation were not very pronounced in that study.

Product formation by OmpF-functionalized nanoreactors was barely higher than by unfunctionalized ones. Since it was demonstrated that the 744 Da cofactor $NADP^+$ was unable to leak through the OmpF channel, it was reasoned why this channel did not produce a greater effect. By comparison of the permeability of plain and OmpF-functionalized polymersomes determined by an influx assay it was shown that the increased permeability due to the presence of the channels corresponded only to a single-channel flux of $1.5 \cdot 10^{-3}$ s^{-1} at a nominal concentration gradient of 1 mM. Since no data for the transport

of formate through OmpF are published, a direct comparison is not feasible. However, single-channel conductance experiments allowed the determination of the flux of ampicillin through the OmpF channel, which amounts to $1.4 \cdot 10^{1}$ molecules s^{-1} at a concentration gradient of 1 mM (Hajjar *et al.*, 2010). From the relative diffusion rates of various substrates through OmpF, determined by liposome-swelling by Nikaido and Rosenberg (1983), it can be further deduced that the flux of the 45 Da formate should be about 100 times faster, i.e. in the range of $1\text{-}2 \cdot 10^{3}$ s^{-1}. The extreme discrepancy between the theoretically possible and the observed flux leaves only one explanation, which is that the channel activity was largely lost before the experiment, probably due to a prolonged storage. The same OmpF preparation was successfully used at an earlier point by Klermund (2017) to determine relative diffusion rates of ATP, *N*-acetylmannosamine, *N*-acetylglucosamine and pyruvate and compare them to a mutant form of the channel, proving that the channel had been functional before. However, the reduced stability of the trimers due to the presence of the purification tag presented chapter 5.2.2 and discussed in chapter 5.4 must have also reduced the long-term stability of the channel. Since the OmpF preparations used in other experiments were also not freshly prepared it is likely that more functional channel preparations might have resulted in a different outcome of the experiments.

Similarly, a combination of different channels was not always advantageous because at least one batch of FocA and PhoE was also not fully functional. Besides, the unexpected variation of reconstitution efficiencies when combining two channel types complicated the interpretation of results. Nevertheless, at least in some cases a positive effect of the combination of an ion channel and a channel for hydrophobic substrates was observed, particularly when TodX was involved. It is possible that with some careful investigation of the factors influencing the simultaneous reconstitution of more than one channel and a consequent use of freshly prepared channel preparations, a superior catalysis using membrane-functionalized enzyme membrane reactors can be achieved.

9 Summary

The use of polymer-based nano-scale enzyme membrane reactors for multienzyme syntheses represents an innovative approach for the evolution of novel biocatalysts. The use of synthetic, self-assembling amphiphilic block copolymers allows the generation of thicker, more stable and significantly less permeable membranes than those composed of lipids. A lower permeability can be a considerable advantage, especially when mutual incompatibilities occur within multienzyme reactions, but at the expense of mass transfer limitations. So far, most nanoreactor systems relied on the unspecific exchange of substrates and products across the membrane by means of chemical modifications of the polymer shell or by the incorporation of unspecific channel proteins (Gaitzsch *et al.*, 2016, Schmitt *et al.*, 2016). Among the amphiphilic block copolymers, poly(2-methyloxazoline)-polydimethylsiloxane-poly(2-methyloxazoline) (PMOXA-PDMS-PMOXA) is of particular merit for the generation of membrane-functionalized nano-scale enzyme membrane reactors, because this polymer proved especially amenable to channel protein incorporation. The implementation of a maximally selective mass transport is of great importance for the development of versatile nano-scale enzyme membrane reactors, but the available toolbox of successfully integrated channel proteins is still very limited. In this thesis, a two-enzyme reaction for the asymmetric reduction of prochiral ketones by means of a fusion enzyme between a formate dehydrogenase (FDH) and a 3-ketoacyl-[acyl-carrier-protein]-reductase (KR) was investigated. The substrates of this reaction are hydrophobic prochiral ketones on the one side and formate for the regeneration of the cofactor NADPH on the other. For the membrane functionalization of nano-scale enzyme membrane reactors, different channel proteins from *E. coli* and various pseudomonads were selected. FocA, PhoE and OprP were identified as potential anion-selective channel proteins and the small monomeric outer membrane proteins AlkL, OmpW, OprG and TodX were chosen for their potential ability to transport more hydrophobic substrates. The general porin OmpF was also included as a reference channel, which had been reconstituted in PMOXA-PDMS-PMOXA polymersomes in the past (Nardin *et al.*, 2000b).

The preparation of sufficient amounts of those channel proteins was a prerequisite for further experiments. Expression of FocA, OmpF, OprP and PhoE was performed in the membrane protein expression strain *E. coli* BL21 omp8 at 20 °C over night. Since OmpF, OprP and PhoE rely on their C-terminal residues for the closure of the β-barrel and contain a cleavable N-terminal leader peptide, a hexahistidine-tag was introduced between the PhoE leader peptide and the mature protein according to van Gelder *et al*. (1996). All proteins were purified by immobilized metal affinity chromatography (IMAC), and the solubilization with a number of detergents was investigated to establish suitable purification strategies for these four oligomeric channel proteins. The non-ionic detergent *n*-Octyl-*β*-D-glucopyranoside (OG) was found to be the best detergent for the isolation of OmpF and OprP, while the isolation of PhoE was most efficient with *N,N*-dimethyldodecylamine *N*-oxide (LDAO). The correct trimeric structure of OprP and PhoE was not significantly affected by the presence of the His-tag,

because 89 % and 95 % of the isolated protein were trimeric. In contrast, the stability of the OmpF trimer was impaired and only 52 % of the final protein was still in its trimeric form. The isolated protein yields for OmpF, OprP and PhoE were 1.0, 0.12 and 2.5mg L^{-1} shake flask culture, respectively. FocA was solubilized most efficiently with *n*-dodecyl-*β*-D-maltoside (DDM; isolated protein yield of 4.0 mg L^{-1}) and appeared primarily pentameric as judged by Blue-native polyacrylamide gel electrophoresis. The circular dichroism (CD) spectrum of purified FocA was identical to the one determined by Falke *et al*. (2010) and single-channel conductance experiments suggested that the protein was functional. Due to the extremely low yield obtained for OprP, this channel protein was not further investigated. For the production of the small monomeric outer membrane proteins AlkL, OmpW, OprG and TodX, another strategy based on the insoluble expression of the His_8-tagged proteins as inclusion bodies and their subsequent isolation, purification and refolding was devised[1]. Subsequent to a screening of refolding conditions on the 1.2 mL-scale, the best conditions (summarized in Table 9-1) were implemented in an automated refolding process based on the liquid-handler-assisted dilution of denatured protein into miniaturized stirred-tank reactors operatable in parallel.

Table 9-1. Summarized results for the isolation and refolding of His_8-tagged small monomeric outer membrane proteins. Isolated protein yields refer to the amount of denatured protein per liter shake flask culture after purification by IMAC. Refolding was performed on the 10 mL-scale using the bioREACTOR 48 system equipped with unbaffled reactors and S-shaped stirrers at 500 min^{-1} in 20 mM Tris-HCl, 1 mM EDTA with a protein feed of 2 µL min^{-1} and a final protein concentration of 0.5 g L^{-1}. Protein folding was allowed to continue for at least 8 h after the end of the feeding phase.

Protein	**Isolated protein yield, mg L^{-1}**	**Best folding conditions**	**Folding efficiency, %**
AlkL	218	40 °C, pH 8, 2 % w/v LDAO, 1 M urea	89 ± 1
OmpW	233	20 °C, pH 9, 4 % w/v *N*-lauroylsarcosine, 1 M urea	71 ± 2
OprG	144	20 °C, pH 8, 2 % w/v *N*-lauroylsarcosine, 0.1 M glutamate	96 ± 2
TodX	70	20 °C, pH 8, 2 % w/v *N*-lauroylsarcosine, 25 mM glycine	52 ± 2

The refolded proteins were characterized by a high thermal stability in the presence of 2 % w/v SDS with apparent melting temperatures T_m of 87 °C, 58 °C and 62 °C for AlkL, OmpW and TodX, while OprG could not be sufficiently denatured within 30 min to calculate T_m. Furthermore, successful

[1] SCHWARZER, T. S., HERMANN, M., KRISHNAN, S., SIMMEL, F. C. & CASTIGLIONE, K. 2017. Preparative refolding of small monomeric outer membrane proteins. *Protein Expression and Purification,* 132**,** 171-181.

refolding was also validated by CD-spectroscopy, protease accessibility and, in case of OprG, by electrophysiology. The refolded OprG displayed a single-channel conductance of roughly 330 pS, which is in the same range as the value of 500 pS published by McPhee *et al*. (2009). The developed process allowed the refolding of all four proteins with a high efficiency of 52-96 % and facilitated the preparative production of the target proteins considerably. In fact, this also represents the first instance where AlkL has been purified with success.

The implementation of protein and cofactor encapsulation into the process for the production of uniform polymersomes recently established by Poschenrieder *et al*. (2016) was important for the application of nano-scale enzyme membrane reactors for the asymmetric reduction of prochiral ketones. For reasons of cofactor stability and enzymatic activity of both the FDH and the KR part of the fusion enzyme, PBS pH 7.5 was chosen as the standard buffer system. It was established that the vesicle formation at 4 °C in PBS was comparable to the process in water, and that cofactor concentrations of up to 10 mM were tolerated. A working concentration of 4.5 mM was found to be sufficient for the coupled reaction and could be encapsulated without difficulties. Encapsulation of the fusion enzyme was more problematic, because the high membrane affinity of the KR, although largely diminished in the FDH-KR fusion enzyme (Hölsch and Weuster-Botz, 2010), still caused an interference with the formation of polymersomes. This resulted in a decreasing encapsulation efficiency with increasing protein concentration. In contrast to the fast process described for the formation of empty polymersomes in water (Poschenrieder *et al.*, 2016) or the slower formation of AGE-loaded polymersomes at 4 °C in Bicine buffer (Klermund, 2017), quality (polydispersity index <0.25) and yield of the FDH-KR-loaded polymersomes were highest after 3 h and deteriorated with longer process times. Thus, for the formation of the nano-scale enzyme membrane reactors loaded with the fusion enzyme and $NADP^+$, a process time of 3 h and a protein concentration of 0.60 g L^{-1} were found to be optimal. Under these conditions, an encapsulation efficiency of 0.66-0.69 % (corresponding to a total enzyme content of 3.9-4.2 mg L^{-1} for a 1 % w/v polymersome suspension) could be achieved, which translates to a statistical encapsulation efficiency of 180-190 % or an equivalent of about 2 FDH-KR molecules per nanoreactor. Another consequence of the observed interaction between FDH-KR and the polymer was that in order to remove non-encapsulated protein from the nanoreactors, size exclusion chromatography was not sufficient and needed to be supplemented by treatment with 0.25 g L^{-1} proteinase K.

Reconstitution of channel proteins for the membrane-functionalization of nano-scale enzyme membrane reactors was first studied with AlkL, which integrated readily when mixed with a suspension of empty polymersomes. It was found at a protein:polymer ratio of 1:100 that reconstitution was 1.5-fold more efficient at 30 °C compared to 4 °C, and that the reconstitution process was fast, although a 1.3-fold improvement could be observed when the incubation was prolonged from 5 min to 1 h. At a lower protein:polymer ratio of 1:500, where the amount of detergent introduced by the protein stock was negligible, the reconstitution was also improved 1.8-fold by doubling the concentration of the detergent

LDAO in the mixture. The greatest influence was exerted by the actual concentration of the channel protein. Therefore, the reconstitution of AlkL was increased 2.6-fold from 51 ± 3 to 130 ± 3 channels per polymersome when the polymersome concentration was increased from 1 % to 2 % w/v at a constant molar protein:polymer ratio of 1:100. At a fixed polymersome concentration of 2 % w/v, a direct comparison of different protein:polymer ratios revealed a striking increase from 24 ± 3 channels per polymersome at a ratio of 1:1,000 to 150 ± 5 at a ratio of 1:100. The latter number amounts to a channel density of 4,854 μm^{-2} or a coverage of 4.3 % of the available surface area. However, there was no linear improvement of the reconstitution, because the efficiency dropped from 55 ± 6 % to 35 ± 1 %. Next, reconstitution into FDH-KR-loaded nano-scale enzyme membrane reactors was assessed for all seven channel proteins at protein:polymer ratios between 1:250-1:100. The highest degree of functionalization was achieved for AlkL with 120 ± 6 channels per polymersome, which is 22% lower than in the previous system with empty polymersomes. PhoE, OprG and OmpF were reconstituted with a maximum of 80 ± 7, 65 ± 2 and 50 ± 5 channels per polymersome, respectively. A lower but still noticeable degree of functionalization was observed for OmpW, TodX and FocA, with 28 ± 2, 19 ± 1 and 17 ± 1 channels per polymersome, respectively. The overall median reconstitution efficiency for the functionalization of nano-scale enzyme membrane reactors ranged from 6.8-33 % for the seven proteins studied. Since only one of these proteins, namely OmpF (Nardin *et al.*, 2000b,) had been reconstituted into polymersomes before, these results represent a considerable increase of the number of channel proteins reconstituted into artificial polymer membranes by 60 % from 10 to 16.

Furthermore, the simultaneous reconstitution of two different channel proteins was also studied, which has been done only for one other channel pair, i.e. bacteriorhodopsin and the F_0F_1-ATPase (Choi and Montemagno, 2005, Choi *et al.*, 2006) by now. In this thesis, one of the two anion-selective channel proteins FocA or PhoE was combined with one of the small monomeric channel proteins AlkL, OmpW, OprG or

TodX. In all cases, both channel species could be reconstituted simultaneously, although a quantitative evaluation was not possible for all combinations. However, reconstitution of the different channel proteins displayed a complex interaction and, depending on the specific proteins involved, was reduced, unchanged or even enhanced. The experiments performed so far served to demonstrate that the simultaneous integration of different channel proteins is feasible, but to make reliable predictions about the outcome of a particular coreconstitution experiment, more detailed studies are required.

The flux of formate through the polymersome membrane was investigated using an influx assay. It was found that the membrane-specific permeability for formate at pH 7.5 was more than 5 orders of magnitude lower than for typical lipid membranes (-log *Pe*: 11.4 ± 0.1 vs. approximately 5.8, estimated from Walter *et al*. (1982)). Using the same assay format, it could also be established that a leakage of $NADP^+$ through reconstituted channel proteins presented no issue for the system. However, a comparison of the formate flux through OmpF with plain polymersomes also revealed that this particular

channel protein was severely destabilized and probably inactive in most experiments as a result of overly long storage and the detrimental effect of the N-terminal His_6-tag.

In order to evaluate the potential of the nano-scale enzyme membrane reactors for the asymmetric reduction of prochiral ketones, 2',3',4',5',6'-pentafluoroacetophenone (PFAP) was chosen as a model substrate because it was the most stable among the KR substrates with an acceptable conversion rate. Analysis of the product formation by gas chromatography was first hampered because the presence of polymersomes interfered with the sample extraction using ethyl acetate. For this reason, a more applicable, modified sample preparation protocol for the upstream removal of polymersomes using Amicon Ultra-0.5 centrifugal filter units was devised.

Interestingly, after a period of 112 h at 25 °C, the nano-scale enzyme membrane reactors were found to produce *(S)*-1-(2',3',4',5',6'-pentafluorophenyl)ethanol (*(S)*-PFE) even in the absence of channel proteins. In contrast to the PFAP conversion by whole cells, which lost their entire activity within 48 h under the experimental conditions, the reaction was found to be linear for a period between the first sampling after 24 h and then for at least 72 h. The half-life of the nanoreactors stored at 4 °C amounted to 32 ± 8 d. 0.42 % w/v nano-scale enzyme membrane reactors in the absence of any channel proteins were able to produce 117 µM *(S)*-PFE within 112 h (at 25 °C with 100 mM formate and 6 mM PFAP). A comparison of these results with the free enzyme system was complicated by the unexpected observation that the fusion enzyme tends to lose activity upon dilution. Since the total enzyme concentrations of the studied nanoreactor systems were extremely low (1.0-1.8 mg L^{-1}), experiments with the free enzyme were performed with a higher enzyme concentration. For the sake of comparison, the results were then corrected for the concentration-dependent activity loss using an empirical function. From this perspective, it appears that the free enzyme produced 14 times more *(S)*-PFE after 112 h than the unfunctionalized nano-scale enzyme membrane reactors. Since the two-enzyme system comprised of FDH and KR does not exhibit any cross-inhibitions nor side reactions even in whole cells, an improved reaction cascade due to compartmentalization was not expected and not possible. The comparison with the free enzyme thus only demonstrates that the reaction within the nanoreactors was mass-transfer limited, and indeed a membrane functionalization of the nanoreactors with different channel proteins resulted in a up to 2.2-fold increased product concentration, demonstrating that mass transfer limitations could be alleviated. Depending on the experiment, the greatest improvements were observed when AlkL (1.6-fold) or OmpW (2.2-fold) were reconstituted. Since AlkL could be reconstituted most readily, the effect was primarily mediated by the sheer number of channels, while the channel-specific effect of OmpW was almost 2-fold higher (0.088 ± 0.02-fold higher product formation per channel). Another observation was that a higher channel density of AlkL also led to a higher product formation, but the activity increase per AlkL channel decreased with increasing channel density. This result is not surprising, since experiments with the different channel protein classes have shown that the reaction system is very delicate and appeared not to be limited by the availability of a single but of both

substrates, at least at some point in the course of the experiment. Besides, the extent to which the compartmentalized reaction in the absence of channel proteins proceeded limits the possible effect of reconstituted channel proteins. The presence of OprG had a low effect on the activity of the nano-scale enzyme membrane reactors. Although the channel-specific transport activity was comparable to AlkL, the reconstitution of OprG did not produce the same degree of membrane functionalization. TodX, although very inefficient in terms of reconstitution, appears to be the channel with the highest specific transport activity towards PFAP with a 0.180 ± 0.04-fold higher product formation per channel.

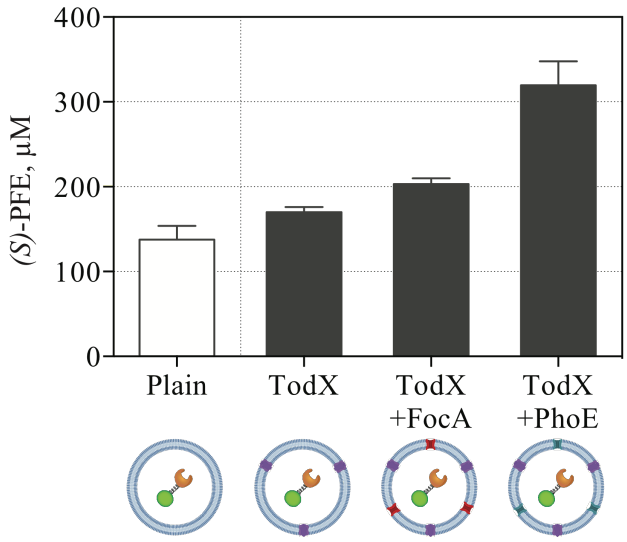

Figure 9-1. *(S)*-PFE formation by different nano-scale enzyme membrane reactor systems after 112 h at 25 °C. The experiment was performed with 0.25 % w/v nanoreactors, 1 M formate and 6 mM PFAP. Nanoreactors were either not functionalized, functionalized with TodX at a protein:polymer ratio of 1:250 or with TodX at a protein:polymer ratio of 1:250 and with FocA or PhoE at a protein:polymer ratio of 1:500.

The effect of the reconstitution of FocA or PhoE on the apparent activity of the nano-scale enzyme membrane reactors was comparable to OmpW, resulting in 2-fold and 1.7-fold higher product concentrations after 112 h. The channel-specific effect of these anion-selective channels was also comparable with a 0.12 ± 0.02 and 0.13 ± 0.01-fold higher product formation per channel. Although experiments with a combination of two different channel proteins were so far not always conclusive because of unpredictable effects on the reconstitution efficiencies of the channel proteins and because of occasional problems with the activity of some ion channel protein batches, a combination of TodX with FocA or PhoE was shown to result in a higher activity than nanoreactors functionalized with TodX alone. The functionalization with TodX alone increased the product concentration 1.2-fold compared to plain nanoreactors. The product concentration achieved with nanoreactors functionalized with a combination of TodX and FocA was 1.6-fold higher compared to plain nanoreactors, while nanoreactors functionalized with TodX and PhoE were 2.3-fold more active than plain nanoreactors and 1.9-fold more active than TodX-functionalized nanoreactors (*cf.* Figure 9-1). At this point it cannot be concluded with

certainty whether the improvement achieved by a combination of TodX with FocA or PhoE is primarily due to an improved channel reconstitution or to the added benefit of a reduced formate transport limitation. Results obtained with nano-scale enzyme membrane reactors only functionalized with FocA or PhoE suggest that the formate transport through the anion-selective channels is of some importance, but possibly both mechanisms contribute.

Finally, it can be concluded that the membrane-functionalization of nano-scale enzyme membrane reactors with a combination of two specialized channel protein species can be advantageous and result in novel and efficient biocatalsysts. However, for a more comprehensive understanding of the occurring phenomena, a detailed investigation of the coreconstitution of different channel protein species and a better control over the functionality of channel proteins would be highly desirable.

10 Outlook

It was shown in this thesis that the reconstitution of substrate-specific channel proteins and the combination of different channel specificities improved the reduction of prochiral ketones by nano-scale enzyme membrane reactors. Yet, some elements of the system still remain poorly understood, such as the interaction between different channel proteins upon coreconstitution and the actual concentration of active KR within the nanoreactors. For a better understanding of the system, a refined kinetic model of the reaction including the membrane-specific permeability coefficients of all involved elements would be of great value. Therefore, some additional effort is required to learn about the permeability towards the KR substrate PFAP and the product PFE, which proved to be difficult to obtain so far. Furthermore, only one substrate could be studied within the scope of this thesis. In order to exploit the full potential of the four newly-established channel proteins for hydrophobic substrates for the membrane-functionalization of polymer membranes in view of a diversified toolbox for the transport of chemically diverse substrates, it would be interesting to evaluate the relative performance of these channel proteins with other substrates. TodX proved to be the best candidate for the transport of PFAP, but due to a low reconstitution efficiency, the overall effect was moderate. On the other hand, given the high reconstitution efficiency of AlkL and considering the natural substrate spectrum ranging from rather aliphatic hydrocarbons and long-chain fatty acids to limonene, membrane-functionalization of nano-scale enzyme membrane reactors with this channel could turn out to be very beneficial for the conversion of other substrates than the one so far investigated.

Another limitation which became apparent was the inability to encapsulate significantly more than two enzyme molecules per nanoreactor, which is rather inefficient considering the tetrameric structure of the KR. A higher encapsulation efficiency could for example be achieved by using a different approach for the production of nanoreactors which is less limited by the interaction between the polymer and the KR at higher protein concentrations. An interesting alternative might be the employment of a micelle-to-vesicle-transition approach as demonstrated by Tangorra *et al*. (2015), which is also very convenient because it allows the simultaneous reconstitution of more delicate channel proteins and could improve the reconstitution of TodX or FocA. An attractive interaction between the membrane and the channel protein would be another interesting strategy, which has been recently demonstrated for the functional reconstitution of proteorhodopsin using a so-called charge-interaction-directed reconstitution (Kuang *et al.*, 2014). Possibly, this strategy could also be employed to achieve a higher loading of the enzyme within the nanoreactor core.

Finally, it must also be recognized that protein channels are not the only option available. Current advances in DNA origami technology have brought about the development of a ligand-responsive ion channel composed of DNA, with channel properties that can be easily tuned by rational design (Burns *et al.*, 2016). Although not likely to be of great use for the specific transport of hydrophobic molecules, such DNA-based structures may prove useful to selectively facilitate the flux of more polar substrates.

11 References

11.1 Literature

AHMED, F. & DISCHER, D. E. 2004. Self-porating polymersomes of PEG-PLA and PEG-PCL: hydrolysis-triggered controlled release vesicles. *Journal of Controlled Release,* 96**,** 37-53.

AHMED, F., PHOTOS, P. J. & DISCHER, D. E. 2006. Polymersomes as viral capsid mimics. *Drug Development Research,* 67**,** 4-14.

AKINC, A. & BATTAGLIA, G. 2013. Exploiting endocytosis for nanomedicines. *Cold Spring Harbor Perspectives in Biology,* 5.

ALBERTS, B., JOHNSON, A., LEWIS, J., RAFF, M., ROBERTS, K. & WALTER, P. 2007. *Molecular biology of the cell*, Garland Science.

ALBRECHT, R., ZETH, K., SODING, J., LUPAS, A. & LINKE, D. 2006. Expression, crystallization and preliminary X-ray crystallographic studies of the outer membrane protein OmpW from *Escherichia coli*. *Acta crystallographica. Section F, Structural biology and crystallization communications,* 62**,** 415-8.

ANDERSEN, O. S. & KOEPPE, R. E. 2007. Bilayer thickness and membrane protein function: An energetic perspective. *Annual Review of Biophysics and Biomolecular Structure,* 36**,** 107-130.

ANFINSEN, C. B., HABER, E., SELA, M. & WHITE, F. H. 1961. Kinetics of formation of native ribonuclease during oxidation of reduced polypeptide chain. *Proceedings of the National Academy of Sciences of the United States of America,* 47**,** 1309-&.

ANGELOVA, M. I., SOLEAU, S., MELEARD, P., FAUCON, J. F. & BOTHOREL, P. 1992. Preparation of giant vesicles by external AC electric fields. Kinetics and applications. *Trends in Colloid and Interface Science VI,* 89**,** 127-131.

ANSELMENT, B., BAEREND, D., MEY, E., BUCHNER, J., WEUSTER-BOTZ, D. & HASLBECK, M. 2010. Experimental optimization of protein refolding with a genetic algorithm. *Protein Science,* 19**,** 2085-2095.

ARAKAWA, T. & TIMASHEFF, S. N. 1983. Preferential interactions of proteins with solvent components in aqueous amino acid solutions. *Archives of Biochemistry and Biophysics,* 224**,** 169-177.

ARBUZOVA, A. & SCHWARZ, G. 1999. Pore-forming action of mastoparan peptides on liposomes: a quantitative analysis. *Biochimica Et Biophysica Acta-Biomembranes,* 1420**,** 139-152.

AVDEEF, A. 2012. *Absorption and drug development: Solubility, permeability and charge State*, Wiley.

AVDEEF, A., NIELSEN, P. E. & TSINMAN, O. 2004. PAMPA - a drug absorption in vitro model 11. Matching the in vivo unstirred water layer thickness by individual-well stirring in microtitre plates. *European Journal of Pharmaceutical Sciences,* 22**,** 365-374.

AVDEEF, A. & TSINMAN, O. 2006. PAMPA - A drug absorption in vitro model 13. Chemical selectivity due to membrane hydrogen bonding: In combo comparisons of HDM-, DOPC-, and DS-PAMPA models. *European Journal of Pharmaceutical Sciences,* 28**,** 43-50.

AXTHELM, F., CASSE, O., KOPPENOL, W. H., NAUSER, T., MEIER, W. & PALIVAN, C. G. 2008. Antioxidant nanoreactor based on superoxide dismutase encapsulated in superoxide-permeable vesicles. *Journal of Physical Chemistry B,* 112**,** 8211-8217.

BAE, J. H., PARK, B. G., JUNG, E., LEE, P.-G. & KIM, B.-G. 2014. fadD deletion and fadL overexpression in *Escherichia coli* increase hydroxy long-chain fatty acid productivity. *Applied Microbiology and Biotechnology,* 98**,** 8917-8925.

BANNWARTH, M. & SCHULZ, G. E. 2003. The expression of outer membrane proteins for crystallization. *Biochimica Et Biophysica Acta-Biomembranes,* 1610**,** 37-45.

BATTAGLIA, G. & RYAN, A. J. 2005. Bilayers and interdigitation in block copolymer vesicles. *Journal of the American Chemical Society,* 127**,** 8757-8764.

BATTAGLIA, G., RYAN, A. J. & TOMAS, S. 2006. Polymeric vesicle permeability: A facile chemical assay. *Langmuir,* 22**,** 4910-4913.

BAUER, K., STRUYVE, M., BOSCH, D., BENZ, R. & TOMMASSEN, J. 1989. One single lysine residue is responsible for the special interaction between polyphosphate and the outer membrane porin PhoE of *Escherichia coli*. *Journal of Biological Chemistry,* 264**,** 16393-16398.

BAUMANN, P., SPULBER, M., DINU, I. A. & PALIVAN, C. G. 2014. Cellular trojan horse based polymer nanoreactors with light-sensitive activity. *Journal of Physical Chemistry B,* 118**,** 9361-9370.

BAUMANN, P., TANNER, P., ONACA, O. & PALIVAN, C. G. 2011. Bio-decorated polymer membranes: A new approach in diagnostics and therapeutics. *Polymers,* 3**,** 173-192.

BEKETSKAIA, M. S., BAY, D. C. & TURNER, R. J. 2014. Outer membrane protein OmpW participates with small multidrug resistance protein member EmrE in Quaternary Cationic Compound Efflux. *Journal of Bacteriology,* 196**,** 1908-1914.

BEN-HAIM, N., BROZ, P., MARSCH, S., MEIER, W. & HUNZIKER, P. 2008. Cell-specific integration of artificial organelles based on functionalized polymer vesicles. *Nano Letters,* 8**,** 1368-1373.

BENZ, R., DARVEAU, R. P. & HANCOCK, R. E. W. 1984a. Outer membrane protein PhoE from *Escherichia coli* forms anion-selective pores in lipid-bilayer membranes. *European Journal of Biochemistry,* 140**,** 319-324.

BENZ, R., EGLI, C. & HANCOCK, R. E. W. 1993. Anion transport through the phosphate-specific OprP-channel of the *Pseudomonas aeruginosa* outer membrane - effects of phosphate, di-basic and tribasic anions and of negatively-charged lipids. *Biochimica et Biophysica Acta-Biomembranes,* 1149**,** 224-230.

BENZ, R. & HANCOCK, R. E. W. 1987. Mechanism of ion transport through the anion-selective channel of the *Pseudomonas aeruginosa* outer membrane. *Journal of General Physiology,* 89**,** 275-295.

BENZ, R., POOLE, K. & HANCOCK, R. E. 1984b. Characterization and chemical modification of small anion specific channels formed in lipid bilayer membranes by outer membrane protein P of *Pseudomonas aeruginosa*. *Biophysical Journal,* 45**,** 81-2.

BENZ, R., SCHMID, A. & HANCOCK, R. E. 1985. Ion selectivity of gram-negative bacterial porins. *Journal of Bacteriology,* 162**,** 722-7.

BERG, J. M., TYMOCZKO, J. L. & STRYER, L. 2007. *Biochemistry*, W.H. Freeman.

BERMUDEZ, H., BRANNAN, A. K., HAMMER, D. A., BATES, F. S. & DISCHER, D. E. 2002. Molecular weight dependence of polymersome membrane structure, elasticity, and stability. *Macromolecules,* 35**,** 8203-8208.

BERMUDEZ, H., HAMMER, D. A. & DISCHER, D. E. 2004. Effect of bilayer thickness on membrane bending rigidity. *Langmuir,* 20**,** 540-543.

BISSWANGER, H. 2000. *Enzymkinetik*, Wiley-VCH.

BOLEN, D. W. & BASKAKOV, I. V. 2001. The osmophobic effect: Natural selection of a thermodynamic force in protein folding. *Journal of Molecular Biology,* 310**,** 955-963.

BOMMARIUS, A. S. & RIEBEL, B. R. 2004. *Biocatalysis*, Wiley-VCH.

BRADSHAW, C. W., FU, H., SHEN, G. J. & WONG, C. H. 1992. A *Pseudomonas Sp.* alcohol dehydrogenase with broad substrate-specificity and unusual stereospecificity for organic synthesis. *Journal of Organic Chemistry,* 57**,** 1526-1532.

BREUER, M., DITRICH, K., HABICHER, T., HAUER, B., KESSELER, M., STURMER, R. & ZELINSKI, T. 2004. Industrial methods for the production of optically active intermediates. *Angewandte Chemie-International Edition,* 43**,** 788-824.

BRIGGS, G. E. & HALDANE, J. B. 1925. A Note on the kinetics of enzyme action. *Biochemical Journal,* 19**,** 338-9.

BROWN, L., MCARTHUR, S. L., WRIGHT, P. C., LEWIS, A. & BATTAGLIA, G. 2010. Polymersome production on a microfluidic platform using pH sensitive block copolymers. *Lab on a Chip,* 10**,** 1922.

BROZ, P., BEN-HAIM, N., SANTINI, F., MARSCH, S., SCHEFFLER, K., MEIER, W. & HUNZIKER, P. 2009. Nano Imaging Technologies: Polymer vesicles loaded with precipitated gadolinium nanoparticles: A novel target-specific contrast agent for magnetic resonance imaging. *European Journal of Nanomedicine,* 2.

BROZ, P., BENITO, S. M., SAW, C., BURGER, P., HEIDER, H., PFISTERER, M., MARSCH, S., MEIER, W. & HUNZIKER, P. 2005. Cell targeting by a generic receptor-targeted polymer nanocontainer platform. *Journal of Controlled Release,* 102**,** 475-488.

BROZ, P., DRIAMOV, S., ZIEGLER, J., BEN-HAIM, N., MARSCH, S., MEIER, W. & HUNZIKER, P. 2006. Toward intelligent nanosize bioreactors: A pH-switchable, channel-equipped, functional polymer nanocontainer. *Nano Letters,* 6**,** 2349-2353.

BUCHANAN, S. K. 1999. Beta-barrel proteins from bacterial outer membranes: structure, function and refolding. *Current Opinion in Structural Biology,* 9**,** 455-461.

BURGESS, N. K., DAO, T. P., STANLEY, A. M. & FLEMING, K. G. 2008. Beta-barrel proteins that reside in the *Escherichia coli* outer membrane in vivo demonstrate varied folding behavior in vitro. *Journal of Biological Chemistry,* 283**,** 26748-26758.

BURNS, J. R., SEIFERT, A., FERTIG, N. & HOWORKA, S. 2016. A biomimetic DNA-based channel for the ligand-controlled transport of charged molecular cargo across a biological membrane. *Nature Nanotechnology,* 11**,** 152-156.

BUSCH, W. & SAIER, M. H. 2004. The IUBMB-endorsed transporter classification system. *Molecular Biotechnology,* 27**,** 253-262.

CALL, T. P., AKHTAR, M. K., BAGANZ, F. & GRANT, C. 2016. Modulating the import of medium-chain alkanes in *E. coli* through tuned expression of FadL. *Journal of Biological Engineering,* 10.

CANTON, I., MASSIGNANI, M., PATIKARNMONTHON, N.*, et al.* 2013. Fully synthetic polymer vesicles for intracellular delivery of antibodies in live cells. *Faseb Journal,* 27**,** 98-108.

CARUGO, O. & ARGOS, P. 1997. NADP-dependent enzymes .1. Conserved stereochemistry of cofactor binding. *Proteins-Structure Function and Genetics,* 28**,** 10-28.

CHEN, Q., RAUSCH, K. G., SCHONHERR, H. & VANCSO, G. J. 2010. α-Chymotrypsin-catalyzed reaction confined in block-copolymer vesicles. *ChemPhysChem,* 11**,** 3534-3540.

CHEN, Q., SCHONHERR, H. & VANCSO, G. J. 2009a. Block copolymer vesicles as nanoreactors for enzymatic reactions. *Small,* 5**,** 1436-1445.

CHEN, Q., SCHÖNHERR, H. & VANCSO, G. J. 2009b. Mechanical properties of block copolymer vesicle membranes by atomic force microscopy. *Soft Matter,* 5**,** 4944.

CHEN, R. R. 2007. Permeability issues in whole-cell bioprocesses and cellular membrane engineering. *Applied Microbiology and Biotechnology,* 74**,** 730-738.

CHENAULT, H. K. & WHITESIDES, G. M. 1987. Regeneration of nicotinamide cofactors for use in organic synthesis. *Applied Biochemistry and Biotechnology,* 14**,** 147-197.

CHI, E. Y., KRISHNAN, S., RANDOLPH, T. W. & CARPENTER, J. F. 2003. Physical stability of proteins in aqueous solution: Mechanism and driving forces in nonnative protein aggregation. *Pharmaceutical Research,* 20**,** 1325-1336.

CHOE, W. S., NIAN, R. & LAI, W. B. 2006. Recent advances in biomolecular process intensification. *Chemical Engineering Science,* 61**,** 886-906.

CHOI, H. J., GERMAIN, J. & MONTEMAGNO, C. D. 2006. Effects of different reconstitution procedures on membrane protein activities in proteopolymersomes. *Nanotechnology,* 17**,** 1825-1830.

CHOI, H. J. & MONTEMAGNO, C. D. 2005. Artificial organelle: ATP synthesis from cellular mimetic polymersomes. *Nano Letters,* 5**,** 2538-2542.

CHRISTIAN, D. A., CAI, S., BOWEN, D. M., KIM, Y., PAJEROWSKI, J. D. & DISCHER, D. E. 2009. Polymersome carriers: From self-assembly to siRNA and protein therapeutics. *European Journal of Pharmaceutics and Biopharmaceutics,* 71**,** 463-474.

CHUANOI, S., ANRAKU, Y., HORI, M., KISHIMURA, A. & KATAOKA, K. 2014. Fabrication of polyion complex vesicles with enhanced salt and temperature resistance and their potential applications as enzymatic nanoreactors. *Biomacromolecules,* 15**,** 2389-2397.

CLELAND, J. L. & WANG, D. I. C. 1990. Cosolvent assisted protein refolding. *Bio-Technology,* 8**,** 1274-1278.

CONRADO, R. J., VARNER, J. D. & DELISA, M. P. 2008. Engineering the spatial organization of metabolic enzymes: mimicking nature's synergy. *Current Opinion in Biotechnology,* 19**,** 492-499.

CORNELISSEN, S., JULSING, M. K., VOLMER, J., RIECHERT, O., SCHMID, A. & BUHLER, B. 2013. Whole-cell-based CYP153A6-catalyzed (S)-limonene hydroxylation efficiency depends

on host background and profits from monoterpene uptake via AlkL. *Biotechnology and Bioengineering,* 110**,** 1282-92.

COWAN, S. W., SCHIRMER, T., RUMMEL, G., STEIERT, M., GHOSH, R., PAUPTIT, R. A., JANSONIUS, J. N. & ROSENBUSCH, J. P. 1992. Crystal structures explain functional properties of two *E. coli* porins. *Nature,* 358**,** 727-33.

CZYZEWSKI, B. K. & WANG, D.-N. 2012. Identification and characterization of a bacterial hydrosulphide ion channel. *Nature,* 483**,** 494-497.

DARGENT, B., HOFMANN, W., PATTUS, F. & ROSENBUSCH, J. P. 1986. The selectivity filter of voltage-dependent channels formed by phosphoporin (PhoE Protein) from *Escherichia coli*. *Embo Journal,* 5**,** 773-778.

DAUßMANN, T., HENNEMANN, H. G., ROSEN, T. C. & DÜNKELMANN, P. 2006. Enzymatische Technologien zur Synthese chiraler Alkohol-Derivate. *Chemie Ingenieur Technik,* 78**,** 249-255.

DE BERNARDEZ-CLARK, E. 2001. Protein refolding for industrial processes. *Current Opinion in Biotechnology,* 12**,** 202-207.

DE BERNARDEZ-CLARK, E., HEVEHAN, D., SZELA, S. & MAACHUPALLI-REDDY, J. 1998. Oxidative renaturation of hen egg-white lysozyme. Folding vs aggregation. *Biotechnology Progress,* 14**,** 47-54.

DE BERNARDEZ-CLARK, E., SCHWARZ, E. & RUDOLPH, R. 1999. Inhibition of aggregation side reactions during in vitro protein folding. *Methods in Enzymology,* 309**,** 217-236.

DE OLIVEIRA, H., THEVENOT, J. & LECOMMANDOUX, S. 2012. Smart polymersomes for therapy and diagnosis: fast progress toward multifunctional biomimetic nanomedicines. *Wiley Interdisciplinary Reviews-Nanomedicine and Nanobiotechnology,* 4**,** 525-546.

DECOCK, H., STRUYVE, M., KLEEREBEZEM, M., VANDERKRIFT, T. & TOMMASSEN, J. 1997. Role of the carboxy-terminal phenylalanine in the biogenesis of outer membrane protein PhoE of *Escherichia coli* K-12. *Journal of Molecular Biology,* 269**,** 473-478.

DEGERBECK, F., FRANSSON, B., GREHN, L. & RAGNARSSON, U. 1992. Direct synthesis of N-protected chiral amino acids from imidodicarbonates employing either Mitsunobu or triflate alkylation - Feasibility study using lactate with particular reference to N-15-labeling. *Journal of the Chemical Society-Perkin Transactions 1***,** 245-253.

DESAI, N. P. & HUBBELL, J. A. 1991. Solution technique to incorporate polyethylene oxide and other water-soluble polymers into surfaces of polymeric biomaterials. *Biomaterials,* 12**,** 144-153.

DICOSIMO, R., MCAULIFFE, J., POULOSE, A. J. & BOHLMANN, G. 2013. Industrial use of immobilized enzymes. *Chemical Society Reviews,* 42**,** 6437-6474.

DILL, K. A. & CHAN, H. S. 1997. From Levinthal to pathways to funnels. *Nature Structural Biology,* 4**,** 10-19.

DISCHER, B. M., WON, Y. Y., EGE, D. S., LEE, J. C. M., BATES, F. S., DISCHER, D. E. & HAMMER, D. A. 1999. Polymersomes: Tough vesicles made from diblock copolymers. *Science,* 284**,** 1143-1146.

DISCHER, D. E. & AHMED, F. 2006. Polymersomes. *Annual Review of Biomedical Engineering,* 8**,** 323-341.

DISCHER, D. E. & EISENBERG, A. 2002. Polymer vesicles. *Science,* 297**,** 967-973.

EATON, R. W. & NITTERAUER, J. D. 1994. Biotransformation of benzothiophene by isopropylbenzene-degrading bacteria. *Journal of Bacteriology,* 176**,** 3992-4002.

EDRINGTON, T. C., KINTZ, E., GOLDBERG, J. B. & TAMM, L. K. 2011. Structural basis for the interaction of lipopolysaccharide with outer membrane protein H (OprH) from *Pseudomonas aeruginosa*. *Journal of Biological Chemistry,* 286**,** 39211-39223.

EGGINK, G., LAGEVEEN, R. G., ALTENBURG, B. & WITHOLT, B. 1987. Controlled and functional expression of the Pseudomonas oleovorans alkane utilizing system in Pseudomonas putida and *Escherichia coli*. *Journal of Biological Chemistry,* 262**,** 17712-8.

ERBAKAN, M., SHEN, Y. X., GRZELAKOWSKI, M., BUTLER, P. J., KUMAR, M. & CURTIS, W. R. 2014. Molecular cloning, overexpression and characterization of a novel water channel protein from *Rhodobacter sphaeroides*. *Plos One,* 9.

ETAYO, P. & VIDAL-FERRAN, A. 2013. Rhodium-catalysed asymmetric hydrogenation as a valuable synthetic tool for the preparation of chiral drugs. *Chemical Society Reviews,* 42**,** 728-754.

EXPERT-BEZANÇON, N., RABILLOUD, T., VUILLARD, L. & GOLDBERG, M. E. 2003. Physical–chemical features of non-detergent sulfobetaines active as protein-folding helpers. *Biophysical Chemistry,* 100**,** 469-479.

FABER, K. 2011. *Biotransformations in organic chemistry*, Springer.

FABIANO, E., GOLDING, B. T. & SADEGHI, M. M. 1987. A Simple conversion of alcohols into amines. *Synthesis-Stuttgart***,** 190-192.

FAIRBANKS, G., STECK, T. L. & WALLACH, D. F. H. 1971. Electrophoretic analysis of the major polypeptides of the human erythrocyte membrane. *Biochemistry,* 10**,** 2606–2617.

FALKE, D., SCHULZ, K., DOBERENZ, C., BEYER, L., LILIE, H., THIEMER, B. & SAWERS, R. G. 2010. Unexpected oligomeric structure of the FocA formate channel of *Escherichia coli*: a paradigm for the formate-nitrite transporter family of integral membrane proteins. *Fems Microbiology Letters,* 303**,** 69-75.

FARQUHAR, K. D., MISRAN, M., ROBINSON, B. H., STEYTLER, D. C., MORINI, P., GARRETT, P. R. & HOLZWARTH, J. F. 1996. The kinetics and mechanism of micelle-vesicle transitions in aqueous solution. *Journal of Physics-Condensed Matter,* 8**,** 9397-9404.

FISCHER, H., KANSY, M., AVDEEF, A. & SENNER, F. 2007. Permeation of permanently positive charged molecules through artificial membranes - Influence of physico-chemical properties. *European Journal of Pharmaceutical Sciences,* 31**,** 32-42.

GAITZSCH, J., APPELHANS, D., GRAFE, D., SCHWILLE, P. & VOIT, B. 2011. Photo-crosslinked and pH sensitive polymersomes for triggering the loading and release of cargo. *Chemical Communications,* 47**,** 3466-3468.

GAITZSCH, J., APPELHANS, D., WANG, L. G., BATTAGLIA, G. & VOIT, B. 2012. Synthetic bio-nanoreactor: Mechanical and chemical control of polymersome membrane permeability. *Angewandte Chemie-International Edition,* 51**,** 4448-4451.

GAITZSCH, J., HUANG, X. & VOIT, B. 2016. Engineering functional polymer capsules toward smart nanoreactors. *Chemical Reviews,* 116**,** 1053-1093.

GARAVITO, R. M., JENKINS, J., JANSONIUS, J. N., KARLSSON, R. & ROSENBUSCH, J. P. 1983. X-ray-diffraction analysis of matrix porin, an integral membrane-protein from *Escherichia coli* outer membranes. *Journal of Molecular Biology,* 164**,** 313-327.

GARAVITO, R. M. & ROSENBUSCH, J. P. 1980. 3-Dimensional crystals of an integral membrane protein - an Initial X-ray analysis. *Journal of Cell Biology,* 86**,** 327-329.

GARAVITO, R. M. & ROSENBUSCH, J. P. 1986. Isolation and crystallization of bacterial porin. *Methods in Enzymology,* 125**,** 309-328.

GARCIA-URDIALES, E., LAVANDERA, I. & GOTOOR, V. 2012. Concepts in biocatalysis. *Enzyme Catalysis in Organic Synthesis.* Wiley-VCH.

GENSBERG, K., SMITH, A. W., BRINKMAN, F. S. L. & HANCOCK, R. E. W. 1999. Identification of oprG, a gene encoding a major outer membrane protein of *Pseudomonas aeruginosa*. *Journal of Antimicrobial Chemotherapy,* 43**,** 607-608.

GHOROGHCHIAN, P. P., FRAIL, P. R., LI, G. Z., ZUPANCICH, J. A., BATES, F. S., HAMMER, D. A. & THERIEN, M. J. 2007. Controlling bulk optical properties of emissive polymersomes through intramembranous polymer-fluorophore interactions. *Chemistry of Materials,* 19**,** 1309-1318.

GIACOMELLI, C., SCHMIDT, V. & BORSALI, R. 2007. Nanocontainers formed by self-assembly of poly(ethylene oxide)-b-poly(glycerol monomethacrylate) - Drug conjugates. *Macromolecules,* 40**,** 2148-2157.

GOLDBERG, K., SCHROER, K., LUTZ, S. & LIESE, A. 2007. Biocatalytic ketone reduction - a powerful tool for the production of chiral alcohols - part I: processes with isolated enzymes. *Applied Microbiology and Biotechnology,* 76**,** 237-248.

GOLDBERG, M. E., RUDOLPH, R. & JAENICKE, R. 1991. A kinetic study of the competition between renaturation and aggregation during the refolding of denatured reduced egg-white lysozyme. *Biochemistry,* 30**,** 2790-2797.

GONZALEZ-PEREZ, A., STIBIUS, K. B., VISSING, T., NIELSEN, C. H. & MOURITSEN, O. G. 2009. Biomimetic triblock copolymer membrane arrays: A stable template for functional membrane proteins. *Langmuir,* 25**,** 10447-10450.

GORDON, E., HORSEFIELD, R., SWARTS, H. G., DE PONT, J. J., NEUTZE, R. & SNIJDER, A. 2008. Effective high-throughput overproduction of membrane proteins in *Escherichia coli*. *Protein Expression and Purification,* 62**,** 1-8.

GOSWAMI, A. 2011. Enzyme catalysis in the synthesis of active pharmaceutical ingredients. *Enzyme Technologies.* John Wiley & Sons.

GRAFF, A., FRAYSSE-AILHAS, C., PALIVAN, C. G., GRZELAKOWSKI, M., FRIEDRICH, T., VEBERT, C., GESCHEIDT, G. & MEIER, W. 2010. Amphiphilic copolymer membranes promote NADH:ubiquinone oxidoreductase activity: Towards an electron-transfer nanodevice. *Macromolecular Chemistry and Physics,* 211**,** 229-238.

GRAFF, A., SAUER, M., VAN GELDER, P. & MEIER, W. 2002. Virus-assisted loading of polymer nanocontainer. *Proceedings of the National Academy of Sciences of the United States of America,* 99**,** 5064-5068.

GRANT, C., DESZCZ, D., WEI, Y.-C.*, et al.* 2014. Identification and use of an alkane transporter plug-in for applications in biocatalysis and whole-cell biosensing of alkanes. *Scientific Reports,* 4.

GRANT, C., WOODLEY, J. M. & BAGANZ, F. 2011. Whole-cell bio-oxidation of *n*-dodecane using the alkane hydroxylase system of *P. putida* GPo1 expressed in *E. coli*. *Enzyme and Microbial Technology,* 48**,** 480-486.

GRÖGER, H. & ASANO, Y. 2012. Introduction - principles and historical landmarks of enzyme catalysis in organic synthesis. *Enzyme Catalysis in Organic Synthesis.* Wiley-VCH.

GRZELAKOWSKI, M., ONACA, O., RIGLER, P., KUMAR, M. & MEIER, W. 2009. Immobilized protein-polymer nanoreactors. *Small,* 5**,** 2545-8.

GUNKEL-GRABOLE, G., SIGG, S., LOMORA, M., LORCHER, S., PALIVAN, C. G. & MEIER, W. P. 2015. Polymeric 3D nano-architectures for transport and delivery of therapeutically relevant biomacromolecules. *Biomaterials Science,* 3**,** 25-40.

HABEL, J., HANSEN, M., KYNDE, S.*, et al.* 2015. Aquaporin-based biomimetic polymeric membranes: Approaches and challenges. *Membranes,* 5**,** 307-351.

HAJJAR, E., MAHENDRAN, K. R., KUMAR, A., BESSONOV, A., PETRESCU, M., WEINGART, H., RUGGERONE, P., WINTERHALTER, M. & CECCARELLI, M. 2010. Bridging timescales and length scales: from macroscopic flux to the molecular mechanism of antibiotic diffusion through porins. *Biophysical Journal,* 98**,** 569-575.

HAMADA, H., ARAKAWA, T. & SHIRAKI, K. 2009. Effect of additives on protein aggregation. *Current Pharmaceutical Biotechnology,* 10**,** 400-407.

HANCOCK, R. E. & BENZ, R. 1986. Demonstration and chemical modification of a specific phosphate binding site in the phosphate-starvation-inducible outer membrane porin protein P of *Pseudomonas aeruginosa*. *Biochimica et Biophysica Acta-Biomembranes,* 860**,** 699-707.

HANCOCK, R. E., POOLE, K. & BENZ, R. 1982. Outer membrane protein P of *Pseudomonas aeruginosa*: regulation by phosphate deficiency and formation of small anion-specific channels in lipid bilayer membranes. *Journal of Bacteriology,* 150**,** 730-8.

HANCOCK, R. E., POOLE, K., GIMPLE, M. & BENZ, R. 1983. Modification of the conductance, selectivity and concentration-dependent saturation of *Pseudomonas aeruginosa* protein P channels by chemical acetylation. *Biochimica et Biophysica Acta-Biomembranes,* 735**,** 137-44.

HANCOCK, R. E. W. 1997. The bacterial outer membrane as a drug barrier. *Trends in Microbiology,* 5**,** 37-42.

HAVEL, J. 2006. *Asymmetrische Synthesen mit phototrophen Mikroorganismen.* Dissertation, Technical University of Munich.

HAVEL, J. & WEUSTER-BOTZ, D. 2007. Cofactor regeneration in phototrophic cyanobacteria applied for asymmetric reduction of ketones. *Applied Microbiology and Biotechnology,* 75**,** 1031-1037.

HEARN, E. M., PATEL, D. R., LEPORE, B. W., INDIC, M. & VAN DEN BERG, B. 2009. Transmembrane passage of hydrophobic compounds through a protein channel wall. *Nature,* 458**,** 367-70.

HEARN, E. M., PATEL, D. R. & VAN DEN BERG, B. 2008. Outer-membrane transport of aromatic hydrocarbons as a first step in biodegradation. *Proceedings of the National Academy of Sciences of the United States of America,* 105**,** 8601-6.

HINDAHL, M. S., CROCKFORD, G. W. K. & HANCOCK, R. E. W. 1984. Outer membrane protein Nmpc of *Escherichia coli*: Pore-forming properties in black lipid bilayers. *Journal of Bacteriology,* 159**,** 1053-1055.

HINDS, T. R. & VINCENZI, F. F. 1985. The effect of ETH 1001 on ion fluxes across red blood-cell membranes. *Cell Calcium,* 6**,** 265-279.

HO, D., CHU, B., LEE, H., BROOKS, E. K., KUO, K. & MONTEMAGNO, C. D. 2005. Fabrication of biomolecule–copolymer hybrid nanovesicles as energy conversion systems. *Nanotechnology,* 16**,** 3120-3132.

HO, E. M., CHANG, H. W., KIM, S. I., KAHNG, H. Y. & OH, K. H. 2004. Analysis of TNT (2,4,6-trinitrotoluene)-inducible cellular responses and stress shock proteome in *Stenotrophomonas sp* OK-5. *Current Microbiology,* 49**,** 346-352.

HOGBOM, M., JAGER, K., ROBEL, I., UNGE, T. & ROHAYEM, J. 2009. The active form of the norovirus RNA-dependent RNA polymerase is a homodimer with cooperative activity. *Journal of General Virology,* 90**,** 281-291.

HÖLSCH, K. 2009. *Asymmetrische Synthesen mit neuen Oxidoreduktasen aus Cyanobakterien.* Dissertation at the Technical University of Munich.

HÖLSCH, K., HAVEL, J., HASLBECK, M. & WEUSTER-BOTZ, D. 2008. Identification, cloning, and characterization of a novel ketoreductase from the cyanobacterium *Synechococcus sp* Strain PCC 7942. *Applied and Environmental Microbiology,* 74**,** 6697-6702.

HÖLSCH, K., SUHRER, I., HEUSEL, M. & WEUSTER-BOTZ, D. 2013. Engineering of formate dehydrogenase: synergistic effect of mutations affecting cofactor specificity and chemical stability. *Applied Microbiology and Biotechnology,* 97**,** 2473-2481.

HÖLSCH, K. & WEUSTER-BOTZ, D. 2010. Enantioselective reduction of prochiral ketones by engineered bifunctional fusion proteins. *Biotechnology and Applied Biochemistry,* 56**,** 131-140.

HÖLSCH, K. & WEUSTER-BOTZ, D. 2011. Kinetic mechanism of 3-ketoacyl-(acyl-carrier-protein) reductase from *Synechococcus sp* strain PCC 7942: A useful enzyme for the production of chiral alcohols. *Journal of Molecular Catalysis B: Enzymatic,* 69**,** 89-94.

HONG, H., PATEL, D. R., TAMM, L. K. & VAN DEN BERG, B. 2006. The outer membrane protein OmpW forms an eight-stranded beta-barrel with a hydrophobic channel. *Journal of Biological Chemistry,* 281**,** 7568-77.

HORST, R., STANCZAK, P. & WUTHRICH, K. 2014. NMR polypeptide backbone conformation of the *E. coli* outer membrane protein W. *Structure,* 22**,** 1204-1209.

HUANG, K. S., BAYLEY, H., LIAO, M. J., LONDON, E. & KHORANA, H. G. 1981. Refolding of an integral membrane-protein: Denaturation, renaturation, and reconstitution of intact bacteriorhodopsin and 2 proteolytic fragments. *Journal of Biological Chemistry,* 256**,** 3802-3809.

HUMMEL, W. 1997. New alcohol dehydrogenases for the synthesis of chiral compounds. *Advances in Biochemical Engineering/Biotechnology,* 58**,** 145-84.

HUMMEL, W. & KULA, M. R. 1989. Dehydrogenases for the synthesis of chiral compounds. *European Journal of Biochemistry,* 184**,** 1-13.

HUNGER, D., DOBERENZ, C. & SAWERS, R. G. 2014. Identification of key residues in the formate channel FocA that control import and export of formate. *Biological Chemistry,* 395.

INOUYE, M. & YEE, M. L. 1973. Homogeneity of Envelope Proteins of Escherichia-Coli Separated by Gel-Electrophoresis in Sodium Dodecyl Sulfate. *Journal of Bacteriology,* 113**,** 304-312.

ITEL, F., CHAMI, M., NAJER, A., LÖRCHER, S., WU, D., DINU, I. A. & MEIER, W. 2014. Molecular organization and dynamics in polymersome membranes: a lateral diffusion study. *Macromolecules,* 47**,** 7588-7596.

ITEL, F., NAJER, A., PALIVAN, C. G. & MEIER, W. 2015. Dynamics of membrane proteins within synthetic polymer membranes with large hydrophobic mismatch. *Nano Letters,* 15**,** 3871-3878.

IUBMB 1992a. *Enzyme Nomenclature*, Academic Press, San Diego.

IUBMB 1992b. Nomenclature Committee of IUBMB (NC-IUBMB) and IUPAC-IUBMB Joint Commission on Biochemical Nomenclature (JCBN). *European Journal of Biochemistry,* 204**,** 1-3.

JAENICKE, R. 1996. How do proteins acquire their three-dimensional structure and stability? *Naturwissenschaften,* 83**,** 544-554.

JULSING, M. K., SCHREWE, M., CORNELISSEN, S., HERMANN, I., SCHMID, A. & BUHLER, B. 2012. Outer membrane protein AlkL boosts biocatalytic oxyfunctionalization of hydrophobic substrates in *Escherichia coli*. *Applied and Environmental Microbiology,* 78**,** 5724-33.

JUNGBAUER, A. & KAAR, W. 2007. Current status of technical protein refolding. *Journal of Biotechnology,* 128**,** 587-596.

JUNGBAUER, A., KAAR, W. & SCHLEGL, R. 2004. Folding and refolding of proteins in chromatographic beds. *Current Opinion in Biotechnology,* 15**,** 487-494.

JUNGE, F., SCHNEIDER, B., RECKEL, S., SCHWARZ, D., DÖTSCH, V. & BERNHARD, F. 2008. Large-scale production of functional membrane proteins. *Cellular and Molecular Life Sciences,* 65**,** 1729-1755.

KADAS, J., BOROSS, P., WEBER, I. T., BAGOSSI, P., MATUZ, K. & TOZSER, J. 2008. C-terminal residues of mature human T-lymphotropic virus type 1 protease are critical for dimerization and catalytic activity. *Biochemical Journal,* 416**,** 357-364.

KADISCH, M., JULSING, M. K., SCHREWE, M., JEHMLICH, N., SCHEER, B., VON BERGEN, M., SCHMID, A. & BÜHLER, B. 2016. Maximization of cell viability rather than biocatalyst activity improves whole-cell ω-oxyfunctionalization performance. *Biotechnology and Bioengineering*.

KATAOKA, M., KITA, K., WADA, M., YASOHARA, Y., HASEGAWA, J. & SHIMIZU, S. 2003. Novel bioreduction system for the production of chiral alcohols. *Applied Microbiology and Biotechnology,* 62**,** 437-445.

KATOH, S. & KATOH, Y. 2000. Continuous refolding of lysozyme with fed-batch addition of denatured protein solution. *Process Biochemistry,* 35**,** 1119-1124.

KIEFHABER, T., RUDOLPH, R., KOHLER, H. H. & BUCHNER, J. 1991. Protein aggregation in vitro and in vivo: A quantitative model of the kinetic competition between folding and aggregation. *Bio-Technology,* 9**,** 825-829.

KIM, H., KANG, Y. J., KANG, S. & KIM, K. T. 2012. Monosaccharide-responsive release of insulin from polymersomes of polyboroxole block copolymers at neutral pH. *Journal of the American Chemical Society,* 134**,** 4030-4033.

KIM, K. T., CORNELISSEN, J. J. L. M., NOLTE, R. J. M. & VAN HEST, J. C. M. 2009. A polymersome nanoreactor with controllable permeability induced by stimuli-responsive block copolymers. *Advanced Materials,* 21**,** 2787–2791.

KIM, M. S. & LEE, D. S. 2010. Biodegradable and pH-sensitive polymersome with tuning permeable membrane for drug delivery carrier. *Chemical Communications,* 46**,** 4481-4483.

KITA-TOKARCZYK, K., GRUMELARD, J., HAEFELE, T. & MEIER, W. 2005. Block copolymer vesicles - using concepts from polymer chemistry to mimic biomembranes. *Polymer,* 46**,** 3540-3563.

KLEINSCHMIDT, J. H., WIENER, M. C. & TAMM, L. K. 1999. Outer membrane protein A of *E. coli* folds into detergent micelles, but not in the presence of monomeric detergent. *Protein Science,* 8**,** 2065-2071.

KLERMUND, L. 2017. *Surface functionalization of nano-scale membrane reactors for multienzyme syntheses.* Dissertation, Technical University of Munich.

KLERMUND, L., POSCHENRIEDER, S. T. & CASTIGLIONE, K. 2016. Simple surface functionalization of polymersomes using non-antibacterial peptide anchors. *Journal of Nanobiotechnology,* 14.

KOEBNIK, R., LOCHER, K. P. & VAN GELDER, P. 2000. Structure and function of bacterial outer membrane proteins: barrels in a nutshell. *Molecular Microbiology,* 37**,** 239-53.

KROGH, A., LARSSON, B., VON HEIJNE, G. & SONNHAMMER, E. L. L. 2001. Predicting transmembrane protein topology with a hidden Markov model: Application to complete genomes. *Journal of Molecular Biology,* 305**,** 567-580.

KROUTIL, W., MANG, H., EDEGGER, K. & FABER, K. 2004. Recent advances in the biocatalytic reduction of ketones and oxidation of sec-alcohols. *Current Opinion in Chemical Biology,* 8**,** 120-126.

KUANG, L., FERNANDES, D. A., O'HALLORAN, M., ZHENG, W., JIANG, Y., LADIZHANSKY, V., BROWN, L. S. & LIANG, H. 2014. "Frozen" block copolymer nanomembranes with light-driven proton pumping performance. *ACS Nano,* 8**,** 537-545.

KUCHARSKA, I., EDRINGTON, T. C., LIANG, B. & TAMM, L. K. 2015a. Optimizing nanodiscs and bicelles for solution NMR studies of two β-barrel membrane proteins. *Journal of Biomolecular NMR,* 61**,** 261-274.

KUCHARSKA, I., SEELHEIM, P., EDRINGTON, T., LIANG, B. & TAMM, LUKAS K. 2015b. OprG harnesses the dynamics of its extracellular loops to transport small amino acids across the outer membrane of *Pseudomonas aeruginosa*. *Structure,* 23**,** 2234-2245.

KUMAR, M., GRZELAKOWSKI, M., ZILLES, J., CLARK, M. & MEIER, W. 2007. Highly permeable polymeric membranes based on the incorporation of the functional water channel protein Aquaporin Z. *Proceedings of the National Academy of Sciences of the United States of America,* 104**,** 20719-20724.

KUMAR, M., HABEL, J. E. O., SHEN, Y. X., MEIER, W. P. & WALZ, T. 2012. High-density reconstitution of functional water channels into vesicular and planar block copolymer membranes. *Journal of the American Chemical Society,* 134**,** 18631-18637.

KYTE, J. & DOOLITTLE, R. F. 1982. A simple method for displaying the hydropathic character of a protein. *Journal of Molecular Biology,* 157**,** 105-132.

LACADENA, J., DELPOZO, A. M., GASSET, M.*, et al.* 1995. Characterization of the antifungal protein secreted by the mould *Aspergillus giganteus*. *Archives of Biochemistry and Biophysics,* 324**,** 273-281.

LAMZIN, V. S., DAUTER, Z., POPOV, V. O., HARUTYUNYAN, E. H. & WILSON, K. S. 1994. High resolution structures of holo and apo formate dehydrogenase. *Journal of Molecular Biology,* 236**,** 759-785.

LANGOWSKA, K., PALIVAN, C. G. & MEIER, W. 2013. Polymer nanoreactors shown to produce and release antibiotics locally. *Chemical Communications,* 49**,** 128-130.

LE MEINS, J. F., SANDRE, O. & LECOMMANDOUX, S. 2011. Recent trends in the tuning of polymersomes' membrane properties. *European Physical Journal E,* 34.

LECOMMANDOUX, S. B., SANDRE, O., CHECOT, F., RODRIGUEZ-HERNANDEZ, J. & PERZYNSKI, R. 2005. Magnetic nanocomposite micelles and vesicles. *Advanced Materials,* 17**,** 712-+.

LEE, J. C. M., BERMUDEZ, H., DISCHER, B. M., SHEEHAN, M. A., WON, Y. Y., BATES, F. S. & DISCHER, D. E. 2001. Preparation, stability, and in vitro performance of vesicles made with diblock copolymers. *Biotechnology and Bioengineering,* 73**,** 135-145.

LEE, J. C. M., SANTORE, M., BATES, F. S. & DISCHER, D. E. 2002. From membranes to melts, rouse to reptation: Diffusion in polymersome versus lipid bilayers. *Macromolecules,* 35**,** 323-326.

LEROY, J., HEBERT, E. & WAKSELMAN, C. 1979. Maximum optical rotation of 2-fluorooctane: Survey of fluorinating reagents. *Journal of Organic Chemistry,* 44**,** 3406-3408.

LEVINTHAL, C. 1968. Are there pathways for protein folding? *Journal De Chimie Physique Et De Physico-Chimie Biologique,* 65**,** 44-45.

LEVINTHAL, C. How to Fold Graciously. Mossbauer Spectroscopy in Biological Systems: Proceedings of a meeting held at Allerton House, Monticello, Illinois, 1969. 22-24.

LEWIS, E. S. & BOOZER, C. E. 1952. The kinetics and stereochemistry of the decomposition of secondary alkyl chlorosulfites. *Journal of the American Chemical Society,* 74**,** 308-311.

LI, F., KETELAAR, T., MARCELIS, A. T. M., LEERMAKERS, F. A. M., STUART, M. A. C. & SUDHOLTER, E. J. R. 2007. Stabilization of polymersome vesicles by an interpenetrating polymer network. *Macromolecules,* 40**,** 329-333.

LI, J. J., LIU, Y. D., WANG, F. W., MA, G. H. & SU, Z. G. 2004. Hydrophobic interaction chromatography correctly refolding proteins assisted by glycerol and urea gradients. *Journal of Chromatography A,* 1061**,** 193-199.

LI, W. Y., WEN, L. Y., LI, C. C., CHEN, R., YE, Z. C., ZHAO, J. & PAN, J. Y. 2016. Contribution of the outer membrane protein OmpW in *Escherichia coli* to complement resistance from binding to factor H. *Microbial Pathogenesis,* 98**,** 57-62.

LIESE, A., SEELBACH, K. & WANDREY, C. 2000. *Industrial biotransformations*, Wiley-VCH.

LIN, X. M., WU, L. N., LI, H., WANG, S. Y. & PENG, X. X. 2008. Downregulation of Tsx and OmpW and upregulation of OmpX are required for iron homeostasis in *Escherichia coli*. *Journal of Proteome Research,* 7**,** 1235-1243.

LIU, G. H., WANG, X. R., HU, J. M., ZHANG, G. Y. & LIU, S. Y. 2014. Self-immolative polymersomes for high-efficiency triggered release and programmed enzymatic reactions. *Journal of the American Chemical Society,* 136**,** 7492-7497.

LIU, Y. F. & BOLEN, D. W. 1995. The peptide backbone plays a dominant role in protein stabilization by naturally-occurring osmolytes. *Biochemistry,* 34**,** 12884-12891.

LOMAS, H., JOHNSTON, A. P. R., SUCH, G. K., ZHU, Z., LIANG, K., VAN KOEVERDEN, M. P., ALONGKORNCHOTIKUL, S. & CARUSO, F. 2011. Polymersome-loaded capsules for controlled release of DNA. *Small,* 7**,** 2109-2119.

LOMAS, H., MASSIGNANI, M., ABDULLAH, K. A*., et al.* 2008. Non-cytotoxic polymer vesicles for rapid and efficient intracellular delivery. *Faraday Discussions,* 139**,** 143-159.

LOPRESTI, C., LOMAS, H., MASSIGNANI, M., SMART, T. & BATTAGLIA, G. 2009. Polymersomes: Nature inspired nanometer sized compartments. *Journal of Materials Chemistry,* 19**,** 3576-3590.

LOUZAO, I. & VAN HEST, J. C. M. 2013. Permeability effects on the efficiency of antioxidant nanoreactors. *Biomacromolecules,* 14**,** 2364-2372.

LU, L., ZOU, Y., YANG, W. J., MENG, F. H., DENG, C., CHENG, R. & ZHONG, Z. Y. 2015. Anisamide-decorated pH-sensitive degradable chimaeric polymersomes mediate potent and targeted protein delivery to lung cancer cells. *Biomacromolecules,* 16**,** 1726-1735.

LU, W., DU, J., SCHWARZER, N. J., GERBIG-SMENTEK, E., EINSLE, O. & ANDRADE, S. L. 2012. The formate channel FocA exports the products of mixed-acid fermentation. *Proceedings of the National Academy of Sciences of the United States of America,* 109**,** 13254-9.

LU, W., DU, J. A., WACKER, T., GERBIG-SMENTEK, E., ANDRADE, S. L. A. & EINSLE, O. 2011. pH-dependent gating in a FocA formate channel. *Science,* 332**,** 352-354.

MACHADO, I., COQUET, L., JOUENNE, T. & PEREIRA, M. O. 2013. Proteomic approach to *Pseudomonas aeruginosa* adaptive resistance to benzalkonium chloride. *Journal of Proteomics,* 89**,** 273-279.

MARGUET, M., EDEMBE, L. & LECOMMANDOUX, S. 2012. Polymersomes in polymersomes: Multiple loading and permeability control. *Angewandte Chemie-International Edition,* 51**,** 1173-1176.

MATHAI, J. C., TRISTRAM-NAGLE, S., NAGLE, J. F. & ZEIDEL, M. L. 2008. Structural determinants of water permeability through the lipid membrane. *Journal of General Physiology,* 131**,** 69-76.

MATHEW, M. K. & BALARAM, P. 1983. Alamethicin and related membrane channel forming polypeptides. *Molecular and Cellular Biochemistry,* 50.

MAY, S., ANDREASSON-OCHSNER, M., FU, Z., LOW , Y. X., TAN, D., DE HOOG, H.-P. M., RITZ, S., NALLANI, M. & SINNER, E.-K. 2013. *In vitro* expressed GPCR inserted in polymersome membranes for ligand-binding studies. *Angewandte Chemie-International Edition,* 52**,** 749-753.

MCPHEE, J. B., TAMBER, S., BAINS, M., MAIER, E., GELLATLY, S., LO, A., BENZ, R. & HANCOCK, R. E. 2009. The major outer membrane protein OprG of *Pseudomonas aeruginosa* contributes to cytotoxicity and forms an anaerobically regulated, cation-selective channel. *Fems Microbiology Letters,* 296**,** 241-7.

MEEUWISSEN, S. A., RIOZ-MARTINEZ, A., DE GONZALO, G., FRAAIJE, M. W., GOTOR, V. & VAN HEST, J. C. M. 2011. Cofactor regeneration in polymersome nanoreactors: Enzymatically catalysed Baeyer-Villiger reactions. *Journal of Materials Chemistry,* 21**,** 18923-18926.

MENG, X., SHANG, H., ZHENG, Y. & ZHANG, Z. 2013. Free fatty acid secretion by an engineered strain of *Escherichia coli*. *Biotechnology Letters,* 35**,** 2099-2103.

MESSAGER, L., GAITZSCH, J., CHIERICO, L. & BATTAGLIA, G. 2014. Novel aspects of encapsulation and delivery using polymersomes. *Current Opinion in Pharmacology,* 18**,** 104-111.

MEYER, H. P. 2011. Sustainability and biotechnology. *Organic Process Research & Development,* 15**,** 180-188.

MICHAELIS, L., MENTEN, M. L. 1913. Die Kinetik der Invertinwirkung. *Biochemische Zeitung***,** 333-369.

MIDDELBERG, A. P. J. 2002. Preparative protein refolding. *Trends in Biotechnology,* 20**,** 437-443.

MILES, A. J. & WALLACE, B. A. 2016. Circular dichroism spectroscopy of membrane proteins. *Chemical Society Reviews,* 45**,** 4859-4872.

MIROUX, B. & WALKER, J. E. 1996. Over-production of proteins in *Escherichia coli:* Mutant hosts that allow synthesis of some membrane proteins and globular proteins at high levels. *Journal of Molecular Biology,* 260**,** 289-298.

MORAES, T. F., BAINS, M., HANCOCK, R. E. & STRYNADKA, N. C. 2007. An arginine ladder in OprP mediates phosphate-specific transfer across the outer membrane. *Nat Struct Mol Biol,* 14**,** 85-7.

MORALES, E. H., CALDERON, I. L., COLLAO, B., GIL, F., PORWOLLIK, S., MCCLELLAND, M. & SAAVEDRA, C. P. 2012. Hypochlorous acid and hydrogen peroxide-induced negative regulation of *Salmonella enterica* serovar Typhimurium ompW by the response regulator ArcA. *BMC Microbiology,* 12.

MORTON, D., MORTEZAEI, S., YEMENICIOGLU, S., ISAACMAN, M. J., NOVA, I. C., GUNDLACH, J. H. & THEOGARAJAN, L. 2015. Tailored polymeric membranes for *Mycobacterium smegmatis* porin A (MspA) based biosensors. *Journal of Materials Chemistry B,* 3**,** 5080-5086.

NAKAMURA, K. & MIZUSHIMA, S. 1976. Effects of heating in dodecyl-sulfate solution on conformation and electrophoretic mobility of isolated major outer membrane proteins from *Escherichia coli* K-12. *Journal of Biochemistry,* 80**,** 1411-1422.

NAKAMURA, K., YAMANAKA, R., MATSUDA, T. & HARADA, T. 2003. Recent developments in asymmetric reduction of ketones with biocatalysts. *Tetrahedron-Asymmetry,* 14**,** 2659-2681.

NALLANI, M., ANDREASSON-OCHSNER, M., TAN, C. W. D., SINNER, E. K., WISANTOSO, Y., GEIFMAN-SHOCHAT, S. & HUNZIKER, W. 2011. Proteopolymersomes: In vitro production of a membrane protein in polymersome membranes. *Biointerphases,* 6**,** 153-157.

NALLANI, M., BENITO, S., ONACA, O., GRAFF, A., LINDEMANN, M., WINTERHALTER, M., MEIER, W. & SCHWANEBERG, U. 2006. A nanocompartment system (synthosome) designed for biotechnological applications. *Journal of Biotechnology,* 123**,** 50-59.

NANDI, B., NANDY, R. K., SARKAR, A. & GHOSE, A. C. 2005. Structural features, properties and regulation of the outer-membrane protein W (OmpW) of *Vibrio cholerae*. *Microbiology,* 151**,** 2975-2986.

NAPOLI, A., BOERAKKER, M. J., TIRELLI, N., NOLTE, R. J. M., SOMMERDIJK, N. A. J. M. & HUBBELL, J. A. 2004a. Glucose-oxidase based self-destructing polymeric vesicles. *Langmuir,* 20**,** 3487-3491.

NAPOLI, A., VALENTINI, M., TIRELLI, N., MÜLLER, M. & HUBBELL, J. A. 2004b. Oxidation-responsive polymeric vesicles. *Nature Materials,* 3**,** 183-189.

NARDIN, C., HIRT, T., LEUKEL, J. & MEIER, W. 2000a. Polymerized ABA triblock copolymer vesicles. *Langmuir,* 16**,** 1035-1041.

NARDIN, C., THOENI, S., WIDMER, J., WINTERHALTER, M. & MEIER, W. 2000b. Nanoreactors based on (polymerized) ABA-triblock copolymer vesicles. *Chemical Communications***,** 1433-1434.

NARDIN, C., WIDMER, J., WINTERHALTER, M. & MEIER, W. 2001. Amphiphilic block copolymer nanocontainers as bioreactors. *European Physical Journal E,* 4**,** 403-410.

NEHER, T. M. & LUEKING, D. R. 2009. *Pseudomonas fluorescens* ompW: plasmid localization and requirement for naphthalene uptake. *Canadian Journal of Microbiology,* 55**,** 553-563.

NESTL, B. M., HAMMER, S. C., NEBEL, B. A. & HAUER, B. 2014. Biokatalysatoren für die organische Synthese - die neue Generation. *Angewandte Chemie,* 126**,** 3132-3158.

NGUYEN-MISRA, M., MISRA, S. & MATTICE, W. L. 1996. Bridging by end-adsorbed triblock copolymers. *Macromolecules,* 29**,** 1407-1415.

NI, Y. & CHEN, R. R. 2004. Accelerating whole-cell biocatalysis by reducing outer membrane permeability barrier. *Biotechnology and Bioengineering,* 87**,** 804-811.

NI, Y. & CHEN, R. R. 2005. Lipoprotein mutation accelerates substrate permeability-limited toluene dioxygenase-catalyzed reaction. *Biotechnology Progress,* 21**,** 799-805.

NIKAIDO, H. 1992. Porins and specific channels of bacterial outer membranes. *Molecular Microbiology,* 6**,** 435-442.

NIKAIDO, H. 1994a. Porins and specific diffusion channels in bacterial outer membranes. *Journal of Biological Chemistry,* 269**,** 3905-3908.

NIKAIDO, H. 1994b. Prevention of drug access to bacterial targets: Permeability barriers and active efflux. *Science,* 264**,** 382-388.

NIKAIDO, H. & ROSENBERG, E. Y. 1983. Porin channels in *Escherichia coli: S*tudies with liposomes reconstituted from purified proteins. *Journal of Bacteriology,* 153**,** 241-252.

NOINAJ, N., KUSZAK, A. J. & BUCHANAN, S. K. 2015. Heat Modifiability of Outer Membrane Proteins from Gram-Negative Bacteria. *Methods in Molecular Biology,* 1329**,** 51-56.

NOOR, M., DWORECK, T., SCHENK, A., SHINDE, P., FIORONI, M. & SCHWANEBERG, U. 2012. Polymersome surface decoration by an eGFP fusion protein employing Cecropin A as peptide "anchor". *Journal of Biotechnology,* 157**,** 31-37.

NOYORI, R. & OHKUMA, T. 2001. Asymmetric catalysis by architectural and functional molecular engineering: Practical chemo- and stereoselective hydrogenation of ketones. *Angewandte Chemie-International Edition,* 40**,** 40-73.

NOYORI, R., YAMAKAWA, M. & HASHIGUCHI, S. 2001. Metal-ligand bifunctional catalysis: A nonclassical mechanism for asymmetric hydrogen transfer between alcohols and carbonyl compounds. *Journal of Organic Chemistry,* 66**,** 7931-7944.

OHNISHI, S., KAMEYAMA, K. & TAKAGI, T. 1998. Characterization of a heat modifiable protein, Escherichia coli outer membrane protein OmpA in binary surfactant system of sodium dodecyl sulfate and octylglucoside. *Biochimica Et Biophysica Acta-Biomembranes,* 1375**,** 101-109.

ONACA, O., HUGHES, D. W., BALASUBRAMANIAN, V., GRZELAKOWSKI, M., MEIER, W. & PALIVAN, C. G. 2010. SOD antioxidant nanoreactors: Influence of block copolymer composition on the nanoreactor efficiency. *Macromolecular Bioscience,* 10**,** 531-538.

ONACA, O., NALLANI, M., IHLE, S., SCHENK, A. & SCHWANEBERG, U. 2006. Functionalized nanocompartments (Synthosomes): limitations and prospective applications in industrial biotechnology. *Biotechnology Journal,* 1**,** 795-805.

ONACA, O., SARKAR, P., ROCCATANO, D., FRIEDRICH, T., HAUER, B., GRZELAKOWSKI, M., GUVEN, A., FIORONI, M. & SCHWANEBERG, U. 2008. Functionalized nanocompartments (synthosomes) with a reduction-triggered release system. *Angewandte Chemie-International Edition,* 47**,** 7029-7031.

OTZEN, D. E. & ANDERSEN, K. K. 2013. Folding of outer membrane proteins. *Archives of Biochemistry and Biophysics,* 531**,** 34-43.

PALIVAN, C. G., FISCHER-ONACA, O., DELCEA, M., ITEL, F. & MEIER, W. 2012. Protein-polymer nanoreactors for medical applications. *Chemical Society Reviews,* 41**,** 2800-2823.

PALIVAN, C. G., GOERS, R., NAJER, A., ZHANG, X. Y., CAR, A. & MEIER, W. 2016. Bioinspired polymer vesicles and membranes for biological and medical applications. *Chemical Society Reviews,* 45**,** 377-411.

PANGBURN, T. O., BATES, F. S. & KOKKOLI, E. 2012. Polymersomes functionalized via "click" chemistry with the fibronectin mimetic peptides PR_b and GRGDSP for targeted delivery to cells with different levels of alpha(5)beta(1) expression. *Soft Matter,* 8**,** 4449-4461.

PANKE, S., HELD, M. & WUBBOLTS, M. 2004. Trends and innovations in industrial biocatalysis for the production of fine chemicals. *Current Opinion in Biotechnology,* 15**,** 272-279.

PARK, K., PERCZEL, A. & FASMAN, G. D. 1992. Differentiation between transmembrane helices and peripheral helices by the deconvolution of circular dichroism spectra of membrane proteins. *Protein Science,* 1**,** 1032-1049.

PATA, V., AHMED, F., DISCHER, D. E. & DAN, N. 2004. Membrane solubilization by detergent: Resistance conferred by thickness. *Langmuir,* 20**,** 3888-3893.

PATA, V. & DAN, N. 2003. The effect of chain length on protein solubilization in polymer-based vesicles (polymersomes). *Biophysical Journal,* 85**,** 2111-2118.

PAULSEN, I. T., SLIWINSKI, M. K., NELISSEN, B., GOFFEAU, A. & SAIER, M. H. 1998a. Unified inventory of established and putative transporters encoded within the complete genome of *Saccharomyces cerevisiae*. *Febs Letters,* 430**,** 116-125.

PAULSEN, I. T., SLIWINSKI, M. K. & SAIER, M. H. 1998b. Microbial genome analyses: Global comparisons of transport capabilities based on phylogenies, bioenergetics and substrate specificities. *Journal of Molecular Biology,* 277**,** 573-592.

PAWAR, P. V., GOHIL, S. V., JAIN, J. P. & KUMAR, N. 2013. Functionalized polymersomes for biomedical applications. *Polymer Chemistry,* 4**,** 3160-3176.

PENG, X. X., XU, C. X., REN, H. X., LIN, X. M., WU, L. & WANG, S. Y. 2005. Proteomic analysis of the sarcosine-insoluble outer membrane fraction of *Pseudomonas aeruginosa* responding to ampicilin, kanamycin, and tetracycline resistance. *Journal of Proteome Research,* 4**,** 2257-2265.

PHALE, P. S., PHILIPPSEN, A., KIEFHABER, T., KOEBNIK, R., PHALE, V. P., SCHIRMER, T. & ROSENBUSCH, J. P. 1998. Stability of trimeric OmpF porin: The contributions of the latching loop L2. *Biochemistry,* 37**,** 15663-15670.

PHALE, P. S., SCHIRMER, T., PRILIPOV, A., LOU, K. L., HARDMEYER, A. & ROSENBUSCH, J. P. 1997. Voltage gating of *Escherichia coli* porin channels: Role of the constriction loop. *Proceedings of the National Academy of Sciences of the United States of America,* 94**,** 6741-6745.

PILIPENKO, O. S., ATYAKSHEVA, L. F., POLTORAK, O. M. & CHUKHRAI, E. S. 2007. Dissociation and catalytic activity of oligomer forms of beta-galactosidases. *Russian Journal of Physical Chemistry A,* 81**,** 990-994.

PILSL, H., SMAJS, D. & BRAUN, V. 1999. Characterization of colicin S4 and its receptor, OmpW, a minor protein of the *Escherichia coli* outer membrane. *Journal of Bacteriology,* 181**,** 3578-3581.

POPOT, J.-L. 2014. Folding membrane proteins in vitro: A table and some comments. *Archives of Biochemistry and Biophysics,* 564**,** 314-326.

POPOT, J.-L. & ENGELMAN, D. M. 2016. Membranes do not tell proteins how to fold. *Biochemistry,* 55**,** 5-18.

POPOV, V. O. & LAMZIN, V. S. 1994. NAD^+-dependent formate dehydrogenase. *Biochemical Journal,* 301**,** 625-643.

POSCHENRIEDER, S. T. 2017. *Prozess zur skalierbaren Herstellung von Nanokompartimenten aus ABA-Triblock-Copolymeren.* Dissertation, Technical University of Munich.

POSCHENRIEDER, S. T., SCHIEBEL, S. K. & CASTIGLIONE, K. 2017. Polymersomes for biotechnological applications: Large-scale production of nano-scale vesicles. *Engineering in Life Sciences,* 17**,** 58-70.

POSCHENRIEDER, S. T., WAGNER, S. G. & CASTIGLIONE, K. 2016. Efficient production of uniform nanometer-sized polymer vesicles in stirred-tank reactors. *Journal of Applied Polymer Science,* 133**,** 43274.

PRATS, R. & DEPEDRO, M. A. 1989. Normal growth and division of *Escherichia coli* with a reduced amount of murein. *Journal of Bacteriology,* 171**,** 3740-3745.

PRILIPOV, A., PHALE, P. S., VAN GELDER, P., ROSENBUSCH, J. P. & KOEBNIK, R. 1998. Coupling site-directed mutagenesis with high-level expression: Large scale production of mutant porins from *E. coli*. *Fems Microbiology Letters,* 163**,** 65-72.

PRINOS, J. & PANAYIOTOU, C. 1995. Glass-transition temperature in hydrogen-bonded polymer mixtures. *Polymer,* 36**,** 1223-1227.

QIN, S., GENG, Y., DISCHER, D. E. & YANG, S. 2006. Temperature-controlled assembly and release from polymer vesicles of poly(ethylene oxide)-block-poly(*N*-isopropylacrylamide). *Advanced Materials,* 18**,** 2905-2909.

QIN, Y., MI, Y. M. & BAKKER, E. 2000. Determination of complex formation constants of 18 neutral alkali and alkaline earth metal ionophores in poly(vinyl chloride) sensing membranes

plasticized with bis(2-ethylhexyl)sebacate and o-nitrophenyloctylether. *Analytica Chimica Acta,* 421**,** 207-220.

RANK, A., HAUSCHILD, S., FORSTER, S. & SCHUBERT, R. 2009. Preparation of monodisperse block copolymer vesicles via a thermotropic cylinder-vesicle transition. *Langmuir,* 25**,** 1337-1344.

RANQUIN, A., VERSEES, W., MEIER, W., STEYAERT, J. & VAN GELDER, P. 2005. Therapeutic nanoreactors: Combining chemistry and biology in a novel triblock copolymer drug delivery system. *Nano Letters,* 5**,** 2220-2224.

RASSAM, P., COPELAND, N. A., BIRKHOLZ, O.*, et al.* 2015. Supramolecular assemblies underpin turnover of outer membrane proteins in bacteria. *Nature,* 523**,** 333-336.

REN, Q., SIERRO, N., WITHOLT, B. & KESSLER, B. 2000. FabG, an NADPH-dependent 3-ketoacyl reductase of *Pseudomonas aeruginosa*, provides precursors for medium-chain-length poly-3-hydroxyalkanoate biosynthesis in *Escherichia coli*. *Journal of Bacteriology,* 182**,** 2978-2981.

RENGGLI, K., BAUMANN, P., LANGOWSKA, K., ONACA, O., BRUNS, N. & MEIER, W. 2011. Selective and Responsive Nanoreactors. *Advanced Functional Materials,* 21**,** 1241-1259.

RIEDLBERGER, P., BRÜNING, S. & WEUSTER-BOTZ, D. 2012. Characterization of stirrers for screening studies of enzymatic biomass hydrolyses on a milliliter scale. *Bioprocess and Biosystems Engineering,* 36**,** 927-935.

RIGLER, P. & MEIER, W. 2006. Encapsulation of fluorescent molecules by functionalized polymeric nanocontainers: Investigation by confocal fluorescence imaging and fluorescence correlation Spectroscopy. *Journal of the American Chemical Society,* 128**,** 367-373.

RITTER, A., COM, E., BAZIRE, A.*, et al.* 2012. Proteomic studies highlight outer-membrane proteins related to biofilm development in the marine bacterium *Pseudoalteromonas sp* D41. *Proteomics,* 12**,** 3180-3192.

ROSENBUSCH, J. P. 1974. Characterization of the major envelope protein from *Escherichia coli.* Regular arrangement on the peptidoglycan and unusual dodecyl sulfate binding. *J Biol Chem,* 249**,** 8019-29.

ROSENBUSCH, J. P. 1988. Ion-transport across biological-membranes: Diffusion in water solution or conduction in the solid-state. *Biophysical Chemistry,* 29**,** 79-84.

ROZZELL, J. D. 1999. Commercial scale biocatalysis: Myths and realities. *Bioorganic & Medicinal Chemistry,* 7**,** 2253-2261.

RUDOLPH, R. & LILIE, H. 1996. In vitro folding of inclusion body proteins. *Faseb Journal,* 10**,** 49-56.

RUFF, A. J., ARLT, M., VAN OHLEN, M., KARDASHLIEV, T., KONARZYCKA-BESSLER, M., BOCOLA, M., DENNIG, A., URLACHER, V. B. & SCHWANEBERG, U. 2016. An engineered outer membrane pore enables an efficient oxygenation of aromatics and terpenes. *Journal of Molecular Catalysis B: Enzymatic,* 134**,** 285-294.

RUYSSCHAERT, T., SONNEN, A. F. P., HAEFELE, T., MEIER, W., WINTERHALTERT, M. & FOURNIER, D. 2005. Hybrid nanocapsules: Interactions of ABA block copolymers with liposomes. *Journal of the American Chemical Society,* 127**,** 6242-6247.

SAIER, M. H. 2000. Families of proteins forming transmembrane channels. *Journal of Membrane Biology,* 175**,** 165-180.

SAINT, N., LOU, K. L., WIDMER, C., LUCKEY, M., SCHIRMER, T. & ROSENBUSCH, J. P. 1996. Structural and functional characterization of OmpF porin mutants selected for larger pore size: 2. Functional characterization. *Journal of Biological Chemistry,* 271**,** 20676-20680.

SAKAMOTO, R., NISHIKORI, S. & SHIRAKI, K. 2004. High temperature increases the refolding yield of reduced lysozyme: Implication for the productive process for folding. *Biotechnology Progress,* 20**,** 1128-1133.

SANTACOLOMA, P. A., SIN, G., GERNAEY, K. V. & WOODLEY, J. M. 2011. Multienzyme-catalyzed processes: Next-generation biocatalysis. *Organic Process Research & Development,* 15**,** 203-212.

SAUER, M., HAEFELE, T., GRAFF, A., NARDIN, C. & MEIER, W. 2001. Ion-carrier controlled precipitation of calcium phosphate in giant ABA triblock copolymer vesicles. *Chemical Communications***,** 2452-2453.

SCHAGGER, H., CRAMER, W. A. & VON JAGOW, G. 1994. Analysis of molecular masses and oligomeric states of protein complexes by blue native electrophoresis and isolation of membrane protein complexes by two-dimensional native electrophoresis. *Anal Biochem,* 217**,** 220-30.

SCHECHTER, B., SCHECHTER, I., RAMACHANDRAN, J., CONWAY-JACOBS, A. & SELA, M. 1971. the synthesis and circular dichroism of a series of peptides possessing the structure (l-tyrosyl-l-alanyl-l-glutamyl)n. *European Journal of Biochemistry,* 20**,** 301-308.

SCHEPS, D., HONDA MALCA, S., RICHTER, S. M., MARISCH, K., NESTL, B. M. & HAUER, B. 2013. Synthesis of ω-hydroxy dodecanoic acid based on an engineered CYP153A fusion construct. *Microbial Biotechnology***,** 694-707.

SCHMID, A., DORDICK, J. S., HAUER, B., KIENER, A., WUBBOLTS, M. & WITHOLT, B. 2001. Industrial biocatalysis today and tomorrow. *Nature,* 409**,** 258-268.

SCHMITT, C., LIPPERT, A. H., BONAKDAR, N., SANDOGHDAR, V. & VOLL, L. M. 2016. Compartmentalization and transport in synthetic vesicles. *Frontiers in Bioengineering and Biotechnology,* 4.

SCHNEIDER, S., WUBBOLTS, M. G., SANGLARD, D. & WITHOLT, B. 1998. Biocatalyst engineering by assembly of fatty acid transport and oxidation activities for in vivo application of cytochrome P-450(BM-3) monooxygenase. *Applied and Environmental Microbiology,* 64**,** 3784-3790.

SCHRAGE, S. 2002. *Selbstorganisation von Ionomeren zu phasenseparierten Vesikeln.* Dissertation, University of Potsdam.

SCHREWE, M., JULSING, M. K., LANGE, K., CZARNOTTA, E., SCHMID, A. & BÜHLER, B. 2014. Reaction and catalyst engineering to exploit kinetically controlled whole-cell multistep biocatalysis for terminal FAME oxyfunctionalization. *Biotechnology and Bioengineering,* 111**,** 1820-1830.

SCHUBERT, T., HUMMEL, W., KULA, M. R. & MULLER, M. 2001. Enantioselective synthesis of both enantiomers of various propargylic alcohols by use of two oxidoreductases. *European Journal of Organic Chemistry***,** 4181-4187.

SCHUBERT, T., HUMMEL, W. & MULLER, M. 2002. Highly enantioselective preparation of multifunctionalized propargylic building blocks. *Angewandte Chemie-International Edition,* 41**,** 634–637.

SCHULTZ, C. P. 2000. Illuminating folding intermediates. *Nature Structural Biology,* 7**,** 7-10.

SCHULZ, G. E. 1993. Bacterial porins: structure and function. *Current Opinion in Cell Biology,* 5**,** 701-707.

SCHWARZER, T. S., HERMANN, M., KRISHNAN, S., SIMMEL, F. C. & CASTIGLIONE, K. 2017. Preparative refolding of small monomeric outer membrane proteins. *Protein Expression and Purification,* 132**,** 171-181.

SCHWEIZER, M., HINDENNACH, I., GARTEN, W. & HENNING, U. 1978. Major Proteins of the *Escherichia coli* Outer Cell Envelope Membrane. Interaction of Protein II* with Lipopolysaccharide. *European Journal of Biochemistry,* 82**,** 211-217.

SEDDON, A. M., CURNOW, P. & BOOTH, P. J. 2004. Membrane proteins, lipids and detergents: not just a soap opera. *Biochimica et Biophysica Acta-Biomembranes,* 1666**,** 105-117.

SEELBACH, K., RIEBEL, B., HUMMEL, W., KULA, M. R., VI, T., EGOROV, A. M., WANDREY, C. & KRAGL, U. 1996. A novel, efficient regenerating method of NADPH using a new formate dehydrogenase. *Tetrahedron Letters,* 37**,** 1377-1380.

SEGEL, I. H. 1996. *Enzyme Kinetics: Behavior and Analysis of Rapid Equilibrium and Steady-State Enzyme Systems*, Wiley.

SHI, Y., JIANG, C. S., CHEN, Q. & TANG, H. 2003. One-step on-column affinity refolding purification and functional analysis of recombinant human VDACI. *Biochemical and Biophysical Research Communications,* 303**,** 475-482.

SIEHNEL, R. J., WOROBEC, E. A. & HANCOCK, R. E. 1988. Cloning of the *Pseudomonas aeruginosa* outer membrane porin protein P gene: evidence for a linked region of DNA homology. *Journal of Bacteriology,* 170**,** 2312-8.

SITI, W., DE HOOG, H. P. M., FISCHER, O., SHAN, W. Y., TOMCZAK, N., NALLANI, M. & LIEDBERG, B. 2014. An intercompartmental enzymatic cascade reaction in channel-equipped polymersome-in-polymersome architectures. *Journal of Materials Chemistry B,* 2**,** 2733-2737.

SOLOV'EVA, T. F., NOVIKOVA, O. D. & PORTNYAGINA, O. Y. 2012. Biogenesis of beta-barrel integral proteins of bacterial outer membrane. *Biochemistry-Moscow,* 77**,** 1221-1236.

SOO, P. L. & EISENBERG, A. 2004. Preparation of block copolymer vesicles in solution. *Journal of Polymer Science Part B-Polymer Physics,* 42**,** 923-938.

SPULBER, M., BAUMANN, P., SAXER, S. S., PIELES, U., MEIER, W. & BRUNS, N. 2014. Poly(*N*-vinylpyrrolidone)-poly(dimethylsiloxane)-based polymersome nanoreactors for laccase-catalyzed biotransformations. *Biomacromolecules,* 15**,** 1469-1475.

SPULBER, M., NAJER, A., WINKELBACH, K., GLAIED, O., WASER, M., PIELES, U., MEIER, W. & BRUNS, N. 2013. Photoreaction of a hydroxyalkyphenone with the membrane of polymersomes: a versatile method to generate semipermeable nanoreactors. *J Am Chem Soc,* 135**,** 9204-12.

SRINIVAS, G., DISCHER, D. E. & KLEIN, M. L. 2004. Self-assembly and properties of diblock copolymers by coarse-grain molecular dynamics. *Nature Materials,* 3**,** 638-644.

SRINIVAS, G., DISCHER, D. E. & KLEIN, M. L. 2005. Key roles for chain flexibility in block copolymer membranes that contain pores or make tubes. *Nano Letters,* 5**,** 2343-2349.

STOENESCU, R., GRAFF, A. & MEIER, W. 2004. Asymmetric ABC-triblock copolymer membranes induce a directed insertion of membrane proteins. *Macromolecular Bioscience,* 4**,** 930-935.

STRUYVE, M., MOONS, M. & TOMMASSEN, J. 1991. Carboxy-terminal phenylalanine is essential for the correct assembly of a bacterial outer membrane protein. *Journal of Molecular Biology,* 218**,** 141-148.

SÜHRER, I. 2015. *One-step expression and enzyme immobilisation in cellular envelopes of Escherichia coli.* Dissertation, Technical University of Munich.

SÜHRER, I., HASLBECK, M. & CASTIGLIONE, K. 2014. Asymmetric synthesis of a fluoxetine precursor with an artificial fusion protein of a ketoreductase and a formate dehydrogenase. *Process Biochemistry,* 49**,** 1527-1532.

SUKHAN, A. & HANCOCK, R. E. W. 1996. The role of specific lysine residues in the passage of anions through the *Pseudomonas aeruginosa* porin OprP. *Journal of Biological Chemistry,* 271**,** 21239-21242.

SUPPMANN, B. & SAWERS, G. 1994. Isolation and characterization of hypophosphite-resistant mutants of *Escherichia coli*: Identification of the FocA protein, encoded by the pfl operon, as a putative formate transporter. *Molecular Microbiology,* 11**,** 965-982.

SURREY, T., SCHMID, A. & JAHNIG, F. 1996. Folding and membrane insertion of the trimeric beta-barrel protein OmpF. *Biochemistry,* 35**,** 2283-2288.

TAMM, L. K., HONG, H. & LIANG, B. Y. 2004. Folding and assembly of beta-barrel membrane proteins. *Biochimica Et Biophysica Acta-Biomembranes,* 1666**,** 250-263.

TAN, S., TAN, H. T. & CHUNG, M. C. M. 2008. Membrane proteins and membrane proteomics. *Proteomics,* 8**,** 3924-3932.

TANGORRA, R. R., OPERAMOLLA, A., MILANO, F.*, et al.* 2015. Assembly of a photosynthetic reaction center with ABA tri-block polymersomes: highlights on protein localization. *Photochemical and Photobiological Sciences,* 14**,** 1844-1852.

TANNER, P., BALASUBRAMANIAN, V. & PALIVAN, C. G. 2013. Aiding nature's organelles: Artificial peroxisomes play their role. *Nano Letters,* 13**,** 2875-2883.

TANNER, P., EGLI, S., BALASUBRAMANIAN, V., ONACA, O., PALIVAN, C. G. & MEIER, W. 2011a. Can polymeric vesicles that confine enzymatic reactions act as simplified organelles? *Febs Letters,* 585**,** 1699-1706.

TANNER, P., ONACA, O., BALASUBRAMANIAN, V., MEIER, W. & PALIVAN, C. G. 2011b. Enzymatic cascade reactions inside polymeric nanocontainers: A means to combat oxidative stress. *Chemistry-a European Journal,* 17**,** 4552-4560.

TIMASHEFF, S. N. 2002. Protein-solvent preferential interactions, protein hydration, and the modulation of biochemical reactions by solvent components. *Proceedings of the National Academy of Sciences of the United States of America,* 99**,** 9721-9726.

TISHKOV, V. I., GALKIN, A. G. & EGOROV, A. M. 1989. Kinetic isotope effect and the presteady-state kinetics of the reaction catalyzed by the bacterial formate dehydrogenase. *Biochimie,* 71**,** 551-557.

TISHKOV, V. I., GALKIN, A. G., MARCHENKO, G. N., EGOROVA, O. A., SHELUHO, D. V., KULAKOVA, L. B., DEMENTIEVA, L. A. & EGOROV, A. M. 1993. Catalytic properties and stability of a *Pseudomonas sp* 101 formate dehydrogenase mutants containing Cys-255-Ser and Cys-255-Met replacements. *Biochemical and Biophysical Research Communications,* 192**,** 976-981.

TISHKOV, V. I. & POPOV, V. O. 2004. Catalytic mechanism and application of formate dehydrogenase. *Biochemistry-Moscow,* 69**,** 1252-1268.

TISHKOV, V. I. & POPOV, V. O. 2006. Protein engineering of formate dehydrogenase. *Biomolecular Engineering,* 23**,** 89-110.

TOMMASSEN, J., OVERDUIN, P., LUGTENBERG, B. & BERGMANS, H. 1982. Cloning of phoE, the structural gene for the *Escherichia coli* phosphate limitation-inducible outer-membrane pore protein. *Journal of Bacteriology,* 149**,** 668-672.

TOUW, D. S., PATEL, D. R. & VAN DEN BERG, B. 2010. The crystal structure of OprG from *Pseudomonas aeruginosa*, a potential channel for transport of hydrophobic molecules across the outer membrane. *PLoS One,* 5**,** e15016.

TRAUT, T. W. 1994. Dissociation of enzyme oligomers: A mechanism for allosteric regulation. *Critical Reviews in Biochemistry and Molecular Biology,* 29**,** 125-163.

TSUMOTO, K., EJIMA, D., KUMAGAI, I. & ARAKAWA, T. 2003. Practical considerations in refolding proteins from inclusion bodies. *Protein Expression and Purification,* 28**,** 1-8.

TUCKER, A. D., JACKMAN, S., PARKER, M. W. & TSERNOGLOU, D. 1991. Crystallization and preliminary-x-ray analysis of phosphoporin from the outer membrane of *Escherichia coli*. *Journal of Molecular Biology,* 222**,** 881-884.

VALAX, P. & GEORGIOU, G. 1993. Molecular characterization of beta-lactamase inclusion bodies produced in *Escherichia coli*: 1. Composition. *Biotechnology Progress,* 9**,** 539-547.

VALLEJO, L. F. & RINAS, U. 2004. Strategies for the recovery of active proteins through refolding of bacterial inclusion body proteins. *Microbial Cell Factories,* 3.

VAN BEILEN, J. B., EGGINK, G., ENEQUIST, H., BOS, R. & WITHOLT, B. 1992. DNA sequence determination and functional characterization of the OCT-plasmid-encoded alkJKL genes of *Pseudomonas oleovorans*. *Molecular Microbiology,* 6**,** 3121-36.

VAN DEN BERG, B. 2005. The FadL family: Unusual transporters for unusual substrates. *Current Opinion in Structural Biology,* 15**,** 401-407.

VAN DER DONK, W. A. & ZHAO, H. M. 2003. Recent developments in pyridine nucleotide regeneration. *Current Opinion in Biotechnology,* 14**,** 421-426.

VAN DONGEN, S. F. M., NALLANI, M., CORNELISSEN, J. L. L. M., NOLTE, R. J. M. & VAN HEST, J. C. M. 2009. A three-enzyme cascade reaction through positional assembly of enzymes in a polymersome nanoreactor. *Chemistry-a European Journal,* 15**,** 1107-1114.

VAN GELDER, P., SAINT, N., PHALE, P., EPPENS, E. F., PRILIPOV, A., VANBOXTEL, R., ROSENBUSCH, J. P. & TOMMASSEN, J. 1997. Voltage sensing in the PhoE and OmpF outer membrane porins of *Escherichia coli*: Role of charged residues. *Journal of Molecular Biology,* 269**,** 468-472.

VAN GELDER, P., STEIERT, M., EL KHATTABI, M., ROSENBUSCH, J. P. & TOMMASSEN, J. 1996. Structural and functional characterization of a His-tagged PhoE pore protein of *Escherichia coli*. *Biochemical and Biophysical Research Communications,* 229**,** 869-75.

VIJAYAN, K., DISCHER, D. E., LAL, J., JANMEY, P. & GOULIAN, M. 2005. Interactions of membrane-active peptides with thick, neutral, nonzwitterionic bilayers. *Journal of Physical Chemistry B,* 109**,** 14356-14364.

VINCENTELLI, R., CANAAN, S., CAMPANACCI, V., *et al.* 2004. High-throughput automated refolding screening of inclusion bodies. *Protein Science,* 13**,** 2782-2792.

VRIEZEMA, D. M., ARAGONES, M. C., ELEMANS, J. A. A. W., CORNELISSEN, J. J. L. M., ROWAN, A. E. & NOLTE, R. J. M. 2005. Self-assembled nanoreactors. *Chemical Reviews,* 105**,** 1445-1489.

VRIEZEMA, D. M., GARCIA, P. M. L., OLTRA, N. S., HATZAKIS, N. S., KUIPER, S. M., NOLTE, R. J. M., ROWAN, A. E. & VAN HEST, J. C. M. 2007. Positional assembly of enzymes in polymersome nanoreactors for cascade reactions. *Angewandte Chemie-International Edition,* 46**,** 7378-7382.

VUILLARD, L., BRAUN-BRETON, C. & RABILLOUD, T. 1995. Non-detergent sulphobetaines: a new class of mild solubilization agents for protein purification. *The Biochemical Journal,* 305 (Pt 1)**,** 337-43.

WAIGHT, A. B., LOVE, J. & WANG, D.-N. 2009. Structure and mechanism of a pentameric formate channel. *Nature Structural & Molecular Biology,* 17**,** 31-37.

WALLACE, B. A. 1990. Gramicidin channels and pores. *Annual Review of Biophysics and Biophysical Chemistry,* 19**,** 127-157.

WALTER, A., HASTINGS, D. & GUTKNECHT, J. 1982. Weak acid permeability through lipid bilayer-membranes: Role of chemical-reactions in the unstirred layer. *Journal of General Physiology,* 79**,** 917-933.

WANG, F., GUO, J., BAI, Q. & WANG, L. 2014. Refolding and purification of recombinant human (Pro)renin receptor from *Escherichia coli* by ion exchange chromatography. *Biotechnol Prog,* 30**,** 864-71.

WANG, H., ANDERSEN, K. K., VAD, B. S. & OTZEN, D. E. 2013. OmpA can form folded and unfolded oligomers. *Biochimica Et Biophysica Acta-Proteins and Proteomics,* 1834**,** 127-136.

WANG, L. G., CHIERICO, L., LITTLE, D., PATIKARNMONTHON, N., YANG, Z., AZZOUZ, M., MADSEN, J., ARMES, S. P. & BATTAGLIA, G. 2012. Encapsulation of biomacromolecules within polymersomes by electroporation. *Angewandte Chemie-International Edition,* 51**,** 11122-11125.

WANG, Y., HUANG, Y., WANG, J., *et al.* 2009. Structure of the formate transporter FocA reveals a pentameric aquaporin-like channel. *Nature,* 462**,** 467-72.

WANG, Y., RAWLINGS, M., GIBSON, D. T., LABBE, D., BERGERON, H., BROUSSEAU, R. & LAU, P. C. K. 1995. Identification of a membrane-protein and a truncated LysR-type regulator associated with the toluene degradation pathway in *Pseudomonas putida* F1. *Molecular and General Genetics,* 246**,** 570-579.

WANG, Y. M., MATTICE, W. L. & NAPPER, D. H. 1992. Simulation of the self-assembly of symmetrical triblock copolymers in dilute solution. *Macromolecules,* 25**,** 4073-4077.

WEUSTER-BOTZ, D., PUSKEILER, R., KUSTERER, A., KAUFMANN, K., JOHN, G. T. & ARNOLD, M. 2005. Methods and milliliter scale devices for high-throughput bioprocess design. *Bioprocess and Biosystems Engineering,* 28**,** 109-119.

WHITE, S. W., ZHENG, J., ZHANG, Y. M. & ROCK, C. O. 2005. The structural biology of type II fatty acid biosynthesis. *Annual Review of Biochemistry,* 74**,** 791-831.

WITTIG, I., BRAUN, H. P. & SCHAGGER, H. 2006. Blue native PAGE. *Nature Protocols,* 1**,** 418-428.

WONG, D., JEON, T.-J. & SCHMIDT, J. 2006. Single molecule measurements of channel proteins incorporated into biomimetic polymer membranes. *Nanotechnology,* 17**,** 3710-3717.

WOODLE, M. C., ENGBERS, C. M. & ZALIPSKY, S. 1994. New amphipatic polymer lipid conjugates forming long-circulating reticuloendothelial system-evading liposomes. *Bioconjugate Chemistry,* 5**,** 493-496.

WOODLEY, J. M. 2008. New opportunities for biocatalysis: Making pharmaceutical processes greener. *Trends in Biotechnology,* 26**,** 321-327.

WOROBEC, E. A., MARTIN, N. L., MCCUBBIN, W. D., KAY, C. M., BRAYER, G. D. & HANCOCK, R. E. 1988. Large-scale purification and biochemical characterization of crystallization-grade porin protein P from *Pseudomonas aeruginosa*. *Biochimica et Biophysica Acta,* 939**,** 366-74.

WRIGHT, H. T. 2004. Cofactors in fatty acid biosynthesis - Active site organizers and drug targets. *Structure,* 12**,** 358-359.

WU, J. T., WU, L. H. & KNIGHT, J. A. 1986. Stability of NADPH: Effect of various factors on the kinetics of degradation. *Clinical Chemistry,* 32**,** 314-319.

WU, X. B., TIAN, L. H., ZOU, H. J., WANG, C. Y., YU, Z. Q., TANG, C. H., ZHAO, F. K. & PAN, J. Y. 2013. Outer membrane protein OmpW of *Escherichia coli* is required for resistance to phagocytosis. *Research in Microbiology,* 164**,** 848-855.

XIE, Y. S. & WETLAUFER, D. B. 1996. Control of aggregation in protein refolding: The temperature-leap tactic. *Protein Science,* 5**,** 517-523.

XU, C., REN, H., WANG, S. & PENG, X. 2004. Proteomic analysis of salt-sensitive outer membrane proteins of *Vibrio parahaemolyticus*. *Research in Microbiology,* 155**,** 835-842.

XU, C., WANG, S., REN, H., LIN, X., WU, L. & PENG, X. 2005. Proteomic analysis on the expression of outer membrane proteins of *Vibrio alginolyticus* at different sodium concentrations. *Proteomics,* 5**,** 3142-3152.

YANG, L., HARROUN, T. A., WEISS, T. M., DING, L. & HUANG, H. W. 2001. Barrel-stave model or toroidal model? A case study on melittin pores. *Biophysical Journal,* 81**,** 1475-1485.

YASSIN, M. A., APPELHANS, D., MENDES, R. G., RUMMELI, M. H. & VOIT, B. 2012. pH-dependent release of doxorubicin from fast photo-cross-linkable polymersomes based on benzophenone units. *Chemistry-a European Journal,* 18**,** 12227-12231.

YATES, J. M., MORRIS, G. & BROWN, M. R. W. 1989. Effect of iron concentration and growth-rate on the expression of protein G in *Pseudomonas-Aeruginosa*. *Fems Microbiology Letters,* 58**,** 259-262.

YILDIZ, U. H., DE HOOG, H. P. M., FU, Z. K., TOMCZAK, N., PARIKH, A. N., NALLANI, M. & LIEDBERG, B. 2014. Third-party ATP Sensing in polymersomes: A label-free assay of enzyme reactions in vesicular compartments. *Small,* 10**,** 442-447.

YILGOR, I., STECKLE, W. P., YILGOR, E., FREELIN, R. G. & RIFFLE, J. S. 1989. Novel triblock siloxane copolymers: Synthesis, characterization, and their use as surface modifying additives. *Journal of Polymer Science Part A: Polymer Chemistry,* 27**,** 3673-3690.

YOUNG, R. & BLASI, U. 1995. Holins: Form and function in bacteriophagelysis. *Fems Microbiology Reviews,* 17**,** 191-205.

YU, S. Y., AZZAM, T., ROUILLER, I. & EISENBERG, A. 2009. "Breathing" vesicles. *Journal of the American Chemical Society,* 131**,** 10557-10566.

ZETTLMEISSL, G., RUDOLPH, R. & JAENICKE, R. 1979. Reconstitution of lactic-dehydrogenase. Non-covalent aggregation vs. reactivation: 1. Physical-properties and kinetics of aggregation. *Biochemistry,* 18**,** 5567-5571.

ZHANG, X., LOMORA, M., EINFALT, T., MEIER, W., KLEIN, N., SCHNEIDER, D. & PALIVAN, C. G. 2016. Active surfaces engineered by immobilizing protein-polymer nanoreactors for selectively detecting sugar alcohols. *Biomaterials,* 89**,** 79-88.

ZHOU, J., WANG, K., XU, S., WU, J., LIU, P., DU, G., LI, J. & CHEN, J. 2015. Identification of membrane proteins associated with phenylpropanoid tolerance and transport in *Escherichia coli* BL21. *Journal of Proteomics,* 113**,** 15-28.

ZHOU, Y. F., YAN, D. Y., DONG, W. Y. & TIAN, Y. 2007. Temperature-responsive phase transition of polymer vesicles: Real-time morphology observation and molecular mechanism. *Journal of Physical Chemistry B,* 111**,** 1262-1270.

11.2 Websites

- Anatrace (CMCs of LDAO and O-POE)
  https://www.anatrace.com/Products/Detergents/AMINE-OXIDES/D360
  https://www.anatrace.com/Products/Specialty-Detergents-Products/OTHER/T350
  Last accessed: March 2017

- BioTek, 2006 (application note on the detection of NADPH by fluorescence spectroscopy)
  http://www.biotek.com/resources/docs/FL600_Determining_NADH_&_NADPH_Concentrations.pdf
  Last accessed: March 2017

- Chemicalize Beta by ChemAxon Ltd.
  http://www.chemicalize.org
  Last accessed: December 2016

- Thermo Fisher Scientific (CMCs of Brij-35, CHAPS, DDM, NP-40, Triton X-100, Tween 20 and Tween 80).
  https://www.thermofisher.com/de/de/home/life-science/protein-biology/protein-purification-isolation/cell-lysis-fractionation/detergents-protein-solubilization.html
  Last accessed: March 2017

- Sigma Aldrich (CMC of *N*-lauroylsarcosine)
  http://www.sigmaaldrich.com/catalog/product/sigma/l5777?lang=de&region=DE
  Last accessed: January 2017

12 Abbreviations

Abbreviation	Description
(S)-PFE	*(S)*-1-(2',3',4',5',6'-Pentafluorophenyl)ethanol
AA	Amino acid
ACP	Acyl carrier protein
ADH	Alcohol dehydrogenase
AEX	Anion exchange chromatography
AGE	*N*-Acetylglucosamine 2-epimerase
APS	Ammonium persulfate
ATP	Adenosine triphosphate
BCA	Bicinchoninic acid
BLAST	Basic Local Alignment Search Tool
BLM	Black lipid membrane
BR	Bacteriorhodopsin
bp	Base pair
BN-PAGE	Blue native polyacrylamide gel electrophoresis
Brij-35	Polyoxyethylene lauryl ether
BR	Bacteriorhodopsin
BSA	Bovine serum albumin
CAC	Critical aggregation concentration
CalB	*Candida antarctica* lipase B
CD	Circular dichroism
cdw	Cell dry weight
CHAPS	3-[(3-Cholamidopropyl)dimethylammonio]-1-propansulfonate
CMC	Critical micelle concentration
CV	Column volume
ddH_2O	Double-distilled water
DDM	*n*-Dodecyl-*β*-D-maltoside
DLS	Dynamic light scattering
dNTP	Desoxyribonucleotide triphosphate
DPhPC	1,2-Diphytanoyl-*sn*-glycero-3-phosphocholine
EC	Enzyme comission
ECAA	Ethyl 4-chloroacetoacetate

Abbreviation	Description
EDTA	Ethylenediaminetetraacetic acid
FAD	Flavin adenine dinucleotide
FAS	fatty acid synthase
FC-11	*n*-Undecylphosphocholine
FDH	Formate dehydrogenase
FhuA	Ferric hydroxamate uptake component A
FMN	Flavin mononucleotide
G6PDH	Glucose 6-phosphate dehydrogenase
GC	Gas chromatography
GDH	Glucose dehydrogenase
GOx	Glucose oxidase
GRAVY	Grand Average of Hydropathicity
HRP	Horseradish peroxidase
IB	Inclusion body
IMAC	Immobilized metal affinity chromatography
IPTG	Isopropyl-*β*-D-1-thiogalactopyranoside
KR	3-Ketoacyl-[acyl-carrier-protein]-reductase
LB	Lysogeny broth
LDAO	*N,N*-Dimethyldodecylamine *N*-oxide
LPS	Lipopolysaccharide
MM	Molecular mass
MMCO	Molecular mass cut-off
MOPS	3-(*N*-Morpholino)-propanesulfonic acid
NAD^+/NADH	Nicotinamide adenine dinucleotide (oxidized/reduced form)
$NADP^+$/NADPH	Nicotinamide adenine dinucleotide phosphate (oxidized/reduced form)
NDSB	Non-detergent sulfobetaine
NP-40	Nonidet P40 substitute
OG	*n*-Octyl-*β*-D-glucopyranoside
O-POE	*n*-Octylpolyoxyethylene
OTG	*n*-Octyl-*β*-D-thioglucopyranoside
PAA	Poly(acrylic acid)
PAGE	Polyacrylamide gel electrophoresis
PAMO	Phenylacetone monooxygenase

Abbreviation	Description
PB	Polybutadiene
PBS	Phosphate-buffered saline
PCR	Polymerase chain reaction
PDI	Polydispersity index
PDMS	Polydimethylsiloxane
PEE	Polyethylethylene
PEG	Poly(ethylene glycol)
PEO	Poly(ethylene oxide)
PEtOz	Poly(2-ethyl-2-oxazoline)
PFAP	2',3',4',5',6'-Pentafluoroacetophenone
PHT	PhoE-leader, His-tag, Tev-cleavage-site
pI	Isoelectric point
PIAT	Poly(isocyanoalanine(2-thiophene-3-yl-ethyl)amide)
PIB	Polyisobutadiene
PMOXA	Poly(2-methyloxazoline)
PMSF	Phenylmethylsulfonyl fluoride
POPC	1-Palmitoyl-2-oleoyl-*sn*-glycero-3-phosphocholine
PS	Polystyrene
SDS	Sodium dodecyl sulfate
SEC	Size exclusion chromatography
TAE buffer	Tris-acetate-ethylenediaminetetraacetic acid buffer
TB	Terrific Broth
TEA	Triethanolamine
TEM	Transmission electron microscopy
TEMED	Tetramethylethylenediamine
TEV	Tobacco etch virus
Tricine	*N*-Tris-(hydroxymethyl)-methyl-glycine
Tris	Tris(hydroxymethyl)-aminomethane
Triton X-100	Polyethylene glycol alkylphenyl ether
Tween 20	Polyoxyethylene (20) sorbitan monolaureate
Tween 80	Polyoxyethylene (80) sorbitan monolaureate
Z-average	Intensity-based mean hydrodynamic diameter

13 Symbols

Symbol	Meaning	Dimension
A	Total surface area of the polymer membrane	cm^2
A_{280}	Absorbance at 280 nm	-
A_{340}	Absorbance at 340 nm	-
$AC_{vesicle}$	Dimensionless number describing the concentration in the acceptor phase relative to the equilibrium concentration	-
c	Concentration	$mol\ L^{-1}$
c_A	Concentration in the acceptor phase	$mol\ cm^{-3}$
c_{eq}	Equilibrium concentration	$mol\ cm^{-3}$
d	Layer thickness	cm
d_M	Membrane thickness	nm
d_N	Number-based mean diameter	nm
d_i	Inner polymersome diameter	nm
ε	Molar extinction coefficient	$L\ mol^{-1}\ cm^{-1}$
ee	Enantiomeric excess	%
E	Enzyme concentration	$g\ L^{-1}$
$E_{Applied}$	Total enzyme concentration used for encapsulation	$g\ L^{-1}$
$E_{Encapsulated}$	Encapsulated enzyme concentration (relative to the total volume of the polymersome suspension)	$g\ L^{-1}$
E_{inside}	Encapsulated enzyme concentration (relative to the inner volume of a single polymersome)	$g\ L^{-1}$
G	Conductance	S
I	Current	A
J	Flux density	$mol\ cm^{-2}\ s^{-1}$
K_a	Acid dissociation constant	$mol\ L^{-1}$
k_{cat}	Catalytic constant	s^{-1}
K_d	Dissociation constant	$mol\ L^{-1}$
K_d'	Apparent dissociation constant	$mg\ L^{-1}$
k_{inact}	Inactivation constant	h^{-1}
K_M	Half-saturation constant	$mol\ L^{-1}$
M_E	Molecular mass of the enzyme	$g\ mol^{-1}$
n	Hill coefficient	-
N_A	Avogadro constant ($6.022 \cdot 10^{23}$)	mol^{-1}

Symbol	Meaning	Dimension
N_{Agg}	Aggregation number	-
$N_{Polymersomes}$	Number of polymersomes per volume	L^{-1}
n_R / n_S	Amount of *(R)*/*(S)*-enantiomer	mol
OD_{600}	Optical density at 600 nm	-
p	Probability	-
P	Octanol-water partition coefficient	-
Pe	Permeability	cm s^{-1}
Pe_0	Intrinsic permeability	cm s^{-1}
pK_A	Negative decadic logarithm of the acid dissociation constant	-
t	Incubation time	s
T	Temperature	°C
T_m	Melting temperature	°C
v	Reaction rate	U mg^{-1}
v_0	Initial reaction rate at $t = 0$	U mg^{-1}
V_A	Total volume of the acceptor phase	cm^3
V_D	Total volume of the donor phase	cm^3
V_i	Encapsulated volume of a polymersome suspension	L
$V_{i,\ 1\ Polymersome}$	Inner volume of a single polymersome	L
V_E	Elution volume	L
v_{max}	Maximal specific activity	U mg^{-1}
V_{total}	Total volume of a polymersome suspension	L
$(1-\alpha)$	Protonated fraction	-
$\tau_{1/2}$	Half-life	h

14 Appendix A

14.1 Equipment

Table A 1. General equipment.

Equipment	Supplier
Analytical scale Explorer E1M213	Ohaus, Gießen, Germany
Analytical scale Extend ED124S	Sartorius, Göttingen, Germany
Autoclave 5075 ELV	Systec GmbH, Wettenberg, Germany
Autoclave Varioklav 500 E H+P	H+P Labortechnik, Oberschleißheim, Germany
Bandelin Sonoplus HD2070	Bandelin, Berlin, Germany
Biospectrometer Basic + µCuvette G 1.0	Eppendorf, Hamburg, Germany
CD spectrometer J815	Jasco, Groß-Umstadt, Germany
Centrifuge Heraeus Biofuge Stratos	Thermo Fisher Scientific, Braunschweig, Germany
Centrifuge Heraeus Fresco 17	Thermo Fisher Scientific, Braunschweig, Germany
Centrifuge Heraeus Megafuge 16R	Thermo Fisher Scientific, Braunschweig, Germany
Centrifuge Mikro 20	Hettich, Tuttlingen, Germany
Centrifuge Rotixa 50 RS	Hettich, Tuttlingen, Germany
Dounce homogenizer 40 mL	Carl Roth, Karlsruhe, Germany
Dialysis chamber, custom-made from high-density polyethylene	Entleutner, Haag, Germany
Drying oven E28	Binder, Tuttlingen, Germany
Electroporator GenePulser Xcell	Bio-Rad, Hercules, CA, USA
Gel iX Imager	Intas, Göttingen, Germany
Gel electrophoresis chamber MGU-402T	C.B.S. Scientific, Del Mar, CA, USA
Hamilton 5 µL syringe 75 N SYR	BGB Analytik, Schlossbockelheim, Germany
Incubator Multitron II	Infors, Einsbach, Germany
Magnetic Stirrer Variomag Multipoint 15	Thermo Fisher Scientific, Braunschweig, Germany
Magnetic Stirrer Variomag Poly 16	Thermo Fisher Scientific, Braunschweig, Germany
Mastercycler gradient	Eppendorf, Hamburg, Germany

Equipment	Supplier
Microliter Digital Syringe 700 Series	Hamilton, Reno, NV, USA
Micropipette 20 µL, 200 µL, 1000 µL	Brand, Wertheim, Germany
Mixer Mill MM 200	Retsch, Haan, Germany
MJ Mini Thermal Cycler	Bio-Rad, Hercules, CA, USA
MTP-photometer Infinite M200	Tecan, Männedorf, Switzerland
MTP-photometer Multiskan FC	Thermo Fisher Scientific, Braunschweig, Germany
MTP-Shaker DTS-1	NeoLab, Heidelberg, Germany
Peltier-cooled incubator IPP 500	Memmert, Schwabach, Germany
pH-electrode BlueLine 24 pH	Schott, Mainz, Germany
pH-meter CG 843	Schott, Mainz, Germany
Photometer Genesys 10 S UV-Vis	Thermo Spectronic, Neuss, Germany
Power supply E802	Consort, Fournhout, Belgium
Power supply pegPOWER E300	Peqlab, Erlangen, Germany
Rotary shaker	NeoLab, Heidelberg, Germany
SDS-PAGE gel chamber P8DS Class II	OWI, Portsmouth, NH, USA
Shaker MTS 2/4 digital	Ika, Staufen, Germany
Suprasil 110-QS 0.5 mm Quartz cuvette	Hellma Analytics, Müllheim, Germany
Thermo Shaker TS-100	Biosan, Riga, Latvia
Thermomixer comfort	Eppendorf, Hamburg, Germany
Transmission electron microscope CM100	Philips, Leiden, Netherlands
Transmission electron microscope JEM 100 CX	Jeol, Freising, Germany
Ultra-Turrax T18 digital	Ika, Staufen, Germany
Ultracentrifuge Optima LE-70	Beckman Coulter, Krefeld, Germany
Ultracentrifuge Optima Max-E	Beckman Coulter, Krefeld, Germany
Ultracentrifuge Optima Max-TL	Beckman Coulter, Krefeld, Germany
Ultracentrifuge rotor TLA-45	Beckman Coulter, Krefeld, Germany
Ultracentrifuge rotor TLA-110	Beckman Coulter, Krefeld, Germany
Ultracentrifuge rotor type 70-Ti	Beckman Coulter, Krefeld, Germany
Vortex-shaker VF2	Ika, Staufen, Germany
WiseCube shaking incubator WIS-20	Witeg Labortechnik, Wertheim, Germany
ZetaSizer Nano-S	Malvern Instruments, Worcestershire, UK

Table A 2. Chromatography equipment.

Component	Supplier
4-channel online degasser	Knauer, Berlin, Germany
ÄKTA Pure Workstation	GE Healthcare, Uppsala, Sweden
ÄKTA Software UNICORN 6.4.1 WkSt pure-BP-exp	GE Healthcare, Uppsala, Sweden
HisTrap FF crude columns, 1 mL	GE Healthcare, Uppsala, Sweden
HisTrap FF crude columns, 5 mL	GE Healthcare, Uppsala, Sweden
HiTrap Capto Q, 1 mL	GE Healthcare, Uppsala, Sweden
Laboratory column (12.5 mL, 10 µm filter pore size)	MobiTec, Göttingen, Germany
Laboratory column (2.5 mL, 10 µm filter pore size)	MobiTec, Göttingen, Germany
Mobicol "classic" spin columns (1 mL, 10 µm filter pore size)	MobiTec, Göttingen, Germany
Preparative column, empty (25x500 mm)	Kronlab, Dinslaken, Germany
Profinity IMAC uncharged resin	Bio-Rad, Hercules, CA, USA
Sepharose 4B chromatography medium	GE Healthcare, Uppsala, Sweden
Superdex 200 Increase 10/300 GL column	GE Healthcare, Uppsala, Sweden

Table A 3. bioREACTOR 48 equipment.

Component	Supplier
C/DC-Open-Bath Circulator Haake W15	PSL Systemtechnik, Osterode am Harz, Germany
Cooling unit DLK-402	G. Heinemann, Schwäbisch Hall, Germany
Liquid handler Genesis Workstation 150	Tecan, Männedorf, Switzerland
Liquid handler software Gemini V4.2.17.304	Gemini, Trivandrum, India
Paddle-stirrer	2mag, Munich, Germany
Parallel bioreactor unit	2mag, Munich, Germany
Single-use bioreactor without sensors (HTBD)	PreSens, Regensburg, Germany
S-stirrer	2mag, Munich, Germany
Stirrer control device	2mag, Munich, Germany
Thermostat ME-12	Julabo, Seelbach, Germany
Tip low volume PTFE coated SP	Tecan, Männedorf, Switzerland
Tubing pump Analog MS 4-4/12	Ismatec, Wertheim, Germany

Table A 4. Gas chromatography equipment.

Component	Supplier
Gas chromatograph CP-3800	Varian, Darmstadt, Germany
Injector 1079 PTV, temperature programmable	Varian, Darmstadt, Germany
Split regulation - electronic flow control (EFC)	Varian, Darmstadt, Germany
FID detector, Fuel gas: hydrogen/air, helium: carrier gas	Varian, Darmstadt, Germany
Software Star Version 5.51	Varian, Darmstadt, Germany
Sample handler CombiPal	CTC Analytics, Zwingen, Switzerland
BGB-174 Column, length 30 m, inner diameter 0.25 mm, film thickness 0.25 µm	BGB Analytik, Schlossbockelheim, Germany
Helium 99.999 % (v/v)	Air Liquide, Krefeld, Germany
Hydrogen 99.999 % (v/v)	Air Liquide, Krefeld, Germany
Synthetic air	House internal gas supply

Table A 5. Electrophysiology equipment.

Component	Supplier
Axopatch 200B Amplifier + Accessories	Molecular Devices, Sunnyvale, CA, USA
Dagan PC one patch clamp amplifier	Dagan, Minneapolis, MN, USA
Orbit mini system	Nanion Technologies, Munich, Germany
MECA4 recording chip	Ionera, Freiburg, Germany
GePulse software	Michael Pusch (http://users.ge.ibf.cnr.it/pusch/programs-mik.htm)
MATLAB R2010b, R2012b	MathWorks, Natick, MA, USA

14.2 Consumables

Table A 6. Consumables.

Consumable	Art.-No.	Supplier
96-well Microplate, PS, black, half area, µCL	675096	Greiner
96-well plates MicroWell	243656	Nunc
Amicon Ultra-0.5 centrifugal filters (100 kDa)	UFC510096	Merck Millipore
Amicon Ultra-15 centrifugal filters (10 kDa)	UFC901008	Merck Millipore

Consumable	Art.-No.	Supplier
Amicon Ultra-15 centrifugal filters (100 kDa)	UFC810096	Merck Millipore
Amicon Ultra-15 centrifugal filters (30 kDa)	UFC903008	Merck Millipore
Amicon Ultra-4 centrifugal filters (10 kDa)	UFC801024	Merck Millipore
Amicon Ultra-4 centrifugal filters (100 kDa)	UFC810096	Merck Millipore
Cuvettes, Q-VETTES half micro, PS	2712120	Ratiolab
Dialysis tube ZelluTrans T4, MMCO: 12,000-14,000	E684.1	Carl Roth
Electroporation cuvettes LE 1 mm	71-2010-LE	Peqlab
Isopore polycarbonate membrane 0,22 µm Ø 13 mm	GTTP01300	Merck Millipore
Isopore polycarbonate membrane 0,4 µm Ø 13 mm	HTTP01300	Merck Millipore
Isopore polycarbonate membrane 1,2 µm Ø 13 mm	RTTP01300	Merck Millipore
Micro-inserts for GC vials	LC07.1	Carl Roth
Polyallomer microfuge tubes 1.5 mL	357448	Beckman Coulter
Polycarbonate tube 38.5 mL	355631	Beckman Coulter
Screw cap KG PP with septum	548-0086	VWR
ServaGel TG PRiME 4-20%	004327801	Serva
Steritop Millipore Express Plus	SCGPS02RE	Merck Millipore
Swinnex 13 mm filter holder	SX0001300	Merck Millipore
Cross-shaped magnetic stirrer Ø 10 mm	442-0394	VWR
Rotilabo sample vials Ø 15 mm	H306.1	Carl Roth
1.5 mL short-thread vials	548-0028	VWR
UVette Cuvettes	003106.318	Eppendorf
0.22 µm syringe filters CA membrane	90491011	Sartorius

14.3 Chemicals

Table A 7. General chemicals.

Chemical	Purity	Art.-No.	Supplier
(3-1-Pyridino)-1-propane sulfonate (NDSB-201)	-	NDSB-201	Anatrace
(S)-1-(2',3',4',5',6'-pentafluorophenyl)ethanol	-	858330	Interchim
2',3',4',5',6'-Pentafluoroacetophenone	97.0 %	32258	Interchim

Chemical	Purity	Art.-No.	Supplier
3-(1-Methylpiperidinium)-1-propane sulfonate (NDSB-221)	-	NDSB-221	Anatrace
3-(*N*-Morpholino)-propanesulfonic acid (MOPS)	PUFFERAN, ≥ 99,5 %	6979	Carl Roth
Acetic acid	≥ 99.8 % for analysis, ACS	10313699	Honeywell
Acetone	> 99.5 %	5025	Carl Roth
Acetophenone	Puriss. p.a., ≥ 99.0 %	00790-250ML	Sigma
Agar-agar	Bacteriology grade	A0949	Applichem
Agarose NEEO	DNA grade	2267	Carl Roth
Ammoniumperoxodisulfate (APS)	0.98 %		Carl Roth
Ampicillin sodium salt	≥ 99 %	K029	Carl Roth
Bromophenol blue	ACS, Reag. Ph. Eur.	108122	Merck
Calcein sodium salt, ca 2-3 Na	-	L10255	VWR
Coomassie Blue G 250	-	9598	Carl Roth
Coomassie Blue R 250	-	3862	Carl Roth
D(+)-Glucose monohydrate	≥ 99.5 %, Ph. Eur.	6780	Carl Roth
Di-Potassium hydrogen phosphate	≥ 99 %, p.a., anhydrous	P749	Carl Roth
Di-sodium hydrogen phosphate	≥ 99 %, p.a., ISO	T106	Carl Roth
Di-sodium hydrogen phosphate	≥ 98 %, Ph. Eur., USP, anhydrous	T876	Carl Roth
Ethanol	99.8 %	9065	Carl Roth
Ethyl 4-chloroacetoacetate (ECAA)	-	532079314	Merck
Ethyl acetate	> 99.5 %, for synthesis	7338	Carl Roth
Ethylenediamine tetraacetic acid (EDTA)	≥ 99 %, p.a., ACS	8040	Carl Roth
Ethylenedinitrilotetraacetic acid, disodium salt dihydrate	ACS, ISO, Reag. Ph Eur.	108418	Merck
Fluoresceine disodium salt	Highly pure	0681	VWR
Glycerol	≥ 98 %, Ph. Eur., anhydrous	7530	Carl Roth
Glycine	PUFFERAN, ≥ 99 %, p.a.	3908	Carl Roth
Guanidine hydrochloride	≥ 99.5 % for biochemistry	0037	Carl Roth
Hydrochloric acid 32%	Pro analysi	100319	Merck

Chemical	Purity	Art.-No.	Supplier
Imidazole	PUFFERAN ≥ 99 %, p.a., ultra quality	X998	Carl Roth
Isopropanol	ROTISOLV, HPLC	7343	Carl Roth
Isopropyl-*β*-D-thiogalactopyranoside (IPTG)	≥ 99 %, for biochemistry	CN08	Carl Roth
Kanamycin sulfate	≥ 750 I.U./mg for biochemistry	T823	Carl Roth
L-Arginine	reagent grade, ≥ 98 %	A5006	Sigma
L-Glutamic acid	≥ 98.5 %, Ph. Eur., for biochemistry	3774	Carl Roth
L-Glutamine	≥ 99 %, USP, for biochemistry	3772	Carl Roth
Magnesium chloride	≥ 98.5 %, water free	KK36	Carl Roth
Magnesium sulphate heptahydrate	≥ 99 %, Ph. Eur., USP, BP	T888	Carl Roth
N,N,N′,N′-Tetramethylethylenediamine (TEMED)	≥ 99 %, p.a., for electrophoresis	2367	Carl Roth
N,N-Bis-(2-hydroxyethyl)-glycine (Bicine)	≥ 99 %	9162	Carl Roth
Nickel(II) chloride hexahydrate	≥ 98 %, p.a.	4489	Carl Roth
Nicotinamide adenine dinucleotide (NAD^+)	~ 98 % for biochemistry	AE11	Carl Roth
Nicotinamide adenine dinucleotide phosphate ($NADP^+$), disodium salt	≥ 97 % for biochemistry	AE13	Carl Roth
Nicotinamide adenine dinucleotide phosphate reduced (NADPH), tetrasodium salt	≥ 97 % for biochemistry	AE14	Carl Roth
n-Octane	≥ 99%, anhydrous	296988	Sigma Aldrich
n-Pentane	≥ 99%, anhydrous	236705	Sigma Aldrich
N-Tris-(hydroxymethyl)-methyl-glycine (Tricine)	PUFFERAN, ≥ 99 %	6977	Carl Roth
ortho-Phosphoric acid 85%	Ph. Eur.	100563	Merck
Peptone ex casein	tryptic digest, microbiology grade	8986	Carl Roth
Phenylmethylsulphonyl fluoride (PMSF)	≥ 99 %, for biochemistry	6367	Carl Roth
Polyethylene glycol 4000	For Synthesis	8074901000	Merck
Potassium dihydrogen phosphate	≥ 99 %, p.a., ACS	3904	Carl Roth

Chemical	Purity	Art.-No.	Supplier
Roti GelStain	-	3865	Carl Roth
Rotiphorese 10x SDS-PAGE buffer	-	3060	Carl Roth
Rotiphorese Gel 40 (19:1)	-	3030	Carl Roth
Sodium chloride	≥ 99.5 %, p.a., ACS, ISO	3957	Carl Roth
Sodium chloride	≥ 99 %, Ph. Eur., USP	P029	Carl Roth
Sodium dihydrogen phosphate monohydrate	Pro analysi	106346	Merck
Sodium dodecyl sulphate (SDS) ultra pure	≥99.5 %, for electrophoresis	2326	Carl Roth
Sodium formate	≥ 99 % p.a., ACS	4404	Carl Roth
Sodium hydroxide	≥ 99 %, p.a., ISO	6771	Carl Roth
β-Mercaptoethanol	≥ 99 %, p.a.	4227	Carl Roth
Tris(hydroxymethyl)-aminomethane (Tris)	PUFFERAN, ≥ 99.9 %, p.a.	4855	Carl Roth
Tris(hydroxymethyl)aminomethane hydrochloride (Tris-HCl)	PUFFERAN, ≥ 99 %, p.a.	9090	Carl Roth
Urea	For biochemistry	108488	Carl Roth
Yeast extract	Powder for Bacteriology	2363	Carl Roth

14.4 Bacterial strains

Table A 8. *Escherichia coli* strains.

Strain	Genotype	Supplier
E. coli BL21 (DE3)	F⁻ *ompT gal dcm Ion hsd*SB(rB^-mB^-) ʎ(DE3)	Novagen, San Diego, CA, USA
E. coli BL21 (DE3) omp8	F⁻ *ompT gal dcm Ion hsd*SB(rB^-mB^-) ʎ(DE3) ΔlamB ompF::Tn5 ΔompA ΔompC	Prilipov *et al.*, 1998
E. coli C41 (DE3)	F⁻ *ompT gal dcm Ion hsd*SB(rB^-mB^-) ʎ(DE3)	Lucigen, Middleton, WI, USA
E. coli C43 (DE3)	F⁻ *ompT gal dcm Ion hsd*SB(rB^-mB^-) ʎ(DE3)	Lucigen, Middleton, WI, USA
E. coli DH5α	F⁻ *endA1 glnV44 thi-1 recA1 relA1 gyrA96 deoR nupG purB20 φ80dlacZ*ΔM15 Δ(*lacZYA-argF*)U169, hsdR17($r_K^-m_K^+$), λ^-	Invitrogen, Carlsbad, CA, USA

14.5 Enzymes, standards and kits

Table A 9. Enzymes.

Component	Art.-No.	Supplier
Antarctic Phosphatase	M0289	New England Biolabs
BamHI-HF	R3136	New England Biolabs
Deoxyribonuclease I (DNAse I)from bovine pancreas	DN25	Sigma-Aldrich
HindIII-HF	R3104	New England Biolabs
Lysozyme	L6876	Sigma Aldrich
NdeI	R0111	New England Biolabs
NheI-HF	R3131	New England Biolabs
Phusion High-Fidelity DNA Polymerase	M0530	New England Biolabs
Proteinase K, ≥30 mAnson U/mg	7528	Carl Roth
T4 DNA Ligase	M0202	New England Biolabs
Taq DNA-Polymerase	M0267	New England Biolabs
Trypsin, 2.500 U/mg USP	785	VWR
Quick Ligation Kit	M2200	New England Biolabs
XhoI	R0146	New England Biolabs

Table A 10. Standards and kits.

Component	Art.-No.	Supplier
DNA-ladder 100 bp extended	T835	Carl Roth
dNTP-Mix	N0447S	New England Biolabs
Gel Filtration Markers Kit for Protein Molecular Weights 12,000-200,000 Da	MWGF200	Sigma Aldrich
GenElute Gel Extraction Kit	NA1111	Sigma Aldrich
GenElute PCR Clean-Up Kit	NA1020	Sigma Aldrich
JustBlue Protein Marker	MWP05	Nippon Genetics
Perfect Protein Marker 15-150 kDa	US169149-3	Merck, Darmstadt, Germany
Quick-Load 100 bp DNA Ladder	N0467	New England Biolabs
Roti-Mark Standard	T851	Carl Roth

14.6 Buffers

All buffers for use with proteins or polymersomes were prepared with ddH_2O.

Table A 11. Buffers for IMAC of enzymes.

Component	IMAC binding buffer	IMAC elution buffer
Sodium phosphate pH 7.4	20 mM	20 mM
NaCl	500 mM	500 mM
Imidazole	40 mM	300 mM

Table A 12. Buffers for IMAC of channel proteins. Depending on the channel protein of choice, the buffers were supplemented with the respective additives listed in Table A 14. For detergent screenings, the buffers were supplemented with the detergents listed in Table A 13. IMAC MP washing buffer was only used for the screenings.

Component	IMAC MP binding buffer	IMAC MP washing buffer	IMAC MP elution buffer
Tris-HCl pH 8	20 mM	20 mM	20 mM
NaCl	100 mM	100 mM	100 mM
Imidazole	20 mM	25 mM	300 mM

Table A 13. Properties of detergents employed for the solubilization and initial refolding screening experiments. The name of the detergent, its class, Critical micelle concentrations (CMCs) and concentrations for solubilization / refolding and IMAC / dialysis buffers is given. CMCs were derived from ([1]) Anatrace, ([2]) Sigma Aldrich or ([3]) Thermo Fisher Scientific.

Detergent	Class	CMC	MP solubilization / refolding buffer	MP IMAC / dialysis buffer
Brij-35	Non-ionic	0.011 % v/v	2 % v/v	0.05 % v/v [(3)]
CHAPS	Zwitterionic	0.5 % v/v	2 % v/v	1 % v/v [(3)]
DDM	Non-ionic	0.009 % v/v	2 % v/v	0.02 % v/v [(3)]
LDAO	Zwitterionic	0.023 % v/v	2 % v/v	0.05 % v/v [(1)]
NP-40	Non-ionic	0.018 % v/v	2 % v/v	0.05 % v/v [(3)]
N-Lauroylsarcosine	Anionic	0.43 % v/v	1 % v/v	0.8 % v/v [(2)]
OG	Non-ionic	0.67-0.73 % v/v	2 % v/v	1 % v/v [(3)]
OTG	Non-ionic	0.28 % v/v	2 % v/v	0.6 % v/v [(3)]
O-POE	Non-ionic	~0.25 % v/v	2 % v/v	0.8 % v/v [(1)]
Triton X-100	Non-ionic	0.016 % v/v	2 % v/v	0.03 % v/v [(3)]

Detergent	Class	CMC	MP solubilization / refolding buffer	MP IMAC / dialysis buffer
Tween 20	Non-ionic	0.0074 % v/v	2 % v/v	0.015 % v/v [3]
Tween 80	Non-ionic	0.0016 % v/v [3]	2 % v/v	0.005 % v/v

Table A 14. Additives for the preparative IMAC of channel proteins.

Protein	Detergent	MP solubilization buffer	MP IMAC buffers
FocA	DDM	1 % w/v	0.03 % w/v
	sodium formate	5 mM	5 mM
OmpF	OG	2 % w/v	1 % w/v
OprP	OG	2 % w/v	1 % w/v
PhoE	LDAO	2 % w/v	0.05 % w/v

Table A 15. Buffers for AEX of channel proteins.

Component	AEX binding buffer	AEX wash buffer	AEX elution buffer
Tris-HCl pH 8	10 mM	20 mM	20 mM
NaCl	-	-	300 mM
LDAO	> 0.05 % w/v	0.05 % w/v	0.05 % w/v

Table A 16. Lysis buffer for the isolation of inclusion bodies.

Component	IB lysis buffer
Tris-HCl pH 7.5	50 mM
NaCl	50 mM
Glycerol	20 mM

Table A 17. Washing buffers for the isolation of inclusion bodies.

Component	4x membrane extraction buffer	IB wash buffer I	IB wash buffer II
Tris-HCl pH 7.5	-	50 mM	50
NaCl	1.5 M	50 mM	50
Triton X-100	6 % w/v	1 % w/v	-

Component	4x membrane extraction buffer	IB wash buffer I	IB wash buffer II
Na_2-EDTA	60 mM	-	-
Guanidine-HCl	-	1 M	-

Table A 18. Buffers for IMAC of inclusion body proteins.

Component	IB solubilization buffer	IB-IMAC buffer A	IB-IMAC buffer B
Tris-HCl pH 8	50 mM	50 mM	50 mM
NaCl	100 mM	500 mM	500 mM
Guanidine-HCl	6 M	6 M	6 M
Imidazole	10 mM	10 mM	500 mM

Table A 19. Refolding buffer composition.

Component	TE buffer
Tris-HCl	20 mM
EDTA	1 mM

Table A 20. Refolding additives for initial refolding screening experiments.

Additive	1st concentration	2nd concentration
NaCl	100 mM	500 mM
Glycerol	5 % w/v	15 % w/v
PEG 4000	0.1 % w/v	0.2 % w/v
Urea	500 mM	1000 mM
NDSB -201	500 mM	1500 mM
Glycine	25 mM	100 mM
Arginine	100 mM	500 mM
Glutamine	50 mM	100 mM
Glutamate	100 mM	200 mM

Table A 21. Refolding conditions for preparative refolding.

Protein	Protein concentration	pH	Temperature	Additives
AlkL	0,5 g L^{-1}	8	40 °C	2 % w/v LDAO, 1 M urea
OmpW	0,5 g L^{-1}	9	20 °C	4 % w/v *N*-Lauroylsarcosine, 1 M urea
TodX	0,5 g L^{-1}	8	20 °C	2 % w/v *N*-Lauroylsarcosine, 25 mM glycine
OprG	0,5 g L^{-1}	8	20 °C	2 % w/v *N*-Lauroylsarcosine, 100 mM glutamate

Table A 22. Buffers for SDS-PAGE.

Component	Stacking gel buffer (2x)	Resolving gel buffer (4x)	Laemmli buffer (5x)
Tris-HCl	250 mM, pH 6.8	1.5 M, pH 8.8	300 mM
SDS	0.4 % w/v	0.8 % w/v	10 % w/v
Glycerol	-	-	50 % v/v
β-Mercaptoethanol	-	-	5 % v/v
Bromophenol blue	-	-	0.05 % w/v

Table A 23. Buffers for Blue native PAGE (modified from (Wittig *et al.*, 2006))

Component	Cathode buffer	Anode buffer	Sample loading buffer (10x)
Tricine pH 7	50	-	-
Imidazole	7.5	25	-
Coomassie blue G-250	0.002 % w/v	0.002 % w/v	-
Glycerol	-	-	50 % w/v
Poinceau S	-	-	0.1 % w/v

Table A 24. Buffers SDS-PAGE protein staining.

Component	Fairbanks A	Fairbanks B	Fairbanks C
Isopropanol	25 % v/v	10 % v/v	-
Acetic acid	10 % v/v	10 % v/v	10 % v/v
Coomassie blue R-250	0.05 % w/v	0.005 % w/v	-

Table A 25. Buffers for agarose gel electrophoresis.

Component	TAE buffer	DNA loading buffer (11x)
Tris-HCl pH 8	40 mM	-
EDTA	1 mM	-
Acetic acid	0.114 % v/v	-
Glycerol	-	55 % v/v
Bromophenol blue	-	0.01 % w/v

Table A 26. Buffer for storage of DNAse I.

Component	DNAse I storage buffer
Tris-HCl, pH 8.0	10 mM
NaCl	50 mM
$MgCl_2$	10 mM
0.1 mM PMSF	0.1 mM
50 % Glycerol	50 % w/v

14.7 Media

Media and medium supplements were prepared using deionized water.

Table A 27. Media compositions. The pH was adjusted to 7.4. KH_2PO_4 and K_2HPO_4 were added after the medium had been autoclaved.

Component	Lysogeny broth (LB)	Terrific broth (TB)	SOC
Peptone (Casein)	10 g L^{-1}	12 g L^{-1}	10 g L^{-1}
Yeast extract	5 g L^{-1}	24 g L^{-1}	5 g L^{-1}
NaCl	5 g L^{-1}	4 g L^{-1}	0.5 g L^{-1}
Glycerol	-	0.5 % w/v	-
KH_2PO_4	-	2.13 g L^{-1}	-
K_2HPO_4	-	12.54 g L^{-1}	-
KCl	-	-	0.2 g L^{-1}
$MgCl_2$	-	-	2 g L^{-1}
Glucose	-	-	3.6 g L^{-1}

Table A 28. Supplement for self-inducing medium (modified from (Gordon *et al.*, 2008)). The supplement was sterile-filtered and added to the already autoclaved medium.

Component	**Self-inducing supplement (50x)**
Glycerol	250 g L^{-1}
Glucose	25 g L^{-1}
α-Lactose	50 g L^{-1}

14.8 Oligonucleotides

Table A 29. Oligonucleotides for assembly of the PHT-modules.

Name	**Sequence (5' → 3')**
PHT2-flanking-f	GATACACATATGAAAAAGAGCACTCTG
PHT2-flanking-r	TGTATCGCTAGCTCCCTGAAAATACAGG
PHT-assembly1	GATACACATATGAAAAAGAGCACTCTGGCATTAGTGGTGA
PHT-assembly2	CCTGTACAGATGCAGATGCCACAATGCCCATCACCACTAATGCCA GAGTG
PHT-assembly3	GCATCTGCATCTGTACAGGCTGCACACCACCACCACCACCACGAA AACC
PHT1-assembly4	TGTATCGGATCCCTGAAAATACAGGTTTTCGTGGTGGTGGTG
PHT2-assembly4	TGTATCGCTAGCTCCCTGAAAATACAGGTTTTCGTGGTGGTGGTG
PHT1-flanking-f	GATACACCATGGAAAAAGAGCACTCTG
PHT1-flanking-r	TGTATCGGATCCCTGAAAATACAGG

Table A 30. Oligonucleotides for cloning native channel proteins.

Name	**Sequence (5' → 3')**
alkL-for1	GATACACATATGAGTTTTTCTAATTATAAAGTAATCGCGA
alkL-rev1	ACATAGAAGCTTGAAAACATAAGACGCACCAAG
focA-for1	GATACACATATGAAAGCTGACAACCCTTTTGATCTTTTA
focA-rev1	ACATAGAAGCTTATGGTGGTCGTTTTCACGCAGGTA
ompf-for1	GATACAGGATCCGCAGAAATCTATAACAAAGATGG
ompF-rev1	GATACAAAGCTTTTAGAACTGGTAAACGATACCC
ompW-for1	GATACACATATGAAAAAGTTAACAGTGGCGGCTTT
ompW-rev1	ACATAGAAGCTTAAAACGATATCCTGCTGAGAACATAAACAC
oprG-for1	GATACACATATGCGTAAGTCCTGGCTTACCGC

Name	Sequence (5’ → 3’)
oprG-rev1	ACATAGAAGCTTGAACTTGTAGCCGAAACCGATCATGT
oprP-for2	GATACAGCTAGCGGGACCGTGACCACCGACGGTG
oprP-rev2	GATACAGAGCTCTCATCAGAACACGTACTGCAGGCGCATC
phoE-for1	GATACAGGATCCGCAGAAATATATAATAAAGACGGTAATAAACTGGA
phoE-rev1	ACATAGAAGCTTTTAAAACTGATACGTCATGCCAACCGC
todX-for1	GATACACATATGAAGATTGCCAGCGTGCTCG
todX-rev1	ACATAGAAGCTTAAAATTTTTGCTATAGGAAACCACTGCATTT

Table A 31. Oligonucleotides for cloning truncated channel proteins.

Name	Sequence (5’ → 3’)
alkL-IB-for1	GATACACATATGAATGAAAATTATCCGGCGAAATCTGC
alkL-rev1	ACATAGAAGCTTGAAAACATAAGACGCACCAAG
ompW-IB-for1	GGAATTCCATATGGCGCATGAAGCAGGCG
ompW-rev1	ACATAGAAGCTTAAAACGATATCCTGCTGAGAACATAAACAC
oprG-IB-for1	GATACACATATGGATATTCAAGGACACAAGGCCGGTGAC
oprG-rev1	ACATAGAAGCTTGAACTTGTAGCCGAAACCGATCATGT
pET28a_His8_rev	ACATAGCTCGAGTCATCAGTGGTGGTGGTGGTGGTGGTGCTCAAGTGCGGCCGCAAGC
todX-IB-for1	GATACACATATGCAGGTTTTCGACCTGGAAGGTTATGGAGC
todX-rev1	ACATAGAAGCTTAAAATTTTTGCTATAGGAAACCACTGCATTT

Table A 32. Sequencing oligonucleotides.

Name	Sequence (5’ → 3’)
T7	TAATACGACTCACTATAGGG
T7 term	CTAGTTATTGCTCAGCGGT

14.9 Plasmids

Table A 33. Plasmids used in this thesis. ΔAA denotes truncated amino acids at the corresponding positions.

Plasmid	Purpose	Source
pET21a(+)	Backbone for the construction of channel protein expression vectors	Novagen, San Diego, USA
pET21a-PHT1	Modified expression vector containing an N-terminal PhoE-leader sequence followed by a His_6-tag and a TEV-cleavage site (BamHI restriction site)	This thesis
pET21a-PHT2	Modified expression vector containing an N-terminal PhoE-leader sequence followed by a His_6-tag and a TEV-cleavage site (NheI restriction site)	This thesis
pCOLA-Duet1-*fdh*(M7)-SG-*kr*-His_6	Expression of the FDH-KR-fusion protein	(Sührer *et al.*, 2014)
pET21a-*fdh*-His_6	Expression of FDH_{wt}	Gebhardt, 2006
pEX-A-*P. oleovorans alkL*	Cloning vector carrying the synthesized *alkL* gene, template for the construction of AlkL expression vectors	Eurofins Genomics
pET21a-*alkL*	Expression of native AlkL with a C-terminal His_6-tag, template for the construction of truncated IB constructs	This thesis
pET21a-*alkL*-IB1	Expression of truncated AlkL (ΔAA 2-27) with a C-terminal His_6-tag, for inclusion body purification	This thesis
pET21a-*alkL*-IB2	Expression of truncated AlkL (ΔAA 2-27) with a C-terminal His_8-tag, for inclusion body purification	This thesis
pET21a-*ompW*	Expression of native OmpW with a C-terminal His_6-tag, template for the construction of truncated IB constructs	This thesis
pET21a-*ompW*-IB1	Expression of truncated OmpW (ΔAA 2-20) with a C-terminal His_6-tag, for inclusion body purification	This thesis
pET21a-*ompW*-IB2	Expression of truncated OmpW (ΔAA 2-20) with a C-terminal His_8-tag, for inclusion body purification	This thesis
pET21a-*oprG*	Expression of native OprG with a C-terminal His_6-tag, template for the construction of truncated IB constructs	This thesis
pET21a-*oprG*-IB1	Expression of truncated OprG (ΔAA 2-27) with a C-terminal His_6-tag, for inclusion body purification	This thesis
pET21a-*oprG*-IB2	Expression of truncated OprG (ΔAA 2-27) with a C-terminal His_8-tag, for inclusion body purification	This thesis
pET21a-*focA*	Expression of native FocA with a C-terminal His_6-tag	This thesis

Plasmid	Purpose	Source
pET21a-*focA2*-H8	Expression of native FocA with a C-terminal His_8-tag	This thesis
pET21a-PHT1-*ompF*	Expression of native OmpF with an N-terminal His_6-tag and a TEV-cleavage site	This thesis
pET21a-PHT1-*phoE*	Expression of native PhoE with an N-terminal His_6-tag and a TEV-cleavage site	This thesis
pET21a-PHT2-*oprP*	Expression of native OprP with an N-terminal His_6-tag and a TEV-cleavage site	This thesis
pET21a-*todX*	Expression of native TodX with a C-terminal His_6-tag, template for the construction of truncated IB constructs	This thesis
pET21a-*todX*-IB1	Expression of truncated TodX (ΔAA 2-21) with a C-terminal His_6-tag, for inclusion body purification	This thesis
pET21a-*todX*-IB2	Expression of truncated TodX (ΔAA 2-21) with a C-terminal His_8-tag, for inclusion body purification	This thesis

14.10 Nucleotide sequences of the proteins used in this thesis

Table A 34. Nucleotide sequences of native channel protein genes.

Name	Sequence (5' → 3')
alkL	ATGAGTTTTTCTAATTATAAAGTAATCGCGATGCCGGTGTTGGTTGCTA ATTTTGTTTTGGGGGCGGCCACTGCATGGGCGAATGAAAATTATCCGG CGAAATCTGCTGGCTATAATCAGGGTGACTGGGTCGCGAGCTTCAATT TTTCTAAGGTCTATGTGGGTGAGGAGCTTGGCGATCTAAATGTTGGAG GGGGGGCTTTGCCAAATGCTGATGTAAGTATTGGTAATGATACAACAC TTACGTTTGATATCGCCTATTTTGTTAGCTCAAATATAGCGGTGGATTT TTTTGTTGGGGTGCCAGCTAGGGCTAAATTTCAAGGTGAGAAATCAAT CTCCTCGCTGGGAAGAGTCAGTGAAGTTGATTACGGCCCTGCAATTCT TTCGCTTCAATATCATTACGATAGCTTTGAGCGACTTTATCCGTATGTT GGGGTTGGTGTTGGTCGGGTGCTATTTTTTGATAAAACCGACGGTGCTT TGAGTTCGTTTGATATTAAGGATAAATGGGCGCCTGCTTTTCAGGTTGG CCTTAGATATGACCTTGGTAACTCATGGATGCTAAATTCAGATGTGCGT TATATTCCTTTCAAAACGGACGTCACAGGTACTCTTGGCCCGGTTCCTG TTTCTACTAAAATTGAGGTTGATCCTTTCATTCTCAGTCTTGGTGCGTCT TATGTTTTCAAGCTTGCGGCCGCACTCGAGCACCACCACCACCACCAC TGA

Name	Sequence (5' → 3')
focA	ATGAAAGCTGACAACCCTTTTGATCTTTTACTTCCTGCTGCAATGGCCA AAGTGGCCGAAGAGGCGGGTGTCTATAAAGCAACGAAACATCCGCTT AAGACTTTCTATCTGGCGATTACCGCCGGTGTTTTCATCTCAATCGCAT TCGTCTTCTATATCACAGCAACCACTGGCACAGGCACAATGCCCTTCG GCATGGCAAAACTGGTTGGCGGCATTTGCTTCTCTCTGGGGCTGATTCT TTGTGTTGTCTGCGGAGCCGATCTCTTTACTTCCACCGTGTTGATTGTTG TTGCTAAGGCGAGTGGGCGCATCACCTGGGGTCAGTTGGCGAAAAACT GGCTAAATGTCTATTTTGGCAACCTGGTCGGCGCACTGCTGTTTGTACT TTTAATGTGGCTTTCCGGCGAGTATATGACCGCAAATGGTCAATGGGG ACTAAACGTCCTACAAACCGCCGACCACAAAGTGCACCATACTTTTAT TGAGGCCGTCTGTCTTGGTATCCTGGCAAACCTGATGGTATGTCTGGCA GTATGGATGAGTTATTCTGGCCGCAGCCTGATGGACAAAGCGTTCATT ATGGTGCTGCCGGTCGCGATGTTTGTTGCCAGCGGTTTTGAGCACAGT ATCGCAAACATGTTTATGATCCCGATGGGTATTGTAATCCGCGACTTCG CATCCCCGGAATTTTGGACCGCAGTCGGTTCTGCACCGGAAAATTTTTC TCACCTGACCGTGATGAATTTCATCACTGATAACCTGATTCCGGTTACG ATCGGCAACATTATCGGTGGTGGTTTGTTGGTTGGGTTGACATACTGGG TCATTTACCTGCGTGAAAACGACCACCATAAGCTTGCGGCCGCACTCG AGCACCACCACCACCACCACTGA
*focA*2-H8	ATGAAAGCTGACAACCCTTTTGATCTTTTACTTCCTGCTGCAATGGCCA AAGTGGCCGAAGAGGCGGGTGTCTATAAAGCAACGAAACATCCGCTT AAGACTTTCTATCTGGCGATTACCGCCGGTGTTTTCATCTCAATCGCAT TCGTCTTCTATATCACAGCAACCACTGGCACAGGCACAATGCCCTTCG GCATGGCAAAACTGGTTGGCGGCATTTGCTTCTCTCTGGGGCTGATTCT TTGTGTTGTCTGCGGAGCCGATCTCTTTACTTCCACCGTGTTGATTGTTG TTGCTAAGGCGAGTGGGCGCATCACCTGGGGTCAGTTGGCGAAAAACT GGCTAAATGTCTATTTTGGCAACCTGGTCGGCGCACTGCTGTTTGTACT TTTAATGTGGCTTTCCGGCGAGTATATGACCGCAAATGGTCAATGGGG ACTAAACGTCCTACAAACCGCCGACCACAAAGTGCACCATACTTTTAT TGAGGCCGTCTGTCTTGGTATCCTGGCAAACCTGATGGTATGTCTGGCA GTATGGATGAGTTATTCTGGCCGCAGCCTGATGGACAAAGCGTTCATT ATGGTGCTGCCGGTCGCGATGTTTGTTGCCAGCGGTTTTGAGCACAGT ATCGCAAACATGTTTATGATCCCGATGGGTATTGTAATCCGCGACTTCG CATCCCCGGAATTTTGGACCGCAGTCGGTTCTGCACCGGAAAATTTTTC TCACCTGACCGTGATGAATTTCATCACTGATAACCTGATTCCGGTTACG ATCGGCAACATTATCGGTGGTGGTTTGTTGGTTGGGTTGACATACTGGG TCATTTACCTGCGTGAAAACGACCACCATAAGCTTGCGGCCGCACTTG AGCACCACCACCACCACCACCACTGA

Name	Sequence (5' → 3')
ompF	ATGAAAAAGAGCACTCTGGCATTAGTGGTGATGGGCATTGTGGCATCT GCATCTGTACAGGCTGCACACCACCACCACCACCACGAAAACCTGTAT TTTCAGGGATCCGCAGAAATCTATAACAAAGATGGCAACAAAGTAGAT CTGTACGGTAAAGCTGTTGGTCTGCATTATTTTTCCAAGGGTAACGGTG AAAACAGTTACGGTGGCAATGGCGACATGACCTATGCCCGTCTTGGTT TTAAAGGGGAAACTCAAATCAATTCCGATCTGACCGGTTATGGTCAGT GGGAATATAACTTCCAGGGTAACAACTCTGAAGGCGCTGACGCTCAAA CTGGTAACAAAACGCGTCTGGCATTCGCGGGTCTTAAATACGCTGACG TTGGTTCTTTCGATTACGGCCGTAACTACGGTGTGGTTTATGATGCACT GGGTTACACCGATATGCTGCCAGAATTTGGTGGTGATACTGCATACAG CGATGACTTCTTCGTTGGTCGTGTTGGCGGCGTTGCTACCTATCGTAAC TCCAACTTCTTTGGTCTGGTTGATGGCCTGAACTTCGCTGTTCAGTACC TGGGTAAAAACGAGCGTGACACTGCACGCCGTTCTAACGGCGACGGTG TTGGCGGTTCTATCAGCTACGAATACGAAGGCTTTGGTATCGTTGGTGC TTATGGTGCAGCTGACCGTACCAACCTGCAAGAAGCTCAACCTCTTGG CAACGGTAAAAAAGCTGAACAGTGGGCTACTGGTCTGAAGTACGACG CGAACAACATCTACCTGGCAGCGAACTACGGTGAAACCCGTAACGCTA CGCCGATCACTAATAAATTTACAAACACCAGCGGCTTCGCCAACAAAA CGCAAGACGTTCTGTTAGTTGCGCAATACCAGTTCGATTTCGGTCTGCG TCCGTCCATCGCTTACACCAAATCTAAAGCGAAAGACGTAGAAGGTAT CGGTGATGTTGATCTGGTGAACTACTTTGAAGTGGGCGCAACCTACTA CTTCAACAAAAACATGTCCACCTATGTTGACTACATCATCAACCAGAT CGATTCTGACAACAAACTGGGCGTAGGTTCAGACGACACCGTTGCTGT GGGTATCGTTTACCAGTTCTAA
ompW	ATGAAAAAGTTAACAGTGGCGGCTTTGGCAGTAACAACTCTTCTCTCT GGCAGTGCCTTTGCGCATGAAGCAGGCGAATTTTTTATGCGTGCAGGT TCTGCAACCGTACGTCCAACAGAAGGTGCTGGTGGTACGTTAGGAAGT CTGGGTGGATTCAGCGTGACCAATAACACGCAACTGGGCCTTACGTTT ACTTATATGGCGACCGACAACATTGGTGTGGAATTACTGGCAGCGACG CCGTTCCGCCATAAAATCGGCACCCGGGCGACCGGCGATATTGCAACC GTTCATCATCTGCCACCAACACTGATGGCGCAGTGGTATTTTGGTGATG CCAGCAGCAAATTCCGTCCTTACGTTGGGGCAGGTATTAACTACACCA CCTTCTTTGATAATGGATTTAACGATCATGGCAAAGAGGCAGGGCTTT CCGATCTCAGTCTGAAAGATTCCTGGGGAGCTGCCGGGCAGGTGGGGG TTGATTATCTGATTAACCGTGACTGGTTGGTTAACATGTCAGTGTGGTA CATGGATATCGATACCACCGCCAATTATAAGCTGGGCGGTGCACAGCA ACACGATAGCGTACGCCTCGATCCGTGGGTGTTTATGTTCTCAGCAGG ATATCGTTTTAAGCTTGCGGCCGCACTCGAGCACCACCACCACCACCA CTGA

Name	Sequence (5' → 3')
oprG	ATGCGTAAGTCCTGGCTTACCGCTTCCCTGCTGGCCCTCACCGTCGCCT CCCCGTTCGCCGCTGCGGATATTCAAGGACACAAGGCCGGTGACTTCA TCATCCGTGGCGGCTTCGCCACCGTCGATCCCGACGACAGCAGTTCCG ACATCAAGCTGGACGGCGCCAAGCAGCGCGGTACCAAGGCGACTGTC GACAGCGACACCCAGCTCGGCCTGACCTTCACCTACATGTTCGCCGAC AAGTGGGGCGTGGAACTGGTCGCCGCCACTCCGTTCAACCACCAGGTC GACGTCAAGGGCCTCGGCCCGGGCCTGGACGGCAAGCTGGCCGACAT CAAGCAACTGCCGCCGACCCTGCTGCTCCAGTACTACCCCATGGGCGG TACCAACAGCGCCTTCCAGCCCTACGGCGGTCTGGGCGTGAACTACAC CACCTTCTTCGACGAAGACCTCGCCAGCAACCGCAAGGCGCAGGGTTT CAGCAGCATGAAGCTGCAGGACTCCTGGGGCCTGGCCGGCGAACTGG GCTTCGACTACATGCTCAACGAGCACGCGCTGTTCAACATGGCCGTCT GGTACATGGACATCGACACCAAGGCCAGCATCAACGGCCCGAGCGCC CTGGGCGTGAACAAGACCAAGGTCGACGTGGACGTCGATCCGTGGGTC TACATGATCGGTTTCGGCTACAAGTTCAAGCTTGCGGCCGCACTCGAG CACCACCACCACCACCACTGA
oprP	ATGAAAAAGAGCACTCTGGCATTAGTGGTGATGGGCATTGTGGCATCT GCATCTGTACAGGCTGCACACCACCACCACCACCACGAAAACCTGTAT TTTCAGGGAGCTAGCGGGACCGTGACCACCGACGGTGCCGACATCGTG ATCAAGACCAAGGGCGGCCTCGAAGTCGCCACCACCGACAAGGAATT CAGCTTCAAGCTCGGCGGCCGCCTGCAGGCCGACTACGGCCGCTTCGA CGGCTACTACACGAACAACGGCAATACCGCCGATGCCGCCTACTTCCG CCGCGCCTACCTGGAGTTCGGCGGCACCGCCTACCGGGACTGGAAGTA CCAGATCAACTACGACCTGTCGCGCAACGTCGGCAACGACAGCGCCGG CTACTTTGACGAAGCTTCGGTCACCTATACCGGCTTCAACCCGGTCAAC CTGAAGTTCGGCCGCTTCTACACCGACTTCGGCCTGGAAAAGGCCACC AGCTCCAAATGGGTCACCGCGCTGGAGCGCAACCTCACCTACGACATC GCCGACTGGGTCAACGACAACGTCGGTACCGGTATCCAAGCCAGCTCG GTGGTGGGCGGCATGGCTTTCCTCTCTGGCAGCGTGTTCAGCGAGAAC AACAACGATACCGACGGCGACAGCGTCAAGCGCTACAACCTGCGCGG CGTGTTCGCGCCGCTGCACGAGCCGGGCAACGTGGTGCACCTGGGCCT GCAATACGCCTATCGCGACCTGGAGGACAGCGCGGTGGATACCCGGAT CCGCCCGCGCATGGGCATGCGCGGCGTCTCCACCAATGGCGGCAACGA TGCCGGCAGCAATGGCAACCGCGGTCTGTTCGGCGGCAGTTCGGCAGT CGAGGGGCTGTGGAAGGACGACTCGGTCTGGGGCCTGGAAGGCGCCT GGGCGCTGGGTGCCTTCTCGGCCCAGGCCGAGTACCTGCGGCGCACGG TCAAGGCCGAGCGCGACCGCGAGGATCTCAAGGCCTCCGGCTATTACG CGCAACTGGCCTACACCCTCACCGGCGAGCCGCGCCTCTACAAGCTGG ACGGCGCCAAGTTCGACACCATCAAGCCGGAGAACAAGGAAATCGGC GCCTGGGAGCTGTTCTACCGCTACGACTCGATCAAGGTCGAGGATGAC AACATCGTCGTCGACAGCGCCACCCGCGAGGTCGGCGACGCCAAGGG CAAGACCCATACCCTGGGCGTCAACTGGTACGCCAACGAGGCGGTGA AGGTTTCCGCCAACTACGTCAAGGCGAAGACCGACAAGATCAGCAAT GCCAACGGCGACGATAGCGGCGATGGCCTGGTGATGCGCCTGCAGTAC GTGTTCTGA

Name	Sequence (5' → 3')
phoE	ATGAAAAAGAGCACTCTGGCATTAGTGGTGATGGGCATTGTGGCATCT GCATCTGTACAGGCTGCACACCACCACCACCACCACGAAAACCTGTAT TTTCAGGGATCCGCAGAAATATATAATAAAGACGGTAATAAACTGGAT GTCTATGGCAAAGTTAAAGCCATGCATTATATGAGTGATAACGCCAGT AAAGATGGCGACCAGAGTTATATCCGTTTTGGTTTCAAAGGCGAAACA CAAATTAACGATCAACTGACTGGTTATGGTCGTTGGGAAGCAGAGTTT GCCGGTAATAAAGCAGAGAGTGATACTGCACAGCAAAAAACGCGTCT CGCTTTTGCCGGGTTGAAATATAAAGATTTGGGTTCTTTCGATTATGGT CGTAACCTGGGGGCGTTGTATGACGTGGAAGCCTGGACCGATATGTTC CCGGAATTTGGTGGCGATTCCTCGGCGCAGACCGACAACTTTATGACC AAACGCGCCAGCGGTCTGGCGACGTATCGGAACACCGACTTCTTCGGC GTTATCGATGGCCTGAACTTAACCCTGCAATATCAAGGGAAAAACGAA AACCGCGACGTTAAAAAGCAAAACGGCGATGGCTTCGGCACGTCATTG ACATATGACTTTGGCGGCAGCGATTTCGCCATTAGTGGGGCCTATACC AACTCAGATCGCACCAACGAGCAGAACCTGCAAAGCCGTGGCACAGG CAAGCGTGCAGAAGCATGGGCAACAGGTCTGAAATACGATGCCAATA ATATTTATCTGGCAACTTTCTATTCTGAAACACGCAAAATGACGCCAAT AACTGGCGGCTTTGCCAATAAGACACAGAACTTTGAAGCGGTCGCTCA ATACCAGTTTGACTTTGGTCTGCGTCCATCGCTGGGTTATGTCTTATCG AAAGGGAAAGATATTGAAGGTATCGGTGATGAAGATCTGGTCAATTAT ATCGACGTCGGTGCTACGTATTATTTCAACAAAAATATGTCAGCGTTTG TTGATTATAAAATCAACCAACTGGATAGCGATAACAAATTGAATATTA ATAATGATGATATTGTCGCGGTTGGCATGACGTATCAGTTTTAA
todX	ATGAAGATTGCCAGCGTGCTCGCACTGCCTTTGAGTGGATATGCTTTCA GTGTGCATGCTACACAGGTTTTCGACCTGGAAGGTTATGGAGCGATCT CTCGTGCCATGGGTGGCACCAGTTCATCGTATTATACCGGTAATGCTGC GCTGATTAGTAATCCCGCTACATTGAGTTTTGCTCCGGACGGAAATCA GTTTGAGCTCGGGCTGGACGTGGTGACTACCGATATCAAGGTTCACGA CAGCCACGGAGCAGAGGCAAAAAGCAGCACGAGATCCAATAATCGAG GCCCCTATGTGGGTCCACAATTGAGCTATGTTGCTCAGTTGGATGACTG GCGTTTCGGTGCTGGATTGTTTGTCAGTAGCGGGTTGGGTACAGAGTAT GGAAGTAAAAGTTTTCTATCACAGACAGAAAACGGAATCCAGACCAG CTTTGATAATTCCAGCCGTCTGATCGTATTGCGCGCTCCTATTGGCTTT AGTTATCAAGCCACATCAAAGCTCACCTTCGGCGCTAGTGTCGATCTG GTCTGGACTTCACTCAACCTTGAACTTCTACTTCCATCATCTCAGGTGG GAGCCCTGACTGCGCAGGGGAATCTTTCAGGCGGTTTAGTTCCCTCGC TGGCTGGATTCGTCGGGACAGGTGGTGCCGCCCATTTCAGTCTAAGTC GCAACAGTACCGCTGGTGGCGCCGTGGATGCGGTCGGTTGGGGCGGGC GCTTGGGACTTACCTACAAACTCACGGATAACACTGTCCTAGGTGCGA TGTACAACTTCAAGACTTCGGTGGGCGATCTCGAGGGGAAGGCGACAC TTTCTGCTATCAGTGGTGATGGAGCGGTGCTTCCATTGGATGGCGATAT CCGTGTAAAAAACTTTGAGATGCCCGCCAGTCTGACGCTTGGCCTCGC TCATCAGTTCAATGAGCGTTGGGTAGTTGCTGCTGATATCAAGCGTGC CTACTGGGGTGATGTAATGGATAGCATGAATGTGGCTTTCATCTCGCA GTTGGGCGGGATCGATGTCGCATTGCCACACCGCTATCAGGATATAAC GGTGGCCTCAATCGGCACTGCTTACAAATATAACAATGATTTAACGCT TCGTGCTGGATATAGCTATGCACAACAGGCGCTAGACAGCGAACTGAT ATTGCCAGTGATTCCTGCTTATTTGAAGCGGCACGTTACTTTCGGTGGC GAGTATGACTTTGACAAGGACTCCAGGATCAATTTGGCAATTTCTTTTG GCCTGAGAGAGCGCGTGCAGACGCCATCGTACTTGGCAGGCACCGAG ATGTTGCGGCAAAGCCACAGTCAAATAAATGCAGTGGTTTCCTATAGC AAAAATTTTAAGCTTGCGGCCGCACTCGAGCACCACCACCACCACCAC TGA

Table A 35. Nucleotide sequences of truncated channel protein genes.

Name	**Sequence (5' → 3')**
alkL-IB1	ATGAATGAAAATTATCCGGCGAAATCTGCTGGCTATAATCAGGGTGAC TGGGTCGCGAGCTTCAATTTTTCTAAGGTCTATGTGGGTGAGGAGCTTG GCGATCTAAATGTTGGAGGGGGGGCTTTGCCAAATGCTGATGTAAGTA TTGGTAATGATACAACACTTACGTTTGATATCGCCTATTTTGTTAGCTC AAATATAGCGGTGGATTTTTTTGTTGGGGTGCCAGCTAGGGCTAAATTT CAAGGTGAGAAATCAATCTCCTCGCTGGGAAGAGTCAGTGAAGTTGAT TACGGCCCTGCAATTCTTTCGCTTCAATATCATTACGATAGCTTTGAGC GACTTTATCCGTATGTTGGGGTTGGTGTTGGTCGGGTGCTATTTTTTGA TAAAACCGACGGTGCTTTGAGTTCGTTTGATATTAAGGATAAATGGGC GCCTGCTTTTCAGGTTGGCCTTAGATATGACCTTGGTAACTCATGGATG CTAAATTCAGATGTGCGTTATATTCCTTTCAAAACGGACGTCACAGGT ACTCTTGGCCCGGTTCCTGTTTCTACTAAAATTGAGGTTGATCCTTTCA TTCTCAGTCTTGGTGCGTCTTATGTTTTCAAGCTTGCGGCCGCACTCGA GCACCACCACCACCACCACTGA
alkL-IB2	ATGAATGAAAATTATCCGGCGAAATCTGCTGGCTATAATCAGGGTGAC TGGGTCGCGAGCTTCAATTTTTCTAAGGTCTATGTGGGTGAGGAGCTTG GCGATCTAAATGTTGGAGGGGGGGCTTTGCCAAATGCTGATGTAAGTA TTGGTAATGATACAACACTTACGTTTGATATCGCCTATTTTGTTAGCTC AAATATAGCGGTGGATTTTTTTGTTGGGGTGCCAGCTAGGGCTAAATTT CAAGGTGAGAAATCAATCTCCTCGCTGGGAAGAGTCAGTGAAGTTGAT TACGGCCCTGCAATTCTTTCGCTTCAATATCATTACGATAGCTTTGAGC GACTTTATCCGTATGTTGGGGTTGGTGTTGGTCGGGTGCTATTTTTTGA TAAAACCGACGGTGCTTTGAGTTCGTTTGATATTAAGGATAAATGGGC GCCTGCTTTTCAGGTTGGCCTTAGATATGACCTTGGTAACTCATGGATG CTAAATTCAGATGTGCGTTATATTCCTTTCAAAACGGACGTCACAGGT ACTCTTGGCCCGGTTCCTGTTTCTACTAAAATTGAGGTTGATCCTTTCA TTCTCAGTCTTGGTGCGTCTTATGTTTTCAAGCTTGCGGCCGCACTTGA GCACCACCACCACCACCACCACTGA
ompW-IB1	ATGGCGCATGAAGCAGGCGAATTTTTTATGCGTGCAGGTTCTGCAACC GTACGTCCAACAGAAGGTGCTGGTGGTACGTTAGGAAGTCTGGGTGGA TTCAGCGTGACCAATAACACGCAACTGGGCCTTACGTTTACTTATATG GCGACCGACAACATTGGTGTGGAATTACTGGCAGCGACGCCGTTCCGC CATAAAATCGGCACCCGGGCGACCGGCGATATTGCAACCGTTCATCAT CTGCCACCAACACTGATGGCGCAGTGGTATTTTGGTGATGCCAGCAGC AAATTCCGTCCTTACGTTGGGGCAGGTATTAACTACACCACCTTCTTTG ATAATGGATTTAACGATCATGGCAAAGAGGCAGGGCTTTCCGATCTCA GTCTGAAAGATTCCTGGGGAGCTGCCGGGCAGGTGGGGGTTGATTATC TGATTAACCGTGACTGGTTGGTTAACATGTCAGTGTGGTACATGGATAT CGATACCACCGCCAATTATAAGCTGGGCGGTGCACAGCAACACGATAG CGTACGCCTCGATCCGTGGGTGTTTATGTTCTCAGCAGGATATCGTTTT AAGCTTGCGGCCGCACTCGAGCACCACCACCACCACCACTGA

Name	Sequence (5' → 3')
ompW-IB2	ATGGCGCATGAAGCAGGCGAATTTTTTATGCGTGCAGGTTCTGCAACC GTACGTCCAACAGAAGGTGCTGGTGGTACGTTAGGAAGTCTGGGTGGA TTCAGCGTGACCAATAACACGCAACTGGGCCTTACGTTTACTTATATG GCGACCGACAACATTGGTGTGGAATTACTGGCAGCGACGCCGTTCCGC CATAAAATCGGCACCCGGGCGACCGGCGATATTGCAACCGTTCATCAT CTGCCACCAACACTGATGGCGCAGTGGTATTTTGGTGATGCCAGCAGC AAATTCCGTCCTTACGTTGGGGCAGGTATTAACTACACCACCTTCTTTG ATAATGGATTTAACGATCATGGCAAAGAGGCAGGGCTTTCCGATCTCA GTCTGAAAGATTCCTGGGGAGCTGCCGGGCAGGTGGGGGTTGATTATC TGATTAACCGTGACTGGTTGGTTAACATGTCAGTGTGGTACATGGATAT CGATACCACCGCCAATTATAAGCTGGGCGGTGCACAGCAACACGATAG CGTACGCCTCGATCCGTGGGTGTTTATGTTCTCAGCAGGATATCGTTTT AAGCTTGCGGCCGCACTTGAGCACCACCACCACCACCACCACTGA
oprG-IB1	ATGGATATTCAAGGACACAAGGCCGGTGACTTCATCATCCGTGGCGGC TTCGCCACCGTCGATCCCGACGACAGCAGTTCCGACATCAAGCTGGAC GGCGCCAAGCAGCGCGGTACCAAGGCGACTGTCGACAGCGACACCCA GCTCGGCCTGACCTTCACCTACATGTTCGCCGACAAGTGGGGCGTGGA ACTGGTCGCCGCCACTCCGTTCAACCACCAGGTCGACGTCAAGGGCCT CGGCCCGGGCCTGGACGGCAAGCTGGCCGACATCAAGCAACTGCCGC CGACCCTGCTGCTCCAGTACTACCCCATGGGCGGTACCAACAGCGCCT TCCAGCCCTACGGCGGTCTGGGCGTGAACTACACCACCTTCTTCGACG AAGACCTCGCCAGCAACCGCAAGGCGCAGGGTTTCAGCAGCATGAAG CTGCAGGACTCCTGGGGCCTGGCCGGCGAACTGGGCTTCGACTACATG CTCAACGAGCACGCGCTGTTCAACATGGCCGTCTGGTACATGGACATC GACACCAAGGCCAGCATCAACGGCCCGAGCGCCCTGGGCGTGAACAA GACCAAGGTCGACGTGGACGTCGATCCGTGGGTCTACATGATCGGTTT CGGCTACAAGTTCAAGCTTGCGGCCGCACTCGAGCACCACCACCACCA CCACTGA
oprG-IB2	ATGGATATTCAAGGACACAAGGCCGGTGACTTCATCATCCGTGGCGGC TTCGCCACCGTCGATCCCGACGACAGCAGTTCCGACATCAAGCTGGAC GGCGCCAAGCAGCGCGGTACCAAGGCGACTGTCGACAGCGACACCCA GCTCGGCCTGACCTTCACCTACATGTTCGCCGACAAGTGGGGCGTGGA ACTGGTCGCCGCCACTCCGTTCAACCACCAGGTCGACGTCAAGGGCCT CGGCCCGGGCCTGGACGGCAAGCTGGCCGACATCAAGCAACTGCCGC CGACCCTGCTGCTCCAGTACTACCCCATGGGCGGTACCAACAGCGCCT TCCAGCCCTACGGCGGTCTGGGCGTGAACTACACCACCTTCTTCGACG AAGACCTCGCCAGCAACCGCAAGGCGCAGGGTTTCAGCAGCATGAAG CTGCAGGACTCCTGGGGCCTGGCCGGCGAACTGGGCTTCGACTACATG CTCAACGAGCACGCGCTGTTCAACATGGCCGTCTGGTACATGGACATC GACACCAAGGCCAGCATCAACGGCCCGAGCGCCCTGGGCGTGAACAA GACCAAGGTCGACGTGGACGTCGATCCGTGGGTCTACATGATCGGTTT CGGCTACAAGTTCAAGCTTGCGGCCGCACTTGAGCACCACCACCACCA CCACCACCACTGA

Name	Sequence (5’ → 3’)
todX-IB1	ATGCAGGTTTTCGACCTGGAAGGTTATGGAGCGATCTCTCGTGCCATG GGTGGCACCAGTTCATCGTATTATACCGGTAATGCTGCGCTGATTAGT AATCCCGCTACATTGAGTTTTGCTCCGGACGGAAATCAGTTTGAGCTC GGGCTGGACGTGGTGACTACCGATATCAAGGTTCACGACAGCCACGGA GCAGAGGCAAAAAGCAGCACGAGATCCAATAATCGAGGCCCCTATGT GGGTCCACAATTGAGCTATGTTGCTCAGTTGGATGACTGGCGTTTCGGT GCTGGATTGTTTGTCAGTAGCGGGTTGGGTACAGAGTATGGAAGTAAA AGTTTTCTATCACAGACAGAAAACGGAATCCAGACCAGCTTTGATAAT TCCAGCCGTCTGATCGTATTGCGCGCTCCTATTGGCTTTAGTTATCAAG CCACATCAAAGCTCACCTTCGGCGCTAGTGTCGATCTGGTCTGGACTTC ACTCAACCTTGAACTTCTACTTCCATCATCTCAGGTGGGAGCCCTGACT GCGCAGGGGAATCTTTCAGGCGGTTTAGTTCCCTCGCTGGCTGGATTC GTCGGGACAGGTGGTGCCGCCCATTTCAGTCTAAGTCGCAACAGTACC GCTGGTGGCGCCGTGGATGCGGTCGGTTGGGGCGGGCGCTTGGGACTT ACCTACAAACTCACGGATAACACTGTCCTAGGTGCGATGTACAACTTC AAGACTTCGGTGGGCGATCTCGAGGGGAAGGCGACACTTTCTGCTATC AGTGGTGATGGAGCGGTGCTTCCATTGGATGGCGATATCCGTGTAAAA AACTTTGAGATGCCCGCCAGTCTGACGCTTGGCCTCGCTCATCAGTTCA ATGAGCGTTGGGTAGTTGCTGCTGATATCAAGCGTGCCTACTGGGGTG ATGTAATGGATAGCATGAATGTGGCTTTCATCTCGCAGTTGGGCGGGA TCGATGTCGCATTGCCACACCGCTATCAGGATATAACGGTGGCCTCAA TCGGCACTGCTTACAAATATAACAATGATTTAACGCTTCGTGCTGGAT ATAGCTATGCACAACAGGCGCTAGACAGCGAACTGATATTGCCAGTGA TTCCTGCTTATTTGAAGCGGCACGTTACTTTCGGTGGCGAGTATGACTT TGACAAGGACTCCAGGATCAATTTGGCAATTTCTTTTGGCCTGAGAGA GCGCGTGCAGACGCCATCGTACTTGGCAGGCACCGAGATGTTGCGGCA AAGCCACAGTCAAATAAATGCAGTGGTTTCCTATAGCAAAAATTTTAA GCTTGCGGCCGCACTCGAGCACCACCACCACCACCACTGA

Name	Sequence (5' → 3')
todX-IB2	ATGCAGGTTTTCGACCTGGAAGGTTATGGAGCGATCTCTCGTGCCATG GGTGGCACCAGTTCATCGTATTATACCGGTAATGCTGCGCTGATTAGT AATCCCGCTACATTGAGTTTTGCTCCGGACGGAAATCAGTTTGAGCTC GGGCTGGACGTGGTGACTACCGATATCAAGGTTCACGACAGCCACGGA GCAGAGGCAAAAAGCAGCACGAGATCCAATAATCGAGGCCCCTATGT GGGTCCACAATTGAGCTATGTTGCTCAGTTGGATGACTGGCGTTTCGGT GCTGGATTGTTTGTCAGTAGCGGGTTGGGTACAGAGTATGGAAGTAAA AGTTTTCTATCACAGACAGAAAACGGAATCCAGACCAGCTTTGATAAT TCCAGCCGTCTGATCGTATTGCGCGCTCCTATTGGCTTTAGTTATCAAG CCACATCAAAGCTCACCTTCGGCGCTAGTGTCGATCTGGTCTGGACTTC ACTCAACCTTGAACTTCTACTTCCATCATCTCAGGTGGGAGCCCTGACT GCGCAGGGGAATCTTTCAGGCGGTTTAGTTCCCTCGCTGGCTGGATTC GTCGGGACAGGTGGTGCCGCCCATTTCAGTCTAAGTCGCAACAGTACC GCTGGTGGCGCCGTGGATGCGGTCGGTTGGGGCGGGCGCTTGGGACTT ACCTACAAACTCACGGATAACACTGTCCTAGGTGCGATGTACAACTTC AAGACTTCGGTGGGCGATCTCGAGGGGAAGGCGACACTTTCTGCTATC AGTGGTGATGGAGCGGTGCTTCCATTGGATGGCGATATCCGTGTAAAA AACTTTGAGATGCCCGCCAGTCTGACGCTTGGCCTCGCTCATCAGTTCA ATGAGCGTTGGGTAGTTGCTGCTGATATCAAGCGTGCCTACTGGGGTG ATGTAATGGATAGCATGAATGTGGCTTTCATCTCGCAGTTGGGCGGGA TCGATGTCGCATTGCCACACCGCTATCAGGATATAACGGTGGCCTCAA TCGGCACTGCTTACAAATATAACAATGATTTAACGCTTCGTGCTGGAT ATAGCTATGCACAACAGGCGCTAGACAGCGAACTGATATTGCCAGTGA TTCCTGCTTATTTGAAGCGGCACGTTACTTTCGGTGGCGAGTATGACTT TGACAAGGACTCCAGGATCAATTTGGCAATTTCTTTTGGCCTGAGAGA GCGCGTGCAGACGCCATCGTACTTGGCAGGCACCGAGATGTTGCGGCA AAGCCACAGTCAAATAAATGCAGTGGTTTCCTATAGCAAAAATTTTAA GCTTGCGGCCGCACTTGAGCACCACCACCACCACCACCACCACTGA

14.11 Amino acid sequences of the proteins used in this thesis

Table A 36. Peptide sequences of native channel proteins. Cleavable leader peptides are underlined.

Name	Sequence (N → C)
AlkL	<u>MSFSNYKVIAMPVLVANFVLGAATAWA</u>NENYPAKSAGYNQGDWVASFN FSKVYVGEELGDLNVGGGALPNADVSIGNDTTLTFDIAYFVSSNIAVDFFV GVPARAKFQGEKSISSLGRVSEVDYGPAILSLQYHYDSFERLYPYVGVGV GRVLFFDKTDGALSSFDIKDKWAPAFQVGLRYDLGNSWMLNSDVRYIPF KTDVTGTLGPVPVSTKIEVDPFILSLGASYVFKLAAALEHHHHHH
FocA	MKADNPFDLLLPAAMAKVAEEAGVYKATKHPLKTFYLAITAGVFISIAFV FYITATTGTGTMPFGMAKLVGGICFSLGLILCVVCGADLFTSTVLIVVAKA SGRITWGQLAKNWLNVYFGNLVGALLFVLLMWLSGEYMTANGQWGLN VLQTADHKVHHTFIEAVCLGILANLMVCLAVWMSYSGRSLMDKAFIMVL PVAMFVASGFEHSIANMFMIPMGIVIRDFASPEFWTAVGSAPENFSHLTVM NFITDNLIPVTIGNIIGGGLLVGLTYWVIYLRENDHHKLAAALEHHHHHH

Name	Sequence (N → C)
FocA2-H8	MKADNPFDLLLPAAMAKVAEEAGVYKATKHPLKTFYLAITAGVFISIAFV FYITATTGTGTMPFGMAKLVGGICFSLGLILCVVCGADLFTSTVLIVVAKA SGRITWGQLAKNWLNVYFGNLVGALLFVLLMWLSGEYMTANGQWGLN VLQTADHKVHHTFIEAVCLGILANLMVCLAVWMSYSGRSLMDKAFIMVL PVAMFVASGFEHSIANMFMIPMGIVIRDFASPEFWTAVGSAPENFSHLTVM NFITDNLIPVTIGNIIGGGLLVGLTYWVIYLRENDHHKLAAALEHHHHHHH H
OmpF	MKKSTLALVVMGIVASASVQAAHHHHHHHENLYFQGSAEIYNKDGNKVD LYGKAVGLHYFSKGNGENSYGGNGDMTYARLGFKGETQINSDLTGYGQ WEYNFQGNNSEGADAQTGNKTRLAFAGLKYADVGSFDYGRNYGVVYD ALGYTDMLPEFGGDTAYSDDFFVGRVGGVATYRNSNFFGLVDGLNFAVQ YLGKNERDTARRSNGDGVGGSISYEYEGFGIVGAYGAADRTNLQEAQPL GNGKKAEQWATGLKYDANNIYLAANYGETRNATPITNKFTNTSGFANKT QDVLLVAQYQFDFGLRPSIAYTKSKAKDVEGIGDVDLVNYFEVGATYYF NKNMSTYVDYIINQIDSDNKLGVGSDDTVAVGIVYQF
OmpW	MKKLTVAALAVTTLLSGSAFAHEAGEFFMRAGSATVRPTEGAGGTLGSL GGFSVTNNTQLGLTFTYMATDNIGVELLAATPFRHKIGTRATGDIATVHH LPPTLMAQWYFGDASSKFRPYVGAGINYTTFFDNGFNDHGKEAGLSDLSL KDSWGAAGQVGVDYLINRDWLVNMSVWYMDIDTTANYKLGGAQQHDS VRLDPWVFMFSAGYRFKLAAALEHHHHHH
OprG	MRKSWLTASLLALTVASPFAAADIQGHKAGDFIIRGGFATVDPDDSSSDIK LDGAKQRGTKATVDSDTQLGLTFTYMFADKWGVELVAATPFNHQVDVK GLGPGLDGKLADIKQLPPTLLLQYYPMGGTNSAFQPYGGLGVNYTTFFDE DLASNRKAQGFSSMKLQDSWGLAGELGFDYMLNEHALFNMAVWYMDI DTKASINGPSALGVNKTKVDVDVDPWVYMIGFGYKFKLAAALEHHHHH H
OprP	MKKSTLALVVMGIVASASVQAAHHHHHHENLYFQGASGTVTTDGADIVI KTKGGLEVATTDKEFSFKLGGRLQADYGRFDGYYTNNGNTADAAYFRR AYLEFGGTAYRDWKYQINYDLSRNVGNDSAGYFDEASVTYTGFNPVNLK FGRFYTDFGLEKATSSKWVTALERNLTYDIADWVNDNVGTGIQASSVVG GMAFLSGSVFSENNNDTDGDSVKRYNLRGVFAPLHEPGNVVHLGLQYAY RDLEDSAVDTRIRPRMGMRGVSTNGGNDAGSNGNRGLFGGSSAVEGLW KDDSVWGLEGAWALGAFSAQAEYLRRTVKAERDREDLKASGYYAQLAY TLTGEPRLYKLDGAKFDTIKPENKEIGAWELFYRYDSIKVEDDNIVVDSAT REVGDAKGKTHTLGVNWYANEAVKVSANYVKAKTDKISNANGDDSGD GLVMRLQYVF
PhoE	MKKSTLALVVMGIVASASVQAAHHHHHHENLYFQGSAEIYNKDGNKLD VYGKVKAMHYMSDNASKDGDQSYIRFGFKGETQINDQLTGYGRWEAEF AGNKAESDTAQQKTRLAFAGLKYKDLGSFDYGRNLGALYDVEAWTDMF PEFGGDSSAQTDNFMTKRASGLATYRNTDFFGVIDGLNLTLQYQGKNEN RDVKKQNGDGFGTSLTYDFGGSDFAISGAYTNSDRTNEQNLQSRGTGKR AEAWATGLKYDANNIYLATFYSETRKMTPITGGFANKTQNFEAVAQYQF DFGLRPSLGYVLSKGKDIEGIGDEDLVNYIDVGATYYFNKNMSAFVDYKI NQLDSDNKLNINNDDIVAVGMTYQF

Name	Sequence (N → C)
TodX	MKIASVLALPLSGYAFSVHATQVFDLEGYGAISRAMGGTSSSYYTGNAAL ISNPATLSFAPDGNQFELGLDVVTTDIKVHDSHGAEAKSSTRSNNRGPYVG PQLSYVAQLDDWRFGAGLFVSSGLGTEYGSKSFLSQTENGIQTSFDNSSRL IVLRAPIGFSYQATSKLTFGASVDLVWTSLNLELLLPSSQVGALTAQGNLS GGLVPSLAGFVGTGGAAHFSLSRNSTAGGAVDAVGWGGRLGLTYKLTD NTVLGAMYNFKTSVGDLEGKATLSAISGDGAVLPLDGDIRVKNFEMPASL TLGLAHQFNERWVVAADIKRAYWGDVMDSMNVAFISQLGGIDVALPHR YQDITVASIGTAYKYNNDLTLRAGYSYAQQALDSELILPVIPAYLKRHVTF GGEYDFDKDSRINLAISFGLRERVQTPSYLAGTEMLRQSHSQINAVVSYSK NFKLAAALEHHHHHH

Table A 37. Peptide sequences of truncated channel proteins.

Name	Sequence (N → C)
AlkL-IB1	MNENYPAKSAGYNQGDWVASFNFSKVYVGEELGDLNVGGGALPNADVS IGNDTTLTFDIAYFVSSNIAVDFFVGVPARAKFQGEKSISSLGRVSEVDYGP AILSLQYHYDSFERLYPYVGVGVGRVLFFDKTDGALSSFDIKDKWAPAFQ VGLRYDLGNSWMLNSDVRYIPFKTDVTGTLGPVPVSTKIEVDPFILSLGAS YVFKLAAALEHHHHHH
AlkL-IB2	MNENYPAKSAGYNQGDWVASFNFSKVYVGEELGDLNVGGGALPNADVS IGNDTTLTFDIAYFVSSNIAVDFFVGVPARAKFQGEKSISSLGRVSEVDYGP AILSLQYHYDSFERLYPYVGVGVGRVLFFDKTDGALSSFDIKDKWAPAFQ VGLRYDLGNSWMLNSDVRYIPFKTDVTGTLGPVPVSTKIEVDPFILSLGAS YVFKLAAALEHHHHHHHH
OmpW-IB1	MAHEAGEFFMRAGSATVRPTEGAGGTLGSLGGFSVTNNTQLGLTFTYMA TDNIGVELLAATPFRHKIGTRATGDIATVHHLPPTLMAQWYFGDASSKFR PYVGAGINYTTFFDNGFNDHGKEAGLSDLSLKDSWGAAGQVGVDYLINR DWLVNMSVWYMDIDTTANYKLGGAQQHDSVRLDPWVFMFSAGYRFKL AAALEHHHHHH
OmpW-IB2	MAHEAGEFFMRAGSATVRPTEGAGGTLGSLGGFSVTNNTQLGLTFTYMA TDNIGVELLAATPFRHKIGTRATGDIATVHHLPPTLMAQWYFGDASSKFR PYVGAGINYTTFFDNGFNDHGKEAGLSDLSLKDSWGAAGQVGVDYLINR DWLVNMSVWYMDIDTTANYKLGGAQQHDSVRLDPWVFMFSAGYRFKL AAALEHHHHHHH
OprG-IB1	MDIQGHKAGDFIIRGGFATVDPDDSSSDIKLDGAKQRGTKATVDSDTQLG LTFTYMFADKWGVELVAATPFNHQVDVKGLGPGLDGKLADIKQLPPTLL LQYYPMGGTNSAFQPYGGLGVNYTTFFDEDLASNRKAQGFSSMKLQDS WGLAGELGFDYMLNEHALFNMAVWYMDIDTKASINGPSALGVNKTKVD VDVDPWVYMIGFGYKFKLAAALEHHHHHH
OprG-IB2	MDIQGHKAGDFIIRGGFATVDPDDSSSDIKLDGAKQRGTKATVDSDTQLG LTFTYMFADKWGVELVAATPFNHQVDVKGLGPGLDGKLADIKQLPPTLL LQYYPMGGTNSAFQPYGGLGVNYTTFFDEDLASNRKAQGFSSMKLQDS WGLAGELGFDYMLNEHALFNMAVWYMDIDTKASINGPSALGVNKTKVD VDVDPWVYMIGFGYKFKLAAALEHHHHHHHH

Name	Sequence (N → C)
TodX-IB1	MQVFDLEGYGAISRAMGGTSSSYYTGNAALISNPATLSFAPDGNQFELGL DVVTTDIKVHDSHGAEAKSSTRSNNRGPYVGPQLSYVAQLDDWRFGAGL FVSSGLGTEYGSKSFLSQTENGIQTSFDNSSRLIVLRAPIGFSYQATSKLTFG ASVDLVWTSLNLELLLPSSQVGALTAQGNLSGGLVPSLAGFVGTGGAAHF SLSRNSTAGGAVDAVGWGGRLGLTYKLTDNTVLGAMYNFKTSVGDLEG KATLSAISGDGAVLPLDGDIRVKNFEMPASLTLGLAHQFNERWVVAADIK RAYWGDVMDSMNVAFISQLGGIDVALPHRYQDITVASIGTAYKYNNDLT LRAGYSYAQQALDSELILPVIPAYLKRHVTFGGEYDFDKDSRINLAISFGL RERVQTPSYLAGTEMLRQSHSQINAVVSYSKNFKLAAALEHHHHHH
TodX-IB2	MQVFDLEGYGAISRAMGGTSSSYYTGNAALISNPATLSFAPDGNQFELGL DVVTTDIKVHDSHGAEAKSSTRSNNRGPYVGPQLSYVAQLDDWRFGAGL FVSSGLGTEYGSKSFLSQTENGIQTSFDNSSRLIVLRAPIGFSYQATSKLTFG ASVDLVWTSLNLELLLPSSQVGALTAQGNLSGGLVPSLAGFVGTGGAAHF SLSRNSTAGGAVDAVGWGGRLGLTYKLTDNTVLGAMYNFKTSVGDLEG KATLSAISGDGAVLPLDGDIRVKNFEMPASLTLGLAHQFNERWVVAADIK RAYWGDVMDSMNVAFISQLGGIDVALPHRYQDITVASIGTAYKYNNDLT LRAGYSYAQQALDSELILPVIPAYLKRHVTFGGEYDFDKDSRINLAISFGL RERVQTPSYLAGTEMLRQSHSQINAVVSYSKNFKLAAALEHHHHHHHH

14.12 Physicochemical properties of the proteins used in this thesis

Table A 38. Physicochemical properties of the proteins used in this thesis. All parameters were estimated using the built-in functions of the GENtle software package. The number of amino acids (#AA) is indicated for the mature protein if the protein contains a cleavable leader sequence.

Protein	# AA	pI	MW, Da	Molar extinction coefficient	Extinction of a 1 g L^{-1} solution
AlkL-IB	217	5.91	23788.69	34380	1.445
AlkL-IB2	219	5.92	24062.97	34380	1.429
OmpW-IB1	206	5.99	22574.23	39420	1.746
OmpW-IB2	208	6.01	22848.51	39420	1.725
OprG-IB1	224	5.9	24556.66	35410	1.442
OprG-IB2	226	5.91	24830.94	35410	1.426
TodX-IB1	446	5.97	47717.49	55810	1.17
TodX-IB2	448	5.98	47991.77	55810	1.163
FocA	298	5.99	32510.42	50420	1.538
FocA2-H8	300	6	32784.7	50420	1.538
OmpF	355	5.86	38917.41	5570	1.431
OprP	427	5.97	47133.84	82740	1.755
PhoE	345	5.88	38668.34	50770	1.313

Protein	# AA	pI	MW, Da	Molar extinction coefficient	Extinction of a 1 g L^{-1} solution
FDHwt	423	6.06	46469.63	58330	1.255
FDH-KR	673	6.06	71659.54	75290	1.051

15 Appendix B: Supplementary data

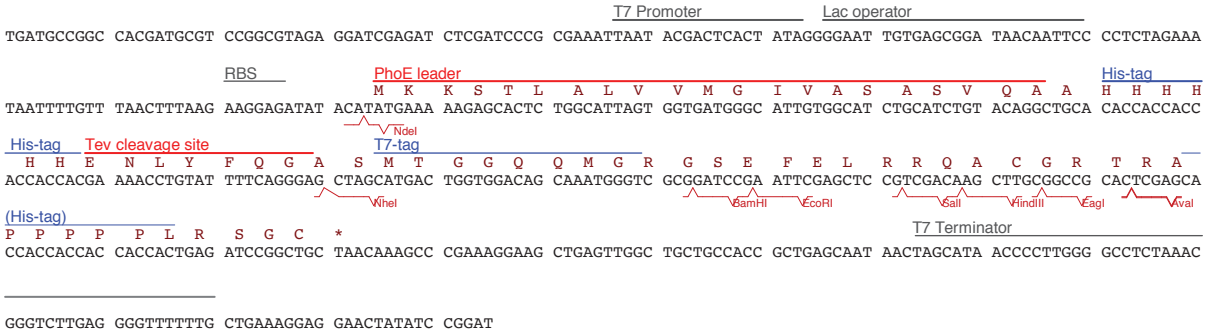

Figure B 1. Structure of the PHT1 cloning site of pET21a-PHT1.

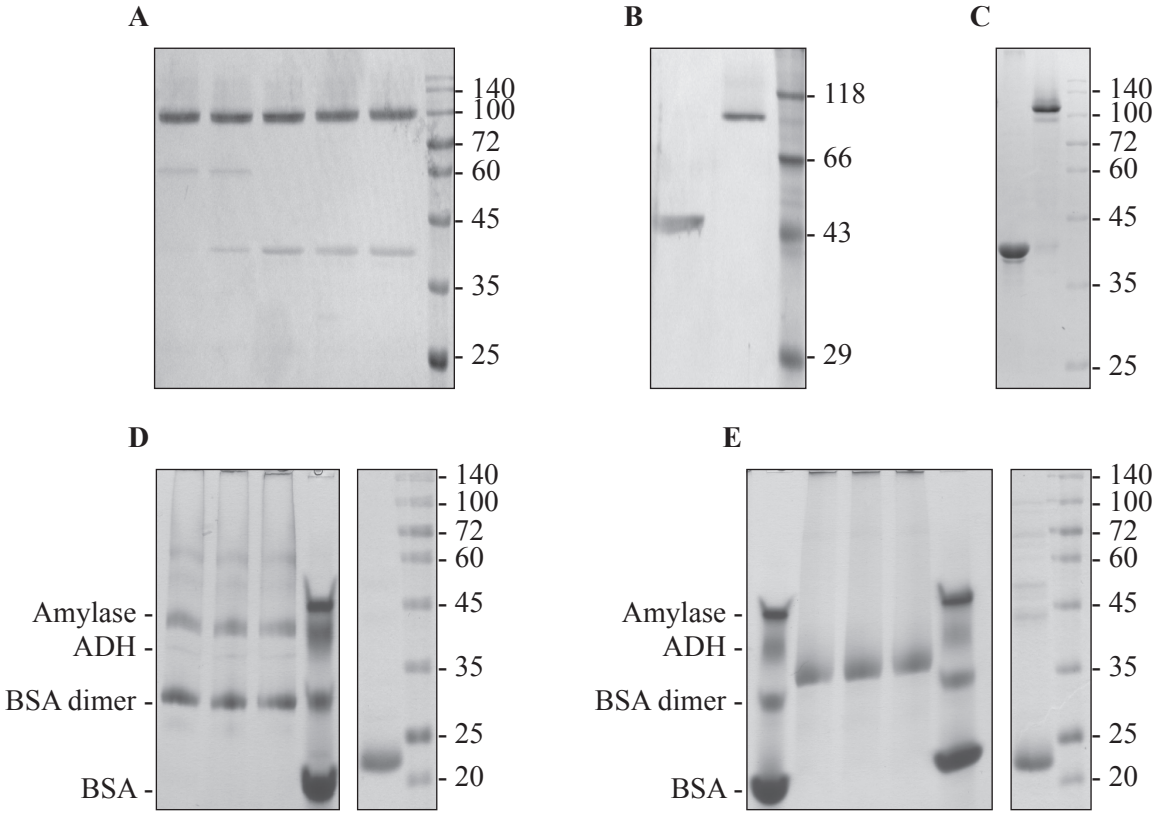

Figure B 2. Upper row: (A) Purified OmpF in LDAO with sample preparation at 40, 45, 50, 55 and 60 °C (from left to right). Note that the trimer band around 100 kDa remains unchanged at these temperatures but vanishes at higher temperatures, while a band corresponding to a dimer disappears above 45 °C and is replaced by the monomer band. This particular behavior, i.e. the presence of the dimer, was not observed in later experiments, although the standard sample preparation temperature for semi-native PAGE of trimeric channel proteins was 37 °C. Just Blue protein marker was used as a guide to the observer. (B) Denatured and native OprP in SDS. Roti-Mark STANDARD was used as a guide to the observer. (C) Denatured and native PhoE in LDAO. Just Blue protein marker was used as a guide to the observer. Lower row: BN-PAGE (left image) and SDS-PAGE (right image) of FocA in (A) DDM and (B) OG. BSA, ADH and amylase were used as marker proteins for BN-PAGE and Just Blue protein marker was used as a guide to the observer for SDS-PAGE.

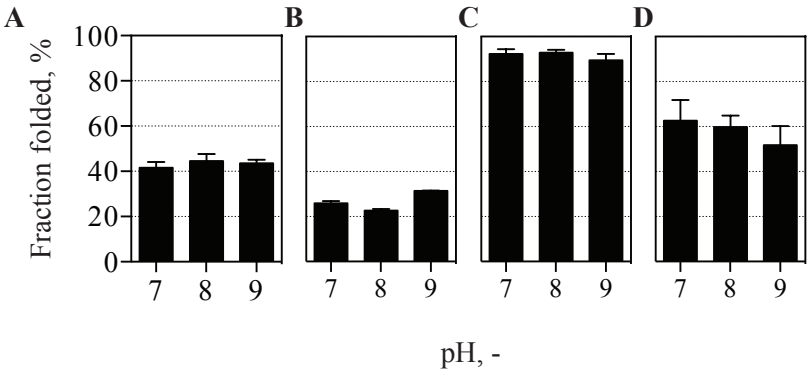

Figure B 3. Folding of (A) AlkL (B) OmpW, (C) OprG and (D) TodX at pH7, 8 or 9.

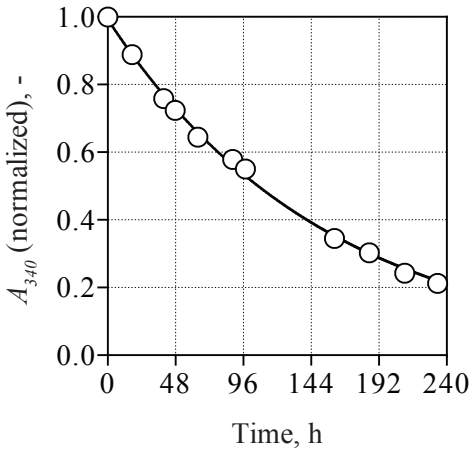

Figure B 4. NADPH stability at 25 °C in PBS pH 7.5. Following the approach of Wu *et al*. (1986), the NADPH concentration was followed over time by measuring the absorbance at 340 nm for 10 days.

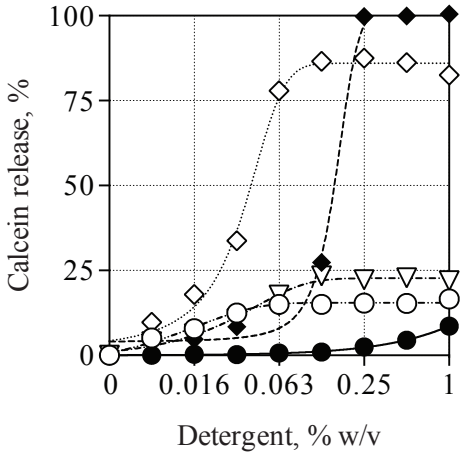

Figure B 5. Calcein release from polymersomes in response to different detergents at concentrations ranging from 0.0078-1 % w/v at 30 °C. DDM (-···○···-), LDAO (···◇···), OG (--●--), O-POE (—◆—) and N-lauroylsarcosine (·-·Δ·-·) were investigated. The release of calcein was assessed by fluorescence measurement after 1 h relative to polymersomes disintegrated with 1 % O-POE. Sigmoidal fits are provided as a guide to the observer only. N=3.